University of Naples Federico II

Alessandra Mazziotti

STRUCTURAL ANALYSIS OF HISTORICAL MASONRY BUILDINGS

Ph.D Thesis
XXVIII cycle

Coordinator:
Prof. Ing. Luciano Rosati

Tutor:
Prof. ing. Antonello De Luca
Co-Tutor:
Prof. Ing. Elena Mele

Dottorato di Ricerca in Ingegneria delle Costruzioni

On the front cover: Piazza Centre (Renzo Piano)- - Eindhoven- The Netherlans

ATMOSPHERIC CORROSION AND DURABILITY DESIGN OF METAL STRUCTURES

CONTENTS

LIST OF FIGURES

LIST OF TABLES

ABSTRACT

The structural analysis of masonry historical buildings is still a challenging task, basically due to: the difficult numerical modelling of the nonlinear behaviour of masonry material, with almost no tensile strength; the arrangement of blocks and mortar joints frequently uncertain and variable; the complexity of morphology; the difficult modeling of the geometry, which drives to three-dimensional models characterized by a large number of degrees of freedom.

The above considerations justify the need for specific modelling and analysis strategies to be developed and established for historical buildings. The most widely used strategies are affected by some limitations and different levels of accuracy. In this study the structural analysis of different types of historical buildings, under seismic loads, is performed by comparing different analysis approaches and pointing out some their criticalities.

In the first part of the thesis (Chapter 2), the seismic capacity of multi-storey masonry buildings is evaluated, comparing different modelling strategies, such as simplified methods (equivalent frame, macro-modelling) and FE method. Four case studies characterized by different geometry (overall height, storey number, slenderness of spandrels and piers, etc.) are analyzed. The results are compared with the horizontal collapse multipliers computed with the limit analysis. The latter has proved to be a powerful simple method to check the results of more complex analysis, often less manageable and influenced by the implemented modelling. A simplified formula is proposed to apply the limit analysis and it was found to provide a good approximate measure of the seismic capacity of the building, being only noted the geometrical characteristics of the walls.

The second part of the thesis focuses on the seismic behavior of masonry churches. The dynamic behavior is first investigated on a sample of fourteen case studies (Chapter 3), then an impressive case study: the gothic cathedral of *Santa Maria del Mar,* is analyzed by means of different analysis methods.

The dynamic analyses of the fourteen masonry churches reveals a considerable dispersion of the vibration modes, which provide very small contribution in terms of participating mass. It leads to low values of the base shears (computed through the response spectrum analysis) and, consequently, to the possibility of adopting reduced forces to be applied on the masonry churches.

The *Santa Maria del Mar* church was analyzed carrying out: linear static analysis, modal analysis, non linear (push-over)analysis and non linear dynamic analysis. The comparison between all these analysis methods provides a convincing picture of the structural weaknesses of the cathedral.

ACKNOWLEDGEMENTS

1 INTRODUCTION

The conservation of historical buildings is intrinsically linked to a correct structural analysis. The structural analysis contributes to all the phases and activities, including diagnosis, reliability assessment and design of intervention, oriented to grant an efficient and respectful conservation of monuments and historical buildings (Roca et al. 2010). Incorrect or non-exhaustive structural analysis can lead to ineffective or counter-productive interventions. The seismic events occurred in Italy in the last decades Umbria-Marche 1997–1998, Abruzzo 2009, Emilia-Romagna 2012) demonstrated that over-strengthening interventions, generally performed with reinforced concrete, does not always safeguarded the structure. Figure 1.1 shows a detail of the damage of the S. Maria di Collemaggio church (L'Aquila, Italy) after the 2009 earthquake. The transept of the church collapsed completely and the presence of the belt courses in reinforced concrete (inserted during the second half of '900), did not help to avoid the collapse.

However it has to be said that the conventional methods of the structural analysis are not immediately applicable to historical constructions. As excellently stated in the preface by Navier (1833), and reported in important literature's treatises (Rondelet 1802 and Breyman 1885), pyramids, mastabas, mosques, churches, domes, cathedrals, towers, castles, palaces, bridges, have been designed starting from the dimensions of similar buildings, under the theory of proportions or from state of art rules. Therefore, these buildings are ill–suited to be studied by means of the numerical models traditionally used in structural engineering. Since the times of realizing marvelous Egyptian temples in the 3000 B.C. up to 18th century, the world's architectural heritage has been constructed with unreinforced masonry. Masonry, being a two-phases material made of assemblage of bricks/blocks connected at interfaces, does not obey to the theory of elasticity. It is characterized by highly non-linear behavior, a brittle response in tension with very low tensile strength, a frictional response in shear and anisotropy. A complete model describing all the complexity of the mechanical behavior of masonry is still an open, challenging issue.

Figure 1.1 S. Maria di Collemaggio church: damage after 2009 earthquake showing the course of reinforced concrete inserted during the second half of '900

Further difficulties, connected to the structural analysis of historical buildings, are related to the highly composite geometry and morphology, which drives to the need of defining three-dimensional (3D) models characterized by a very high number of degrees of freedom.

Moreover, recent studies have proved that a correct structural analysis should take into account the historical events occurred on the structure over the centuries. Studies on different historical structures (Roca 2004, Roca et al.2004) have shown that real deformations are normally much larger (one or even two orders of magnitude) than those predicted by conventional instantaneous calculations. This is due to the fact that these analysis neglect history-related aspects such as (1) deformations occurred during the construction process, (2) initial and historical soil settlements, (3) architectural alterations, (4) the non-reversible effect of multiple thermal and hygrometric cycles, and (4) long term damage of mechanical, physical or chemical nature, among other phenomena (Roca et al.2010).

Since the complexity and variety of the aspects involved, different modelling strategies have been developed and different analysis methods are generally used and compared to carry out the structural analysis of

historical buildings. In the following an overview of the principal modelling strategies and, then, of the analysis methods is presented, pointing out the related advantages and disadvantages.

1.1 OVERVIEW OF MODELLING STRATEGIES

Limit analysis

As mentioned above, the masonry does not obey to the theory of elasticity and its mechanical behavior is difficult to model. However the masonry structures obviously satisfy the equilibrium laws and based on the equilibrium conditions, the first theories for the structural assessments of masonry structures were developed by Gregory, La Hire (1712), Poleni (1748) and Coulomb (1773).

Limit analysis, as it was formulated by Heyman (1966, 1982, 1995), synthetizes all the mentioned classical theories based on equilibrium considerations. It represents a particularly effective tool for estimating the collapse load of structural systems, since it provides a bound of the horizontal capacity. As sketched by Heyman, the hypotheses on the masonry behaviour are: no tensile strength; infinite compression strength and absence of sliding at failure. Under these hypotheses, the masonry material becomes an assemblage of rigid parts, held up by mutual pressure, and the collapse of the structural elements is characterized by the development of non-dissipative hinges transforming the structure into a mechanism. The term 'mechanism' indicates a displacement distribution in the structure produced by inelastic deformations (the formation of hinges) which occur in a finite number of sections due to disconnections and cracking. If a kinematical admissible mechanism can be found, the external forces corresponding to the activation of the mechanism (obtained by applying the virtual work principle), give an upper-bound of the actual ultimate load.

This methodology was applied by Giuffrè, who identified a number of possible failure mechanism of traditional masonry buildings, by observing the real damage experienced by these construction during the earthquake.

Moving from the approach introduced by Heyman, De Luca et al. (2003), Giordano et al. (2007) and more recently Brandonisio et al.

(2015) used the principle of virtual works to derive closed and simplified expressions for computing the collapse multiplier of simple structural elements, such as portal frame and arches.

The need of robust methodologies for predicting the masonry structures behavior or for checking the numerical results obtained from more uncertain advanced analysis methods, is strongly remarked in the scientific literature on masonry structures (Bucchi et al. 2009, Brandonisio et al. 2012, 2014), and led to the recent rediscovery of traditional equilibrium-based methods, such as the "macro-block limit analysis . . ., probably the best analysis tool for practitioners" (Lourenco 2011). On the other hand the limit analysis has the considerable disadvantage of providing only an indication about the safety of the structure regarding a limit condition, but it cannot be helpful in depicting the structural behavior of the building for moderate service load conditions.

Simplified modelling

In order to overcome the mentioned disadvantage of the limit analysis, but with still simple approaches, in the last three decades, many authors have developed simplified or alternative methodologies that, with a reduced computational effort, should be able to predict the nonlinear seismic behaviour of masonry buildings. The most commonly used practical approach for the analysis of unreinforced masonry is the so called 'equivalent frame model', in which the masonry building is represented by an equivalent nonlinear frame structure constituted by nonlinear beam elements and rigid offsets (Magenes et al. 1998, Kappos et al. 2002). According to the equivalent frame model approach, each wall of the building is subdivided into macro-elements representing piers, spandrels and rigid zones. The nonlinear behaviour of piers and spandrels are simulated by nonlinear frame element, while the rigid zones, in which the damage cannot occur, are substituted by rigid offsets. Several different models have been proposed to describe the behavior of the two nodes macro-element implemented in the equivalent frame models of the structure. Much effort was devoted to this issue by Gambarotta and Lagomarsino. In 1996 they proposed a non-linear macro-element model, representative of a whole masonry panel which permits, with a limited number of degrees of freedom, to represent the two main in-plane masonry failure modes, bending-rocking and shear-

sliding (with friction) mechanisms, on the basis of mechanical assumptions. This model considers, by means of internal variables, the shear-sliding damage evolution, which controls the strength deterioration (softening) and the stiffness degradation. This model was later further refined and improved (Brencich and Lagomarsino 1997, 1998, Penna 2002 and Galasco et al. 2004).

However the substitution of a masonry portion with a frame element has some restrictions due to the inaccurate simulation of the interaction between macro-elements, to the difficulties that arise for complex geometry and to the weak modelling of the cracked condition of panels. For these reasons some authors proposed the use of two-dimensional macro-elements, performing an approach defined as macro-element discretization (Lourenco 2002). It has been conceived with the aim of capturing the nonlinear behavior of an entire masonry wall and of the entire building, as an assemblage of several walls. Based on this approach, recently Caliò et al. (2012) proposed a basic macro-element which consists of an articulated quadrilateral with rigid edges in which two diagonal springs govern the shear behaviour. The flexural and sliding shear behaviour is governed by discrete distributions of springs in the sides of the quadrilateral that preside over the interaction with the adjacent macro-elements.

The simplified modellings, discussed above, are implemented in computer codes, nowadays commonly used also for the analysis of historical buildings. However this approach hardly can be used to model historical buildings characterized by complex geometry, combining 1D members (arches, flying arches) with 2D members (vaults, domes) and 3D ones(fillings, pendentives . . .).

Finite element method

The FE method permits to model any geometry and to associate sophisticated material model, taking into account the highly non linear behavior of the masonry. Basically, two different approaches are implemented in the FE method to model the the masonry: the 'micro-model', or 'two-material approach', and the macro-model, or 'equivalent-material approach'.

In the micro-model, the discretization follows the actual geometry of both the blocks and mortar joints, adopting different constitutive models for the two components. Particular attention must be paid in the

modelling of joints, since the sliding at joint level often starts up the crack propagation. Although this approach may appear very straightforward, its major disadvantage comes from the extremely large number of elements to be generated as the structure increases in size and complexity. This renders unlikely the use of micro-models for the global analysis of entire buildings, also considering the fact that the actual distribution of blocks and joints might be impossible to detect unless invasive investigations are performed.

The macro-model assumes that the masonry structure is a homogeneous continuum to be discretized with a finite element mesh which does not copy the wall organism, but obeys the method's own criteria. The single element will thus have a constitutive model which must be capable of reproducing an average behaviour. This assumption bypasses the physical characteristics of the problem. Nevertheless the equivalent material models have proven to be able to grasp certain aspects of the global behaviour without the number of parameters and the computing effort needed in the micro-model (Pegon and Anthoine, 1994).

An exhaustive dissertation on micro and macro FE modelling is provided by Lourenço in his Ph. D. thesis (..). In this reference the adequacy of using homogenization techniques, in which the macro behavior of the composite is predicted from the micro properties of masonry constituents, was discussed and a constitutive macro-model for unreinforced masonry, that includes anisotropic elastic as well as anisotropic inelastic behavior, was proposed.

The macro FE modelling have been extensively used to analyze complex historical monuments and, recently, well known monuments have been studied by using this approach: among the others, the basilica of Hagia Sophia (Almac et al. 2013), the Mallorca gothic cathedral (Roca et al. 2013) and also several Italian masonry churches damaged during the last earthquakes occurred in L'Aquila and in Emilia Romagna (Brandonisio et al. 2013, Gattulli et al. 2013, Milani and Valente 2015a and b).

However, it has to be said that FEM models may be very sensitive to changes in boundary conditions, load history and may predict the formation of cracks in unexpected locations (Huerta 2003). According to Boothby et al. (2006), the solutions provided by an initial FEM model must always be validated against known information on the structure such as testing results, crack location and/or other damage. During the validation process an initial model may probably need to be refined in terms of boundary conditions and material properties. It is also

important to study the influence of the different parameters on the results through a parametric study (Endo 2015).

Discrete element method

The Discrete Element Method (DEM), is currently used for computing the motion of simple unreinforced masonry structures modeled as an assemblage of distinct blocks (rigid or deformable) which interact along the boundaries. This method, originally proposed by Cundall (1971, 1979) in the area of granular and discontinuous materials, is based on the integration of the equation of motion of the discrete elements, and allows for considering the large displacements with the sequential update of the elements positions. In 1987 Lemos, proposed a DEM formulation for two-dimensional blocks in his Ph.D. thesis, and formulated together with Cundall and Hart (1988) a three-dimensional distinct element model for a system composed of many polyhedral blocks. In the last two decades, the application of DEM was extended to masonry to simulate the response of simple structural elements under ground motion; available literature review on DEM of masonry structures is provided by Lemos (2007), where the works of Livesley (1978), Gilbert and Melbourne (1994, 1995) Orduna and Lourenço (2001), Baggio and Trovalusci (1998) are discussed.

In spite of the several studies focused on this approach, he analysis of complex structures such as the historical monuments is still a challenging issue in DEM. The natural field of application of DEMs is composed by structures formed by regularly shaped masonry or stone blocks. Computational viability of analysis may limit severely the number of block elements that can be included in a model.

1.2   OVERVIEW OF ANALYSIS METHOD

Linear static analysis

Linear static analysis is in principle inadequate first of all because it does not take into account the complex non-linear response even for low or moderate stress levels. Secondly the static approach to assess the seismic response of the buildings is based on the predominance of the first vibration modes, which generally give the greatest contribution. The

static approach, traditionally used in the structural engineering, applies equivalent lateral forces generally distributed proportionally to the mass or according to the main vibration mode of the building. However, as it will be extensively discussed in chapter 3, the prerequisites for applying the static approach are not realistic for complex historical buildings, such as the churches.

The seismic demand computed for this analysis method should be reduced through a reduction factor , to take into account the further displacement capacity of the buildings. But the reduction factors provided by the rules are generally reliable for regular buildings, and they can lead to incorrect results, and consequently to ineffective interventions, for historical complex buildings.

However, due to its simplicity, stability and reduced computer effort, many cases of historical monuments have been studied by means of this approach, and among the others: San Marco in Venice (Mola and Vitaliani,1995), the Tower of Pisa (Macchi et al.,1993), the Colosseum of Rome (Croci, 1995). Moreover, especially for vertical loads, linear analysis is always performed, prior to the application of more sophisticated approaches, to allow a quick and first assessment of the adequacy of the structural models regarding the definition of meshes, the values and distribution of loads and reactions, and the likelihood of the overall results (Roca et al. 2010).

Modal dynamic analysis

The response spectrum modal dynamic analysis permits of taking into account all the vibration modes of the structure. Their contribution is compared with the response spectrum and combined through different mode superposition procedures: the direct superposition (SUM) provides an upper bound to the maximum of total response; the root-sum-square (SRSS) provides a satisfactory estimate for system with well separated frequencies; the complete quadratic combination (CQC) used when the natural periods of the structures are very similar.

This analysis method is performed by using an elastic material model and it is based on the superposition principle, therefore it would be in principle inadequate, as well as the linear static analysis.

However the response spectrum analysis has been used to study many examples of historical monuments, especially masonry churches (Gattulli et al. 2013, Dal Cin and Russo 2014, Chellini et al. 2014…).

It involves a dynamic approach to the seismic analysis of this kind of constructions which generally do not obey to the assumptions at the base of the static one. At the same time the response spectrum analysis doe not imply the computational effort of the more complex non linear dynamic analyses.

Non linear static (push-over) analysis

A push-over analysis is performed by subjecting a structure to a monotically increasing pattern of lateral forces, representing the inertial forces which would be experienced by the structure when subjected to ground shaking. This analysis is performed considering a non linear constitutive law of the material and, it can take into account the geometrical non linearity. Under incrementally loads various structural elements yield sequentially. Consequently, at each event, the structure experiences a loss in stiffness (Fajfar 2000). The analysis stopped when an ultimate condition of the structure is reached. A relationship between non linear force and displacement can be determined at the end of a push-over analysis, which provides a capacity curve of the structure. Generally the base shear and the displacement of points at the top of the structures are chosen. In the following chapters the push-over analyses will be carried out conforming this choice.

The selection of an appropriate lateral load is an important step within the push-over analysis. A unique solution does not exist (Fajfar 2000). The Eurocode 8 (CEN, 2004) recommend to use at least two load patterns: a load pattern of forces proportional to the mass and a modal load pattern of forces usually distributed according to the first modal shape.

An exhaustive discussion on pros and cons of the push-over analysis can be found in Krawinkler and Seneviratna (1998). They pointed out that if an invariant load pattern is used, the basic assumptions are that the distribution of inertia forces will be reasonably constant throughout the earthquake and that the maximum deformations obtained from this invariant load pattern will be comparable to those expected in the design earthquake. These assumption may be close to the truth if: a) the structure response is not severely affected by higher mode effects, b) the structure has only a single load yielding mechanism that can be detected by an invariant load pattern. If these hypotheses are verified, the pushover analysis will very likely provide good estimates of global, as

well as local inelastic deformation demands. Otherwise, deformation obtained from a push-over analysis may be very inaccurate.

Recent studies have focused on extending the push-over analysis to the structures affected by higher mode effects (among the others, Chopra and Goel 2002, 2004). Moreover adaptive analysis methods, applying load patterns which follow closely the time variant distribution of inertia forces, have been provided (among the others Bracci et al. 2007). In spite of these studies, the mentioned limitations of the push-over analysis are still a critical point for the reliability of this analysis method.

The push-over analysis provides only a measure of the capacity and has to be combined with a demand measure using methods like capacity spectrum or N2 to complete the assessment study (Elnashay, 2002). In this thesis the N2 method will be used and therefore a brief summary of the procedure is given in the following. The N2 method developed at the University of Ljubljana by Fajfar is exhaustively illustrated in Fajfar 1999 and 2000. This method is also implemented in Eurocode 8 (CEN, 2004). The result of the N2 method is basically the graph of Figure 1.2 (Fajfar 2000). To obtain this graph four steps can be noticed.
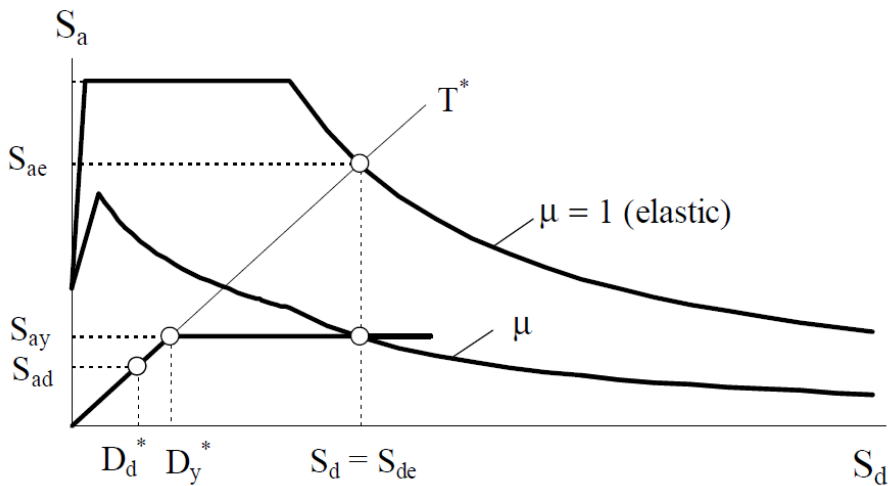
Figure 1.2 Elastic and inelastic demand spectra versus capacity diagram (Fajfar 2000)

In the first step, the elastic response spectrum in the format of time-elastic acceleration is transformed to the displacement-acceleration format using the following relation:

$$S_{de} = \frac{T^2}{4\pi} S_{ae}$$

In the second step, the capacity curve obtained from the pushover analysis is transformed to the equivalent bi-linear curve using the approximate approach of equal area, i.e., the area under the capacity curve is equal to the area under the bi-linear curve
In the third step, the intersection of the radial line, corresponding to the elastic period of the idealized bilinear system T*, with the elastic demand spectrum defines the acceleration demand (strength) required for elastic behavior and the corresponding elastic displacement (Fajfar, 2000).
The elastic spectrum is transformed to the inelastic spectrum using the following relations proposed by Vidic et al. (1994):

$$S_a = \frac{S_{ae}}{R_\mu}$$

$$S_d = \mu \frac{T^2}{4\pi^2} S_a$$

where, R_μ is the reduction factor due to ductility and is evaluated from:

$$R_\mu = (\mu - 1)\frac{T}{T_C} + 1 \qquad\qquad T < T_C$$
$$R_\mu = \mu \qquad\qquad\qquad\qquad T \geq T_C$$

where μ is the ductility factor defined as the ratio between the maximum displacement and the yield displacement $(D_y{}^*)$ and T_c is the characteristic period of the ground motion.
The last step consist of the intersection between the bi-linear capacity curve and the inelastic response spectrum to determine the performance point which defines the performance acceleration and the performance displacement of the structure.

Non linear dynamic analysis

All the previous described analysis methods are simplified ways to assess the seismic response of the masonry buildings. They are based on more

or less reliable assumptions on the mechanical behavior of the material and on the actions applied to the buildings. The non linear dynamic analysis or time history analysis, aimed to provide the seismic response of buildings without any of these major simplifying assumptions. It furnishes the time history of the displacements of the structure, subject to external forces described by an accelerogram, by solving the equations of motion of the structure. When the behavior of the structure is into the non linear range, such as the case of the historical masonry buildings, the equation of the motion has to be solved by using numerical methods. In 1959 N. M. Newmark developed a family of time-stepping numerical methods which, being noted the values of the external force at regular generally constant time step Δt, gives the values of displacement velocity and acceleration of the structure, starting from the results of the previous step. The Newmark method is exhaustively discussed in Chopra 2000 and it was adopted in the non linear dynamic analysis performed and illustrated in the following chapters.

When the Newmark method is adopted two recommendations about the time step size should be respected:

1) it is sufficiently small compared with the accelerogram duration (td):

$$\Delta t \ll t_d$$

2) 20 time steps must be applied in the small period (Ti) of the highest mode, in order to correctly reproduce the system response:

$$\Delta t \leq \frac{1}{20} T_i$$

The highest mode of the structure should be chosen considering that a cumulative participating mass ratio at least equal to 90% is adequate to realistically describe the seismic response of the buildings, according to Eurocode 8 (CEN, 2004) .

Even if some authors consider the non linear dynamic analysis as the only option for irregular structures (Chambers and Kelly, 2004), it has to be said that it involves also some limitations (Powell, 2006). First of all, the time for a dynamic analysis increases substantially as the size of the structure increases and it implies that this kind of analysis for historical masonry building is strongly time demanding. Moreover, if the analysis is carried out for several ground motions, there can be substantial variation in the results. This is partly because nonlinear behavior is inherently sensitive to relatively small changes in the ground motion. The Eurocode

8 promotes the use of at least seven accelerogram, allowing both artificial and real or simulated accelerograms. However, the artificial accelerograms may lead to a non conservative estimation of the seismic response. Great effort is necessary to ensure that their spectra are suitable to seismic analysis (Bazzurro and Luco 2003, Cornell 2004). On the other hand, the recently increasing accessibility to data bases of natural accelerograms recorded during real earthquakes helped significantly in using natural records (Iervolino et al., 2009).

In spite of the above mentioned limitations, the non linear dynamic analysis has been recently used for the structural analysis of complex masonry buildings such as masonry arch bridges (Pelà, 2013), gothic cathedral (Elyamani 2015), masonry churches (Milani and Valente, 2015), and also for the study of macro-elements of historic masonry churches (Giresini et al. 2014, Giresini 2016).

.

2 SEISMIC CAPACITY OF HISTORICAL BUILDINGS: COMPARISON OF DIFFERENT MODELLING STRATEGIES

2.1 INTRODUCTION

The seismic capacity of multi-storey historical buildings (used for residences, public offices, schools etc.) is studied in this chapter, considering a sample of four case studies. In detail the in-plane seismic capacity of the walls is evaluated performing the non linear static (push-over) analysis, compared with the limit analysis.

The masonry walls of such buildings, characterized by openings regularly or irregularly arranged, are usually modelled as equivalent frame 8discussed in section 1.1), as it is also suggested by the Italian technical code (NTC'08). This structural modelling permits to perform a non-linear incremental collapse analysis of the masonry walls with a reduced computational effort, in comparison with the models made of bi or three-dimensional elements. However more sophisticated modelling strategies are used, such as the macro-element modelling, finite element method or discrete element method which have been described in section 1.1.

The mentioned modelling strategies are implemented by different computer codes. Much study in the recent years is focused to compare the results provided by different approaches and different codes. Studies have proven that they are affected by a certain uncertainty and different codes, even if implementing the same modelling strategy, do not give always comparable results.

Bucchi et al. (2009) carried out the push-over analysis of five case studies (masonry schools), comparing the results provided by ANDIL Wall (v. 2.0.1.) and 3Muri (v. 3.2.11.). Both software implement the equivalent frame approach. In terms of base shear, the codes provided average variance equal to 12% with a maximum difference of 32%. In terms of maximum displacements, the average variance was 27% with a maximum value of 70%. It was concluded that the commercial codes were still not able to provide a reliable result and, consequently, the assessment of the

seismic capacity, based only on numerical investigation, was not suggested.

Arangio et al. (2013) studied a simple three-dimensional building by using SAP 2000, to implement the equivalent frame approach. The results were compared with 3Muri. The difference between the results obtained from the two codes reached 50% both in terms of base shear and in terms of displacements.

In this chapter the push-over analysis was carried out by using equivalent frame approach, macro-element modelling and finite element method. 3Muri and 3DMacro, very common in the Italian professional community, were respectively used for the equivalent frame and the macro-element modelling. Abaqus, generally used in the research field, was used for the finite element analysis. The results obtained from the different codes were compared in terms of load multipliers and maximum displacements. The push-over analysis were also compared with the limit analysis. Finally a link between the seismic capacity of single walls and complete building was investigated.

2.2   CASE STUDIES

Four case studies were selected to perform the analyses, two located in Naples, and two in L'Aquila (Fig. 2.1). They have the typical geometrical, and mechanical characteristics of Italian buildings in the XVII-XVIII centuries. The floors do not have any rigid behavior, belonging to first or second class of Pagano classification (Pagano, 1968).

A brief description of each case study is presented in the following.

Figure 2.1 Building case studies: a) *Palazzo Scarpa* (Naples); b) *Ex prison S. Francesco* (Naples); c) *Palazzo Centi* (L'Aquila); d) *De Amicis school* (L'Aquila).

2.2.1 *Palazzo Scarpa* (Naples)

The *Palazzo Scarpa* building was built in 1906, and it can be said a typical example of the Neapolitan residential buildings. Plan and frontal view are plotted in Figure 2.2. It is characterized by a nearly rectangular plan, approximately 20mx40m with a central rectangular core 10mx5m; it consists of six storeys above the ground level and a basement below. The overall height of the building is 27.5m. The walls are made of Neapolitan yellow tuff, except of the basement and the ground floor, consisting of clay-brick. The wall thickness is 120cm, at the basement, and it gradually decreases at the higher levels being 50cm thick at the 5th level is. According to Pagano classification, the building belongs to the second class, having continuous masonry walls and horizontal floors consisting of beams simply supported by the masonry walls.
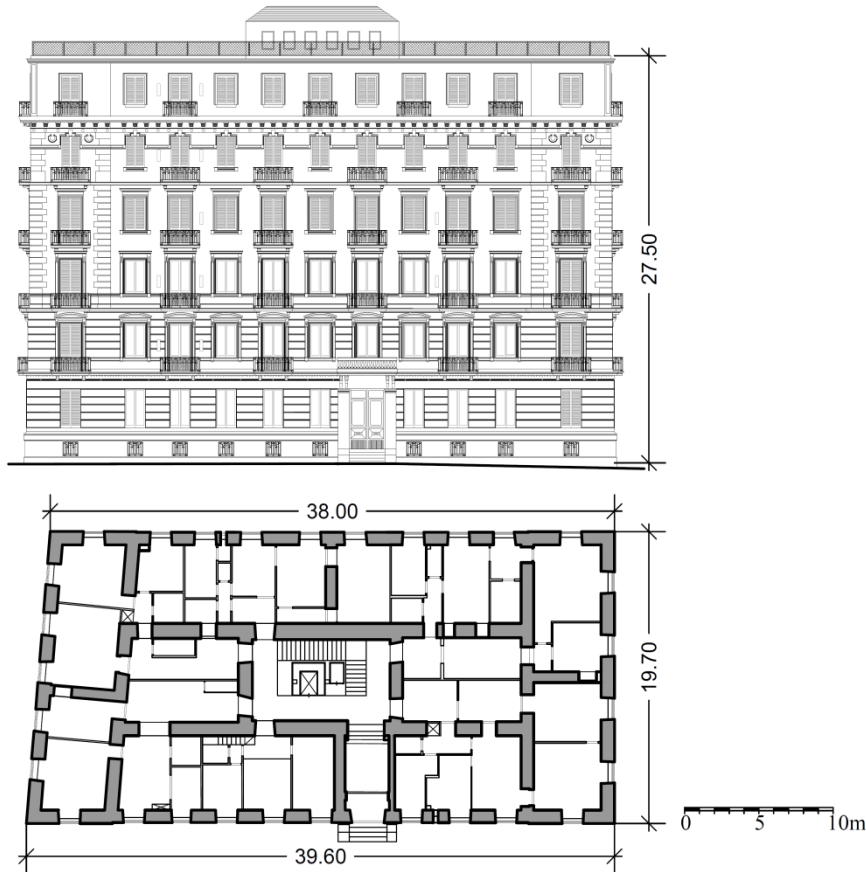
Figure 2.2 *Palazzo Scarpa*: frontal view and plan of the first floor

2.2.2 *Ex prison S. Francesco* (Naples)

The *Ex prison S. Francesco* (Fig. 2.3) is located in the historical center of Naples and has a strong historical interest, in consideration of its different occupancy over time. Originally it was a monastery; at the end of 1700, it was converted into a hospital to serve the city prisons, assuming the nowadays architectural aspect. Later, in 1923, the building was further modified to allow the accommodation of judicial offices.

The building has five floors above ground and it has a rectangular plan, with two courtyards; in plan the total size is about 78x36 m, while the two inner courts, almost square, are 16x17 and 15x19m, respectively.

The overall height of the building is approximately 25.9m. The thickness of the main walls varies from 140 cm, at the first level, to 70cm at the last one.
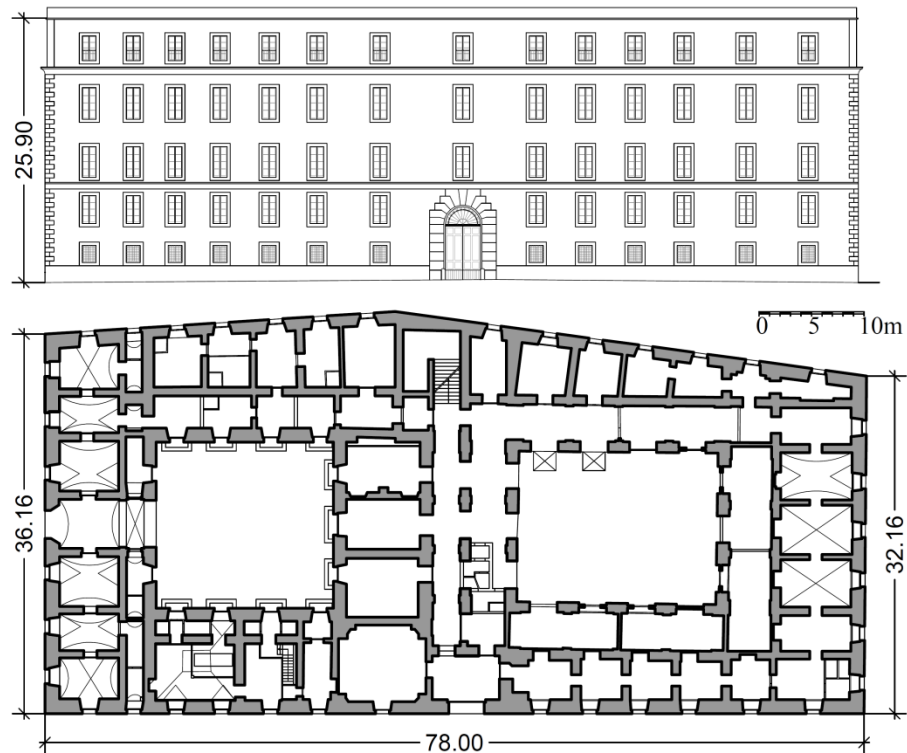
Figure 2.3 *Ex prison S. Francesco* : frontal view and plan of the first floor

The structure is made of tuff masonry except of the top level, built in a subsequent time, made of clay brick and mortar walls. Except of the roof composed of steel beams, the floors consist of tuff vaults. According to the Pagano classification, the building belongs to the first class.

2.2.3   Palazzo Centi (L'Aquila)

Palazzo Centi (Fig. 2.4) was the prestigious residence of the Centi-Colella family. The construction started in 1776 on the basis of the design by Loreto Cicchi da Pescocostanzo. Before the 2009 earthquake, it was the headquarter building of Regione Abruzzo; it is located in Piazza S.

Giusta, in the historical centre of L'Aquila and it represents a masterpiece of the city baroque architecture of the city.
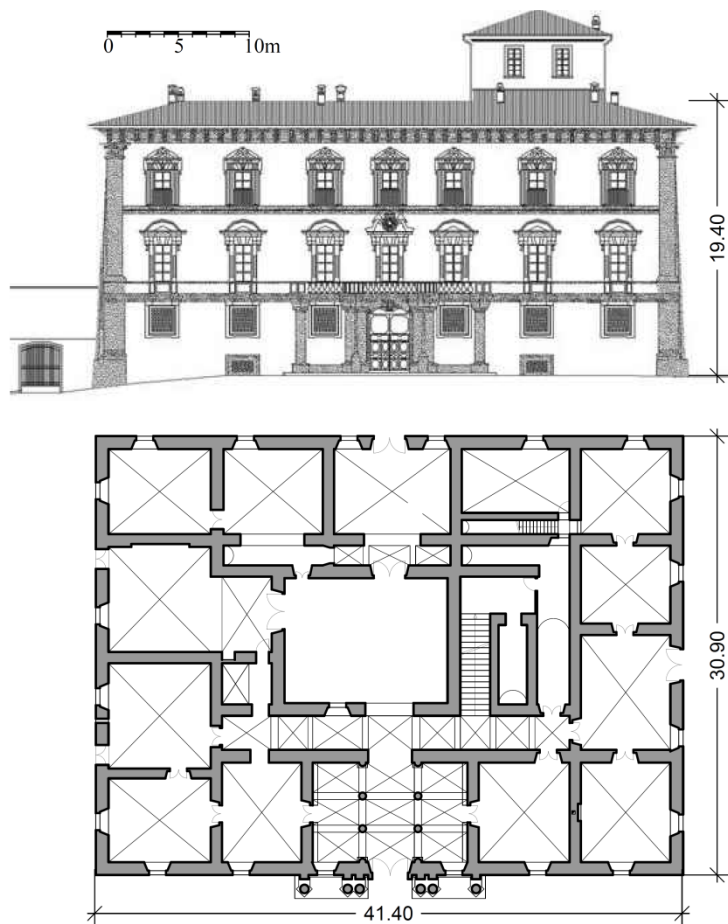
Figure 2.4 *Palazzo Centi*: frontal view and plan of the first floor

The building has a rectangular plan, with dimensions 30.9 x 41.4 m; the internal courtyard is 9 x 11 m. Originally Palazzo Centi had only three levels; more recently, a penthouse called "castellina" was added on the roof. The height from the ground level to the original roof is 19.4 m.
The walls are made of rubble stone masonry, with the two external layers mainly made of mixed roughly squared stones and clay bricks. The façade and the courtyard walls are 90 cm thick, while the internal walls

are usually 80 cm thick, only in few cases 70 cm; for all walls the thickness remains constant from the base to the top.

The horizontal structures are clay bricks pavilion vaults, with thickness at least equal to 12.5 cm. The roof structure is made of wooden trusses (Simple Palladiana type), with underneath ceilings vaults made of bricks or fake vault, called "camorcanna". Thus Palazzo Centi also belongs to the first class of the Pagano classification.

Palazzo Centi experienced significant damage during 2009 L'Aquila earthquake. Detailed informations on the seismic damage and performance of Palazzo Centi after L'Aquila earthquake can be found in Lucibello (2013) and Lucibello et al. (2013).

2.2.4 De Amicis school (L'Aquila)

The *De Amicis School* (Fig.2.5) is located in the historical center of L'Aquila. It is the remaining part of the S. Salvatore hospital, which was built during in XV century.

It has a rectangular plan, on the whole 52.4mx44m, with an internal courtyard of 24.9x13.7m. The building has three levels and the overall height is 19.80 m on the south side (in San Bernardino square) and 17.50 m on the north side.

The walls are very thick and, in some cases, the walls thickness exceeds 2m. However the thickness decreases at the higher level and, at the top, the walls are at most 1m thick.

The horizontal structures consist of barrel vaults and cross vaults at the first floors, while steel beams integrated in the lightweight mortar slab are at the second floor; the roof structure is made of wooden trusses. According to Pagano, the *De Amicis School* can be classified as second class building.
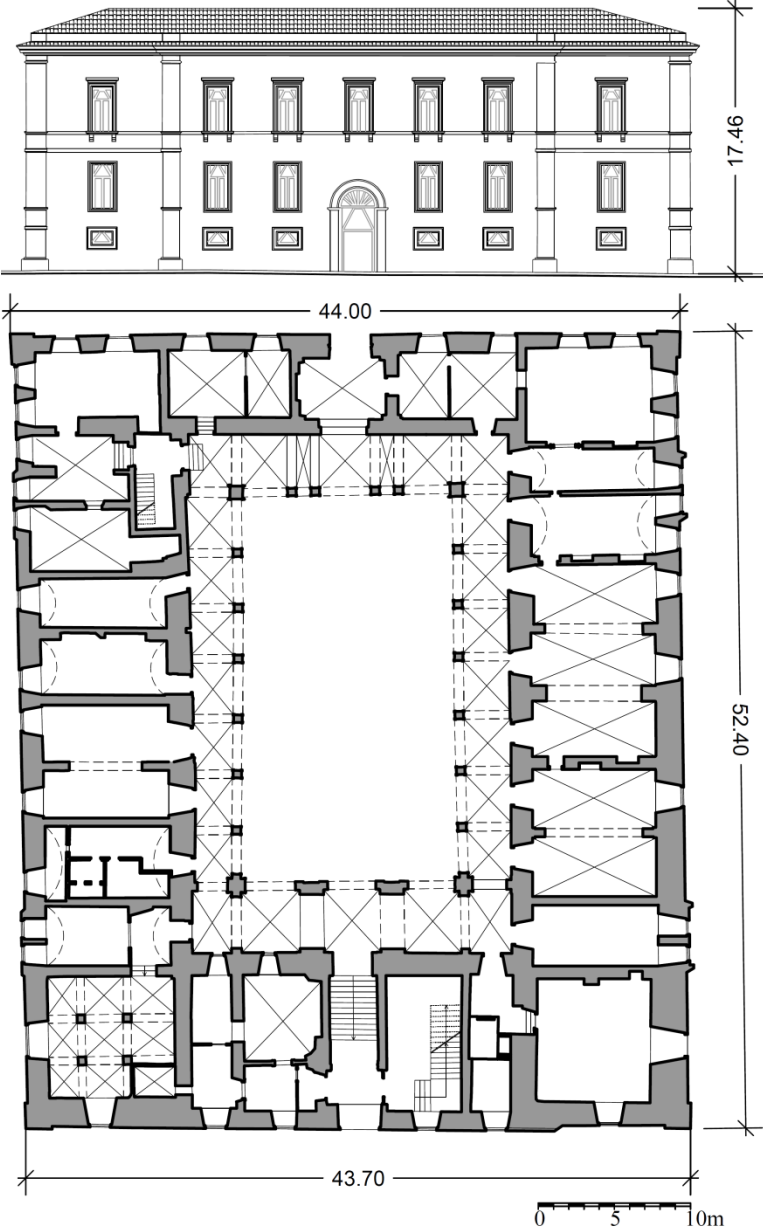
Figure 2.5 *De Amicis school* : frontal view and plan of the first floor

2.3 ANALYSES BY MEANS OF SIMPLIFIED MODELLING

Two types of simplified modelling were first used to perform the push-over analysis: equivalent frame approach and macro-element modelling. The equivalent frame was adopted by using the software 3muri, while the macro-element modelling was implemented through 3DMacro software.

2.3.1 Equivalent frame modelling implemented by 3Muri

Tremuri program, provided by S.T.A. Data S.r.l, is one of the most used software in Italy for the structural analysis of masonry buildings. The modelling implemented in 3Muri can be defined FME (Frame by Macro Elements), because it is based on the non-linear macro-element model, representatives of a whole masonry panel. This macro-element model, mentioned in section 1.1 was firstly developed by Gamabrotta and Lagomarsino (1996) and Brencich and Lagomarsino (1997, 1998). After it was improved with the cooperation of Penna (2002) and Galasco et al. (2004). A more recent refined model is illustrated in Penna et al. (2014).

A complete explanation of the code's theory was detailed by Lagomarsino et al. (2013) and an user manual was provided by STADATA (2012). Here a summary of the modelling strategies implemented by the code is given.

The macro-element permits, with a limited number of degrees of freedom to represent the two main in-plane masonry failure modes, bending-rocking and shear-sliding (with friction) mechanisms, on the basis of mechanical assumptions. This model considers, by means of internal variables, the shear-sliding damage evolution, which controls the strength deterioration (softening) and the stiffness degradation. Figure 2.6 shows the three sub-structures in which a macro- element is divided: two layers, inferior (1) and superior (3), in which the bending and axial effects are concentrated; the central part (2) suffers shear-deformations and presents no evidence of axial or bending deformations. The complete 2D kinematic model takes into account the three degrees of freedom for each node "i" and "j" on the extremities (axial displacement w, horizontal displacement u and rotation φ), and two degrees of freedom for the central zone (axial displacement δ and rotation φ). It is assumed that the extremities have an infinitesimal thickness.
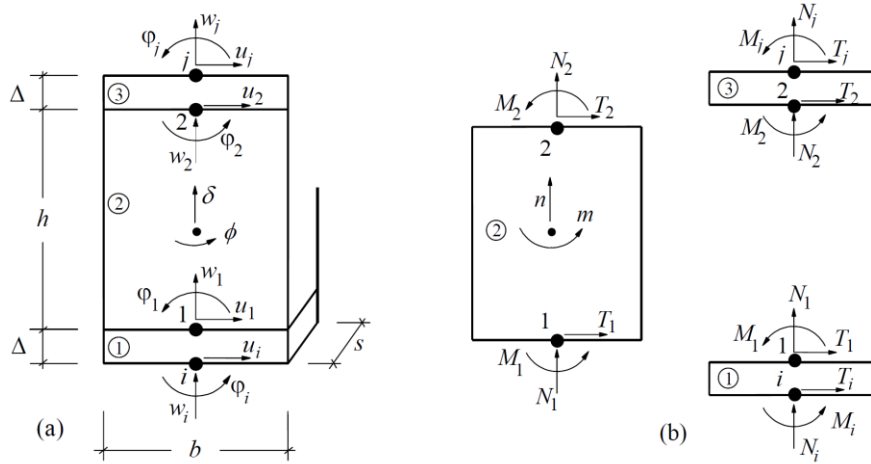
Figure 2.6 Kinematic model for the macro-element *(Gambarotta, 1996)*

3Muri divides each wall in such macro-element and idealizes the wall in an equivalent frame. Figure 2.7 summarizes the main steps of the frame idealization procedure in a regularly perforated masonry wall: from the identification of spandrels and piers (steps 1 and 2), defined on basis of the vertical alignment and overlap of openings, to that of nodes (step 3).
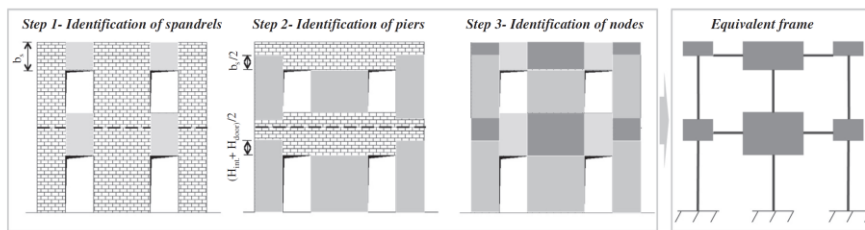
Figure 2.7 Example of equivalent frame idealization in case of regularly distributed openings (Lagomarsino et al.2013)

The geometry of the rigid nodes comes out directly from the previously defined elements that are connected to them. Once having idealized the masonry wall into an assemblage of structural elements, 3Muri considers these as non-linear beam elements with lumped inelasticity idealization (bilinear elastic perfectly plastic behaviour). The deformation and non-linear response are concentrated in spandrels and piers, instead the nodes are considered as portion rigid, which connect the deformable ones (step4). Earthquake damage observation shows, in fact, that only rarely

(very irregular geometry or very small openings) cracks appear in these areas of the wall.

2.3.1.1 Macro-element modelling implemented by 3DMacro

3DMacro program is developed by Gruppo Sismica S.r.l. and validated by numerous research investigations (Caliò et al. 2004, 2005, 2008, 2012). The basic macro-element of the proposed simplified approach, mentioned in section 1.1, has a simple and easy-comprehensive mechanical scheme, shown in Figure 2.8.

It is represented by an articulated quadrilateral constituted by four rigid edges connected by four hinges and two diagonal non-linear springs. Each side of the panel can interact with other panels or elements or supports by means of a discrete distribution of nonlinear springs, denoted as interface. Each interface is constituted by N nonlinear springs, orthogonal to the panel side, and an additional longitudinal spring which controls the relative motion in the direction of the panel edge.

Given a simple masonry wall it is possible defining a minimum number of panels composing. 3DMacro couple each panels with the defined macro-element. However the model can also be refined by using more panels in order to better describe the kinematics of the masonry walls (Fig.2.9).

a)   b)
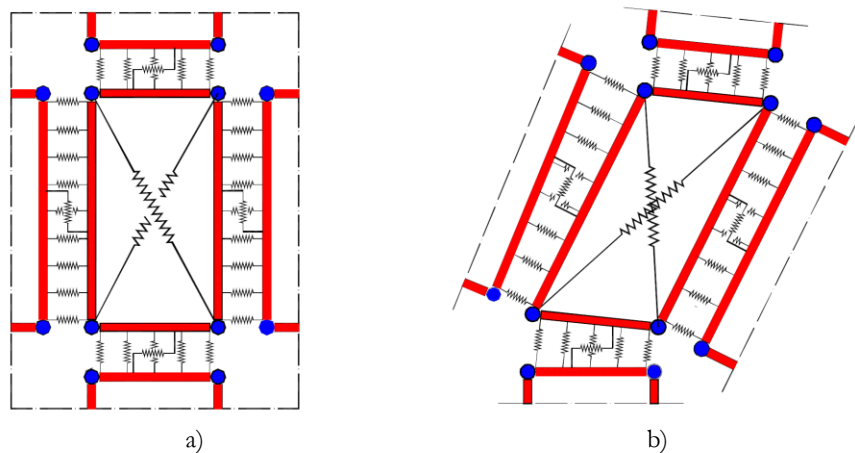
Figure 2.8 The basic macroelement: a) undeformed configuration; b) deformed configuration (Caliò et al. 2005).
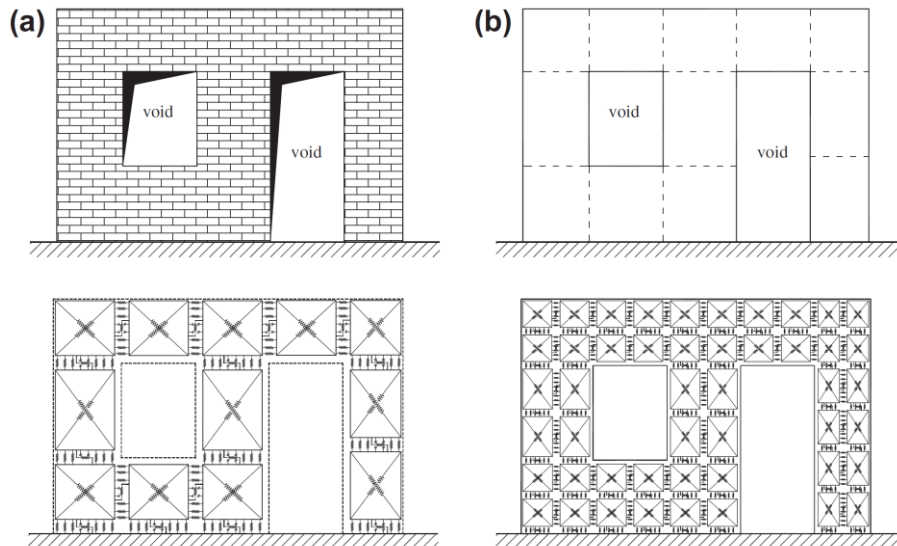
Figure 2.9 Masonry wall and corresponding macro-element discretizations with different mesh resolutions (Caliò et al.2012)

In spite of its great simplicity, such a basic mechanical scheme is able to simulate the main in-plane failures of a portion of masonry wall subjected to horizontal and vertical loads: the flexural failure, the diagonal shear failure and sliding shear failure. The flexural failure mode, associated to the progressive rupture of the panel in the tensile zone and/or to the crushing of the panel in the compressive zone, can be reproduced by the transversal springs of the interfaces that simulate the axial and flexural deformability of the masonry panel. In these nonlinear springs all the flexural properties of the portion of masonry which the panel represents are lumped and each transversal spring has been calibrated by assuming an non-symmetric elasto-plastic behaviour with limited deformability.

The diagonal-shear failure mode and the consequent formation of diagonal cracks along the directions of the principal compression stresses can be governed by means of the two diagonal nonlinear springs which have the role to simulate and predict the nonlinear shear response of the modelled masonry portion. To simulate the shearing behaviour an elasto-plastic constitutive law with a Turnsek & Cacovic yielding surface is considered.

The sliding-shear failure mode is associated to the sliding of the masonry panel in its own plane and it can be controlled by the longitudinal nonlinear springs of the interfaces. This spring is characterised by a rigid plastic constitutive law with a Mohr-Coulomb yielding surface.

The degrees of freedom of the structural scheme are associated to the in-plane motion of the panels. Each panel exhibits three degrees of freedom, associated to the in-plane rigid body motion, plus a further degree of freedom needed for description of the panel deformability. Hence the total degrees of freedom of a N panels structural scheme are 4N corresponding with the four displacements of the rigid edges along their own directions have been chosen.

2.3.1 Push-over analysis performed on the façades of the case studies

2.3.1.1 Input data analysis

The push-over analysis was performed on the façade of the case studies. The geometry of the façade, simplified and deprived of the architectural elements, is plotted in Figure 2.10.

Table 2.1 reports some geometrical characteristics of the principal façades: an average value of the pier width (B_{eq}); the width of the opening (L); the height of the opening (h); the ratio $R=B_{eq}/L$; the ratio $S_n=h/B_{eq}$. The parameters R and S_n were defined by Sparacio in 2009. The ratio R gives a measure of the ratio solids/voids, while the ratio S_n defines the slenderness of the piers. These ratios assume higher values for the buildings in L'Aquila, which in fact are more massive to prevent the higher seismic hazard.

It is noted that the buildings were intentionally ordered on the basis of the R value. The case studies assumes values of R spanning between 1.6 and 3.6; so it can be said that the sample of study is quite representative of a large quantity of masonry walls and, consequently it provides a certain generality of the results.

Table 2.1 Geometrical parameters of the four case studies

Building	$B_{eq}=\Sigma B_i^2/\Sigma B_i$	L	h	$R=B_{eq}/L$	$S_n=h/B_{eq}$
Palazzo Scarpa	2.2	1.4	3.3	1.6	1.5
Ex p. S.Francesco	4.0	1.6	2.9	2.5	0.7
Palazzo Centi	4.2	1.2	2.4	3.5	0.6
De Amicis school	4.6	1.3	2.8	3.6	0.6
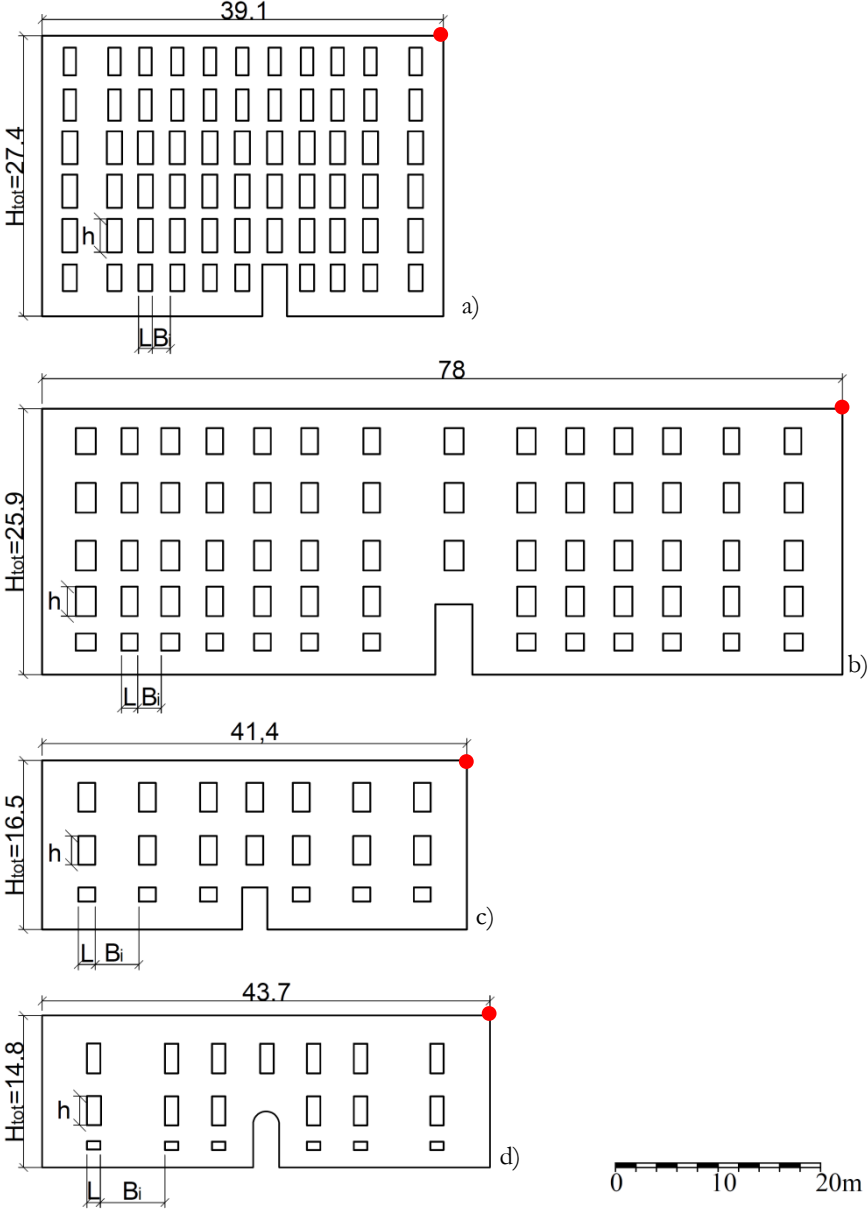
Figure 2.10 Geometry of the principal façade of the building case studies: a) *Palazzo Scarpa*; **b)** *Ex prison S. Francesco*; **c)** *Palazzo Centi*; **d)** *De Amicis school*

The following values were adopted for he material properties requested by the used codes: self-weight $\gamma=20kN/m^3$, Young's modulus E=2000MPa, tangential elastic modulus G=800MPa, compressive strength f_m=2MPa, shear strength f_{vko}=0.03MPa.

The definition of a mesh is not necessary in 3Muri, since an equivalent frame model is automatically created by the code. As mentioned in the previous section, 3DMacro permits a mesh more refined than the basic scheme composed by one macro-element for each panel (spandrel, pier or node). However in this study a basic-mesh was chosen to assure the reliability of the comparison. Sensitivity analysis pointed out a negligible higher accuracy of the results obtained with more refined mesh.

The walls were considered fixed at the base and horizontal loads proportional to the masses were applied. The displacement of the control points, indicated in Figure 2.10, was evaluated during the increasing of the loads.

2.3.1.2 Results

The results obtained for each façade are presented in the Figures from 2.11 to 2.14, where the capacity curves for the façade of each case study are given. The capacity curves are defined in terms of: 1) base shear vs displacement of the control point, 2) base shear divided by the total weight (namely the load multiplier indicated as λ) vs displacement divided by the height of the wall (d/H_{tot}).

It can be noted that the considered simplified modellings gave capacity curves appreciably different. In detail, for *Palazzo Scarpa* façade, 3Muri provided a significant decreasing of the wall stiffness, due to an almost immediate damage of the spandrels. This was not revealed by 3DMacro. However the two codes gave similar results both in terms of load multipliers and in terms of displacements. In the case of *Ex prison S. Francesco,* a decreasing of the wall stiffness can be noted in the 3Muri curve, even if it is less significant than the previous case. On the other hand, the two codes provided appreciable differences in terms of load multipliers and similar values of the displacements. *Palazzo Centi* is the case study procuring the greater variance of results: over the wall stiffness, the results are not consistent both in terms of load multipliers and in terms of displacement. Significant variance of load multiplier was also obtained in the case of *De Amicis school* .
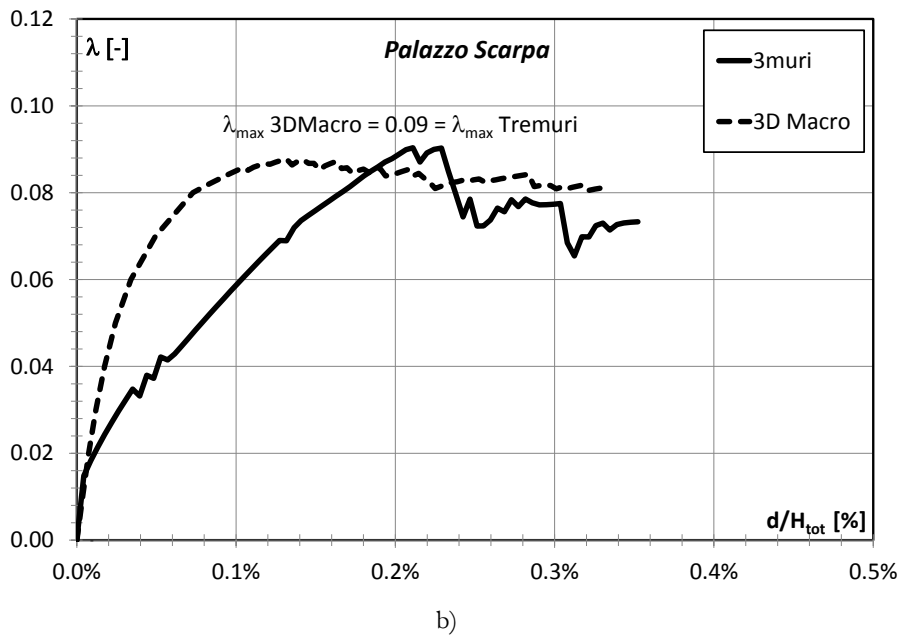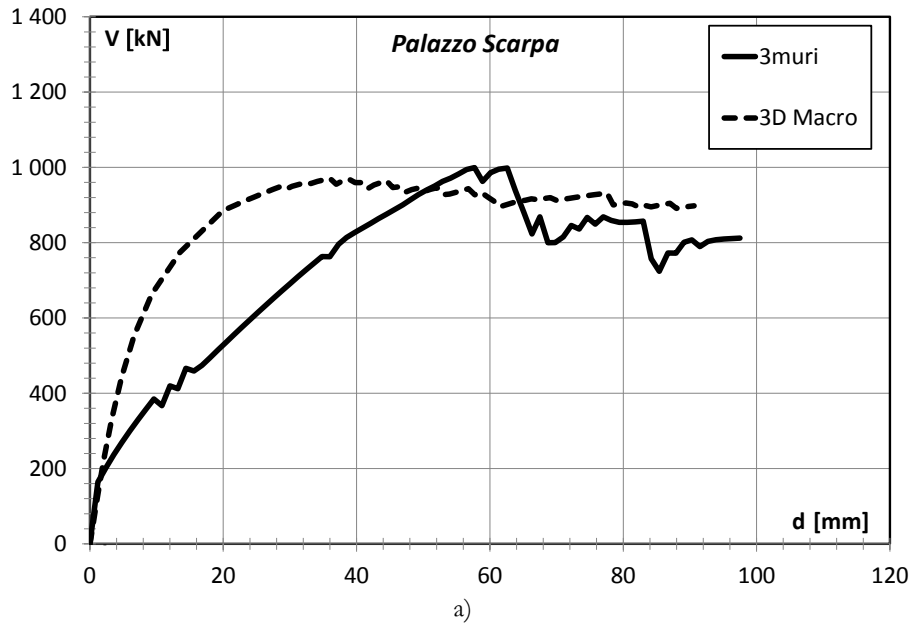
Figure 2.11 *Palazzo Scarpa* **: capacity curves provided by simplified modelling, in terms of : a) force vs displacements; b) load multipliers vs displacements divided by total height of the wall**
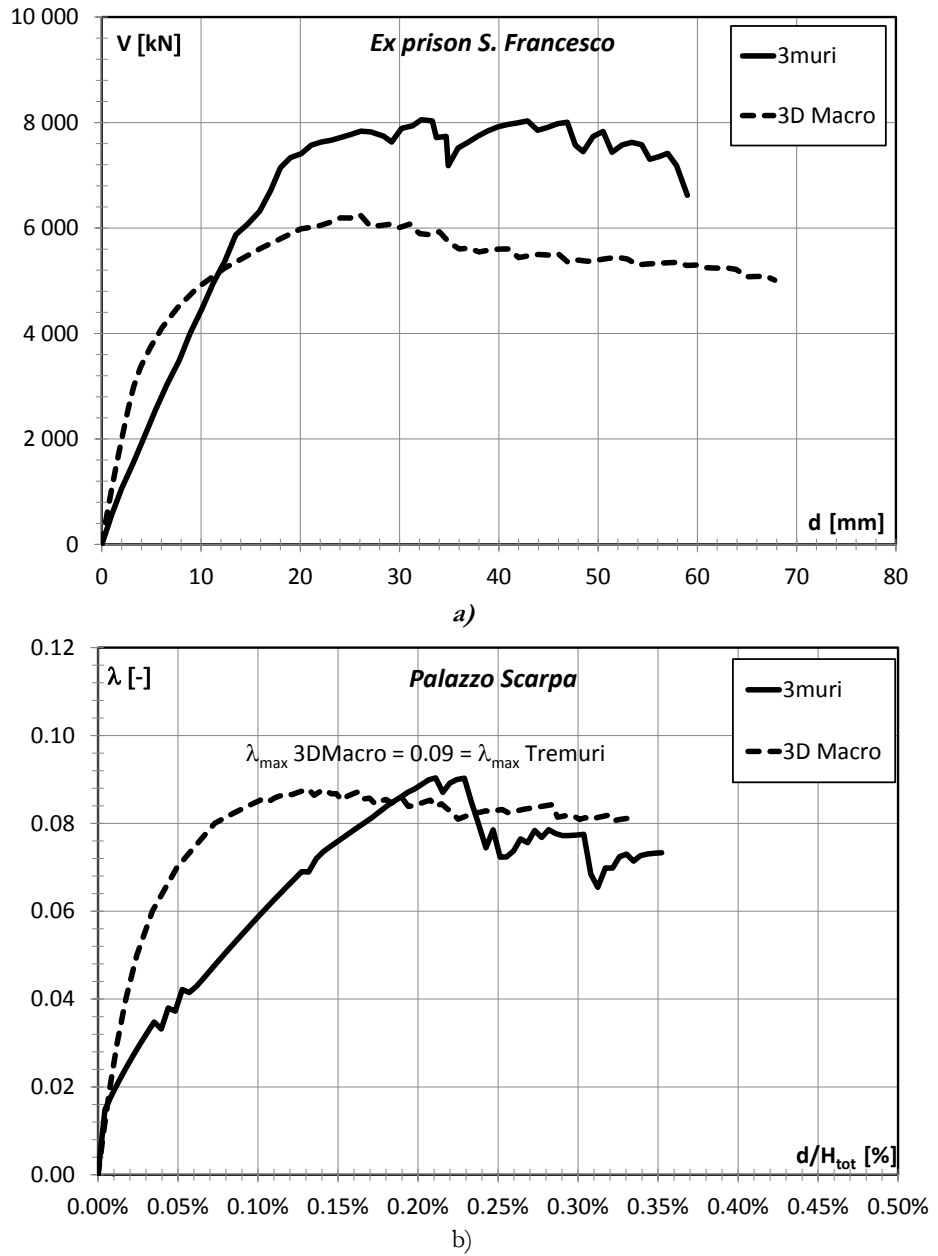
Figure 2.12 *Ex prison S. Francesco*: capacity curves provided by simplified modelling, in terms of : a) force vs displacements; b) load multipliers vs displacements divided by total height of the wall
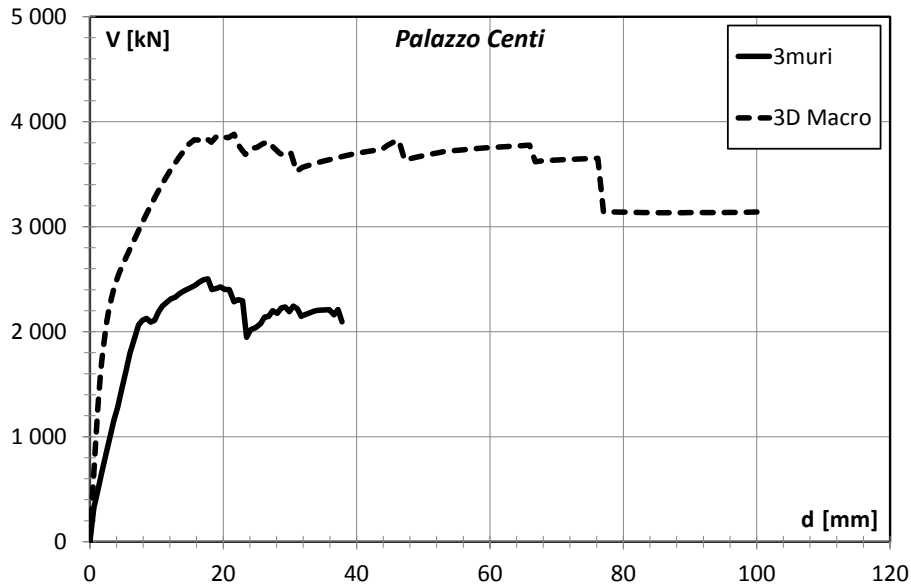
Figure 2.13 *Palazzo Centi*: capacity curves provided by simplified modelling, in terms of : a) force vs displacements; b) load multipliers vs displacements divided by total height of the wall

Figure 2.14 *De Amicis school*: capacity curves provided by simplified modelling, in terms of : a) force vs displacements; b) load multipliers vs displacements divided by total height of the wall

Table 2.2 reports for each case study the value of λ_{max} and d_{max}/H_{tot} reached by the different codes. The variance between the results was also computed and it is reported in the Table. The variance between 3Muri and 3DMacro is in the range 8÷24% in terms of λ, while it is always lower than 13% in terms of displacement, except of Palazzo Centi, which revealed variance equal to 62%.

Table 2.2 Load multipliers, displacements and related variances given by the different commercial codes

		λ_{max}	d_{max}/H_{tot}	Δ_λ	Δ_d
		[-]	%	%	%
Palazzo Scarpa	3Muri	0.09	0.36	8	7.0
	3DMacro	0.08	0.33		
Ex prison S. Francesco	3Muri	0.22	0.23	24	13.0
	3DMacro	0.17	0.26		
Palazzo Centi	3Muri	0.26	0.23	17	62
	3DMacro	0.32	0.61		
De Amicis school	3Muri	0.34	0.13	12	11
	3DMacro	0.39	0.11		

However the three codes agree about the failure mechanism which led the collapse of the wall. Figures 2.15 and 2.16 show the damage observed in the façades at the ultimate state of the analysis. For all the case studies the figures reveal the shear failure of the spandrels, except of the case of De Amicis School that collapsed for the shear failure in the wall piers.

Integro
Plastico per taglio
Rottura per taglio
Plastico per pressoflessione
Rottura per presso flessione
Rottura per compressione
Rottura per trazione
Rottura in fase elastica

a_ 3Muri)

a_ 3Dmacro)
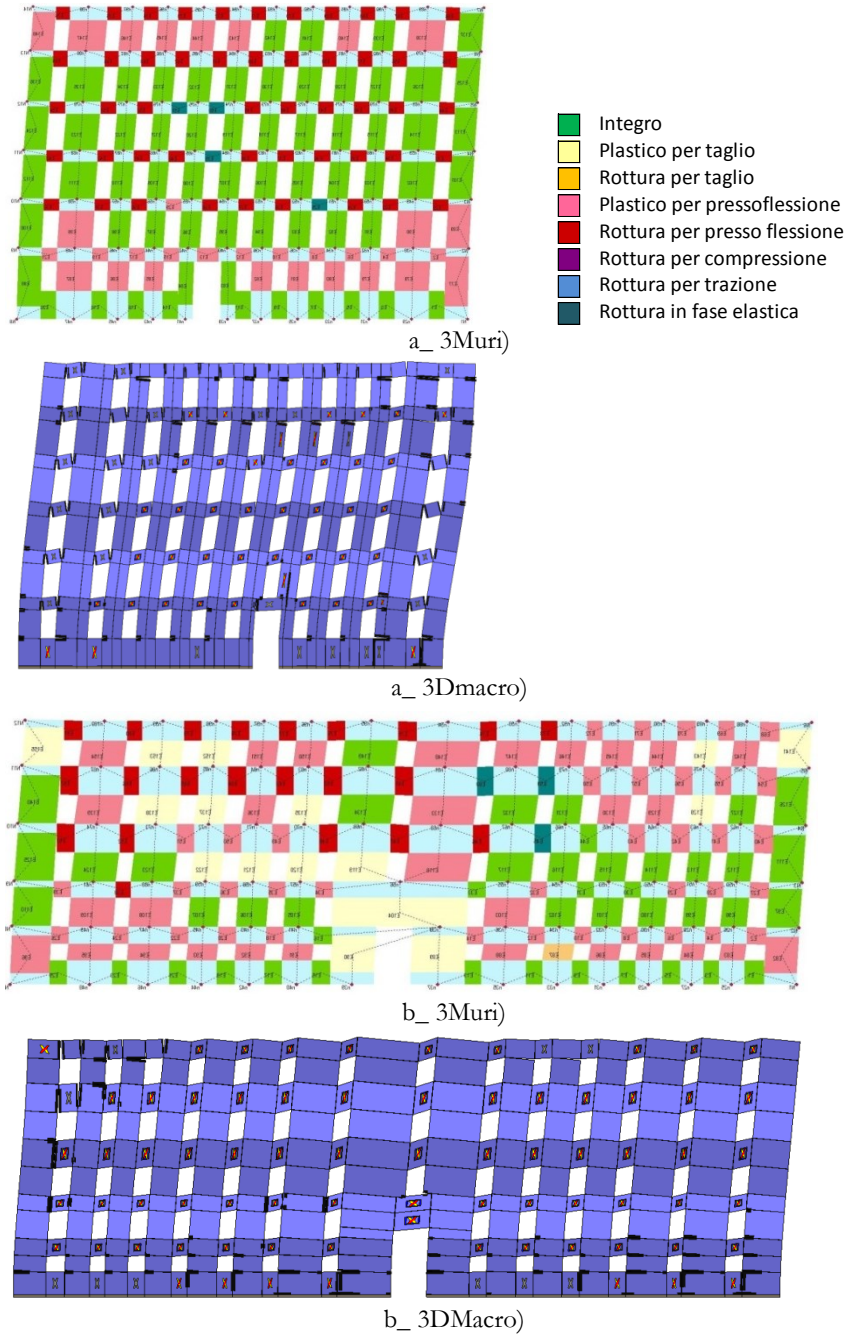
b_ 3Muri)

b_ 3DMacro)

Figure 2.15 Comparison of the damage revealed by 3Muri and 3Dmacro for a) *Palazzo Scarpa***; b)** *Ex prison S. Francesco*

Legend:
- Integro (green)
- Plastico per taglio (pale yellow)
- Rottura per taglio (orange)
- Plastico per pressoflessione (pink)
- Rottura per presso flessione (red)
- Rottura per compressione (purple)
- Rottura per trazione (light blue)
- Rottura in fase elastica (dark teal)

a_ 3Muri)

a_ 3Muri)
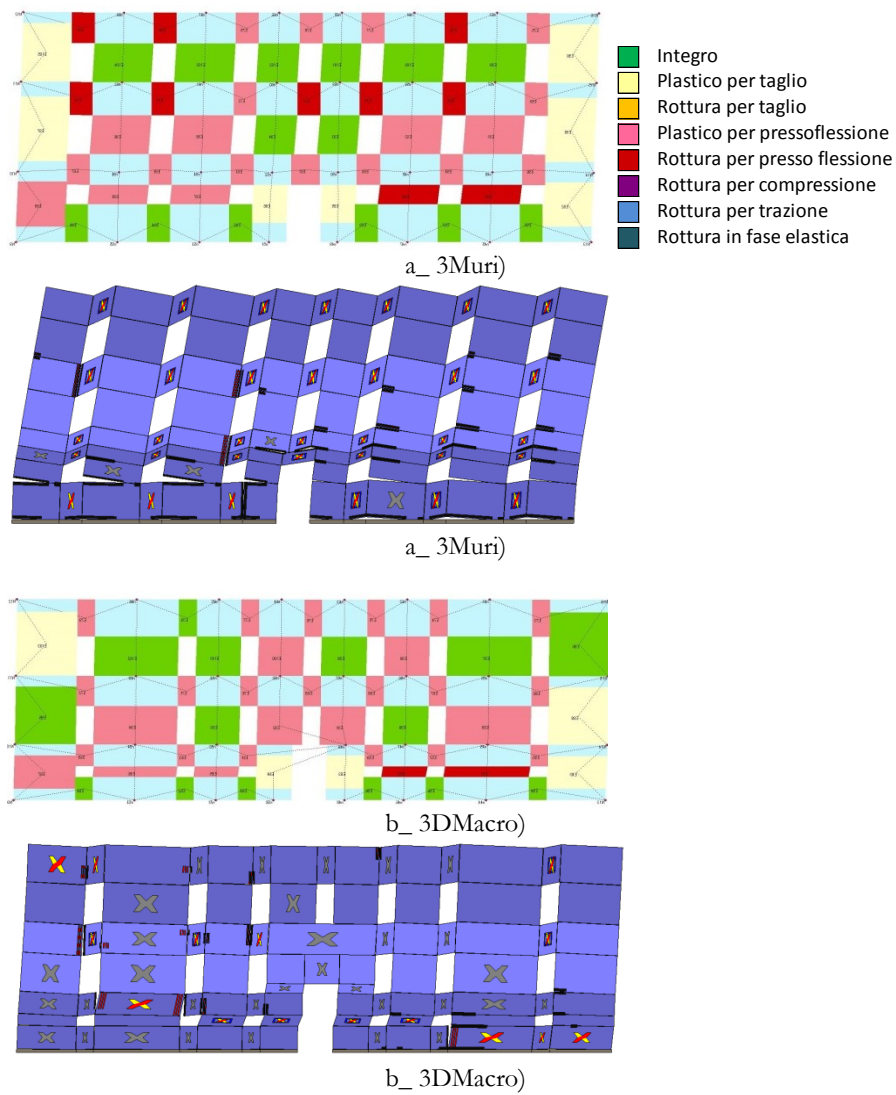
b_ 3DMacro)

b_ 3DMacro)

Figure 2.16 Comparison of the damage revealed by 3Muri and 3Dmacro for a) *Palazzo Centi*, **b)** *De Amicis school*

2.4 FE ANALYSIS

The seismic capacity of the façades was verified by using the finite element method. The Abaqus 6.1 software was used to perform the

analyses. Abaqus has been adopted by the research group of the author for many years, in order to analyze masonry structures. The material model, employed by the software to describe the masonry behavior, was extensively illustrated by Giordano (2001), Santaniello (2010) and Lucibello (2013). Here a brief summary is provided on the basis of the cited references and the Abaqus Manual (Simulia, 2010).

2.4.1   Abaqus concrete model

To model brittle structures, Abaqus provides the "concrete smeared model". It is a fixed multi-crack model based on a simple yield surface with isotropic hardening and associated flow when the state of stress is predominantly compressive, and uses damaged elasticity to account for the cracking, the occurrence of which being defined by a so-called "crack detection surface" (Fig. 2.17). This failure surface is assumed to be a simple Coulomb line written in terms of the first and second stress invariant. The concrete model basically requires: 1) the stress–strain curve in compression to be defined in tabular form as a function of plastic strain, 2) the shape of the failure surface via the "failure ratios" (defined in the following); 3) the post-cracking tensile behaviour defined by the "tension stiffening" option. The tension stiffening implicates that, as the tensile strength is reached, the σ–ε curve goes to 0 following a straight or curve line, according to the user choice (Fig. 2.18). This last feature actually makes no sense for masonry, but a small amount of tensile resistance should be anyway provided to avoid numerical instability problems.
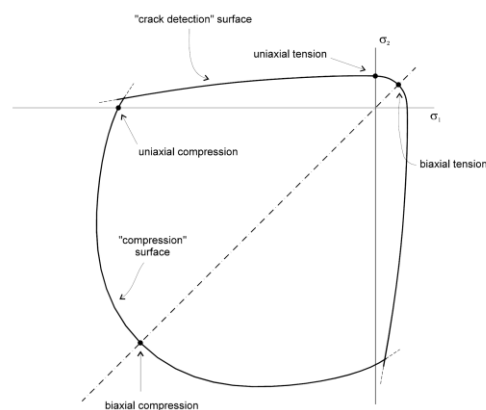
Figure 2.17 Crack detection surface in biaxial stress state

a)   b)
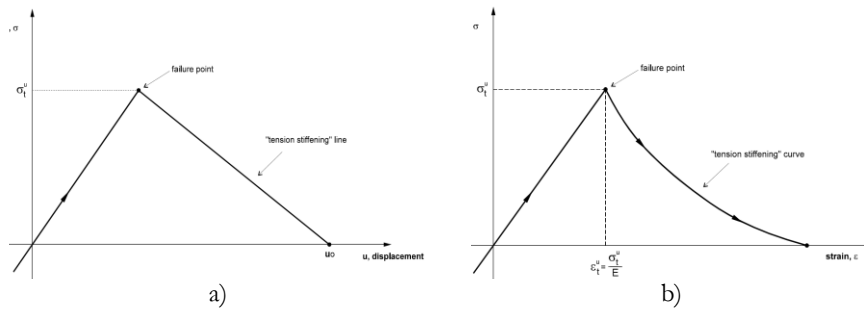
Figure 2.18 Tension stiffening: a) linear and b) curve options

In detail, the "concrete smeared model" uses the classical concepts of plasticity theory: strain rate, decomposition into elastic and inelastic strain rates, elasticity, flow and hardening. In the definition of the compression yield, the value of the magnitude of each nonzero principal stress in biaxial compression and the stress magnitude in uniaxial compression (σ_{bc}/σ_c) is given on the 1st "failure ratio" (indicated as R_1) data line. In the same way, the ratio of the uniaxial tensile stress at failure to the uniaxial compressive stress at failure (σ_t/σ_c) is given on the 2nd "failure ratio" (R_2) data line. In the definition of the flow, the value given on the 3rd "failure ratio" (R_3) option is representative of the ratio of ε_{pl} in a monotonically loaded biaxial compression test to ε_{pl} in a monotonically loaded uniaxial compression test. In tension, cracking dominates the material behaviour. The model uses a "crack detection" plasticity surface in stress space to determine when cracking takes place and the orientation of cracking. Damaged elasticity is then used to describe the post failure behaviour of the material with open cracks. About the crack orientation, although some models have been proposed (fixed model with orthogonal cracks, rotating model, fixed model with multidirectional cracks), the used model by Abaqus is the first one. The perpendicular to the first crack that occurs in a point is parallel to the maximum principal tension stress; the model remembers this direction so that the following cracks could form only in direction perpendicular to the first one. The value of the tensile failure stress σ_I in a state of biaxial stress when the other nonzero principal stress σ_{II}, is at the uniaxial compression ultimate stress state is defined by the 4th "failure ratio" (R_4).

2.4.2 Sensitivity analysis

As discussed in section 1.1, the FE analysis needs an accurate definition of the characteristics of the model. A parametrical analysis was performed to evaluate the sensitivity of the software to the following characteristics:

- Material constitutive law in compression
- Compressive strength
- Ultimate strain
- Tensile strength
- Mesh size

The material properties kept constant are listed in Table 2.3. The failure ratios: R_2, R_3, R_4 were established on the basis of the studies carried out by Giordano (2002). In order to correctly calibrate the model parameters for masonry structures, Giordano adopted a curve-fitting procedure. The results of various experimental tests on tuff masonry panels, were compared with the FE results obtained by using Abaqus.

The sensitivity analysis was performed on a simple geometry: the portal frame plotted in Figure 2.19. I was loaded, at first step, with the self weight and, at the second step, with an forces proportional to the masses incrementally applied.

Table 2.3 Material parameters kept constant

Material Model	Density	Young's modulus	Poisson ratio	R1	R3	R4	Tension stiffening
	[kg/m³]	[MPa]	[-]	[-]	[-]	[-]	[m]
Smeared cracking	2000	1833	0.25	1.16	1.33	0.3	0.003
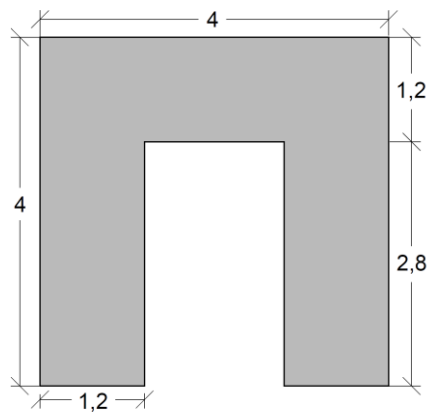
Figure 2.19 Geometry of the masonry portal frame

2.4.2.1 Material constitutive law

The influence of the material constitutive law was assessed analyzing the portal frame by using four different stress-strain curves. These are presented in Figure 2.20. The first one was provided by Kaushik et al. (2007), who developed an analytical model, by regression analysis of experimental data, to plot the masonry stress-strain curves, which follow a combination of parabolic and linear variation. The second law was recommended by the Eurocode6 (CEN 1996). The material constitutive laws 3 and 4 were adopted in previous similar studies by Lucibello (2013) and Brandonisio (2007), respectively.

The comparison of the results obtained with each constitutive law is shown in Figures 2.21, where the capacity curves are plotted in terms of base shear vs displacements and load multipliers vs displacement divided the height of the portal frame. As it can be observed, the different stress-strain laws gave similar results, proving that this parameter does not have a significant influence on the results. In detail the laws 1 and 2 gave exactly the same capacity curve, while minimal differences were found with the law 3. More appreciable variance was noted when the law 4 was adopted, especially in terms of displacement at the ultimate state. This is equal to 5 mm adopting the law four, while it is in the range 6.5÷6.8mm by adopting the other laws.
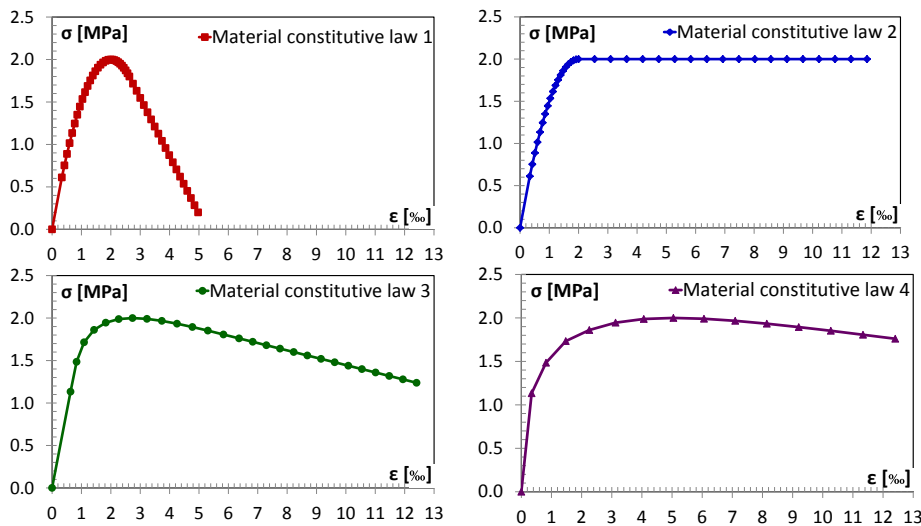
Figure 2.30 Parameter 1: material constitutive laws
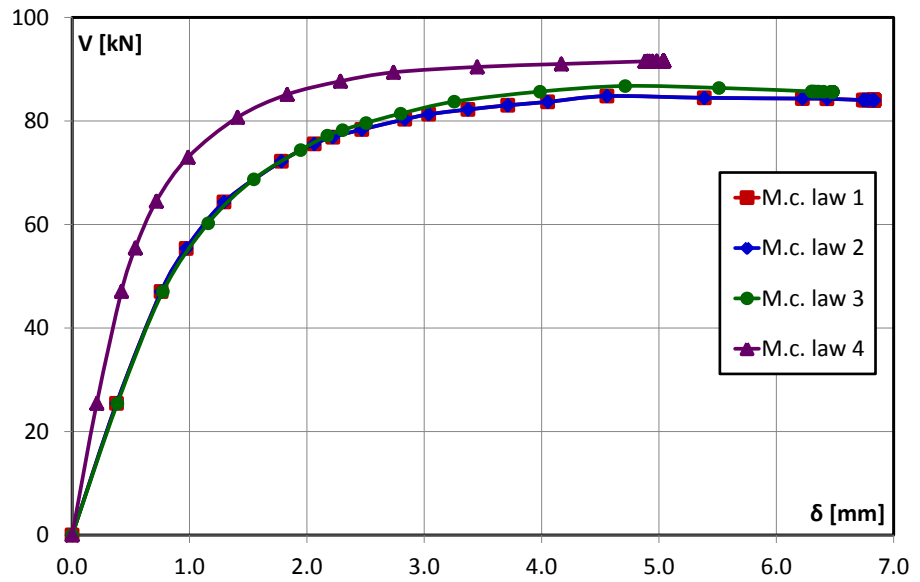
a)
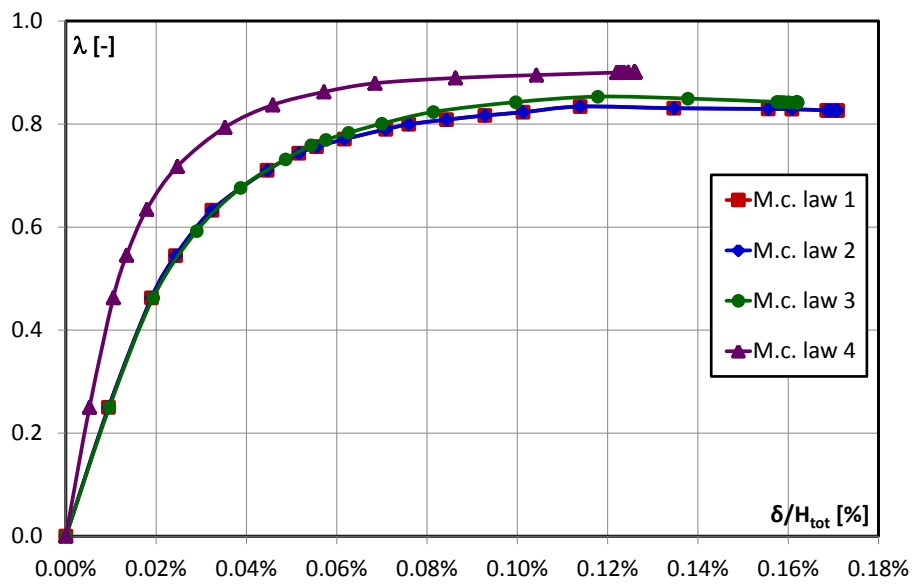
b)

Figure 2.41 Comparison of the curves obtained with different material constitutive laws in terms of: a) force vs displacements, b) load multipliers vs displacements divided by total height of the wall

2.4.2.2 Compressive strength

The sensitivity to the compressive strength (f_c) of the material was evaluated performing the analysis with four different values of f_c, equal to 2, 3, 4, 5 MPa. Figure 2.22 shows the four considered stress-strain relationship. The constitutive law 2 was adopted. In order to keep constant the values of yield strain and ultimate strain, different values of the Young's modulus were assumed. Moreover, different values of the second failure ratio ($R_2 = \sigma_t/\sigma_c$) were assigned to keep constant the tensile strength.

Figure 2.23 shows the resulting capacity curves in terms of base shear vs displacements, and load multipliers vs displacement divided the height of the portal frame. As expected higher values of compressive strength corresponds to higher value of load multipliers, even if the correspondence is not directly proportional, due to the shape of the failure surface. Moreover the maximum ultimate displacement was obtained with the lowest value of the compressive strength because, according to the adopted constitutive law, it associated to the smallest value of the Young's modulus.
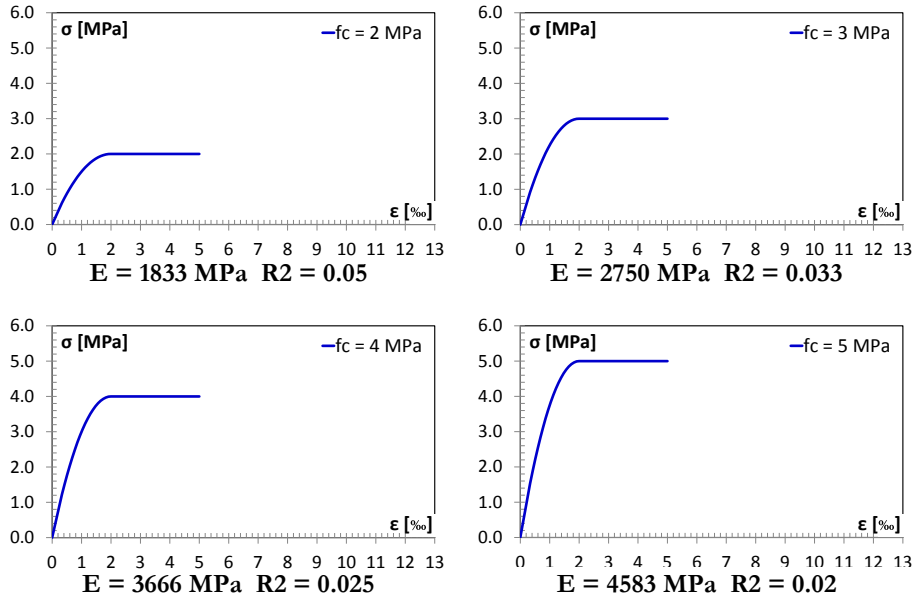
Figure 2.52 Parameter 2: compressive strength
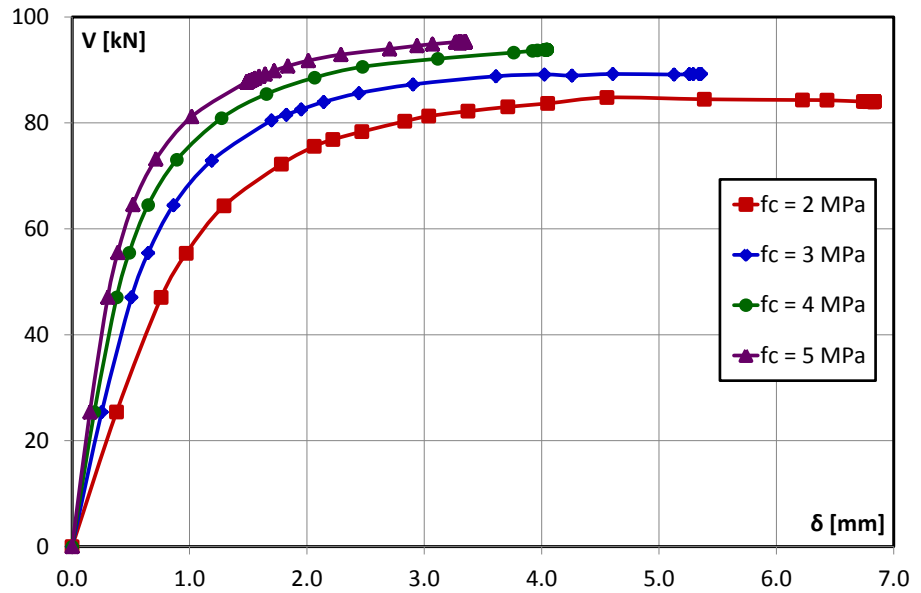
a)
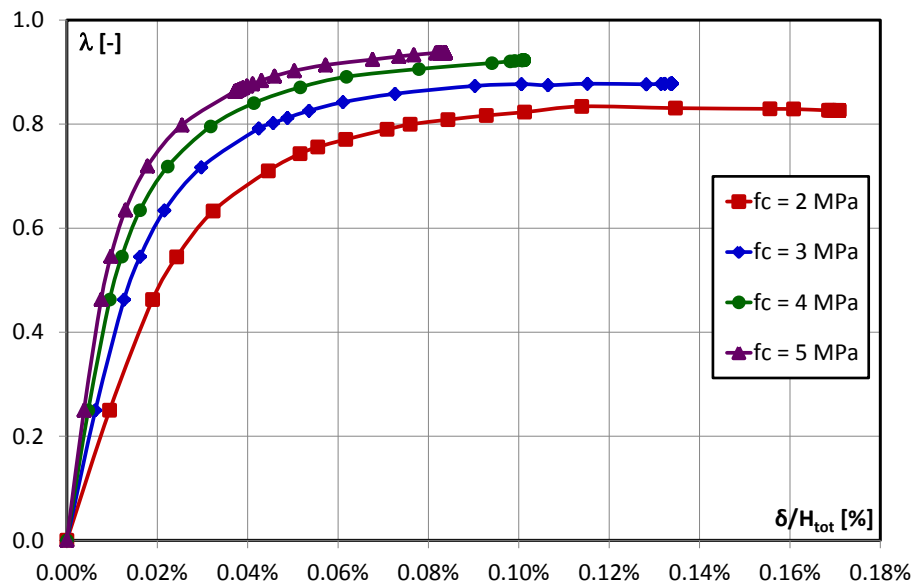
b)

Figure 2.63 Comparison of the curves obtained with different compressive strength (f_c) in terms of: a) force vs displacements, b) load multipliers vs displacements divided by total height of the wall

2.4.2.3   Ultimate strain

The influence of the ultimate strain (ε_u) was evaluated by considering four different values of ε_u equal to: 5‰, 12.5‰, 25‰, 50‰. The material constitutive law 2, with a compressive strength equal to 2 MPa, was assigned. Figure 2.24 shows the four adopted stress-strain relationship. A second failure ratio R_2 equal to 0.05 was assumed.

Similarly to the previous studied parameters, Figure 2.25 shows the comparison of the capacity curves obtained considering the different values of ultimate strain. The capacity curves are identical and then they appear as one curve in the graphs. Therefore the curves, in terms of load multipliers vs displacement divided the height of the portal frame, are individually plotted in Figure 2.26.

It can be deduced that the increasing of the ultimate strain does not influence the results of the analysis, and in particular does not lead to increasing of the ultimate displacement. The collapse of the structure occurred at the same state, for the development of hinges at the base of the pillars and at the connection between the beam and piers.
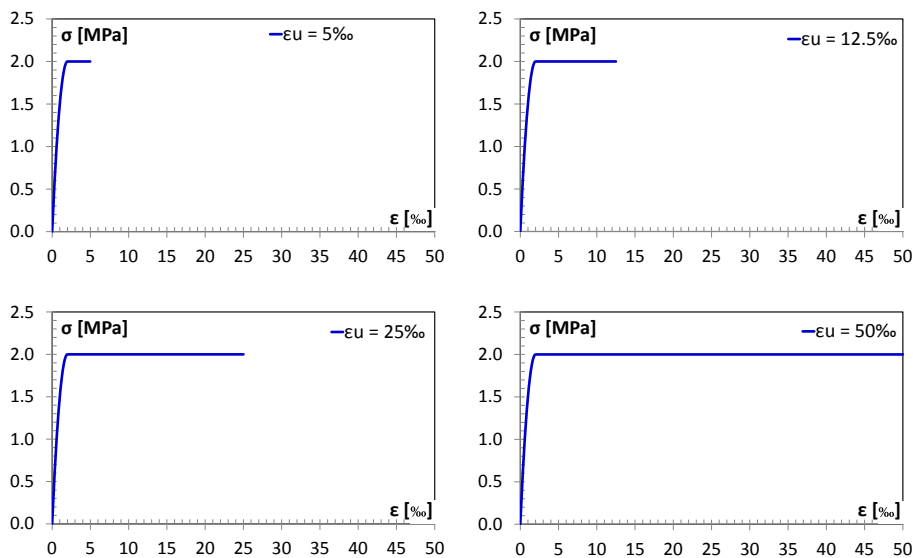
Figure 2.74   Parameter 3: ultimate strain
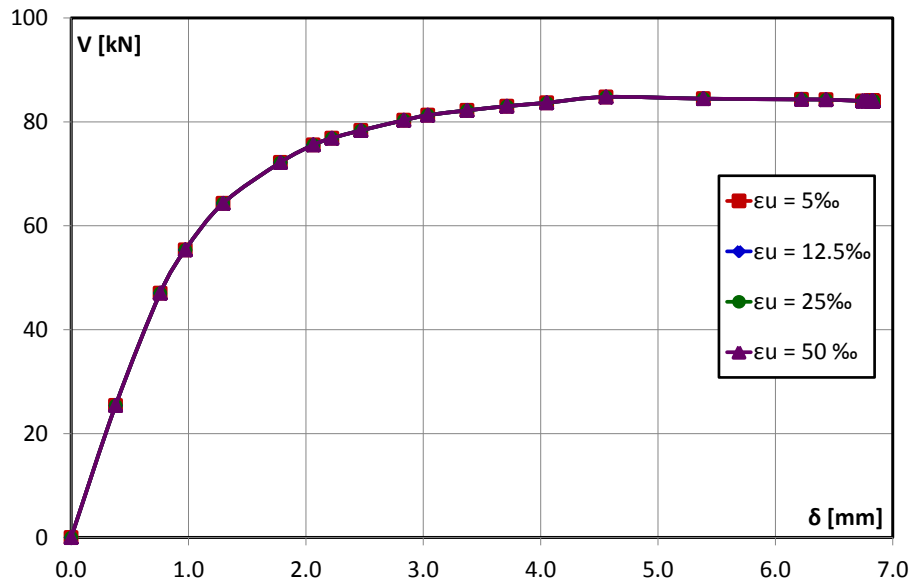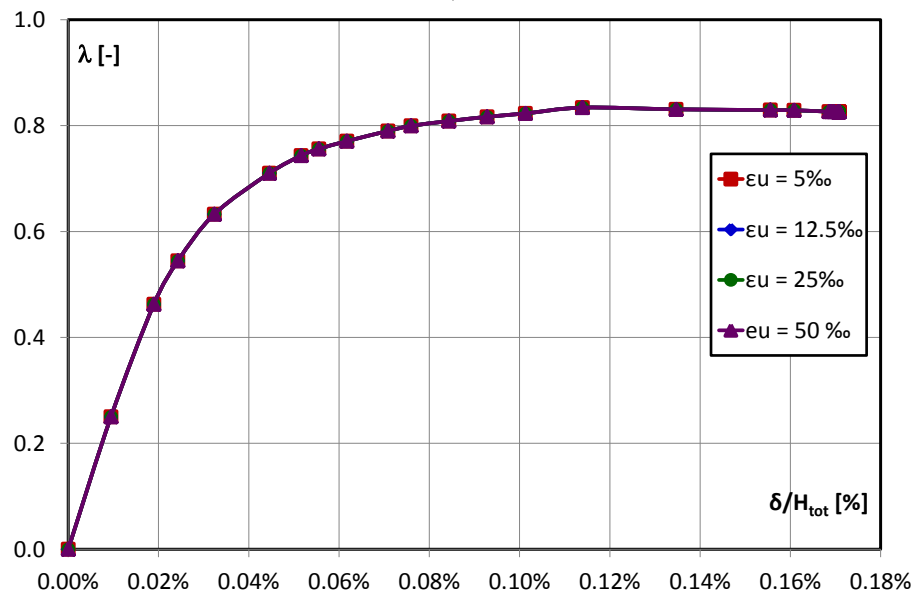
Figure 2.85 Comparison of the curves obtained with different ultimate strain (ε_u) in terms of: a) force vs displacements, b) load multipliers vs displacements divided by total height of the wall
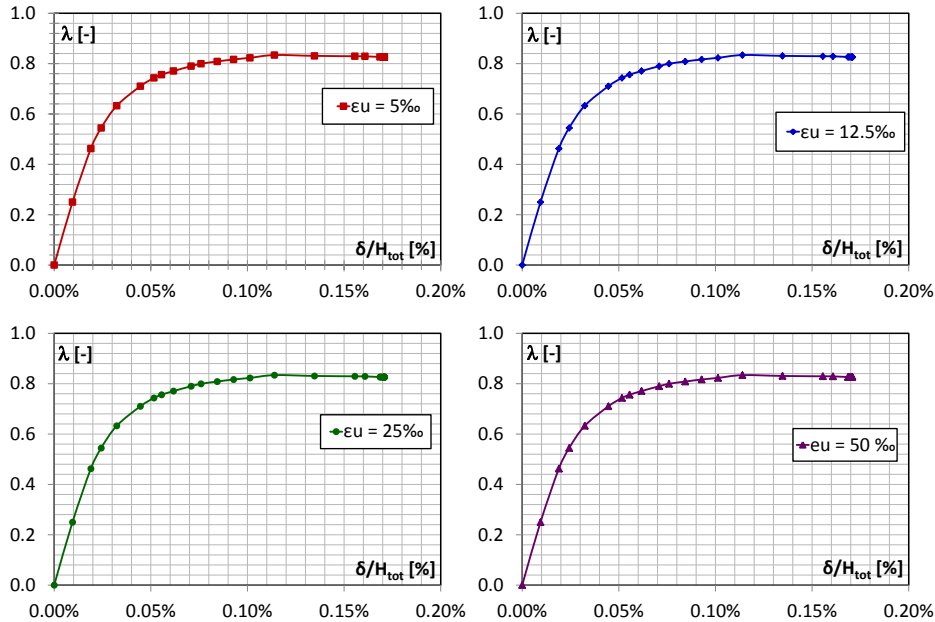
Figure 2.96 Capacity curves obtained with different ultimate strain (ε_u) in terms of load multipliers vs displacements divided by total height of the wall

2.4.2.4 Tensile strength

The tensile strength is the parameter which mainly influences the analysis results. Therefore ten values of the tensile strength were considered, assigning ten different values of the second failure ratio ($R_2 = \sigma_t/\sigma_c$), in the range 0.01÷0.1. The compressive strength was assumed equal to 2 MPa, consequently the tensile strength varied in the range 0.02÷0.2 MPa. Figure 2.27 shows the comparison of the capacity curve obtained for the different value of R_2. Significant variance can be observed among the capacity curves. Considering a tensile strength equal to 1% of the compressive strength, 80% lower load multiplier are obtained than the ones reached considering a tensile strength equal to 10% of the compressive strength. The results are significantly different also in terms of ultimate displacements.
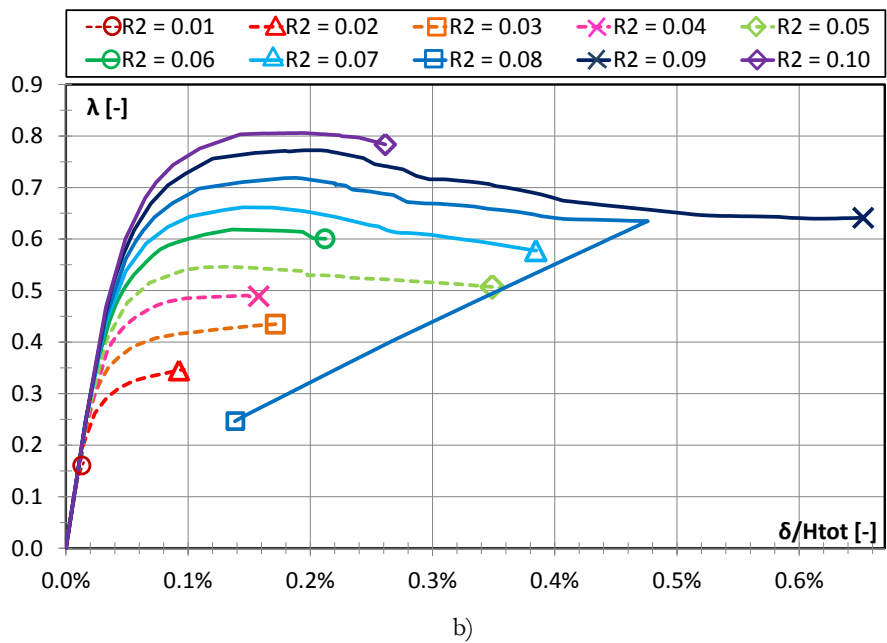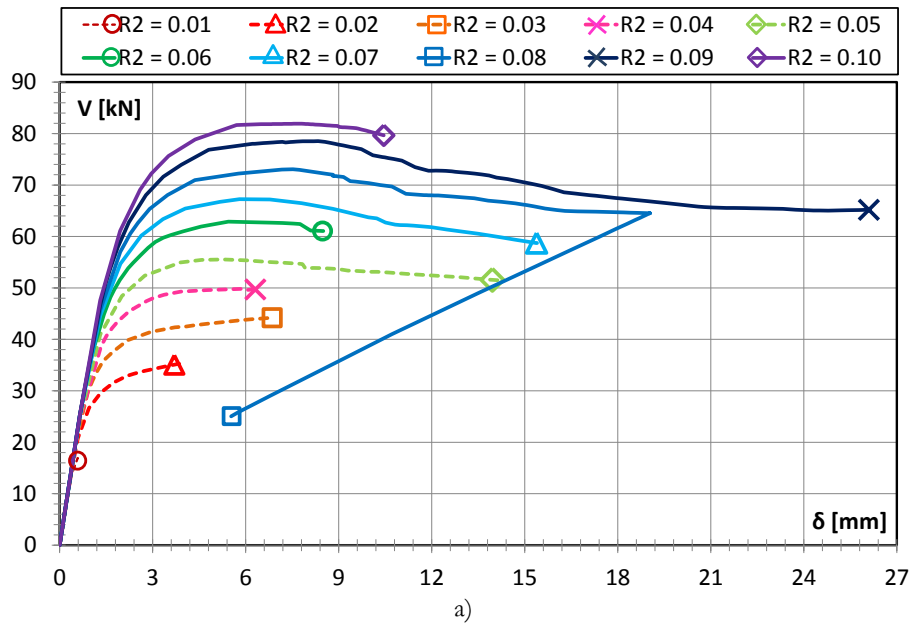
Figure 2.107 Comparison of the curves obtained with different failure ratios (R2 = σt/σc) in terms of: a) force vs displacements, b) load multipliers vs displacements divided by total height of the wall

This result weakens the stability of the FE analysis, because it is noted that the tensile strength for masonry structures is difficult to define, and different methodology and rules are provided in the literature. Casati and Galvez (2009) established that tensile strength is not more than 10% of the compressive strength. Brignola et al. (2008) proposed a methodology for the evaluation of the tensile strength from the diagonal compression test. Zero tensile strength was used without problems of numerical convergence by Silva et al. (2001) and by Ramos and Lourenco (2002, 2003, 2004, 2005). Ceroni et al. used a tensile strength of 5% of the compressive strength, in accordance with the recommendation of the Italian building code (O.P.C.M. 3431, 2005). Although these values, suggested by the literature, appear similar, the parametrical analysis proved that also small difference of the tensile strength procures great difference of the results, both in terms of displacements and in terms of load multipliers.

2.4.2.5 Mesh size

Finally the influence of the mesh size was evaluated. Four different mesh sizes were adopted and they are plotted in fig.2.28. The material constitutive law 2, with compressive strength equal to 2 MPa and R_2 equal to 0.05 was adopted.

The comparison of the capacity curves obtained from the analysis is shown in Figure 2.29. It can be noted that the same value of load multiplier is reached for each considered mesh size. However the maximum ultimate displacement is given by using the largest mesh, proving that the numerical progress of the analysis is improved by the less refined mesh. Similar results were obtained by Santaniello (2010).
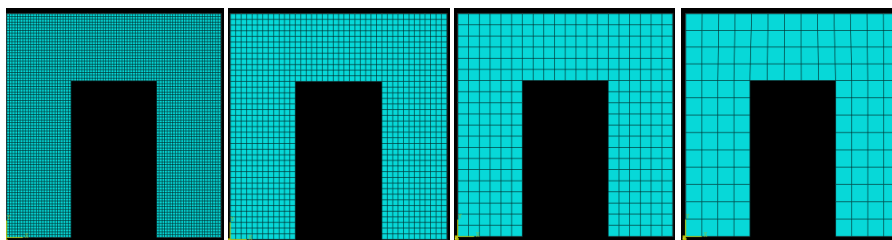
Mesh size = 0.05 m   Mesh size = 0.1 m   Mesh size = 0.2 m   Mesh size = 0.3 m

Figure 2.118 Parameter 4: mesh size
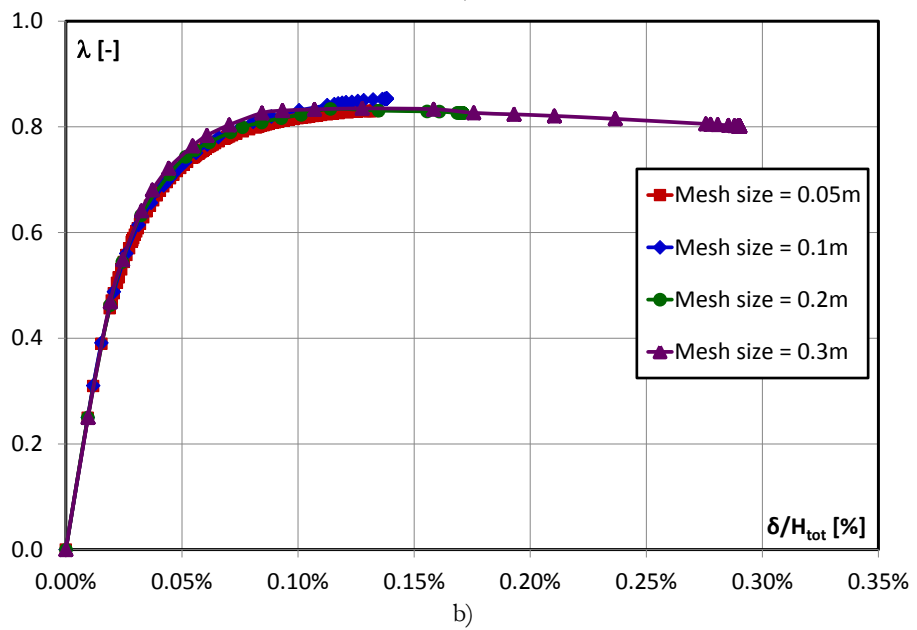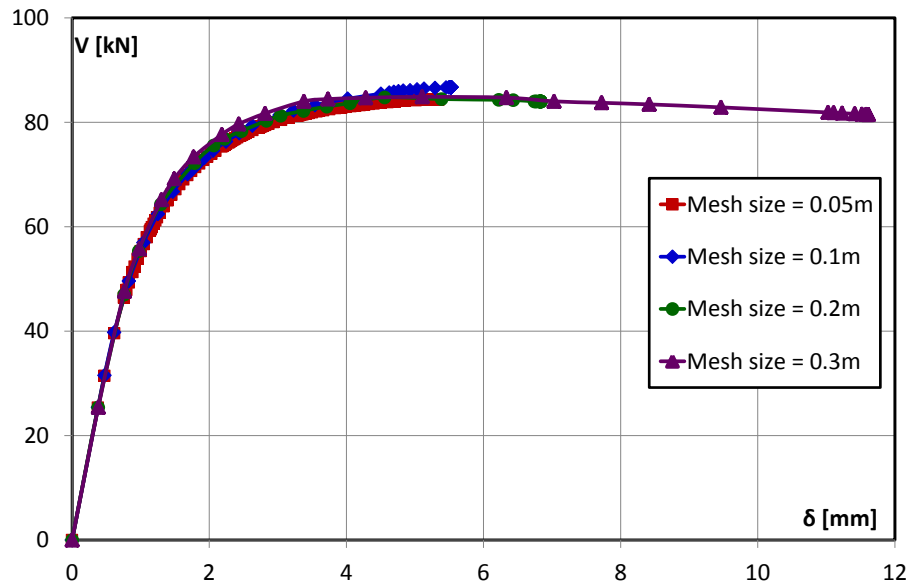
Figure 2.129 Comparison of the curves obtained with different mesh size in terms of: a) force vs displacements, b) load multipliers vs displacements divided by total height of the wall

### 2.4.3 Push-over analysis performed on the façades of the case studies

The façades of the four historical buildings, were analyzed by means of the FE approach. The characteristics of the models were assigned both considering the sensitivity analysis and in order to permit the comparison with the results obtained using the simplified modellings. The material constitutive law 2 with a compressive strength equal to 2 MPa was adopted. The ultimate deformation was considered equal to 5‰. A tensile strength equal to 3% of the compressive strength was used (R_2=0.03). This value was chosen because it is the lowest providing satisfactory numerical progress of the analysis. For the other material properties, the values reported in Table 2.3 were used.

The masonry walls have been modelled using quadrilateral thick shell linear element (S4R). An average value of the mesh size equal to 0.25 m was adopted, which was a good compromise between accuracy of the results, computational effort and provided displacement capacity.

The façades are constrained on the base with a fixed support and loaded at first step with the self weight and at the second step with an horizontal body forces incrementally applied.

The capacity curves of each façade are plotted in Figures 2.30-2.33. As in the previous analysis the curves are given both in terms of base shear vs displacements, and in terms of load multipliers vs displacement divided the height of the portal frame. The displacements of the control points indicated in Figure 2.10 were considered. It can be noted that very small displacements were obtained from the FE analysis. Moreover the capacity curves did not present a decreasing tract, giving rise to doubt about the effective ultimate capacity of the wall. It depends on numerical modelling performed to Abaqus that, up to a certain level of damage, has many difficulty of convergence, so the software aborts the analysis. Therefore, this software seems to be not able to evaluate the realistic maximum displacement of the wall. However reasonable values of the load multipliers were reached, comparable with the results found through the simplified modelling.

Figure 2.34 shows the damage state at the ultimate state of the FE analysis. It can be noted that, in agreement with the simplified modelling, the FE analysis indicates that the collapse of the façades is due to the shear failure of the spandrels, for the most of the cases.
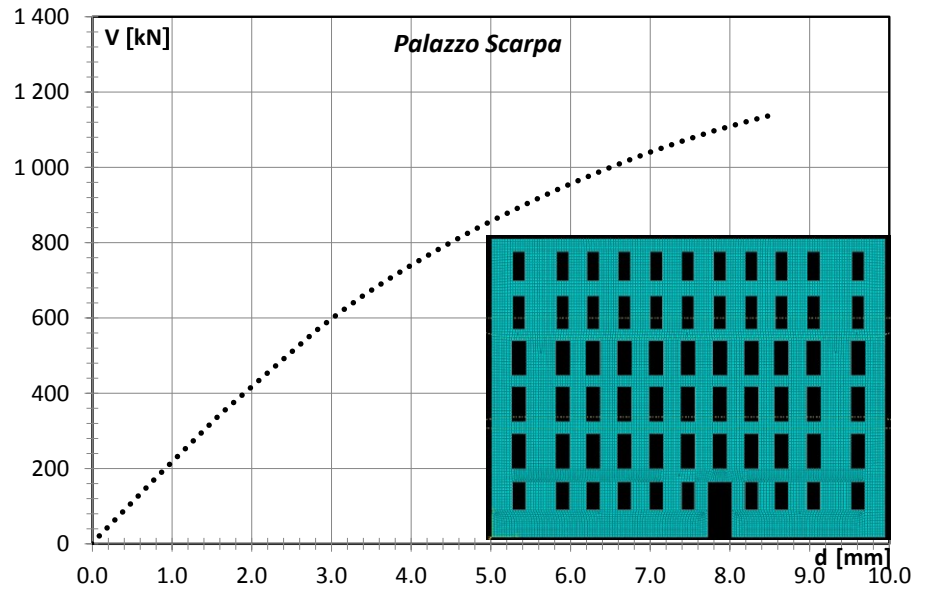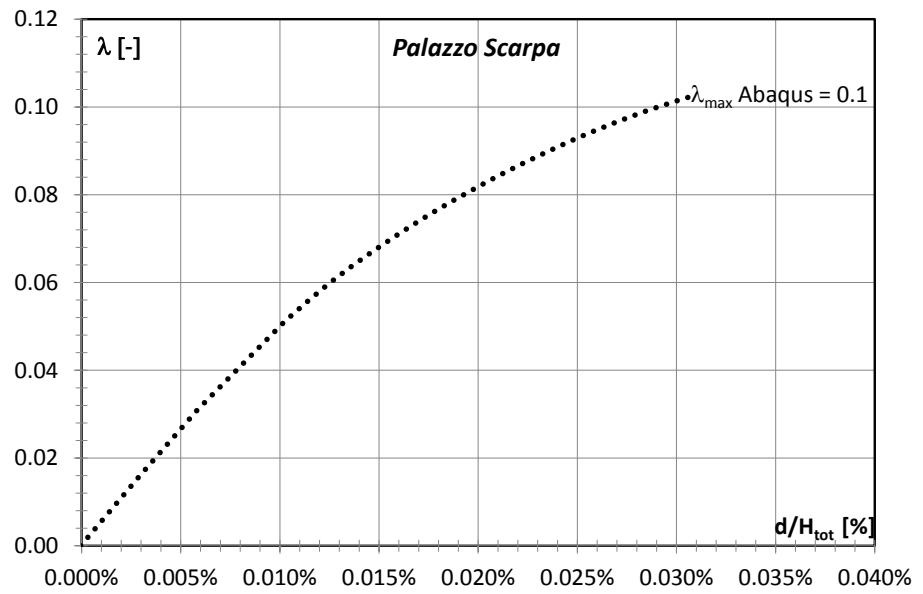
Figure 2.30 *Palazzo Scarpa*: capacity curves provided by FE analysis, in terms of: a) force vs displacements; b) load multipliers vs displacements divided by total height of the wall
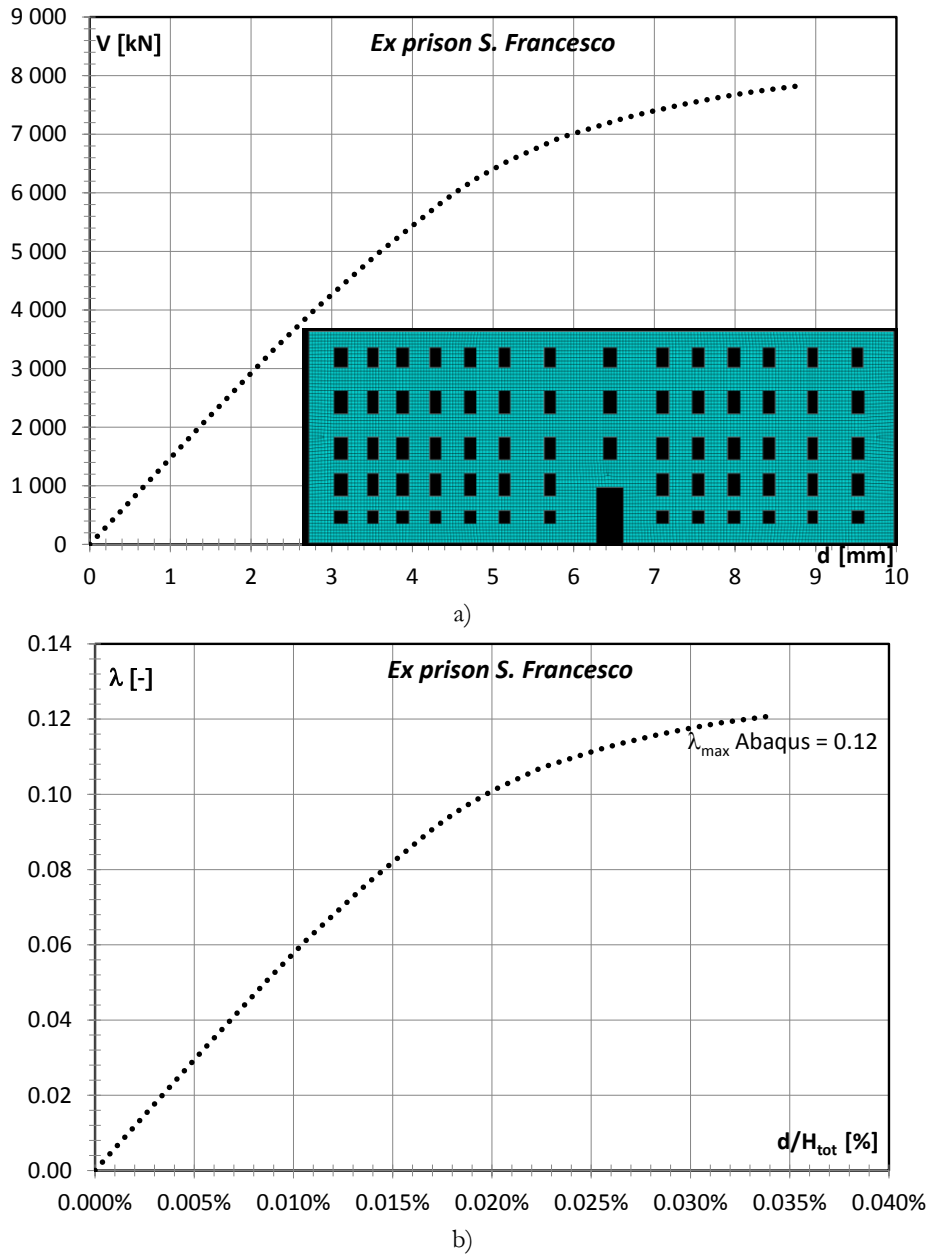
Figure 2.31 *Ex prison S. Francesco*: capacity curves provided by FE analysis, in terms of: a) force vs displacements; b) load multipliers vs displacements divided by total height of the wall

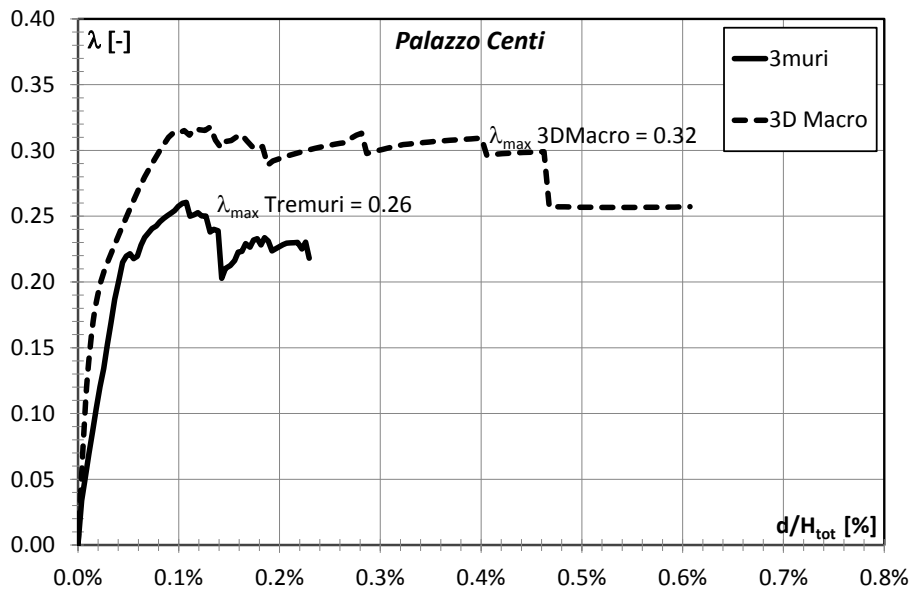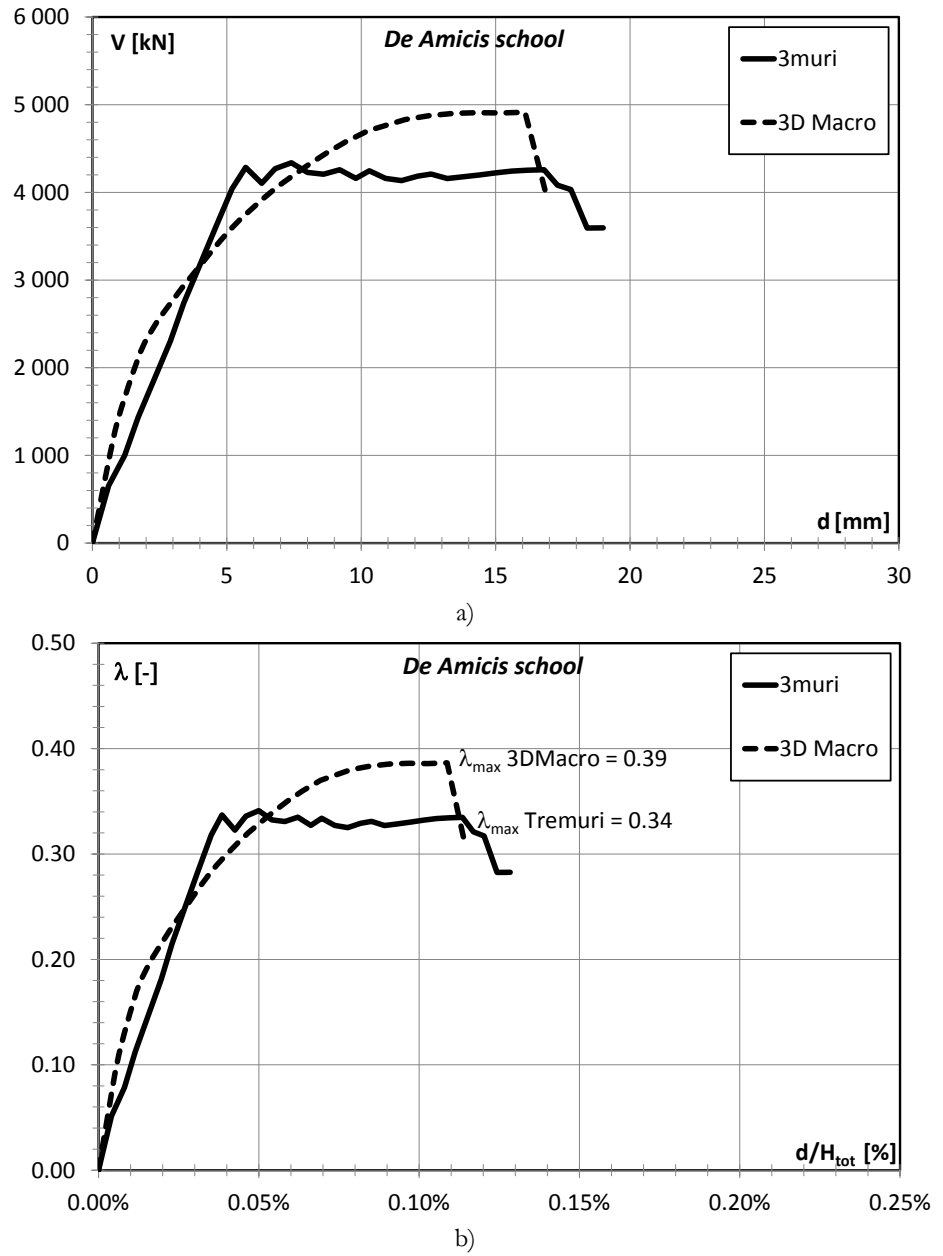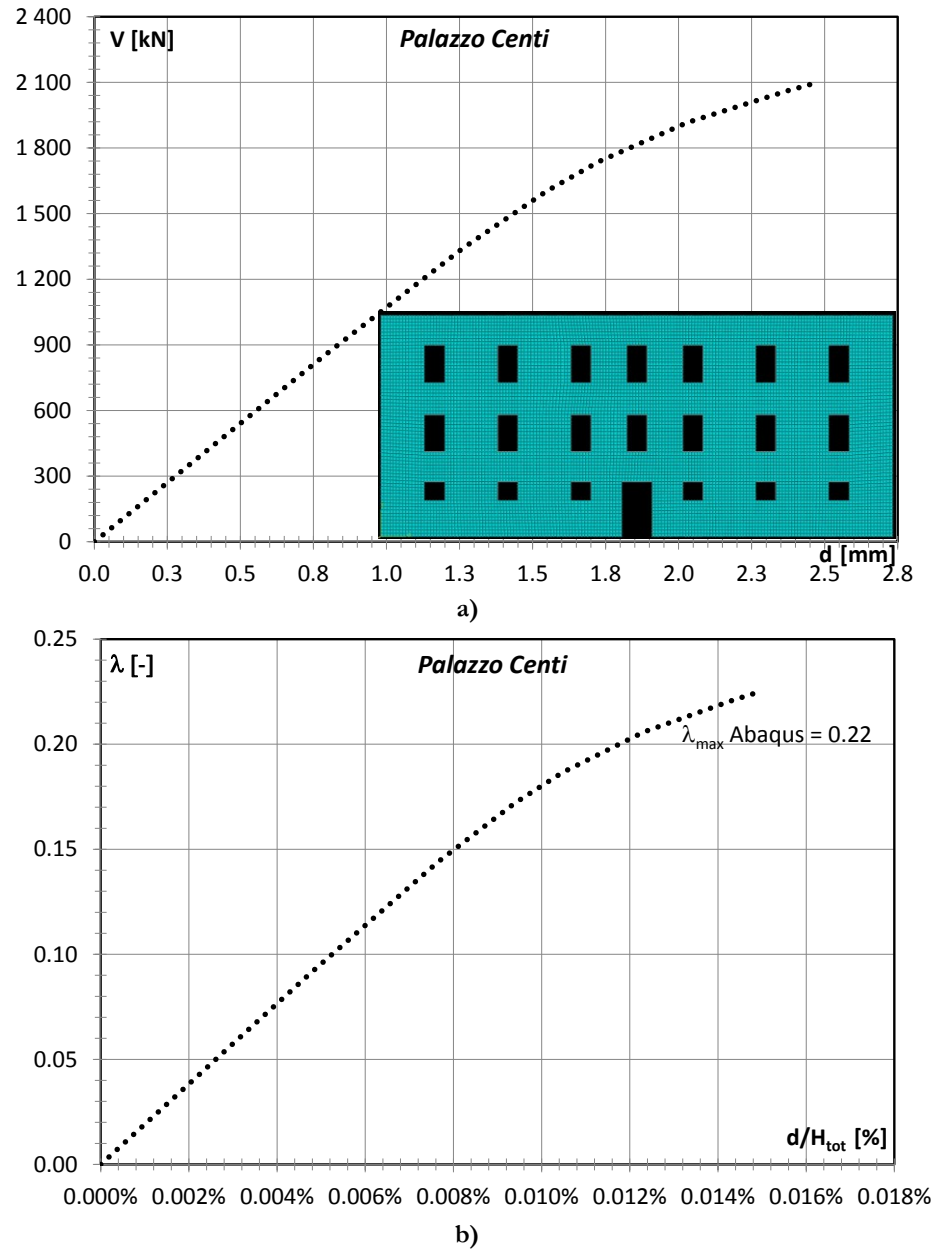**Figure 2.32 Palazzo Centi: capacity curves provided by FE analysis, in terms of: a) force vs displacements; b) load multipliers vs displacements divided by total height of the wall**
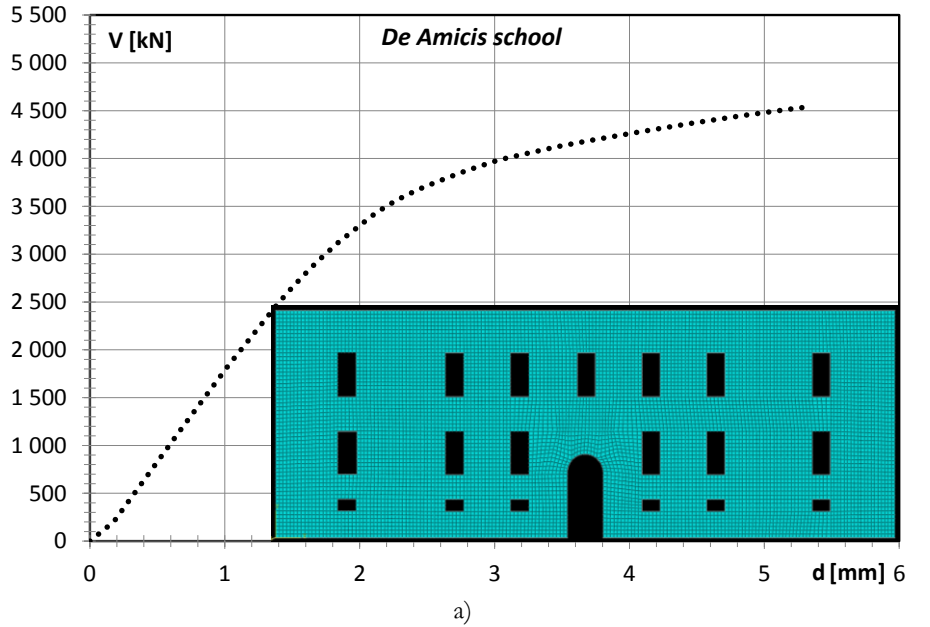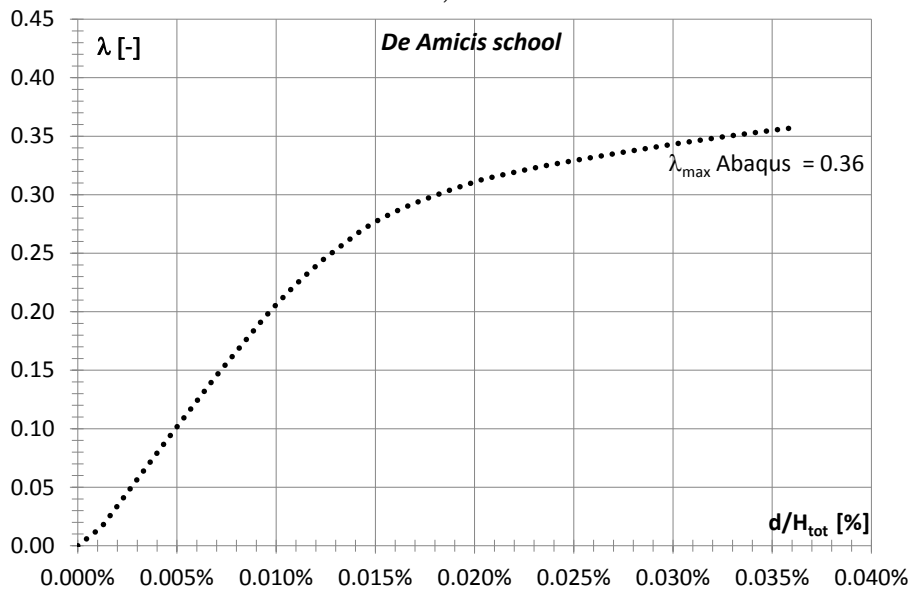
Figure 2.33 *De Amicis school*: capacity curves provided by FE analysis, in terms of: a) force vs displacements; b) load multipliers vs displacements divided by total height of the wall
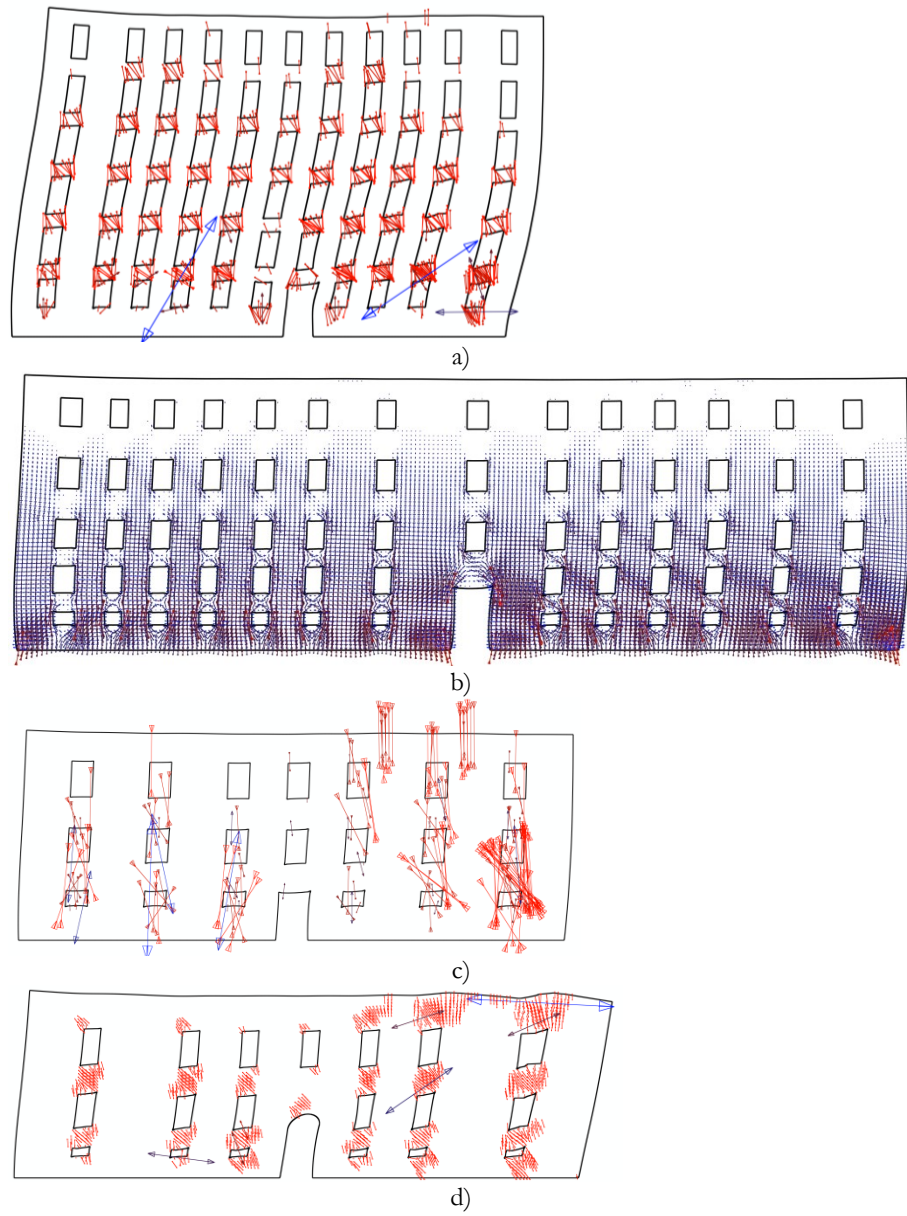
Figure 2.34 Damage at the ultimate state on the façade of: a) *Palazzo Scarpa***, b)** *Ex prison S. Francrsco***, c)** *Palazzo Centi***, d)** *De Amicis school*

2.5 LIMIT ANALYSIS

The in-plane seismic capacity of the four façades was finally evaluated by means of the limit analysis approach which consists in: (i) defining the possible collapse mechanisms; (ii) evaluating the seismic capacity, i.e. the value of horizontal force corresponding to the activation of the mechanism; (iii) comparing the seismic capacity with the seismic demand.

According to the above procedure, the global collapse mechanism of the generic masonry wall of Figure 2.35, was hypothesized for the in-plane failure mode of the principal façade of the building case studies. It is characterized by the formation of hinges at the ends of the girders and at the base of the piers. The corresponding multiplier of the horizontal actions λ, can be evaluated by means of the following closed form expression:

$$\lambda = \frac{B}{H} \cdot \frac{\sum_{i=1}^{n_b+1} W_{p,i} + \sum_{j=1}^{n_b \cdot n_s} W_{s,j}}{\left[n_s \cdot \sum_{i=1}^{n_b+1} W_{p,i} + \left(n_s + 1 - \frac{t}{H} \right) \cdot \sum_{j=1}^{n_b \cdot n_s} W_{s,j} \right]} = \frac{B}{H} \cdot \frac{1}{n_s + \left(1 - \frac{t}{H} \right) \cdot \frac{\sum_{j=1}^{n_b \cdot n_s} W_{s,j}}{W_{tot}}} \quad (1)$$

a)   b)
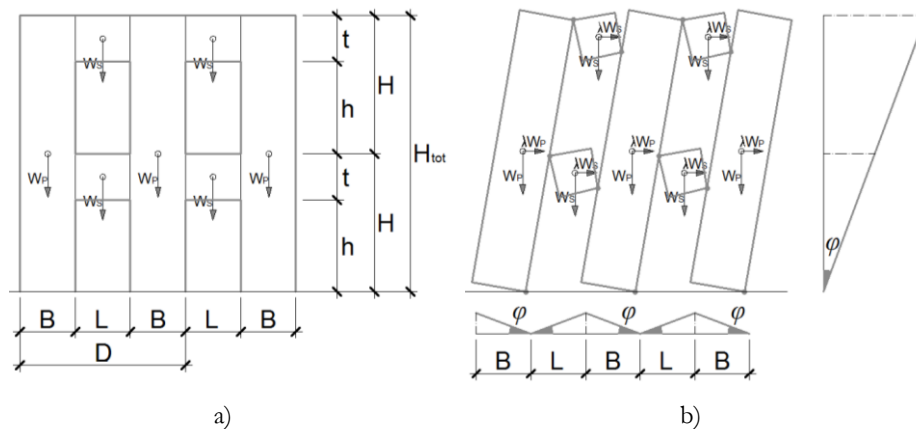
Figure 2.35 Limit analysis: (a) geometrical dimensions of a generic masonry wall; (b) considered frame collapse mechanism

where *B*, *H* and *t* are the parameters that define the wall geometry (Figure 2.35), n_b is the number of bay spans, n_s is the number of storeys, $W_{p,i}$ is the weight of the wall pier i[th], $W_{s,j}$ is the weight of the spandrel j[th], W_{tot} is the total weight.

The Eq. (1) was deduced by Lucibello (2013) on the basis of the methodology adopted by Como and Grimaldi (1983). More detailed information on the expression can be found in Lucibello (2013).

The Eq. (1) was applied to the principal façades of the building case studies. Table 2.4 reports the average values of the geometrical parameters for each façade.

Table 2.4 Geometrical parameters of the façades

Building	B_m [m]	h_m [m]	L_m [m]	t_m [m]	H [m]	n_b [m]	n_s [m]
Palazzo Scarpa	2	2.9	1.3	1	3.9	6	11
Ex p. S.Francesco	3.5	3.4	1.85	2.15	5.55	5	14
Palazzo Centi	3.5	2.7	1.65	2.3	5	3	7
De Amicis school	4.4	3.5	1.3	2.5	6	2	7
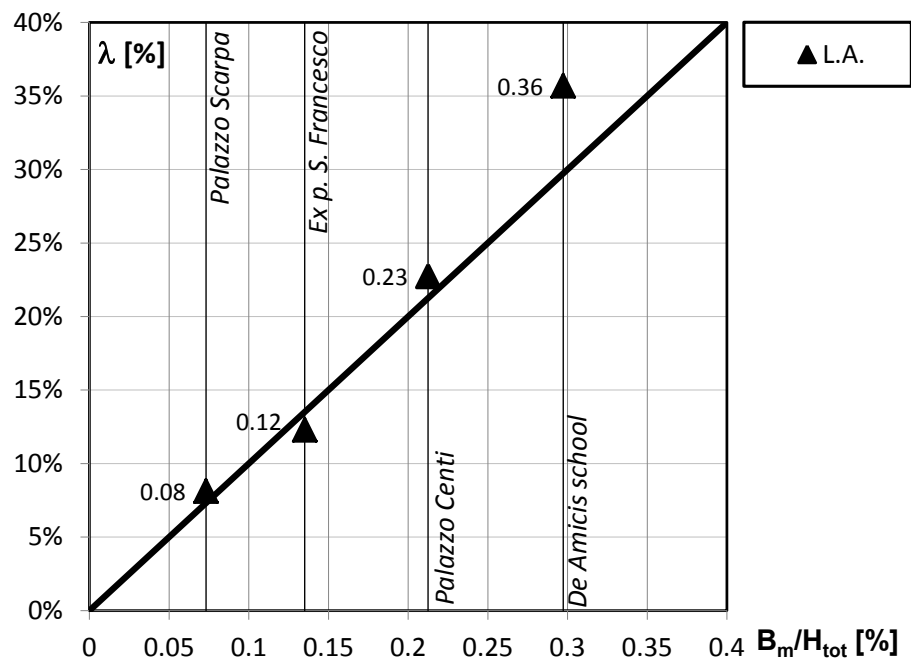
Figure 2.36 Horizontal collapse multipliers for the principal façades of the building case studies

The values of the horizontal collapse multiplier λ are reported in the graph of Figure 2.36, as a function of the B_m/H_{tot} ratio. The points, indicating the limit multipliers, are all allocated very close to the bisector line ($\lambda = B_m/H_{tot}$). This is due to fact that the contribution of the spandrels to the horizontal capacity is always negligible than the contribution of the piers, because the façades are characterized by low values of the $A_{spandrel}/A_{tot}$ ratio, variable in the range 10%-16%. When the total weight of the spandrels is negligible: i.e. $\sum_{j=1}^{n_b \cdot n_s} W_{s,j} \Big/ W_{tot} \cong 0$, the Eq. (1) provides the following approximated expression of the collapse multiplier: $\lambda = B_m/(n_s \cdot H) = B_m/H_{tot}$, corresponding to the bisector line equation.

It can be deduced that, if the contribution of the spandrels is negligible, the complex Eq. (1) could be simplified by a simple ratio: the average value of the pier width, divided by the total height of the wall. Consequently, the following simplified expression (2) is proposed, which implicitly takes into account the simplified modelling of masonry walls, shown in Figure 2.37 .
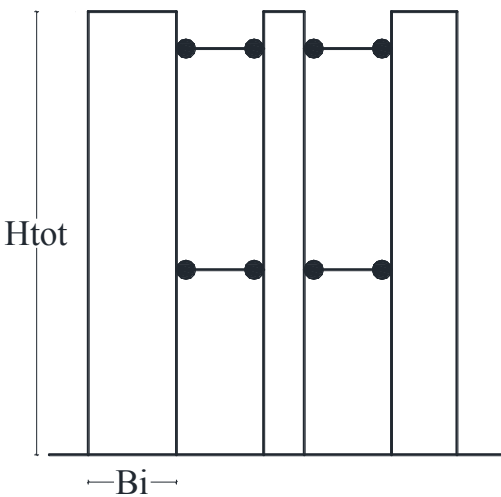
$$\lambda_{eq.} = \frac{\sum B_i^2}{\sum B_i}/H_{tot} \quad (2)$$

Figure 2.37 Simplified formula and corresponding simplified modelling of a generic masonry wall

It can be noted that the ratio $\frac{\sum B_i^2}{\sum B_i}$ has been used, to evaluate the average value of the pier width. It, in fact, provides a more accurate measure of the relative importance of the single piers.

2.6 COMPARISON OF THE RESULTS

Figure 2.38 and2.39 show the comparison between the capacity curves carried out by using the simplified modelling and the FE method. The horizontal lines corresponding to collapse multipliers evaluated with the Eq. (1) and with the simplified Eq. (2) are also reported on the graphs. As expected the displacements reached with the FE analysis are much lower and not comparable with the displacements provided by the simplified modelling. In terms of load multipliers, the variance between FE and simplified modelling is on average equal to 20%. However it should be noted that in the case of the *Ex prison S. Francesco*, the FE analysis gave a maximum load multiplier 45% lower than Tremuri.

On the other hand the FE results are in good agreement with limit analysis. In detail the scatter between the load multipliers is on average equal to 6% and only in the case of *Palazzo Scarpa* the scatter assumes a significant value equal to 19%.

The simplified modelling revealed higher scatter compared with the limit analysis. In detail the difference between the load multipliers is on average equal to 18% and 16%, respectively considering 3Muri and 3DMacro codes. However, as the scatter are always lower than 20%, it can be said that the seismic capacities assessed using the push-over analysis are not very different from those measured with the limit analysis.

Moreover the figures 2.38 and 2.39 confirmed that the collapse multipliers obtained by using the Eq. 1 and 2 are very similar. Therefore, the simplified formula produces a good approximation of the frame collapse mechanism.

a)

b)
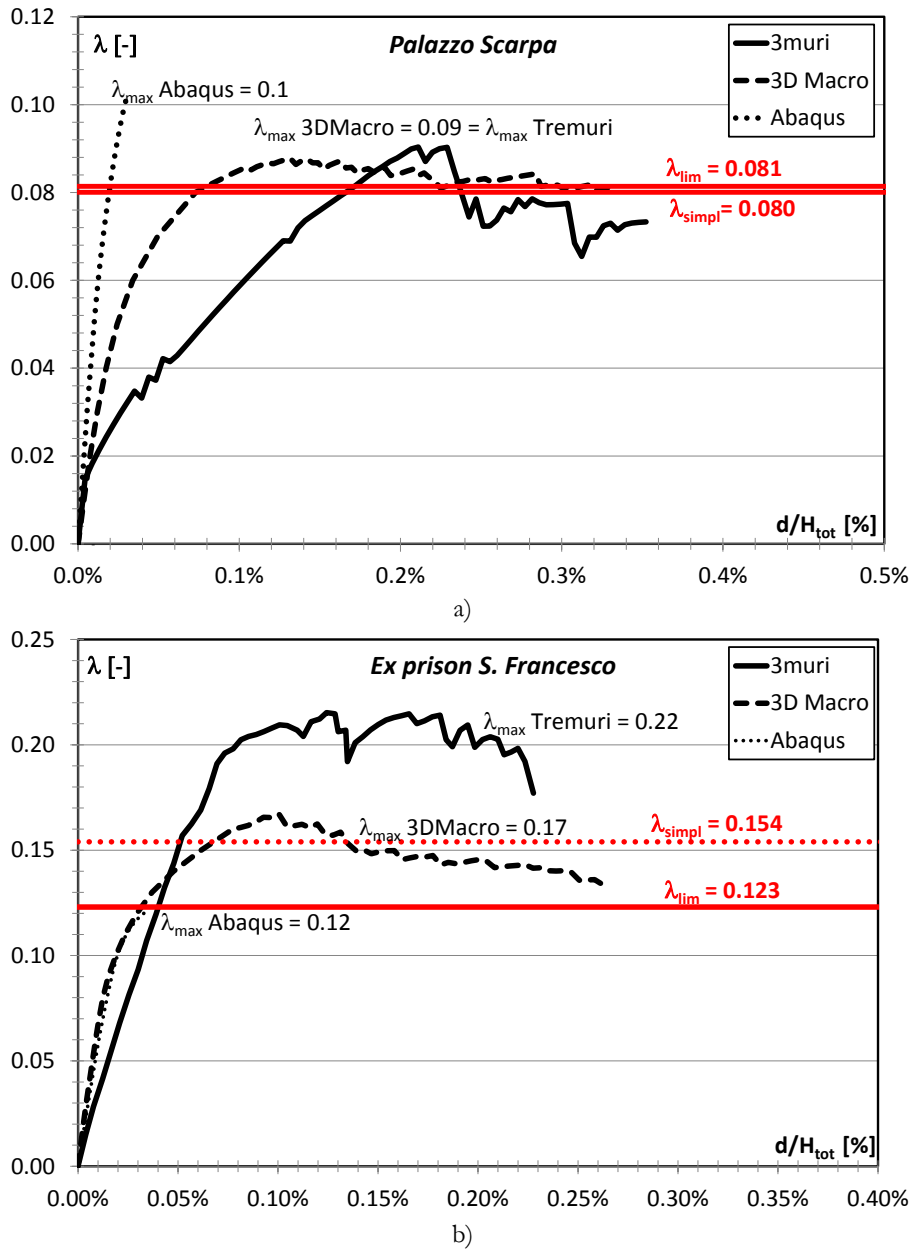
Figure 2.38   Comparison between simplified modelling - FE analysis − limit analysis for a) *Palazzo Scarpa***; b)** *Ex prison S. Francesco*
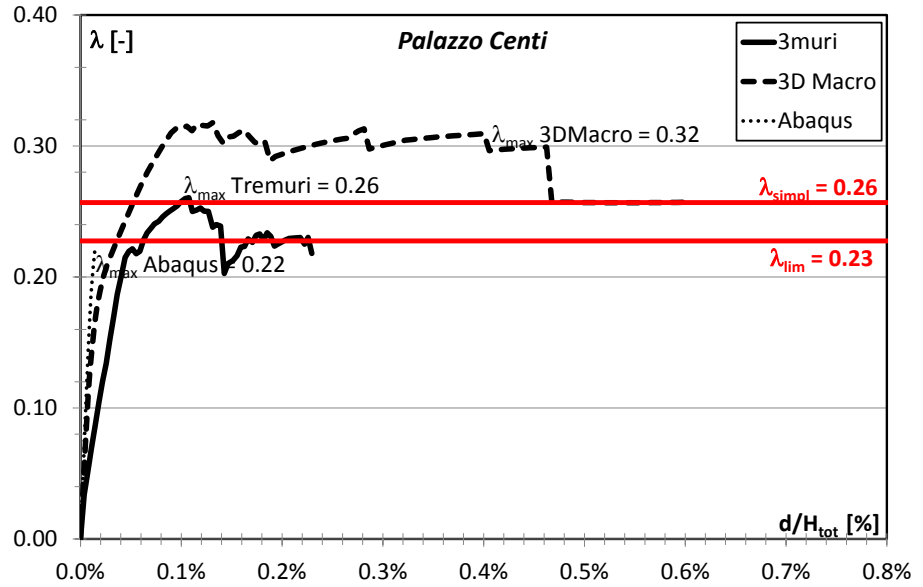
a)
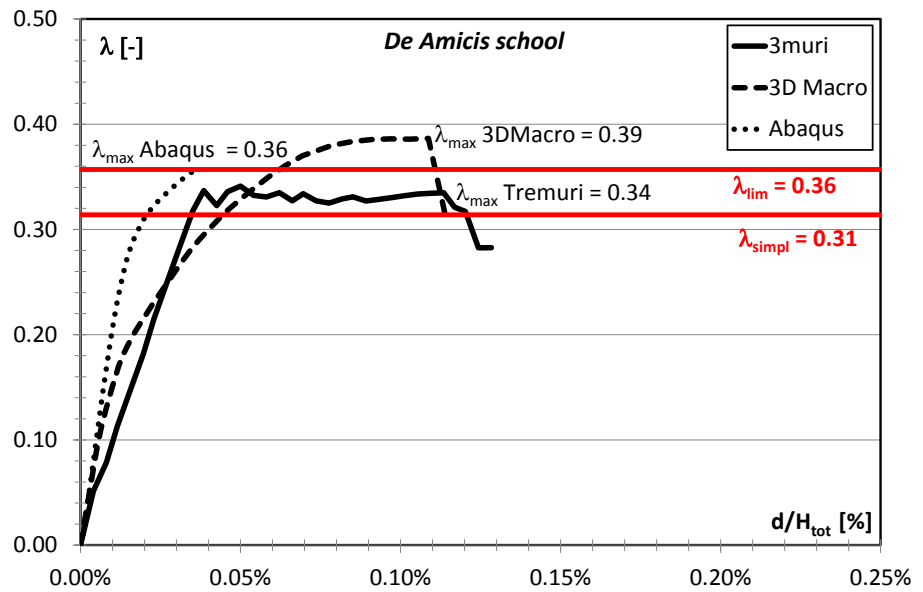
b)

Figure 2.39 Comparison between simplified modelling - FE analysis – limit analysis for a) *Palazzo Centi*; **b)** *De Amicis school*

Finally Figure 2.40 reports on the x axes the ratio $\frac{\sum B_i^2}{\sum B_i}$ /H_{tot} (indicated as B_{eq}/H_{tot}), and on the y axes the load multipliers obtained through simplified modellings, FE method, and limit analysis (considering the Eq. (1)). It can be noted that, with different approximations, all the approaches provided results allocated very close to the bisector line ($\lambda = B_{eq}/H_{tot}$). It suggests that, if the contribution of the spandrels is not so significant, the simplified formula could give a preliminary satisfactory measure of the seismic capacity, being noted only the geometrical characteristics of the wall.
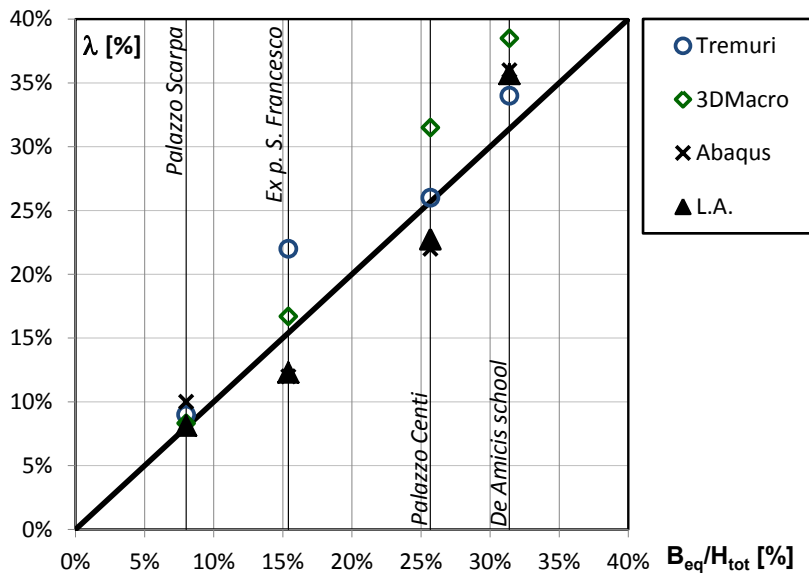
Figure 2.40 Non-linear analysis VS. Limit Analysis (L.A.): comparison of the horizontal collapse multipliers for the principal façades of the building case studies.

2.7 SIMPLIFIED ASSESSING OF THE SEISMIC CAPACITY OF THE WHOLE BUILDING

The seismic capacity of the whole building was estimated for two of the case studies described in section 2.2: the *Ex prison S. Francesco* and *Palazzo Centi*. The seismic capacity of the whole building, was computed as sum

of the in-plane seismic capacity of the single walls. The walls in X direction (evidenced in Fig. 2.41a and 2.42a) furnished the seismic capacity of the building in longitudinal direction, while the walls arranged in Y direction (evidenced in Figure 2.41b and 2.42b) gave the seismic capacity of the building in transversal direction.

The in-plane seismic capacity of each wall was calculated by means of a commercial user friendly code: CDSMa Win (Computer Design of Masonry). It performs push-over analysis of the structures implementing the equivalent frame modelling. A very easy and quick definition of the geometry is allowed by this code. The requested material properties are basically the same requested by the codes 3muri and 3DMacro (see section 2.3.2.1). However it is noted that CDSMa Win adopts the stiffness of the cracked elements, equal to 50% of the stiffness assigned by the user.

The capacity curves of the all the walls in X and Y direction are plotted in the graphs of Figure 2.43-2.46 , both in terms of base shear vs displacements of the control point, and in terms of load multipliers vs displacement divided the height of the portal frame. The capacity curve of each single wall in terms of, is also provided in Appendix A.

The simplified formula of Eq. (2) was applied to each wall and the values of λ_{eq} were found. The graphs of Figure 2.47and 2.48 provide, for each wall, the correspondence between the λ_{eq} (reported on the x axes) and the maximum load multiplier obtained from CDSMa Win (reported on the y axes). It can be noted that, except of a few cases, the points representative of each wall are located very near the bisector line ($\lambda_{max}=B_{eq}/H_{tot}$), in line with the results shown in the previous section.

Finally the capacity curves of the walls were summed to obtain the seismic capacity of the whole building. The graphs in Figures 2.49-2.50 show the capacity curves obtained from the sum, performed until the collapse of a first wall occurred.

The obtained "sum" capacity curves were adimensionalized, dividing the displacements by the total height of the walls, and the base shear by the sum of the weight of the walls. The adimensionalized curves are plotted in Figures 2.51 – 2.52. On the graphs also two horizontal lines are reported: one of them corresponds to the λ_{eq} of the façade; the other one corresponds to the mean of the values of λ_{eq} computed for each wall. First of all, it can be noted that the λ_{eq} of the façade is similar to the mean of the values of λ_{eq}. Then it is remarkable that the λ_{eq} is very close

to the λ_{max} of the whole building capacity curve. Small variance was found between the two load multipliers at most equal to 16%. It could be deduced that the simplified formula of Eq. (2) does not give just a preliminary good estimation of the in-plane seismic capacity of a wall, but it can be also very helpful to provide a first indication of the seismic capacity of a whole building.
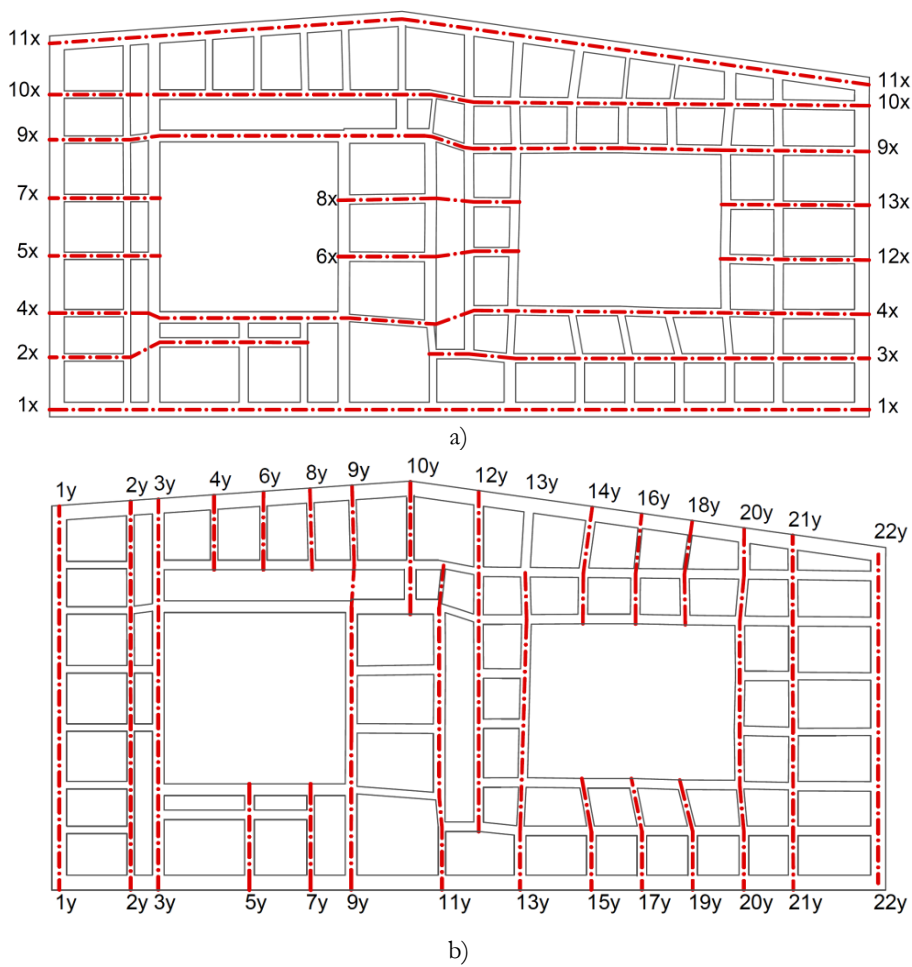
Figure 2.41: *Ex prison S. Francesco*: a) longitudinal walls; b) transversal walls

a)

b)
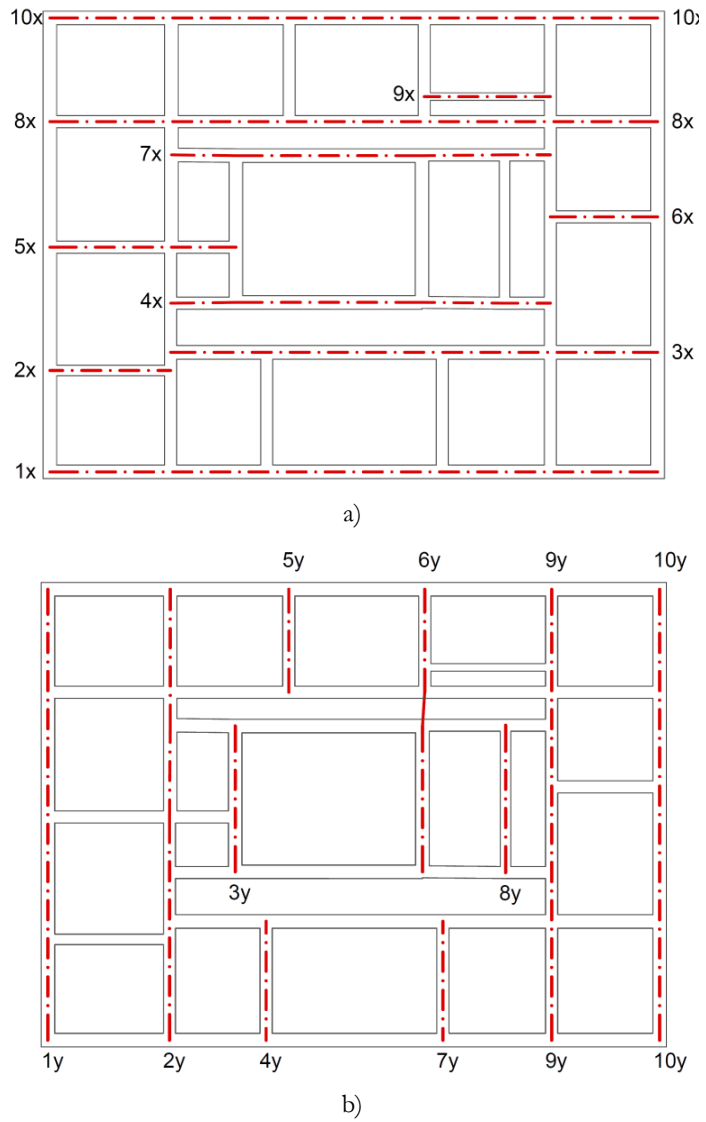
Figure 2.42 *Palazzo Centi*: a) longitudinal walls; b) transversal walls
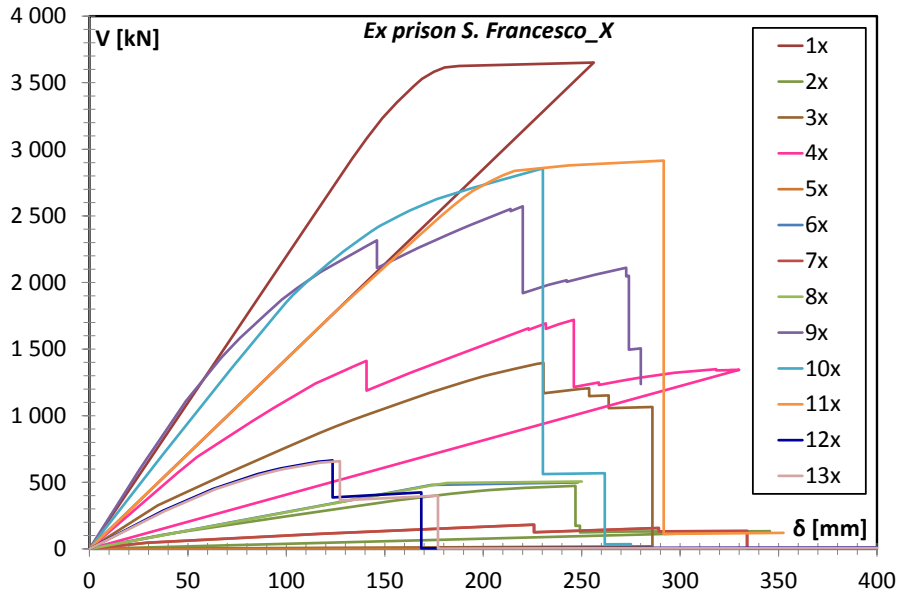
a)
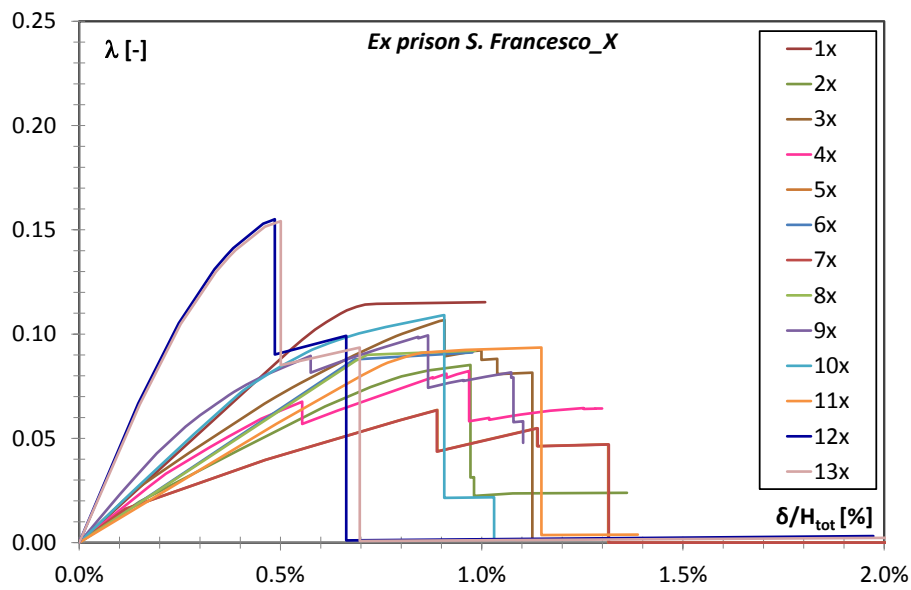
b)

Figure 2.43 *Ex prison S. Francesco*: capacity curves in terms of forces vs displacements of the walls in a) longitudinal direction; b) transversal direction
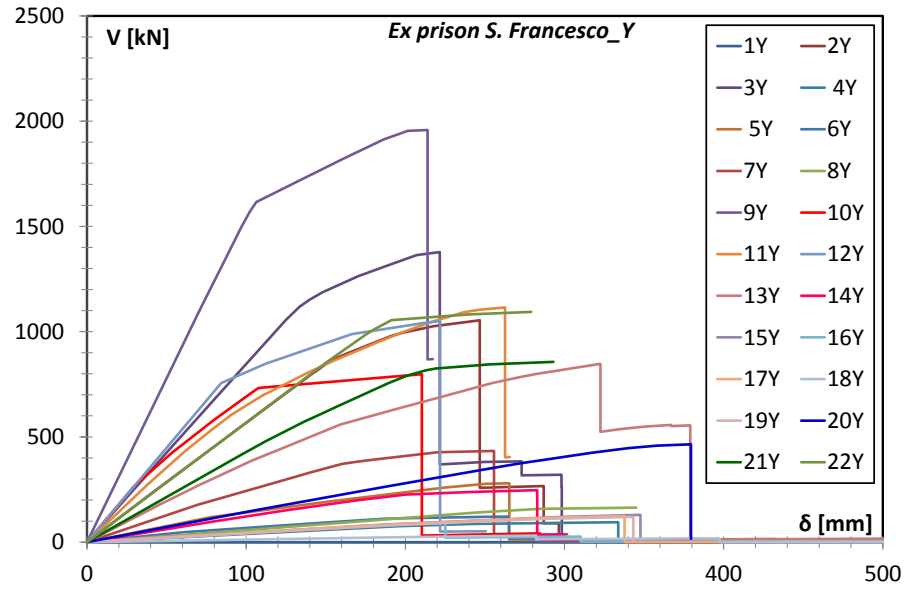
a)
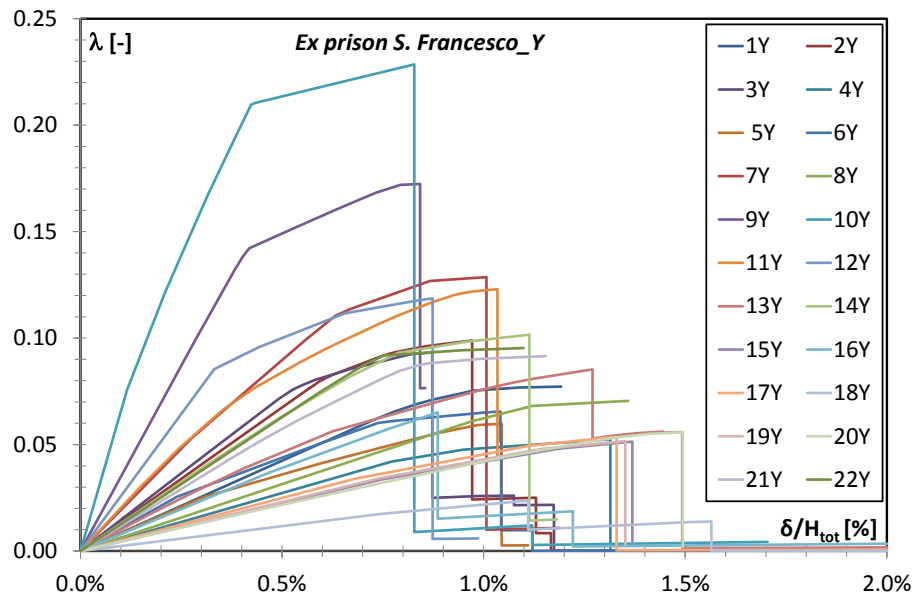
b)

Figure 2.44 *Ex prison S. Francesco*: capacity curves in terms of load multipliers vs displacements divided by total height of the wall in a) longitudinal direction; b) transversal direction
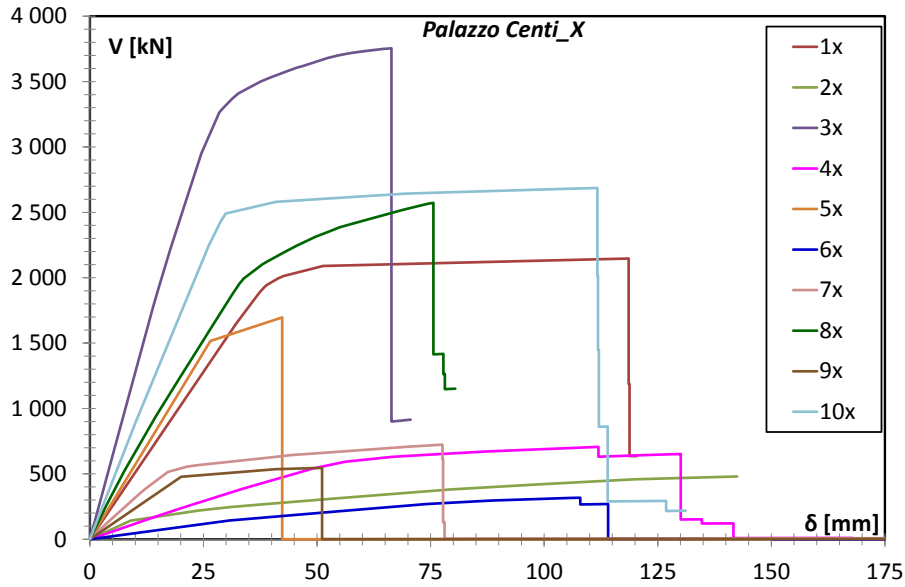
a)
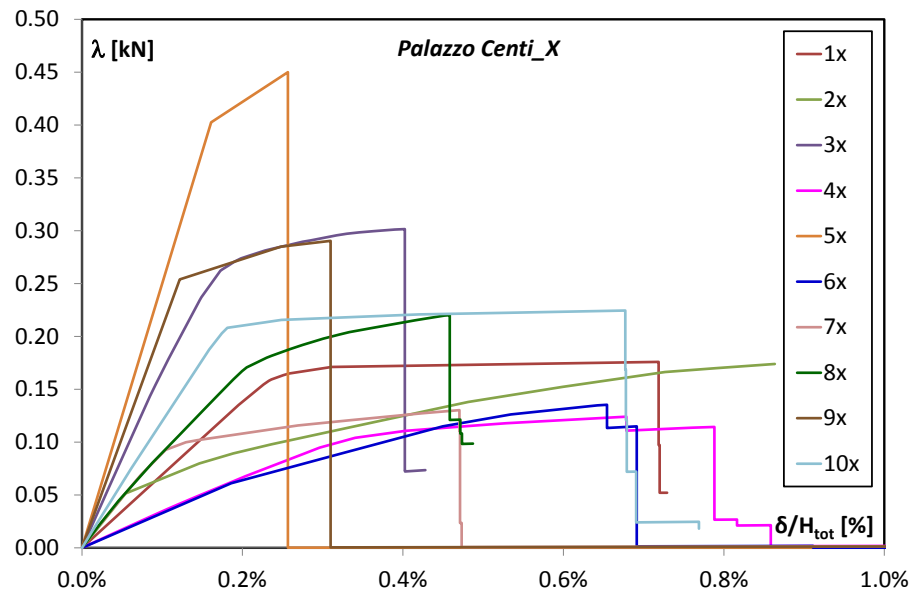
b)

Figure 2.45 *Palazzo Centi*: capacity curves in terms of forces vs displacements of the walls in a) longitudinal direction; b) transversal direction
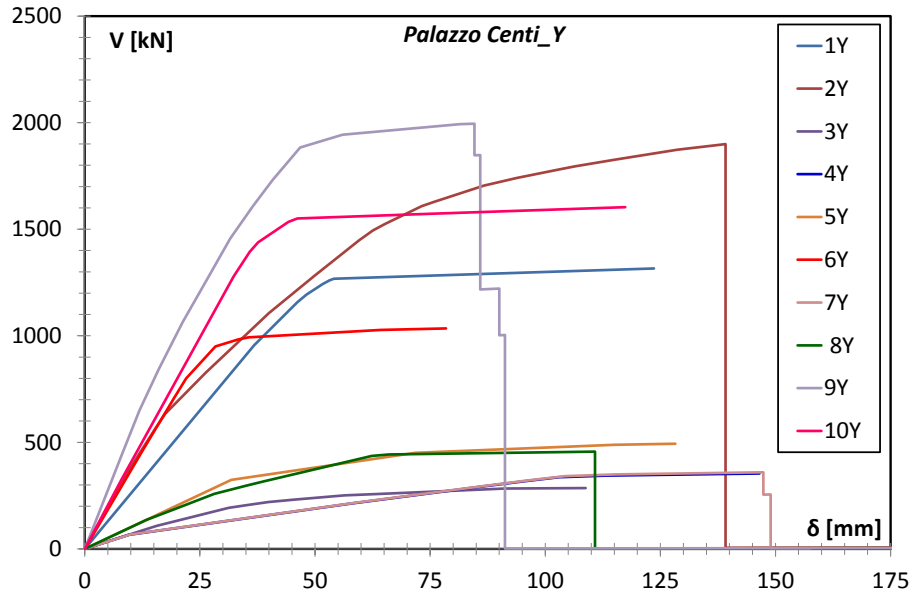
a)
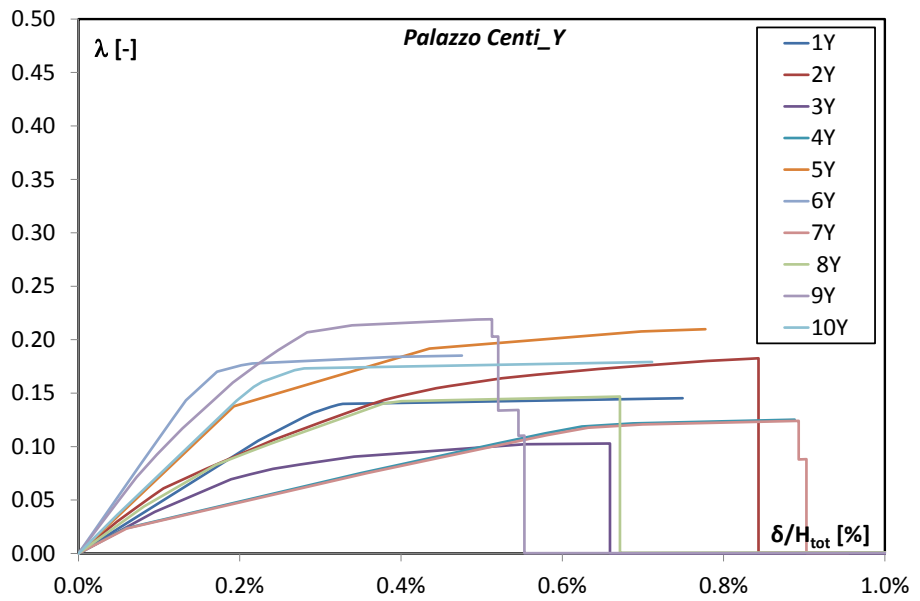
b)

Figure 2.46 *Palazzo Centi*: **capacity curves in terms of load multipliers vs displacements divided by total height of the wall in a) longitudinal direction; b) transversal direction**
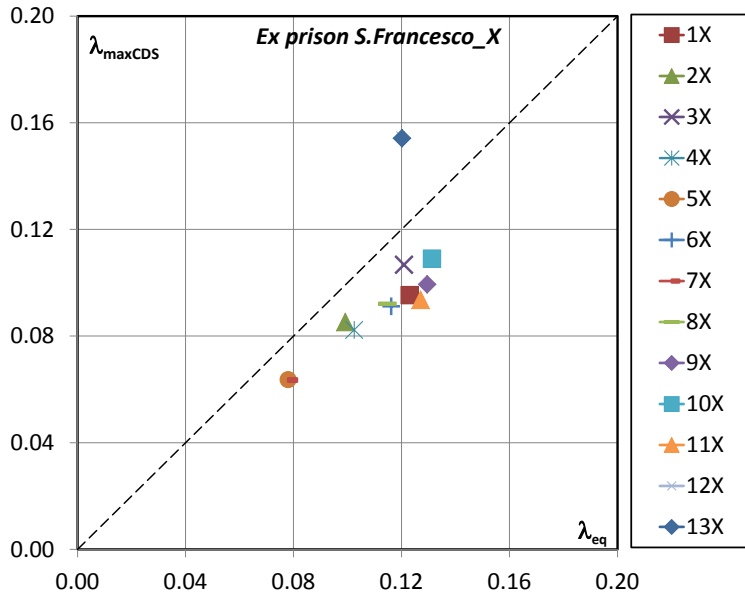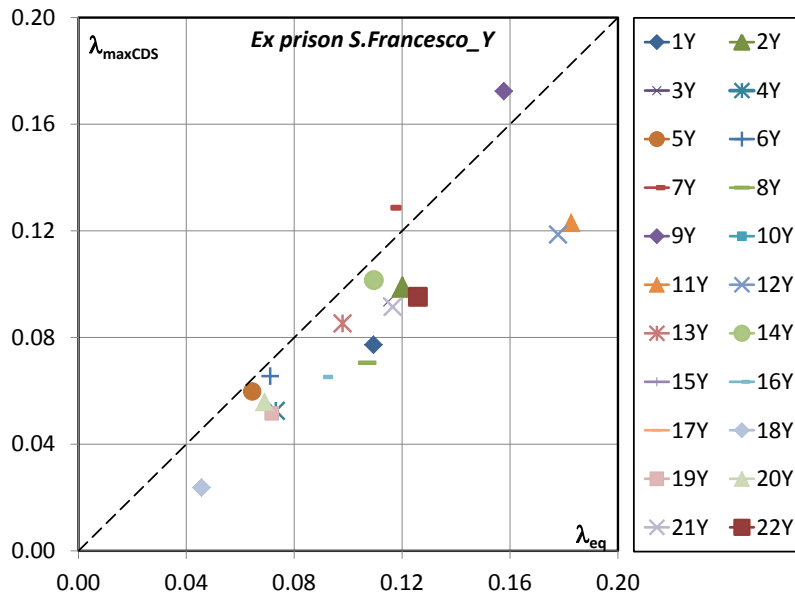
Figure 2.47 *Ex prison S. Francesco*: comparison between λ_{eq} and the load multipliers provided by CDS for each wall in a)longitudinal direction; b) transversal direction
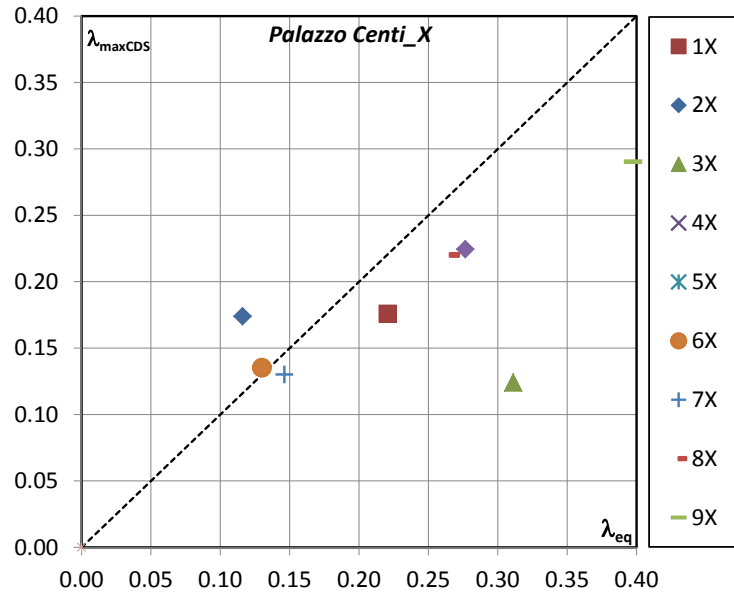
a)
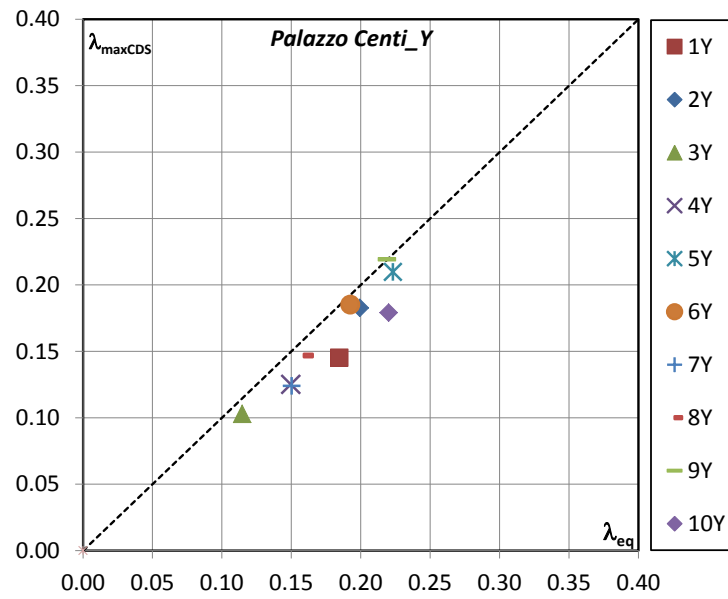
b)

Figure 2.48 Palazzo Centi: comparison between λ_{eq} and the load multipliers provided by CDS for each wall in a)longitudinal direction; b) transversal direction
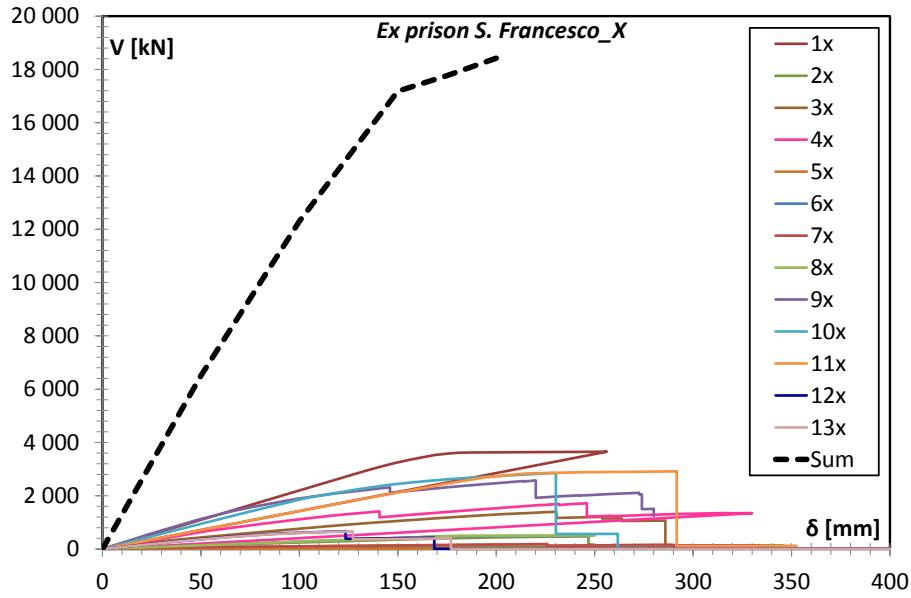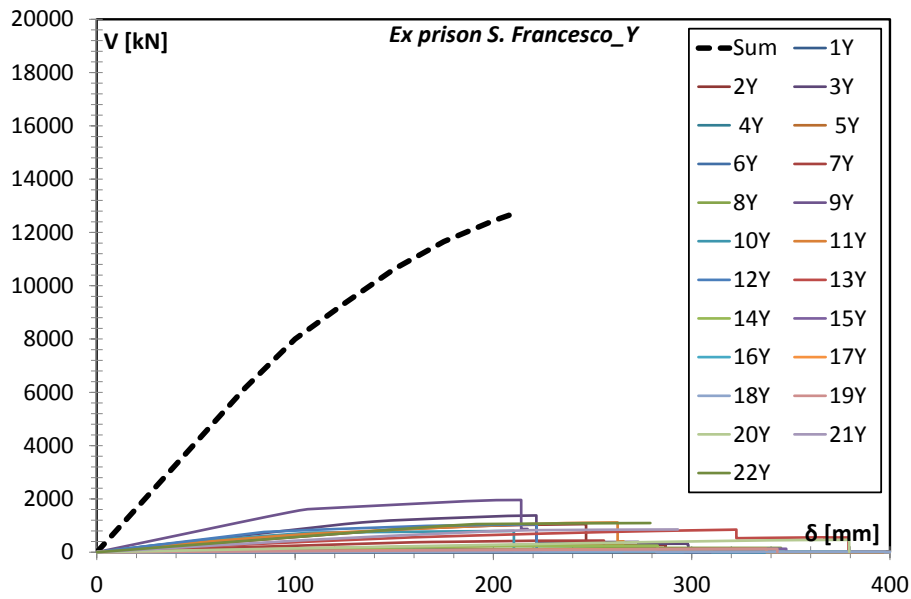
Figure 2.49 *Ex prison S. Francesco*: sum of the capacity curves of the walls in a) longitudinal direction; b) transversal direction
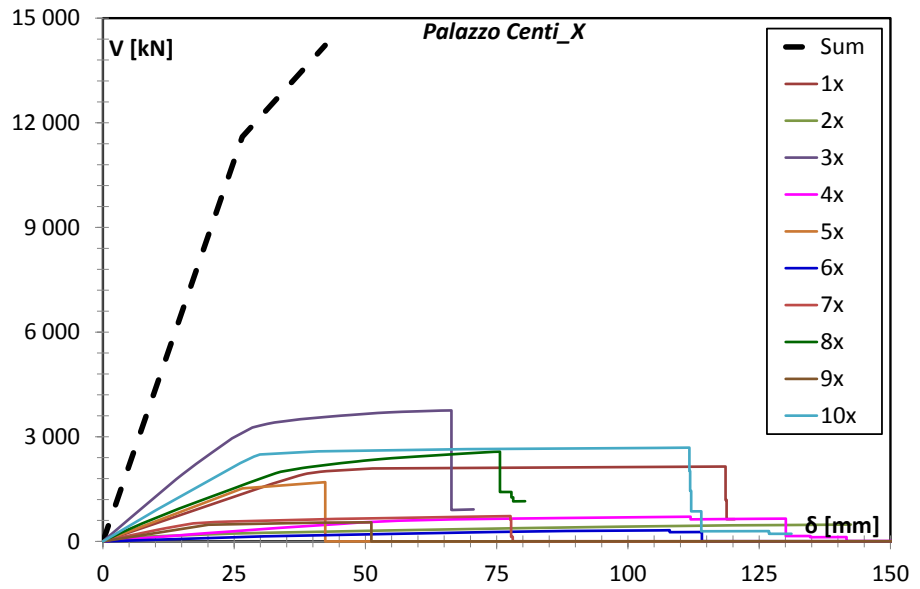
a)
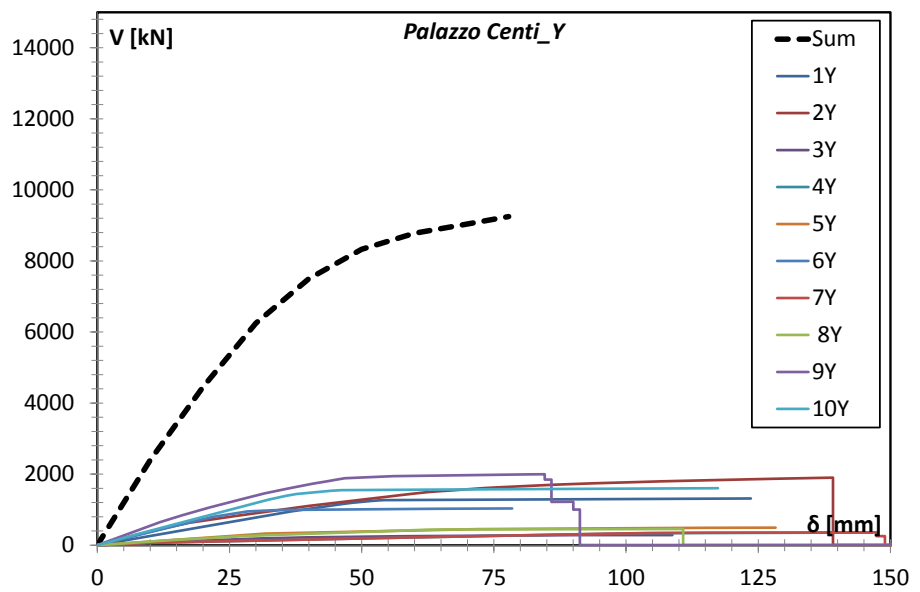
b)

Figure 2.50 *Palazzo Centi*: sum of the capacity curves of the walls in a) longitudinal direction; b) transversal direction
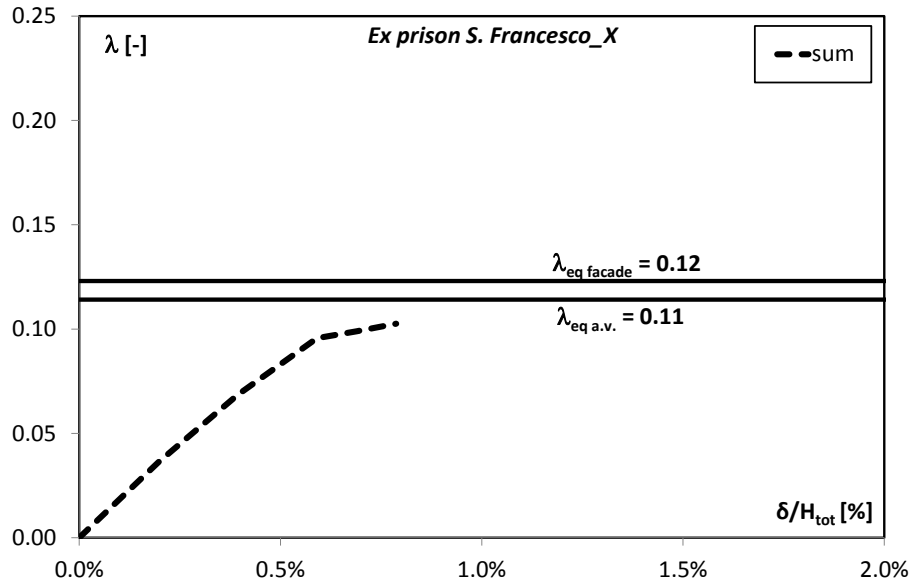
a)
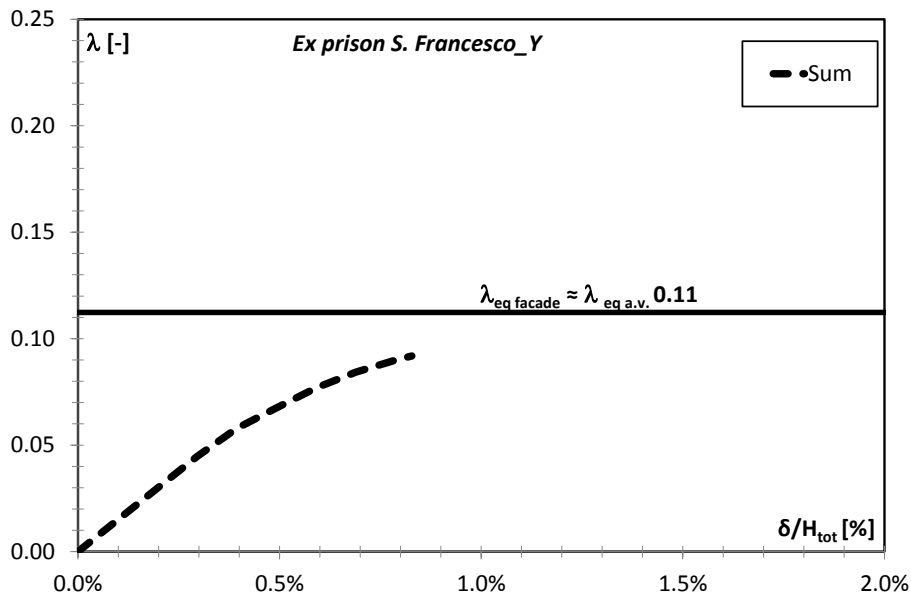
b)

Figure 2.51 *Ex prison S. Francesco*: sum of the capacity curves of the walls in in terms of load multipliers vs displacements divided by total height of the wall: comparison with limit analysis
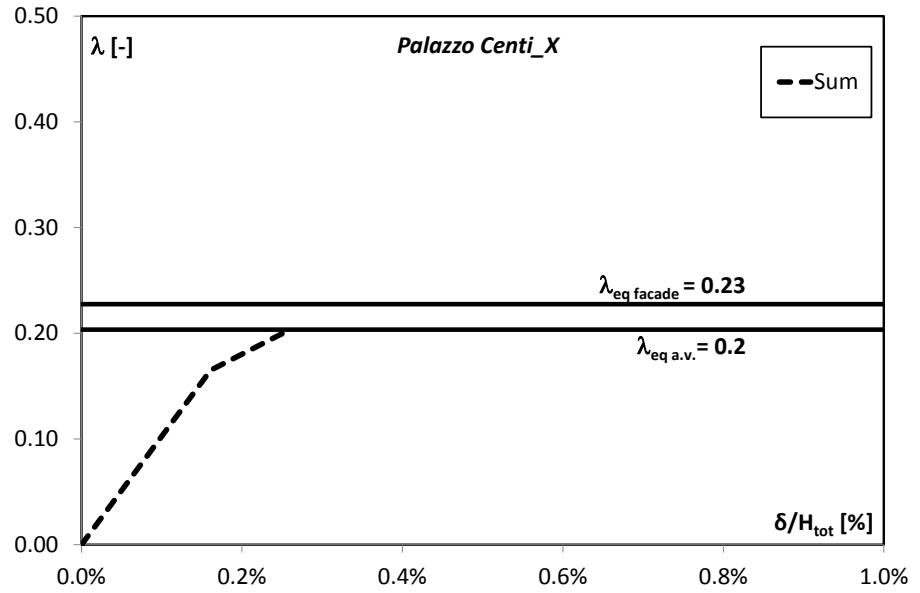
a)
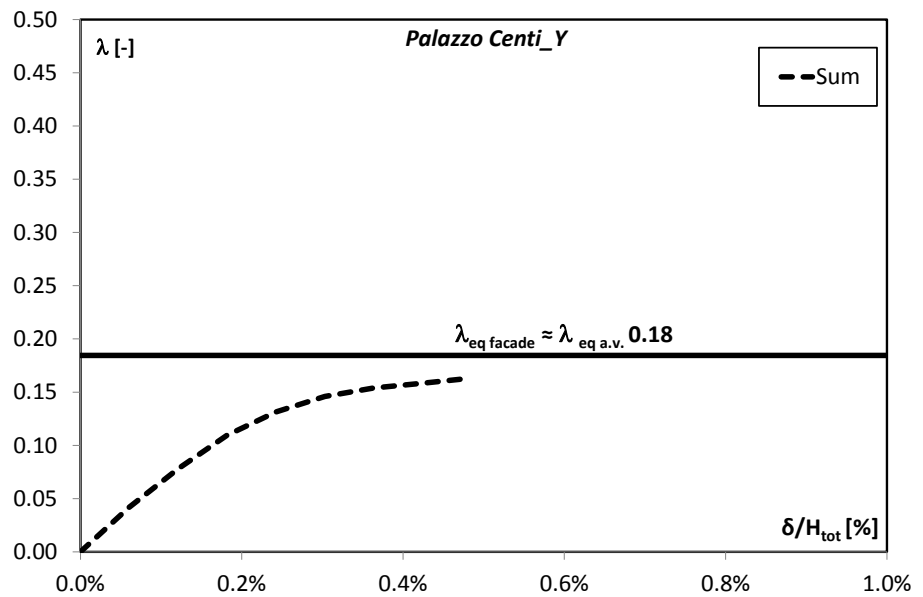
b)

Figure 2.52 *Palazzo Centi*: **sum of the capacity curves of the walls in in terms of load multipliers vs displacements divided by total height of the wall: comparison with limit analysis**

2.8 FINAL REMARKS

The in-plane seismic capacity of multi-storey and multi-bay masonry façades was assessed by adopting both push-over analysis and limit analysis approach. The push-over analysis was performed by using different modelling strategies: equivalent frame, macro-modelling and FE method. The different modelling gave different results both in terms of load multipliers and in terms of displacement. In detail small scatters (on average equal to 15÷20%) were found in terms of maximum load multipliers, while more significant variance was found in terms of ultimate displacement. Especially the FE analysis, probably due to numerical problems of convergence, was not able to predict a plastic tract of the capacity curve and then a reliable value of the ultimate displacement.

The seismic capacity obtained from the push-over analysis was "checked" by applying the limit analysis. A closed expressions was used corresponding to a frame mechanism of the wall. The collapse multipliers found through the limit analysis were in good agreement especially with the FE results. It follows that the limit analysis can be used as simple tool for checking the results of more complex analysis, often less manageable (pushover analysis), closely linked to the different modelling implemented by the computer codes.

A simplified formula for the evaluation of the collapse multiplier was proposed, for masonry walls having a small percentage of spandrel area. It was found that the simplified formula gives results in very good agreement with the closed expression and also with the maximum load multipliers obtained from the push-over analysis. It implies that a satisfactory measure of the seismic capacity of the masonry wall can be performed using the simplified formula, being noted only the geometrical characteristics of the wall.

The simplified formula was found also very helpful to provide a preliminary approximate estimation of the seismic capacity of the whole building. The collapse multiplier of the façade, as well as the average of the collapse multipliers of the walls which form the building, computed by means of the simplified formula, resulted very similar to the maximum load multipliers of the building, computed through the push-over analysis. Further investigations should be carried out in order to generalize this last result, verifying the reliability of the simplified formula on a larger sample of study.

3 MASONRY CHURCHES: DYNAMIC BEHAVIOR AND APPLICABILITY OF CONVENTIONAL ANALYSIS METHOD

3.1 INTRODUCTION

The seismic behavior of historical buildings, as it is known, represents a complex task due to many reasons: the limited knowledge of the mechanical properties of the materials, the highly non linear behavior of the masonry and the complexity of the geometrical configuration. In addition, regarding the masonry churches, the seismic analysis is further complicated by dynamic response of the structure. It cannot be accurately described considering merely the first vibration modes, as it is suitable for regular buildings. Due to the irregular-open plan layout and to the absence of connections among the structural elements, the first modes don't give a significantly higher contribution to the whole seismic response. Therefore the applicability of the conventional analysis methods, based on the predominance of the first natural modes, is questionable for this kind of monumental buildings.

The research group of prof. De Luca has studied this field for many years, adopting different analysis method as the finite element method and the limit analysis. In 1999 Mele and De Luca proposed an alternative approach to the seismic analysis of basilica-churches (Mele & De Luca 1999). It consisted of a two-step procedure: in the step 1 static and dynamic linear analyses of the whole church was performed; in the step 2 nonlinear push-over analyses of the single macro-elements, compared to the collapse loads derived from limit analysis, were carried out. Then, the strength demand on each single structural macro-elements, resulting from the 3D linear analyses, was compared to the macro-element ultimate strength capacity. The comparison demand vs. capacity was carried out for all transversal and longitudinal macro-elements of the church, allowing a direct assessment of the seismic safety level of the church. This approach was first applied to the church of S. Ippolisto Martire (Mele et al. 2003), a basilica type-church located in Atripalda (AV, Italy) and then to a sample study including ten churches located in

Naples (Brandonisio et al. 2008). More recently four churches damaged during the 2009 L'Aquila earthquake were also analyzed using the same procedures (Brandonisio et al. 2013). The dynamic analysis of the fourteen case studies showed the substantial difference between the dynamic behavior of the churches, compared with the regular buildings. Very small contributions in terms of participating mass were provided by each vibration mode and, as the result, the higher modes were taken into account. Therefore, in the following, this aspect of the seismic behavior of these churches will examined in detail.

3.2 CASE STUDIES

The sample study includes fourteen masonry churches characterized by basilica-type plan with three or five naves. The basilica plan is widespread in Italy and it can be found both in the churches of small town and in the big cathedral of the cities. Thus the fourteen case studies are quite different in terms of geometry and sizes and, consequently, they are representative of a wide range of masonry churches. Therefore this selection ensures a certain generality of the obtained results.

Except of one case study, the church of S. Ippolisto which is located in Atripalda (AV, Italy), the fourteen case studies were selected from two historical centers in Italy: Napoli and L'Aquila. Figure 3.1 shows the location of the churches inside of the two historical centers. As it can be observed in figure 2, nine churches are located in Naples and four in L'aquila. In detail, the churches located in Naples are: S. Giovanni Maggiore (indicated as SGM), S. Giovanni a Mare (SGMR), S. Paolo Maggiore (SPM), Sant'Agostino alla Zecca (SAZ), SS. Bernardo e Margherita a Fonseca (SBM), S. Maria in Monteverginella (SMM), S. Maria Vertecoeli (SMV), SS. Gennaro all'Olmo e Biagio Maggiore (SGO), S. Maria in Donnaromita (SMD). The other four churches located in L'aquila are: S. Giusta (SG), S. Maria di Collemaggio (SMC); S. Pietro di Coppito (SPC), S. Silvestro (SS).

In the following, a brief description of each church is given.
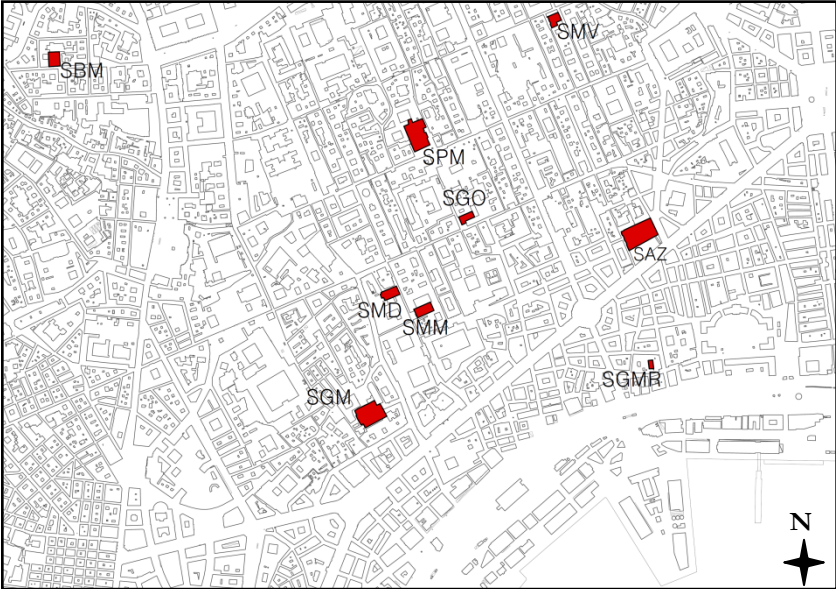
Figure 3.1 Location of the churches in a) Naples; b) L'Aquila

3.2.1   Brief description of the churches located in south of Italy

All the churches located in south of Italy (Fig. 3.2) are made of local materials. In detail yellow and gray tuff were used for the walls and piperno to define the arches and the angles.

The S. Giovanni Maggiore (SGM) church was built during the sixth century d.C., but it was significantly transformed over the centuries, in particular during the baroque epoch. Nowadays it presents a plan 66.1 long and 37.7m large, divided in three naves plan and with an apse having width

of 13.4m and length of 10.2m. The maximum height is equal to 26m. The thickness of the walls varies from 0.7 to 1.5m. The roofing covering the central nave is made of wooden trusses, while the lateral naves are covered by masonry domes as well as the transept. The roofing of the apse consists of a barrel vault.

The S. Giovanni a Mare (SGMR) church was built in the half of twelfth century and it is one of the most significant example of Roman architecture in Naples. The church has a rectangular plan with three naves. The overall width of the plan is 19.5m, its length is about 38.2 m and the maximum height is 13m. The walls are on average 0.8m thick. The roofing of the church consists of cross vaults on the naves, wooden trusses on the transept and barrel vault on the apse.

The San Paolo Maggiore (SPM) church was built at the end of the VIII century on the remains of the temple of the Dioscuri, dating back to first century a.D. . The church shows a Latin cross-plan, with three naves and a large transept characterized by a polygonal apse. Its overall dimensions are equal to 66.6m (length) x 37.8m (width of the three naves). The maximum height of the church reaches 36.2m. The width of the transept is equal to 51.6 m. The masonry walls are from 1 to 2 m thick. The roof structures consist of steel trusses with the exception of the elliptical vaults, covering the lateral chapels and the barrel vault covering the apse zone.

The construction of S. Agostino alla Zecca (SAZ) church started in the second half of thirteenth century ant it was finished at the beginning of fifteenth century. The basilica plan, 43.8m large and 65.8m long, has three naves and an apse of 20.7x13.9m. The maximum height of the church is equal to 37m. The walls have a thickness in the variable between 1 and 2.3m. A large barrel vault cover the main nave, while cross vaults cover the lateral naves.

S. Giovanni Maggiore
(SGM)

S. Giovanni a Mare
(SGMR)

S. Paolo Maggiore
(SPM)

S. Agostino alla Zecca
(SAZ)

SS. Bernardo e Margherita
(SBM)

S. Maria in Monteverginella
(SMM)

0 5 15 30m

S. Maria Vertecoeli   S. Gennaro all'Olmo   S. Maria in Donnaromita   S.Ippolisto
(SMV)   (SGO)   (SMD)   (SI)
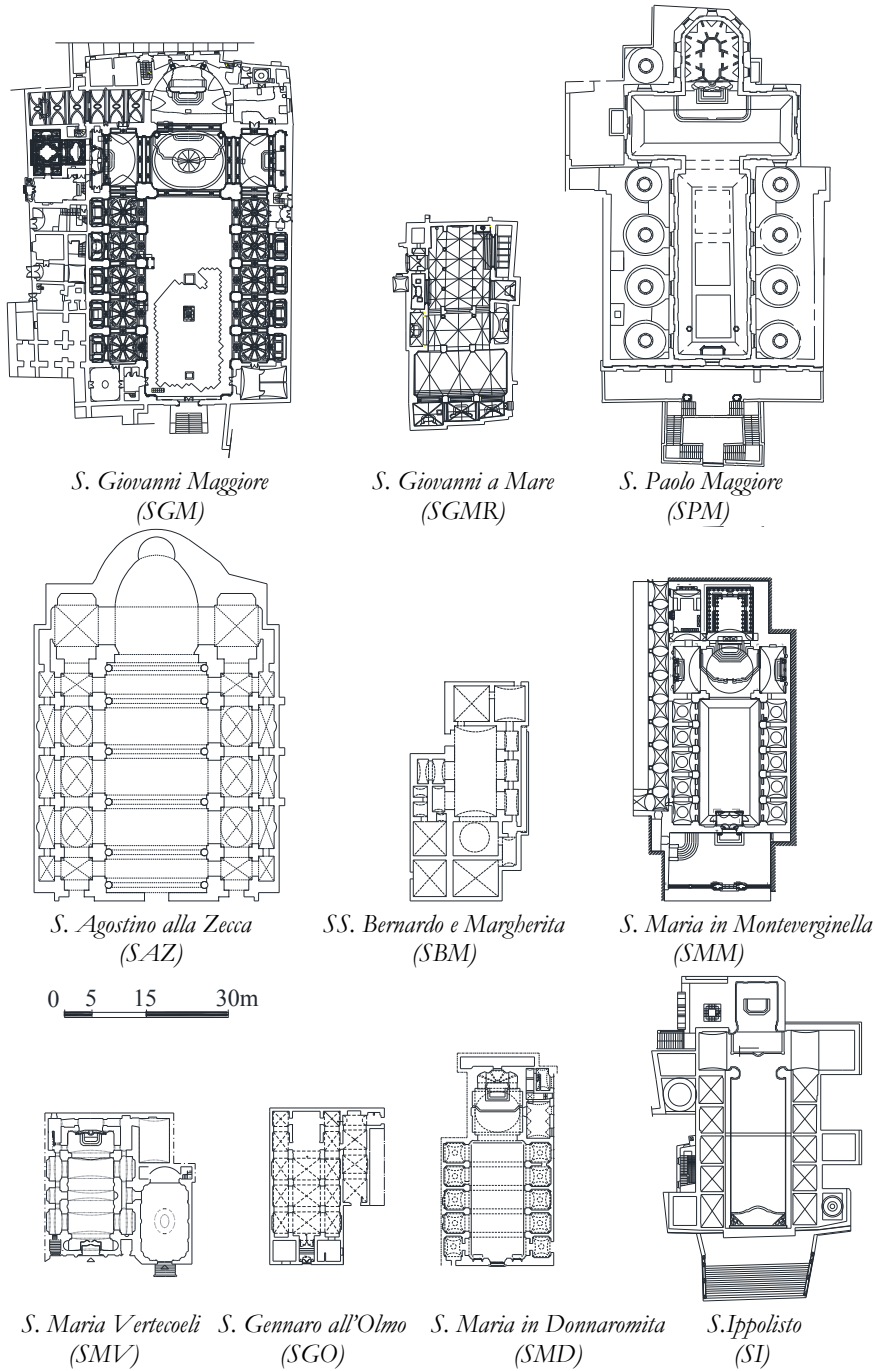
Figure 3.1 Plans of the case studies located in south of Italy

The basilica of SS. Bernardo e Margherita a Fonseca (SBM) was built during fifteenth century and it was completed at the beginning of sixteenth. This church is a single nave structure with a maximum height of 14m. The nave has a length equal to 40.2 and width equal to 20.3m. The walls are from 0.65m to1.8m thick. The roofing of the church consists barrel vaults on the nave with a dome on the transept.

The church of S. Maria in Monteverginella (SMM) was started in 1314, but its construction spanned over three centuries, until 1630, when it was completed. It presents a plan with only one nave and lateral chapels. The overall dimensions are equal to 22.8m (width) and 46.2m (length) and 21m (maximum height). The thickness of the walls ranges among 0.7m and 2.7m. Wooden trusses cover the central nave and a dome is installed on the transept.

The Santa Maria Vertecoeli church (SMV) was built in the second half of the XVII century and a century later it was enlarged. The current shape consists of two spaces similar in terms of sizes: the first (on the right) is the real church, the second one (on the left) is an oratory. The church shows a rectangular layout, 26m long x 17m large, characterized by three naves divided by massive masonry piers. The maximum height is 18 m and the walls are from 1 to 1.5 m thick. Both the main nave and the apse are covered with trusses, while the lateral naves with cross vaults.

The church of S. Gennaro all'Olmo (SGO) was built during the seventh century and it experienced more than one baroque restorations, before the final restoration works in the recent years. The plan presents a vestibule approximately 4.5m large, and inside it is divides in three naves. The church has overall width equal to 21m,overall length equal to 38.7 and maximum height equal to 14m. The thickness of the walls is in the range 0.5÷0.8 m. The roofing is made of cross vaults on the main nave and of ribbed vaults on the lateral ones.

The church of S. Maria in Donnaromita (SMD) was first built during the fourteenth century, but it was significantly transformed in the sixteenth-seventeenth century. It consists of a single nave, 19.6m large and 23.4m long, with lateral chapels and a predominant chancel 13m long. The maximum height is equal to 21m and the walls are from 0.5 to 1.3 thick. The transept is covered with a dome, while trusses and ribbed vaults cover respectively the nave and the lateral chapel.

The S. Ippolisto Martire Church (SI), located in Atripalda was built between 1584 and 1612 on a previous basilica of the IV century AD. In the XVIII century several additions and restorations strongly

transformed the church. The plan shows the typical basilica layout with the main nave, the two lateral aisles, the clerestory and the transept. The nave is 11.6 m large, 28 m long. The chancel has a rectangular plan, 8.8 × 11.6 m. The masonry wall thickness approximately varies between 1.0 and 1.2 m. In 1980, the Irpinia earthquake struck the church and destroyed the transept, which was surmounted by a heavy reinforced concrete roof system, built after the damage occurred following a previous earthquake, in 1930. Other major damages occurred during the 1980 earthquake, namely the collapse of the third order of the bell tower and the separation of the facade from the longitudinal walls, which determined the collapse of the first vault of the west aisle. The roof of the nave is king post timber roof, while the lateral aisles are covered by quadripartite vaulting systems with four diagonal ribs.

Further informations on these churches and their numerical investigations are provided in Brandonisio 2007, Brandonisio Brandonisio et al.2008.

3.2.2 Brief description of the churches located in L'Aquila

Figure 3.3 plots the architectural plans of the L'Aquila churches.

The church of Santa Giusta (SG) was built in the first decades of the XIV century on the ruins of pre-existing masonry walls, according to a basilica layout, with a central nave and lateral chapels. The overall dimensions of the church are 21.9m (width) x 51.6m (length) and 14m as maximum height. The bearing masonry structure is realised by using the sack masonry arrangement, typical of L'Aquila region, with the external leaves made of small calcareous stones and the filling core made of calcareous stones and hydraulic mortar. The thickness of the walls varies between 0.9 and 2.5m. The triumphal arch and its pillars are made of calcareous freestone. The roof structure is made by wood trusses.

Santa Maria di Collemaggio (SMC) church was built in the XIV century. It was greatly modified in the Baroque age, but presently, following a complete dismantlement of the Baroque decorations that occurred in the 1950s, it appears in its native aspect. The building has a basilica plan with central nave, lateral aisles, transept and apse. The plan is 97.2m long and 29.6m large, while the maximum height is equal to 19m. The bearing walls, from 1.1 to 2.6 thick, are made of the typical sack masonry of L'Aquila. Only the most stressed structural elements, such as triumphal arches and pillars, are realised in freestone. The roof structure is made of

wooden trusses for the central nave, and of masonry vaults for the remaining parts.

The San Pietro di Coppito (SPC) church was built at the end of the XIV century. It has an atypical layout consisting of: one almost square nave (20x21m), with a small lateral aisle along one side only; a rectangular transept (20x27m) larger than the nave; an apse constituted by three polygonal chapels. Similarly to the previous case, the masonry walls (from 0.75 to 2 m thick) are realized in sack masonry and free stone, while the roof structures are wooden trusses, with the exception of the cross vaults covering the apse chapels.

The San Silvestro church (SS), was built in the XIV century. It consists of three architectural spaces: the church, the bell tower and the lateral chapel. The church has a typical basilican plan, with three naves, and apse characterized by polygonal chapels. The bearing walls, approximately 0.8 m thick, are made of sack masonry or free stone, while the roof is supported by wooden trusses, with cross vaults only covering the apse zone. The sizes of the basilica are in the middle among the previous case studies: the overall dimensions are equal to 60.2 m in

| S. Giusta (SG) | S. Maria di Collemaggio (SMC) | S. Pietro di Coppito (SPC) | S. Silvestro (SS) |
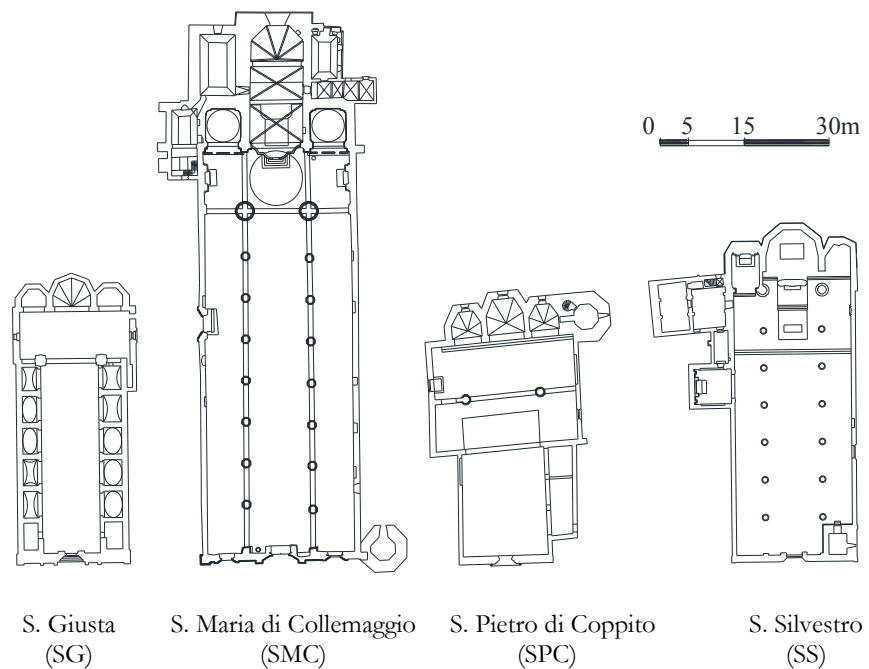
Figure 3.2 Plans of the case studies located in L'Aquila

length and 22.3 m in width. The maximum height reaches 19.5 m in correspondence of the main nave.

Further informations on these churches and their numerical investigations are provided in Brandonisio et al. 2013.

3.2.3 Dimensional sub-groups

As it can be observed in fig. 3.2 and 3.3, especially the churches in Naples, have a quite complex geometry. Therefore the architectural plan of the churches was linearized, in order to simplify the subsequent modeling, without significantly altering the structural characteristics of the building (columns and walls sections). The linearized plans of the fourteen case studies were then grouped into three classes, according to their size. The three dimensional sub-groups include:

1) churches of small size (SGO, SGMR, SMV, SBM, SMD), characterized by maximum length (L_{max}) in the range 21÷41m, maximum width (B_{max}) on average equal to 21m and maximum height on average of 15m. The total weight of this first sub-group varies among 20 MN and 50 MN.

2) churches of intermediate size (SG, SI, SMM, SS, SPC) with maximum length in the range 46÷60m, average width of 25m and average height of 17m. The whole weight is in the range 50÷80 MN.

3) churches of large size (SGM, SMC, SAZ, SPM) with maximum length variable among 66m and 97m, medium width of 33m and average height of 25m. The weight of these cases studies is significantly higher, varying in the range 145÷290 MN.

Table 3.1 summarizes the main dimensions and the weight of each church. The weight is divided into two contributions: weight of the walls (W_w) and weight of the roofing (W_r).

a) Churches of small size

b) Churches of intermediate size

c) Churches of large size
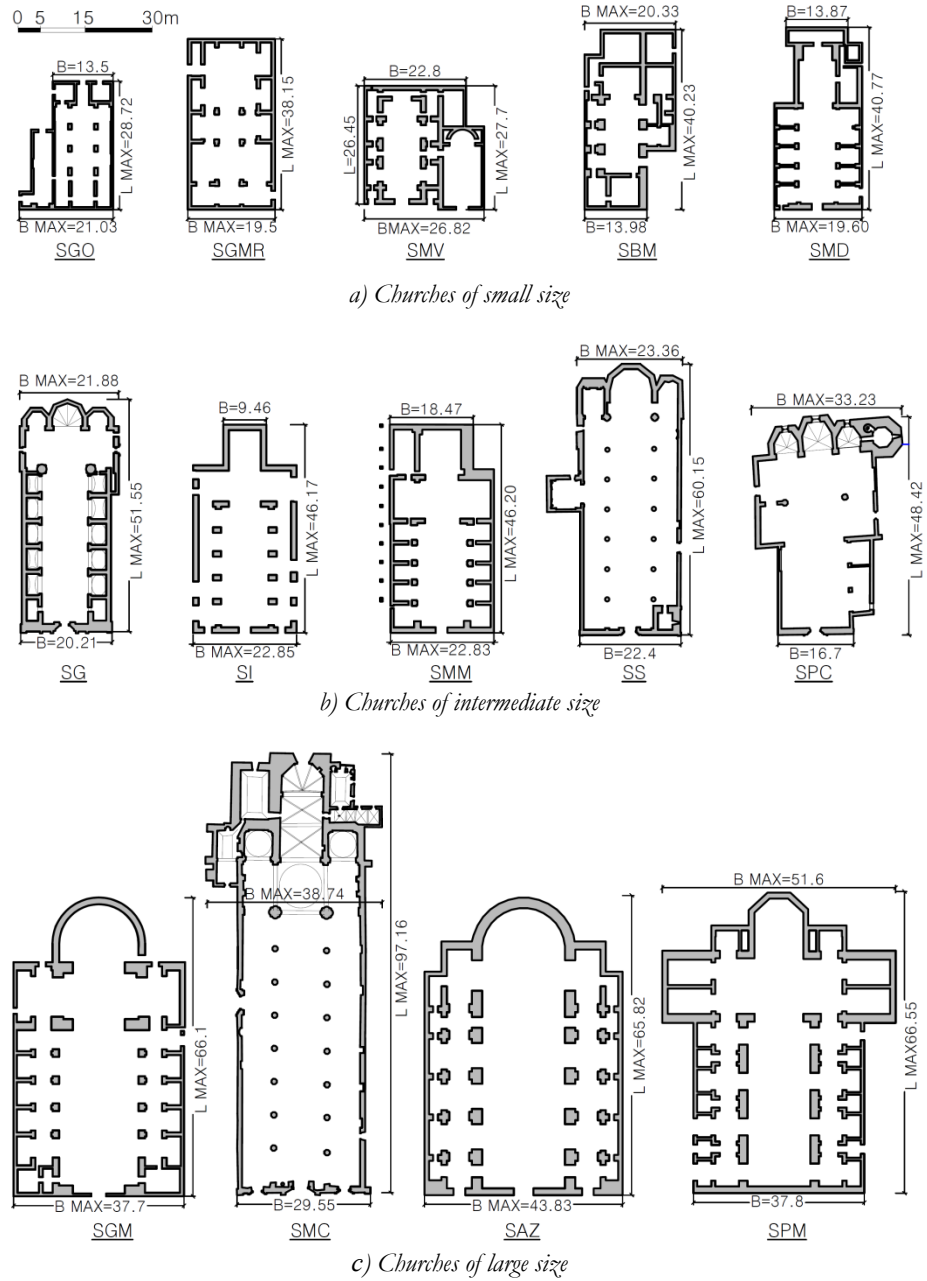
Figure 3.3 Linearized plans of the case studies

Table 3.1 Geometric characteristics and weight of the masonry churches

Churches	B_{max} [m]	L_{max} [m]	H_{max} [m]	W_W [MN]	W_R [MN]	W_{TOT} [MN]
SGO	21.03	29	14	16.2	4.3	20.5
SGMR	19.5	38	13	24	6	30
SMV	26.82	28	15	30	8	38
SBM	20.33	40	14	41	9.6	50.6
SMD	19.6	41	21	32.8	7.7	40.5
SG	21.88	52	14	57.3	2.5	59.8
SI	22.85	46	18	43	7	50
SMM	22.83	46	21	57.4	12.6	70
SS	23.36	60	16.6	77	2.3	79.3
SPC	33.23	48	15.8	76	1.7	77.7
SGM	37.7	66	26	160	20	180
SMC	38.74	97	19	139	5.6	144.6
SAZ	43.83	66	37	230	60	290
SPM	51.6	67	33	160	18	178

It is noted that the roofing provides a marginal contribution for all case studies. The histogram in figure 3.5 reports, on the x axis, the case studies grouped into the three sub-groups and, on the y axis, the total weight of the churches, distinguishing the contribution of the walls and of the roofing. The percentage of the roofing weight on the total, is also indicated and it clearly shows that, in this kind of structure, often for the most part covered by wooden trusses, the most of the weight is provided only by the walls and, the roofing, just in four case studies (SGO, SGMR, SMV, SAZ) reach percentage higher than 20% of the total weight.
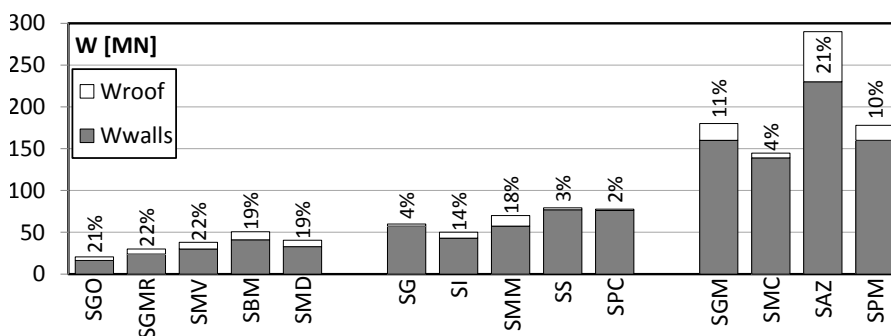
Figure 3.4 Total weight of the case studies and percentage of the roof weight

3.2.4 Geometrical parameters

Starting from the global dimensions of the churches, some geometrical parameters were evaluated. These parameters roughly account for some structural properties providing a first simplified assessment of the structural behavior of the churches. The ratios B/L_{max}, H/L_{max} and H/B, respectively accounting for the plan compactness and the minimum and maximum slenderness, were computed and they are given in the histogram of figure 3.6a. The ratio B_{max}/L_{max} is on average equal to 0.56, and only for the church of SGO and SMV it reaches values higher than 0.7. It proves an uniform distribution of the masses for the most of the case studies. The minimum slenderness H/L_{max} is in the range 0.3÷0.55. The ratio H/B is on average 0.73. It is significantly higher for the church of SMD, characterized by a maximum slenderness equal to 1.07.

Another parameter, useful to evaluate the efficiency and the bearing capacity of a masonry structure, is the ratio A_w/A_{tot} between the total footprint area of the walls (A_w) and the building gross floor area (A_{tot}).
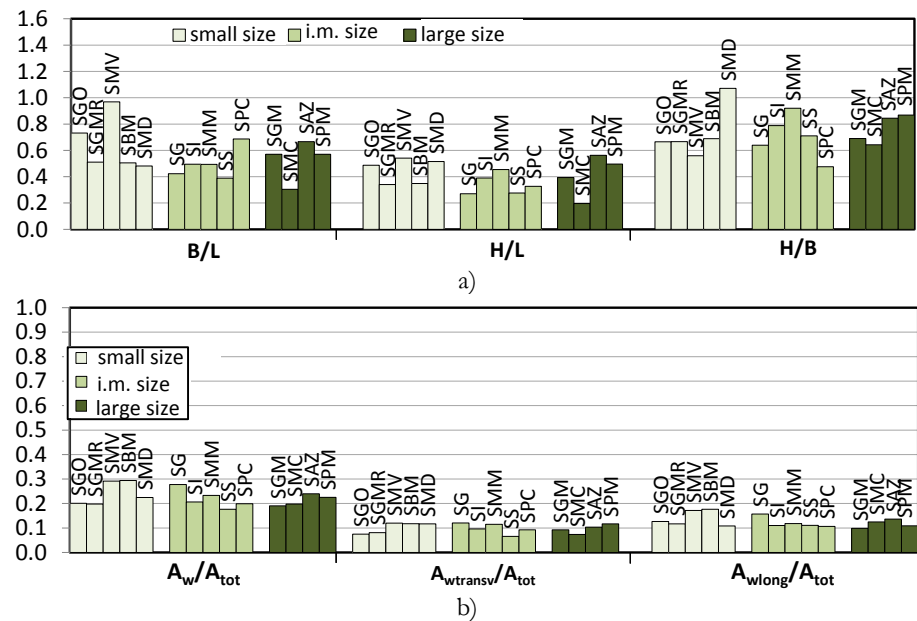
Figure 3.5 Geometrical parameters: a) compactness, minimum and maximum slenderness; b) area ratios

The histogram in fig 3.6b shows, on the right side, this ratio computed for each case study. As it can be observed, it is almost equal to 20% for

all the case studies except of SMV, SBM, SG (28-29%), due to the larger thickness of the walls. If these values are compared to those computed by Rondelet, in his treatise (Rondelet 1807), for some famous ancient monuments such as the Basilica of S. Maria del Fiore (20%), the Pantheon (23%) and Hagia Sofia (23%), it is clear that the sample study respects the rules of the good practice.

Additional geometrical parameters are reported in the histogram of fig. 3.6b: the ratio between the area of masonry walls in each principal direction, and the whole plan area ($A_{w,transv}/A_{tot}$ and $A_{w,long}/A_{tot}$). This ratios are related to the structural behavior under lateral loads and they provides a measure of the shear strength and stiffness of the building in the two directions. The seismic codes suggest minimum values for such parameters, as a function of the number of stories and of the seismic zone. According to the EC8 such limitation is 2÷5%, while more restrictive limitations, equal to 10%, are suggested by Lourenço et al. (2005), for historic building in high-seismicity zone. Considering the value suggested by Lorenço, it can be observed that approximately all the churches satisfy the limitation in both directions, except for the churches of SGO, SGMR, SS, SMC in the transversal direction.

3.3 MODAL ANALYSIS

The modal analysis provides the dynamic properties of the structure: periods of vibration, modal shapes and in particular it gives the contribution provided by each vibration mode to the total dynamic response of the structure. The contribution is estimated by means of two factors: 1) the participation factor which defines the contribution of a modal shapes on the final deformed configuration; 2) the effective mass which represents the mass involved in each vibration mode. The expressions of the two factors are reported below (Clough and Penzien 1975).

$$\Gamma_i = \frac{\Phi^T M 1}{\Phi^T M \Phi} = \frac{\sum m_i \Phi_i}{\sum m_i \Phi_i^2} \; ; \; M_e = \frac{(\sum m_i \Phi_i)^2}{\sum m_i \Phi_i^2}$$

Dividing the effective mass by the total mass of the structure, the modal participating mass ratio is found, in the following indicated as M_p.

The structure of regular buildings vibrates predominantly in a single mode. Consequently these modal factors assume significant values just

for the first modes. Therefore for determining design values of forces and deformations, three vibration modes in each lateral direction are nearly always sufficient for low- and medium-rise buildings (Rosenblueth 1981). Based on the predominance of the first modes, the conventional simplified analysis methods traditionally has replaced the dynamic approach with the static one, which uses equivalent lateral forces generally distributed proportionally to the mass or according to the main vibration mode of the building. For a regular building the results provided by the two different approaches are basically similar.

The hypothesis underlying the static approach: the predominance of the first modes, is rarely verified for masonry churches, as it has been highlighted in the Introduction. In the following the modal analysis of the sample study is illustrated. As it has been described, the sample study is representative of a great variety of churches, in terms of size and geometry. Therefore, the modal analysis performed on this sample provides a quite general results on the dynamic behavior of masonry churches.
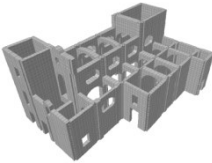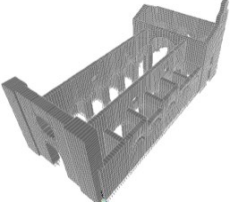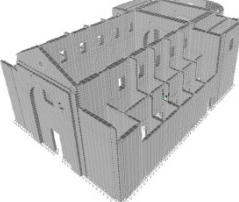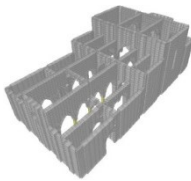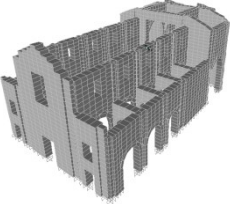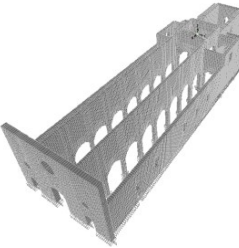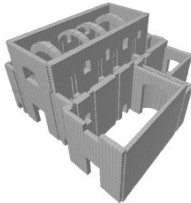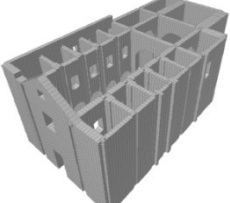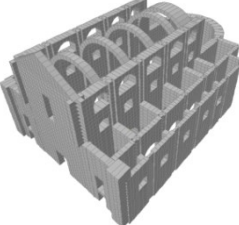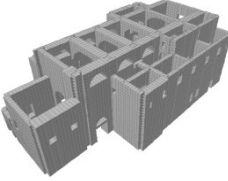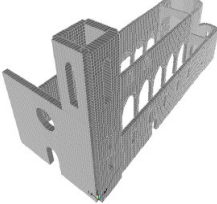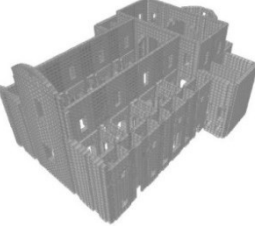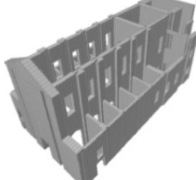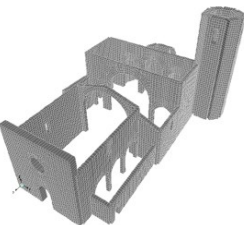
3.3.1   FE models

The modal analysis of the fourteen case studies was performed using finite element models. The FE models were realized by using the software SAP 2000 and they are shown in Table 3.2. The masonry walls were modelled by means of quadrilateral four-node elements, while frame were used, in some cases, for the columns of the nave. The number of the elements is provided in Table 3.3.

The seismic masses involved in the modal analysis are basically the masses of the walls that support the churches in fact, as said above, the weight of the roofing is negligible against the weight of the walls. Moreover the roofing of each case study consists of wooden trusses and/or masonry vaults, which give a negligible contribution to the stiffness of the whole complex. For these reasons the roofing of the churches were not taken into account in the FE models.

All the models were performed as a fixed base models, assuming a rigid ground foundation. Regular interlocking between the masonry walls was assumed. Although this assumption is often not realistic, this issue is not taken into account, in order to consider the dynamic behavior in general condition and not in singular cases.

Table 3.2 FE Models

Churches of small size	*Churches of intermediate size*	*Churches of large size*
SGO	SG	SGM
SGMR	SI	SMC
SMV	SMM	SAZ
SBM	SS	SPM
SMD	SPC	

As reported in the previous section, the churches in Naples are mainly made of tuff, while the churches in L'Aquila of sack masonry. However the same values of mechanical properties were used for all case studies, in order to compare the results, pointing out the effect of the geometry on the dynamic behavior. The poorest masonry, the L'Aquila masonry, was considered, assuming the following mechanical characteristics, according to existing tests of similar masonry (Capecchi et al. 1990): Young's modulus E = 1000 MPa; Poisson modulus ν=0.2, unit weight γ = 19 kN/m³.

Table 3.3 Number of shells and nodes of the FE models

Church	n° Frame	n° Shell	n° nodes
SGO	-	7325	7847
SGMR	8	5924	6401
SMV	-	7900	8343
SBM	-	11525	12177
SMD	-	10252	10691
SG	-	12828	13411
SI	-	5047	5414
SMM	-	16434	16924
SS	-	15172	16077
SPC	-	12561	12760
SGM	-	13966	14516
SMC	-	24414	25611
SAZ	10	9307	10017
SPM	-	12349	13387

3.3.2 Modal analysis results on one church of each sub-group

In this section the results of the modal analysis are described in detail with regard to one case study for each subgroup. In the following, the dynamic properties of all sample study will be illustrated.

The case study selected from each sub-group are: S. Maria Vertecoeli (SMV), S. Pietro di Coppito (SPC) and S. Paolo Maggiore (SPM).

The modal analysis was carried out taking into account one hundred vibration modes. Table 3.4 reports the vibration period and the modal participating mass ratios of the first 20 modes, for the longitudinal and transversal direction of the earthquake. The complete tables, reporting vibration period, modal participating mass ratio and the partial sum of

the ratios, for one hundred modes and for all the case studies are given in Appendix B. The table 3.4 clearly shows that the natural vibration modes are characterized by small participating mass ratios. It can be observed that among the first twenty modes: one vibration mode has M_p in the range 19÷28%; 1 or at most 2 modes have M_p in the range 9÷16%; all the others provide a contribution generally lower than 5%. Moreover, as it is known, generally the contribution of the various modes are greatest for the lower frequencies and tend to decrease for the higher frequencies (Clough and Penzien 1975). Contrary to this general result, the table 3.4 shows that the ninth mode of SMV and the sixth mode of SPC have M_p higher than the previous modes, as well as the eleventh and the twelfth of SPM provide a greater contribution than the previous eight modes.

Table 3.4 Modal participating mass ratio for the first 20 vibration modes

	SMV			SPC			SPM		
Mode	Period	M_{plong}	$M_{ptransv}$	Period	M_{plong}	$M_{ptransv}$	Period	M_{plong}	$M_{ptransv}$
n°	(s)	(%)	(%)	(s)	(%)	(%)	(s)	(%)	(%)
1	0.81	2.4%	0.0%	1.10	2.5%	0.0%	0.82	0.0%	11.0%
2	0.67	21.9%	0.0%	0.74	0.0%	1.4%	0.77	0.0%	2.1%
3	0.57	0.2%	0.0%	0.69	0.6%	5.2%	0.77	19.0%	0.0%
4	0.41	0.1%	0.0%	0.58	5.8%	1.9%	0.64	0.0%	24.0%
5	0.38	2.1%	0.0%	0.58	22.7%	0.0%	0.59	5.1%	0.2%
6	0.36	0.0%	1.1%	0.55	0.4%	25.5%	0.58	0.8%	2.0%
7	0.34	0.0%	2.1%	0.54	0.4%	6.8%	0.57	1.9%	0.0%
8	0.31	0.6%	5.0%	0.51	0.7%	0.0%	0.52	1.0%	0.0%
9	0.31	0.3%	28.1%	0.42	0.3%	0.0%	0.50	0.0%	1.2%
10	0.29	4.2%	0.3%	0.34	0.3%	0.0%	0.46	5.3%	0.0%
11	0.29	0.0%	9.7%	0.34	2.0%	0.4%	0.43	12.0%	1.4%
12	0.29	0.1%	0.8%	0.31	0.1%	0.0%	0.42	1.2%	16.0%
13	0.28	12.6%	0.0%	0.29	0.0%	0.0%	0.41	1.0%	0.1%
14	0.27	0.0%	0.2%	0.28	1.8%	0.1%	0.39	1.4%	0.0%
15	0.27	1.0%	1.7%	0.27	0.5%	0.2%	0.38	9.4%	0.0%
16	0.26	1.6%	0.9%	0.27	5.2%	0.0%	0.38	0.0%	4.2%
17	0.26	0.0%	0.4%	0.27	5.5%	1.3%	0.36	0.0%	1.5%
18	0.25	0.0%	4.1%	0.26	0.0%	0.2%	0.35	2.5%	0.1%
19	0.25	8.6%	0.3%	0.25	0.1%	2.8%	0.32	0.0%	3.8%
20	0.24	6.6%	0.0%	0.25	0.2%	0.2%	0.32	0.3%	0.0%

As a consequence of these results, in order to obtain a total participating mass ratio equal to 85%, as required by the Italian Building code or 90% as indicated in Eurocode 8, it is necessary to consider a great number of

vibration modes. In the graphs of fig 3.7, on the x axis, the number of the vibration modes is reported and, on the y axis, the partial sum of M_p is given.
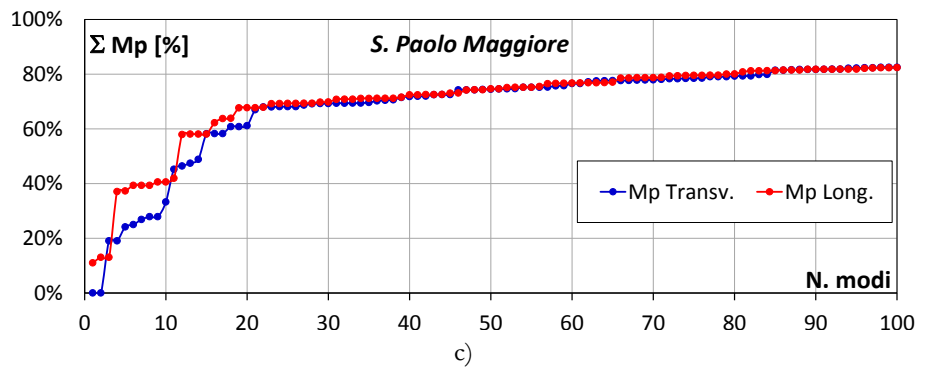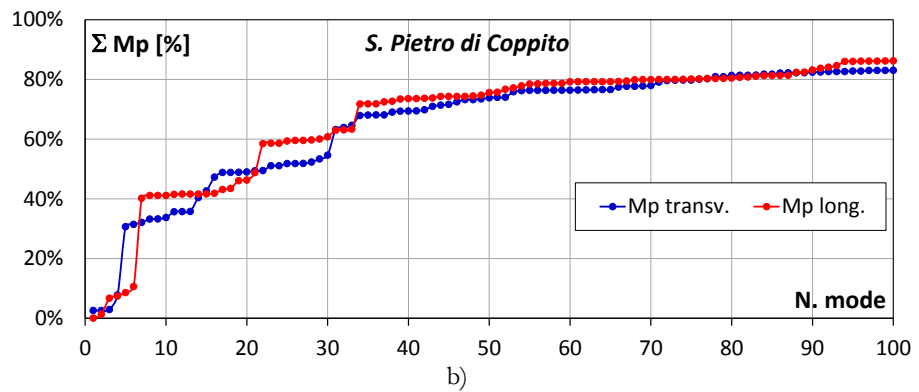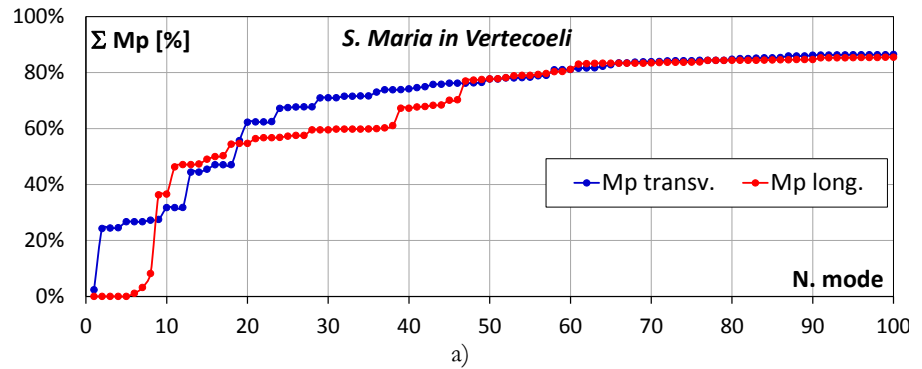
Figure 3.6 Partial sum of the modal participating mass ratio for: a) SMV; b) SPC; c) SPM

 It can be noted that considering one hundred modes a total participating mass about equal to 80÷85% of the total mas can be found. But it is also remarkable that the sum of the participating mass ratio shows only few significant increments, always lower than 30% and generally they do not correspond to the first vibration modes. As 60% of the total mass is reached, the increments become extremely small and always lower than 1%.

These results can be explained observing the modal shapes reported, for a selection of vibration mode, in table 3.5 and 3.6. The table 3.5 shows the modal shapes related to the first three vibration modes, the table 3.6 reports the modal shapes of the vibration modes characterized by the highest participation factors. Both figures clearly show that, due to the absence of connecting elements, each macro-element of the churches moves itself according to a different modes. Table 3.5 reveals that the contribution of the first three modes is not significantly greater than the others, as in the case of regular buildings. Comparing the first modal shapes of the three different churches, it can be seen that just one macro-element is involved, with significant out-of-plane deformation. SMV exhibits the transversal bending of the lateral façade of the oratory, SPM the longitudinal bending of the main façade, SPC the transversal bending of the transept wall. The second and the third modal shape are basically characterized by the transversal bending of the nave walls. When they move symmetrically the contribution of the modes in terms of M_p is almost equal to 0%, (see the third shape of SMV and the second shape of SPC and SPM). It derives from the expression of the effective mass provided above. When the displacement is not symmetrical, the modes 2 and 3 provide a significant contribution, especially for SMV and SPM: the second vibration mode of S. Maria in Vertecoeli is the principal one in the transversal direction as well as the third mode for the S. Paolo Maggiore church, with M_p equal to 19% and 22% respectively for SPM and SMV. The second and the third modal shapes of SPC involve basically one macro-element of the nave, therefore the corresponding M_p results at most equal to 6%.

As the first three modes do not give the major contribution, the three main vibration modes were identified. They are plotted in Table 3.6, where they are organized in three column in order of importance. The main mode, reported in the first column, corresponds with: 9th mode for SMV, 6th for SPC and4th mode for SPM. They give a contribution in terms of Mp in the range 24÷28%. Except for SPC church, these

Table 3.5 Modal shapes of the first three vibration modes
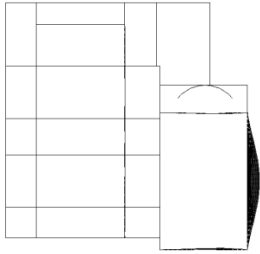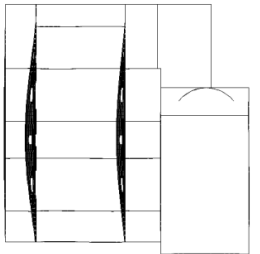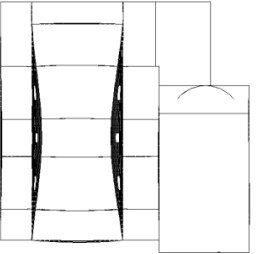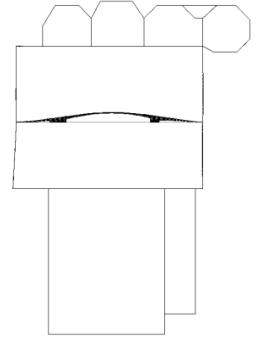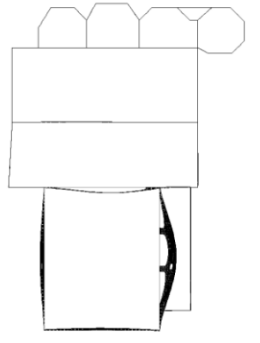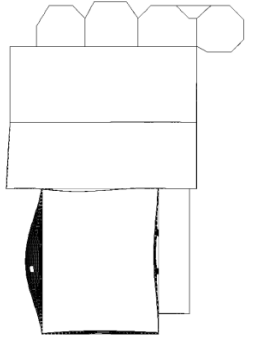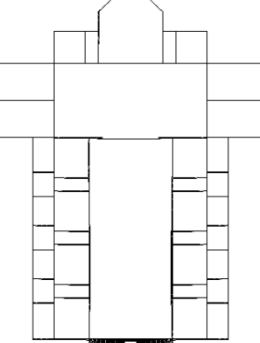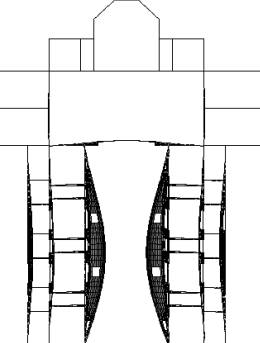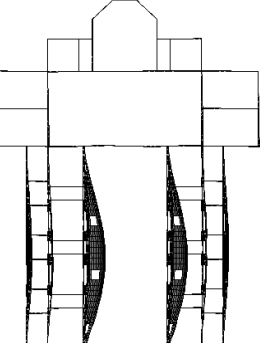
	Mode 1	Mode 2	Mode 3
S M V	 T = 0.81s $M_{pL}=0\%$ $M_{pT}=2\%$	 T = 0.67s $M_{pL}=0\%$ $M_{pT}=22\%$	 T = 0.57s $M_{pL}=0\%$ $M_{pT}=0.2\%$
S P C	 T = 1.1s $M_{pL}=3\%$ $M_{pT}=0\%$	 T = 0.74s $M_{pL}=0\%$ $M_{pT}=1\%$	 T = 0.68s $M_{pL}=1\%$ $M_{pT}=5\%$
S P M	 T = 0.82s $M_{pL}=11\%$ $M_{pT}=0\%$	 T = 0.77s $M_{pL}=2\%$ $M_{pT}=0\%$	 T = 0.76s $M_{pL}=0\%$ $M_{pT}=19\%$

Table 3.6 Modal shapes of the main three vibration mode

	Mode 9	Mode 2	Mode 13
S M V	T = 0.31s M_{pL}=28% M_{pT}=0%	T = 0.67s M_{pL}=0% M_{pT}=22%	T = 0.28s M_{pL}=0% M_{pT}=13%
	Mode 6	Mode 5	Mode 34
S P C	T = 0.55s M_{pL}=0% M_{pT}=26%	T = 0.57s M_{pL}=23% M_{pT}=0%	T = 0.17s M_{pL}=3% M_{pT}=8%
	Mode 4	Mode 3	Mode 12
S P M	T = 0.64s M_{pL}=24% M_{pT}=0%	T = 0.76s M_{pL}=0% M_{pT}=19%	T = 0.42s M_{pL}=16% M_{pT}=1%

vibration modes are translational mode in the longitudinal direction with significant out-of-plane deformation of the orthogonal elements. The church of S. Pietro di Coppito presents a main vibration mode involving predominantly the tower and the transept walls. The second column displays vibration modes characterized by modal participating mass ratio in the range 19÷23%. For the churches in Naples the modal shapes show a transversal bending of the nave walls. SPC presents a local mode involving mainly the tower and the façade in the case of S. Pietro di Coppito. The third column contains higher vibration mode characterized by the transversal bending of almost all elements. It is noted that even if they are higher modes, their contribution is not negligible compared with the others and it reaches 12% of the total for the 12th mode of SPM.

As a consequence of the results illustrated in the Tables 3.5 and 3.6 the following observations were deduced and described through the graphs of Figures 3.8 – 3.10. In the graphs, on the horizontal axis, the vibration periods corresponding to the 100 modes are reported; on the Y-axis (right side) the corresponding modal participating mass ratios (M_p) are provided. The M_p is represented through indicators proportionally increasing with the masses, both for the earthquake acting in transversal and in longitudinal direction. The distribution of M_p is compared with two response spectra, therefore, on the first y-axis (left side), the response spectrum accelerations (Sa/g) are reported. The first spectrum, plotted in red, shows the 5% damped response spectrum, obtained from the acceleration history recorded respectively during the 1980 earthquake in Sturno (for SMV and SPM) and the 2009 earthquake in L'Aquila (for SPC). It was compared with the elastic spectra provided by the Italian Building code respectively for Sturno and L'Aquila, for a returned period TR = 475 years and soil type B (appointed as "NTC'08 EL").
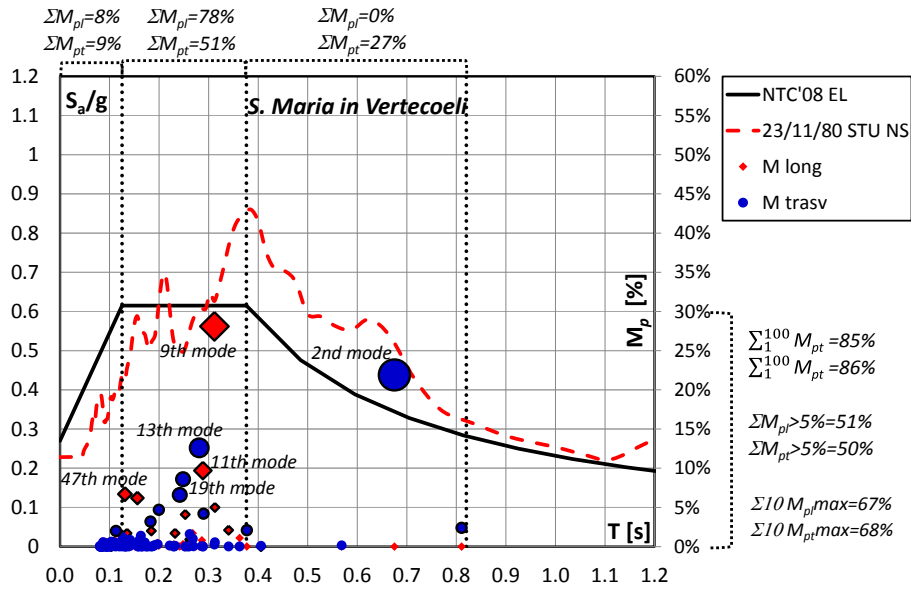
Figure 3.7 Distribution of M_p (modal participating mass ratios) for the first 100 vibration modes and comparison with the response spectra, for SMV church
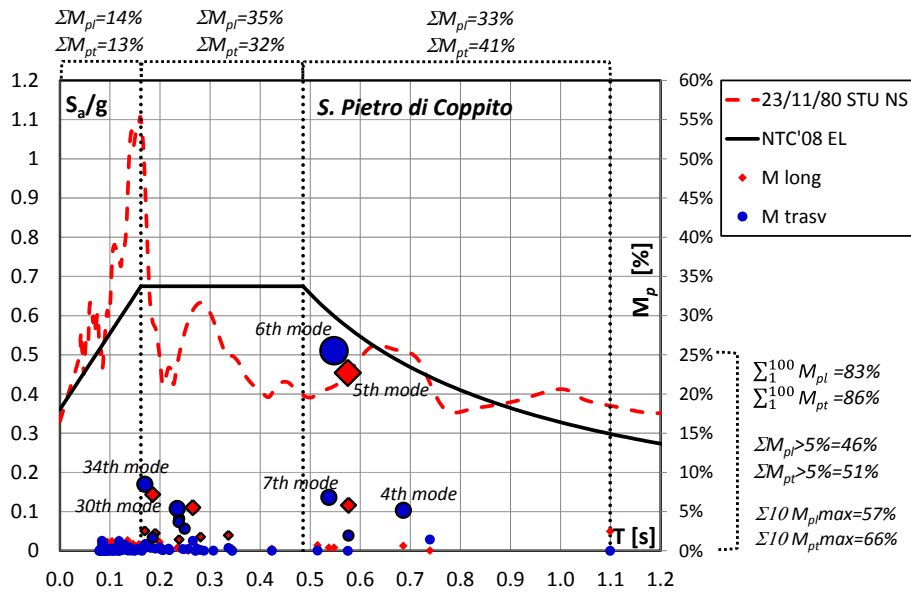
Figure 3.8 Distribution of M_p (modal participating mass ratios) for the first 100 vibration modes and comparison with the response spectra, for SPC church
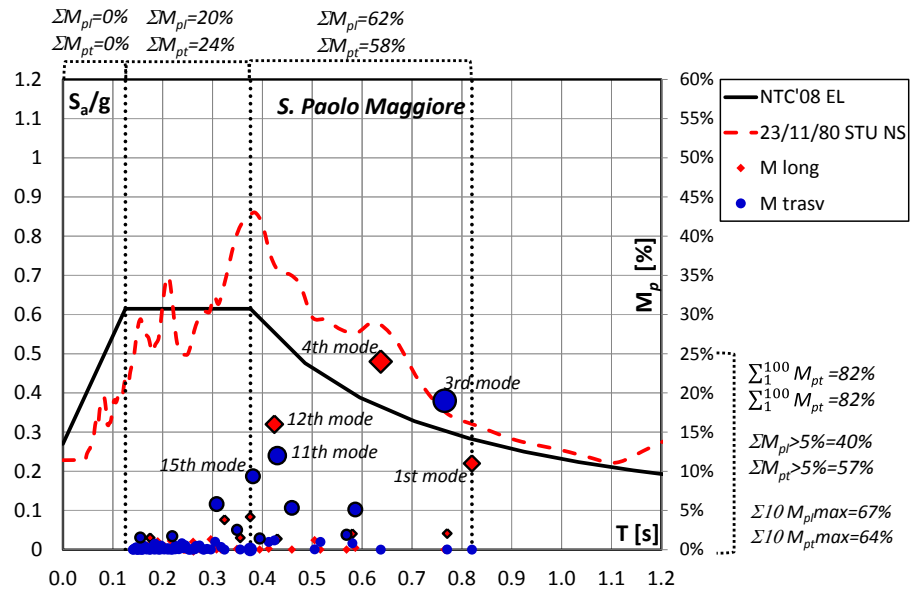
Figure 3.9 Distribution of M_p (modal participating mass ratios) for the first 100 vibration modes and comparison with the response spectra, for SPM church

The graphs show the following results:

- The maximum value of M_p is always lower than 30%. It is in the range 25÷30% for SMV and SPC, 20÷25% for SPM.
- The sum of the M_p corresponding to the first 100 vibration modes ranges from 78 to 87 % of the total mass.
- The M_p is generally less than 5%. It is noted that the Eurocode 8 and the Italian Building Code recommend to consider all vibration modes having modal participating mass ratios higher than 5%, implicitly neglecting the lower values. Thus a total participating mass ratio was computed, considering merely vibration modes having M_p greater than 5%. The results provide quite low values: for the Church of SMV the sum of M_p>5% is equal to 51% and 50% respectively in the longitudinal and transversal direction of the earthquake; for the church of SPC these sums are equal to 46% and 51%; for the church of SPM it was found 40% in longitudinal direction and 57% in transversal direction.
- A subset including ten greater vibration modes, was considered. They are evidenced by a black edge in the graph. It is noted that the subset provided by itself a significant part of the total mass. However values

less than 70% were reached for all the masonry churches. Therefore this subset could not be considered able to fully describe the behavior of the church, according to the indications of the Eurocode 8 and the Italian Building Code. Moreover it is noted that the ten vibration modes providing the greater contribution are not the first ten, but the subsets identified includes higher vibration modes.

– The vibration modes have a spanned distribution. In order to highlight the modal dispersion, the distribution of the modal participating mass ratios is compared with the response spectra plotted in the graphs. Three ranges of vibration periods are considered. The first range includes the increasing zone of the elastic spectrum suggested by the Italian Building Code; the second one includes the plateau; the last range considers the decreasing trend of the spectra. For each range, the total participating mass ratio was computed and reported in the graphs. The church of S. Maria Vertecoeli is the only case study with almost the total participating mass corresponding to the plateau. The others masonry churches, as evident from the graphs, have low percentage (less than 14%) of participating mass included in the first range, significant values (in the range 20÷35%) in the second one and the most of the participating included in the third range, corresponding to low value of spectral accelerations.

3.3.3 Modal analysis results on the complete sample

The parameters which have been defined above - 1) maximum value of the modal participating mass ratio ($Mp\ max$); 2) sum of the M_p corresponding to the first 100 vibration modes; 3) sum of the M_p related to the modes having $M_p > 5\%$; 4) sum of the M_p corresponding to the ten modes which provide the greater contribution – were computed for the complete sample study including fourteen masonry churches. In the following, for each parameter one summary graph is provided, showing the results obtained on all the case studies. However graphs similar to those of figures 3.8-3.10 were elaborated for each church and reported in Appendix B.

The histogram in Fig. 3.11 provides the first parameter. On the x axes the case studies, listed according to the size, are reported, while on the y

axes the maximum value of the modal participating mass ratio is given, for the longitudinal and transversal direction of the church.
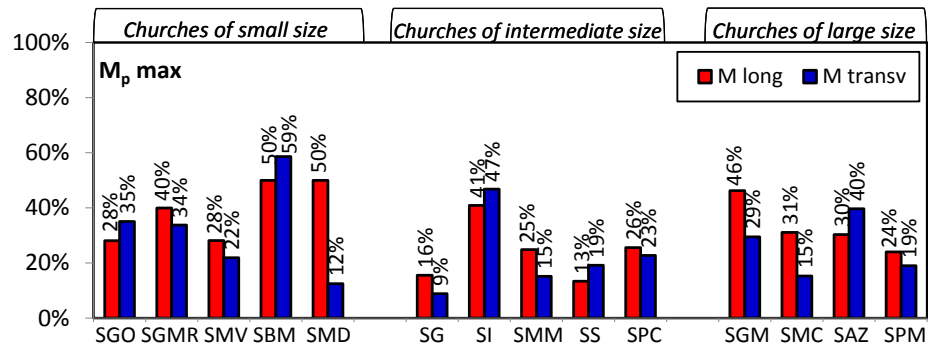
Figure 3.10 Maximum modal participating mass ratio

Except of the case of SBM, the value *Mp max* is always lower than 50% of the total mass for all the case studies and, generally, it reaches at most the percentage of 30-35%, confirming the results described above for the three selected churches (SMV, SPC, SPM). It is noted that the churches of small size, having greater plan compactness, are characterized on average by the highest values of *Mpmax*. Moreover, it can be observed that the churches located in L'Aquila (SG, SS, SPC, SMC) are characterized by small values of the *Mpmax* (in the range of 9÷30%), in comparison with the churches in Naples. It can be explained in the case of SS, SPC, SMC, observing the plans in fig. 3.4: the walls of these churches are the most slender, they are not connected by transversal walls to the pillars, consequently the plans appear as an unique large open space. On the other hand, the maximum value found in the histogram corresponds to the church of SBM. This church has a singular plan and it is almost not attributable to the basilica-type. The longitudinal walls have large thickness and they are well connected by transversal elements. However, even if particular cases can be found, the first parameter, *Mp max*, clearly shows that the modal analysis of masonry churches does not provide a vibration mode markedly predominant compared with the others.

Figure 3.12 presents three histogram providing the other three modal parameters, defined above. Each parameter was computed for all the case studies and divided for the average value (a.v.) obtained from the sample. The first histogram provides this ratio with reference to the sum of the M_p corresponding to the first 100 vibration modes; the second

with reference to the sum of the M_p related to the modes having $M_p >$ 5%; the third one with reference to the sum of the M_p corresponding to the ten greater modes.

The first histogram shows that, except of SMC church, all the case studies minimally deviate from their average value equal to 82% and 85% respectively in longitudinal and transversal direction. The church of SMC (as it can be observed in Appendix b) is characterized from values of M_p, generally lower than 5%. As a result, also taking into account 100 vibration modes, a total participating mass ratio equal to 60% and 78%, respectively in longitudinal and transversal direction was achieved. However, the results of the sample prove that 100 vibration modes is on average a suitable number which can be adopted to compute the total seismic response of the structure.

The second histogram shows a greater dispersion regarding the sum of the modes having $M_p>5\%$: in many cases, especially for the churches of intermediate and large size, it significantly deviates from the average value, assuming lower values. The average value is equal to 54% and 55% respectively in longitudinal and transversal direction. The churches of intermediate size are associated to values of this parameters smaller than 54-55%, variable in the range 35÷50%. Regarding the churches of large size, it can be noted that the church of SGM corresponds to quite higher values, equal to 65% and 64% respectively in longitudinal and transversal direction. The church of SMC, as it was expected, is characterized by the smallest values, equal to 31% in longitudinal and 34% in transversal direction. A similar value was obtained for the church of SPM in longitudinal direction (as illustrated in the previous section). On the whole this results confirms that, for masonry churches, it can be unsuitable to take into account only the modes having $M_p>5\%$.
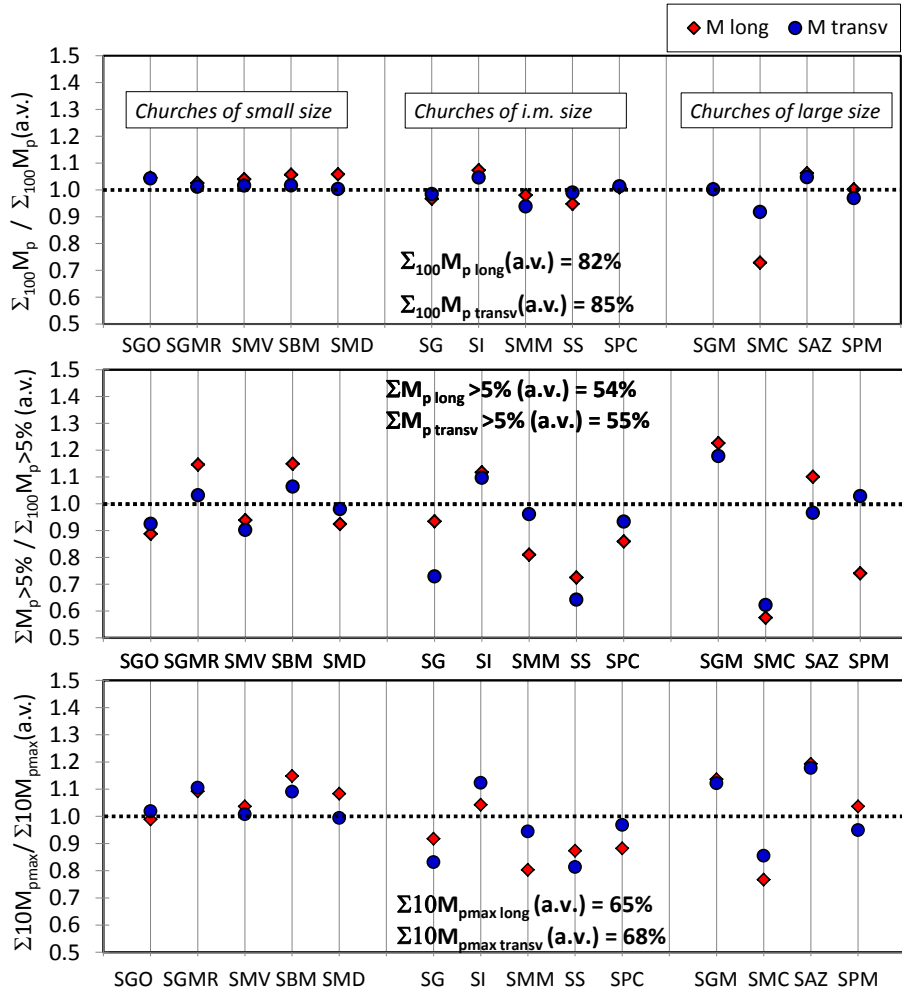
Figure 3.11 Sum of modal participating mass ratios for 100 vibration modes; modes having Mp>5%; 10 modes giving major contribution

The third histogram provides the last parameter, corresponding to the sum of the ten greater vibration modes. It assumes for each case study values quite close to the average value, equal to 65% and 68%, respectively in longitudinal and in transversal direction. In detail: the churches of small size, provides slightly higher results, in the range 67÷75%; the churches of intermediate size, except of SI, provides little lower results in the range 52÷75%; the churches of large size give more spanned results, variable from a minimum value of 50%, corresponding to SMC church, to a maximum value of 80%, corresponding to SAZ

church. This result confirms that, except of one case, also considering a subset of greater ten modes, it was not reached a sufficient a percentage of participating mass.

Finally the dispersion of the vibration modes was evaluated computing the sum of M_p, in the three ranges of vibration periods defined in the previous section. The sum was divided for the Mp corresponding to 100 vibration modes and the results are reported in the histograms of fig. 3.13.

a)

b)
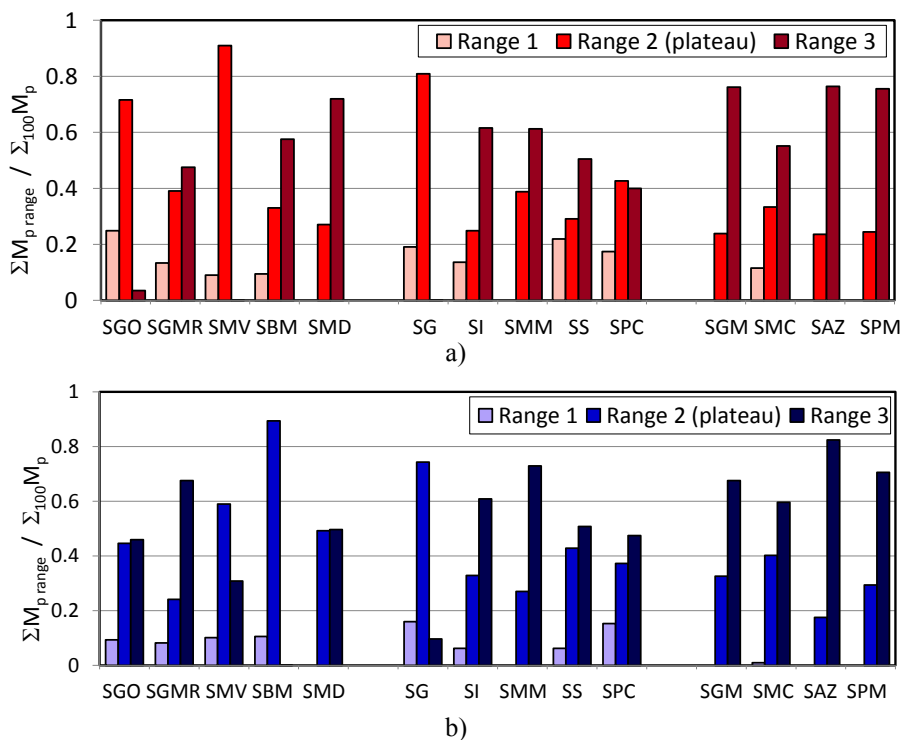
Figure 3.12 Modal Dispersion: a)Longitudinal direction; b)Transversal direction

This ratio is given, for the longitudinal direction, in the histogram of fig.3.13 a, and for the transversal direction in the histogram of fig. 3.13 b. As it can be observed, except for a few cases, like SMV (in longitudinal direction), SBM (in transversal direction) and SG, the participating mass is not predominantly concentrated in one range. Moreover it is noted that, for the majority of the churches, the range which contains the most of the vibration modes is the third one, corresponding to the decreasing trend of the spectra.

It can be concluded that, for all the case studies, the modal analysis provided a multitude of vibration modes, all characterized by small participation factors and by a spanned distribution of the vibration periods. This evidence disproves the predominance of the first mode and, consequently, the assumption underlying the equivalent static analysis, is not verified. Moreover it also influences the total seismic response calculated by a dynamic response spectrum analysis, as it will be seen in the following.

3.3.4 Related works

The complex issue of the dynamic behavior of masonry churches was also highlighted by other authors. Betti and Vignoli, for the analysis of Farneta Abbey, in Cortona, obtained a maximum value of the modal participating mass ratio, equal to 20% (Betti & Vignoli 2008). The same authors analyzing the Church of S. Maria all'Impruneta, evaluated the first 100 vibration modes, with the aim to assure a total effective modal mass at least 90% (Betti &Vignoli 2011). Manos et al., investigating on the seismic behavior of Agia Triada church, located in Drakotrypa, Greece, found that the maximum value of the participating mass ratio was equal to 52% in transversal direction and 47% in longitudinal direction (Manos et al. 2008). However, in another study about the dynamic behavior of greek post-byzantine churches, Manos et al. found that, for the church of Profitis Ilias, the most significant mode has a participating mass ratio equal to 24% (Manos et al. 2013). Similar results were achieved by Lourenço et al., who used a finite element updated by means of dynamic identification results, for the analysis of the Church of S. Georges of the Latins in Famagusta, in Cyprus (Lourenço 2012). A maximum value of the modal participating mass ratio, approximately of 33%, was obtained. Gattulli et al., for the Church of S. Maria di Collemaggio in L'Aquila, found that the modal participating mass ratios assumed a spanned distribution with most of the values always less than 5%, and merely a few modes presented a modal partecipating mass ratio larger than 20% (Gattulli et al. 2013, 2015). Castellazzi et al. analyzed the church of Madre Santa Maria del Borgo, in San Nicandro Garganico (FG, Italy), and the results of the dynamic analysis gave mainly local modes and just one global mode, no. 7. Mass participation sum of the first 30 eigen-modes was equal to 55.5% and 55.2% of the total mass, respectively in the transversal and longitudinal directions (Castellazzi et

al. 2013). Dal Cin and Russo studying the influence of the annex on seismic behavior of the Gesù church in Mirandola (MO, Italy), remarked the relevant dispersion of the mode shapes and highlighted that the highest participating mass calculated was equal to 42.40% in the X axis and 40.00% in Y axis (Dal Cin & Russo 2014). Different results, more consistent with the regular buildings, were obtained by Cakir et al. in the analysis of the historical Ishan Church in Artvin, Turkey. In this case study, a first vibration mode involving more than 60% of the total mass was found (Cakir et al.2014). In the graph of fig. 13, these results extrapolated from related works on historical churches, are summarized. On the x axes the case study and the reference are indicated, while on the y axes the maximum value found, as transversal participating mass ratio, is reported. The software used to perform the analysis is also indicated on the graphs. The dynamic properties were obtained performing FE analysis of the churches, by using different software, which are indicated on the graphs.
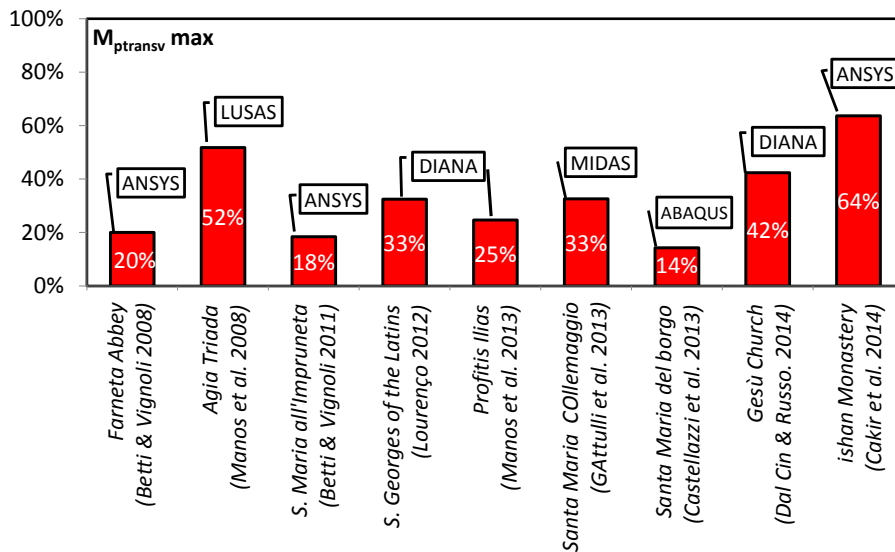
Figure 3.13: Maximum modal participating mass ratio found in related works

3.4 MODAL RESPONSE SPECTRUM ANALYSIS

The atypical dynamic behavior, highlighted in the previous section, strongly influences the total seismic response of the structure, obtained through a response spectrum analysis. Although using this kind of analysis is questionable, as illustrated in section 1.2, it permits to take into account all the vibration modes, without involving the computational effort of the non linear dynamic analysis.

The response spectrum analysis was carried out considering one hundred vibration modes. The response spectra used in the analyses were: the elastic response spectrum of Sturno for the churches located in south of Italy and the response spectrum of L'Aquila for the churches located in L'Aquila. They were obtained according to the Italian building code, for a returned period TR = 475 years and soil type B (appointed as "NTC'08 EL"). Three different mode-superposition procedures were considered: the direct superposition of modal maxima (SUM), the Square Root Sum Squares (SRSS) and the Complete Quadratic Combination (CQC):

$$SUM \ r \leq \sum_{n=1}^{N} |r_n| \quad SRSS \ r = \sqrt{\sum r_n^2} \quad CQC \ r = \sqrt{\sum_{i=1}^{N} \sum_{j=1}^{N} r_i p_{ij} r_j}$$

The first one, direct superposition, provides an upper bound to the maximum of total response; the second one, generally provides a satisfactory estimate for system with well separated frequencies, while the last is used when the natural periods of the structures are very similar.

Similarly to the previous section, the results of the response spectrum analysis will be described first on three case studies, selected from each sub-group of churches, and then they will be extended to the complete sample.

3.4.1 Results on one church of each sub-group

The graphs in Figures 3.15 and 3.16 summarize the results corresponding to the three churches selected: SMV, SPC and SPM. The graphs have the vibration periods on the x axis and the response spectrum acceleration (Sa/g) on the vertical axis. The elastic response

spectra are reported together with the response spectra recorded during the 1980 and 2009 earthquake, respectively occurred in Sturno and in L'Aquila.

The base shears obtained by means of the response spectrum analysis (with the different superposition procedures), were normalized to the weight of the total participating mass considered ($V/(\Sigma_{100}M_p \times g)$) and they are represented as lines on the graphs of the response spectra.

It is noted that also the base shear given by the SUM do not correspond always to the acceleration of the plateau, and it is generally much lower than the peak of the recorded spectra. It depends on the dispersion of the vibration modes: as observed above, generally the modes are not concentrated on the plateau, but they have a spanned distribution and the majority are in the decreasing trend of the spectrum.

Moreover, the lines representing the result of each method are considerably spaced. The direct superposition (SUM) provided a total response comprises in the range 0.54÷0.61g. Accelerations equal to the plateau of the spectrum were approximately reached by the SMV church, which in fact has the most of the participating mass concentrated in the plateau range (see fig.3.8). The Complete Quadratic Combination results range from 0.23 to 0.43g. Except of SMV church, these values are generally little lower than half of the acceleration at the plateau of the spectrum.

The Square Root Sum Squares gave a base shear corresponding to acceleration generally lower than 0.2g. Only SMV church provided, in longitudinal direction, a base shear corresponding to an acceleration equal to 28%. These evidences imply that the results of the response spectrum analysis for masonry churches strongly depends on the choice of the procedure of mode superposition.
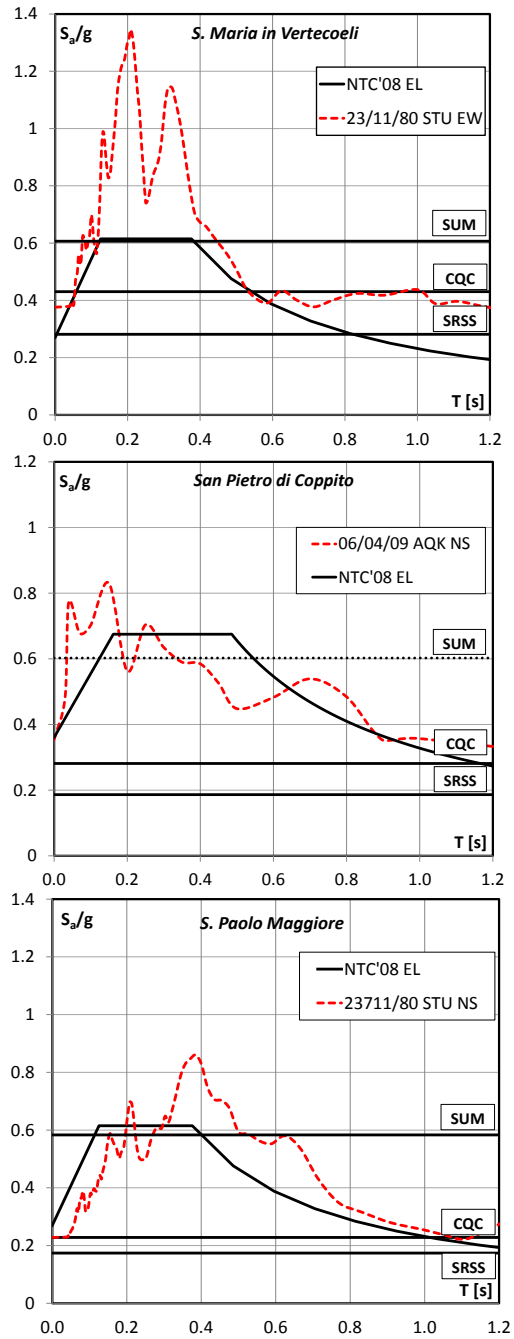
Figure 3.14 Comparison between the response spectra and the longitudinal acceleration deriving from the response spectrum analysis
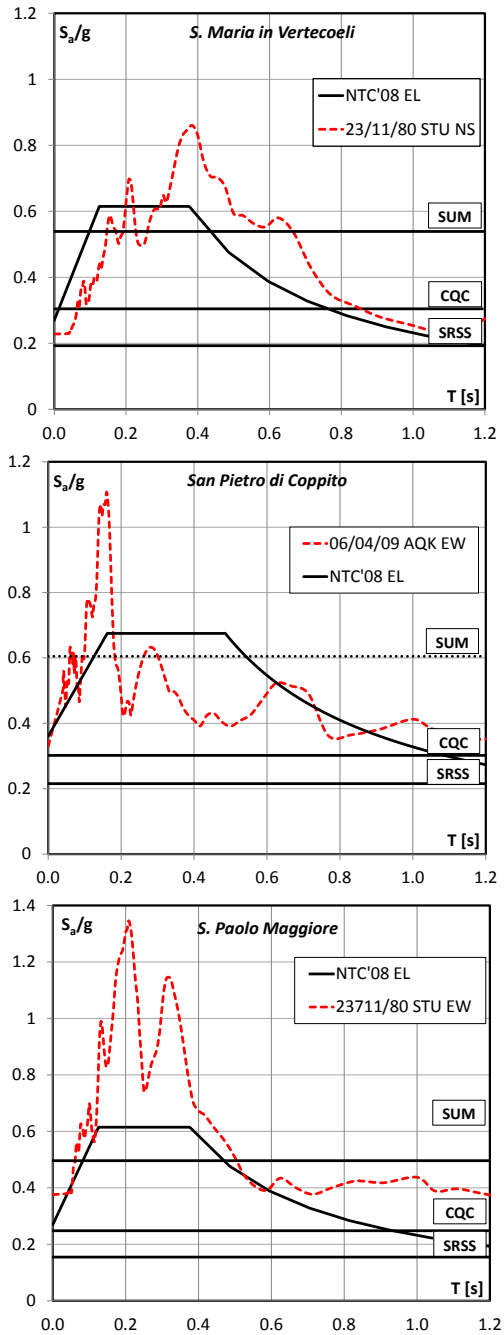
Figure 3.15 Comparison between the response spectra and the transversal acceleration deriving from the response spectrum analysis

The discrepancies between the superposition procedures can be explained by considering that, the square of the very low values of M_p, provides as much low values of base shears. Then, as mentioned above, the SRSS provides a good estimation for system with well separated frequencies, therefore it is not suitable for masonry churches. As it can be observed in the graphs in fig. 3.8-3.11, the natural periods of the vibration modes are extremely close. Therefore it should be used the Complete Quadratic Combination, which, in fact, provided considerably higher results. However the shear resultants obtained by CQC method implies a shear demand approximately equal to half of the plateau acceleration.

It can be concluded that the high spectral values do not give rise to similar high values of seismic loads on the churches. This result is in line with those of Gattulli et al. (2013-2015), and with those of the authors (Dal Cin et al. 2014) reached on different case studies, also performing the analysis considering response spectra obtained from the acceleration history.

3.4.2   Results on the complete sample

The results of the response spectrum analysis for the complete sample are provided in fig.3.17. The acceleration corresponding to the base shears ($V/(\Sigma_{100}M_p \times g)$), computed with the CQC and SRSS procedures, was normalized by the maximum spectral acceleration (plateau). This ratio is reported for each churches on the y axis of the histogram in the figures.

The histogram gives also the results generally obtained from a response spectrum analysis of regular concrete buildings (indicated as R.B.). For regular buildings, usually, the seismic forces correspond to 80-90% of the spectral acceleration. Moreover the two superposition procedures normally give the same results.
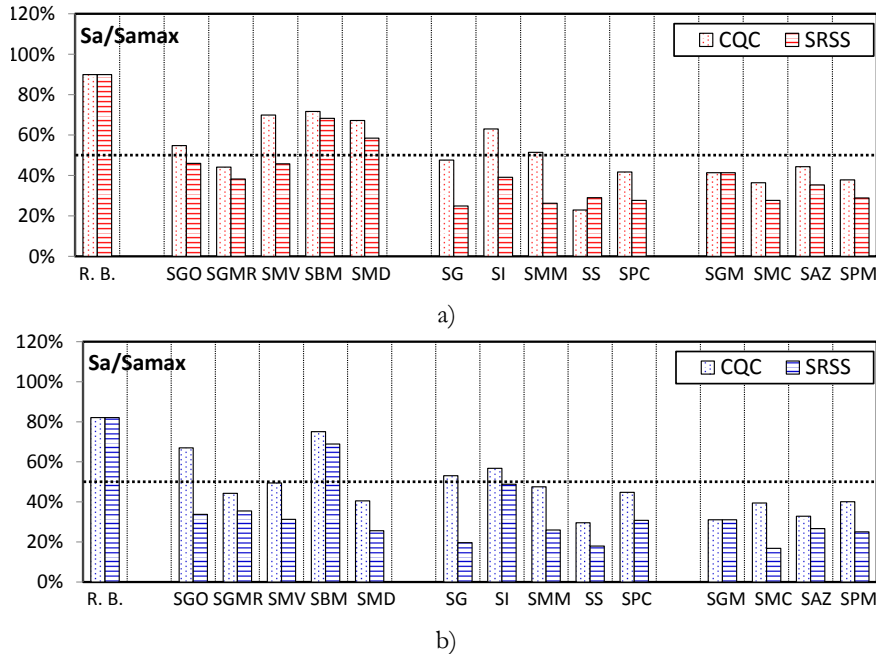
Figure 3.16 Acceleration corresponding to the base shears $(V/(\Sigma_{100}M_P \times g))$ normalized by the maximum spectral acceleration for: a) longitudinal direction of the earthquake, b) transversal direction

The analyses of the masonry churches led to drastically different findings. Both of the procedures gave seismic forces corresponding to accelerations lower than 50% of the maximum spectral acceleration, in most of the case studies. The churches of small size provided results more consistent with a regular building, in particular the case of SBM church. In this case study the acceleration reached 75% of the maximum spectral acceleration. This result was expected since the remarks made in the section 3.3.3 on SBM church.

Due to the distribution of the natural periods, the SRSS procedure gave results significantly lower than the CQC, except of the case of SGM church. The seismic forces obtained through this superposition procedure correspond to acceleration on average equal to 35% of the plateau acceleration, and in some cases (SS, SMC) values lower than 20% were obtained. It can be deduced that the SRSS procedure can excessively underestimate the results.

Certainly the CQC procedure is more suitable for masonry churches and it provided acceleration on average equal to 45-50% of the plateau acceleration.

3.4.3   Final remarks

The dynamic behavior of masonry churches is considerably different from the regular buildings. It has been evidenced in the previous study of the research group of the author and it has been observed in the analyses of many case studies, carried out by other authors, mentioned in section 3.3.1. However these studies have not focused on the dynamics properties of the structures. Therefore in this chapter the results of the modal dynamic analysis were studied in detail, for fourteen churches having different characteristics in terms of size and geometry. Basically four findings were deduced for each case study: 1) each vibration mode involves a small percentage of the total mass of the structure; 2) as the natural modes are characterized by small participating mass ratio, it is necessary to consider 100 vibration modes in order to obtain a total effective mass almost equal to 80% of the total mass; 3) the most of the vibration modes involves less than 5% of the total mass, consequently considering just the modes having M_p greater than 5%, it can be obtained a total participating mass on average equal to 55% of the total; 4) also selecting ten greater mode it cannot be achieved a participating mass sufficient to describe seismic response of the church; 5)the vibration periods have a strongly spanned distribution.
It is clear that this conditions prevent simplified approaches that associate the structure to a SDOF system. The contribution of the higher modes, indeed, is not negligible compared with the others, because every vibration mode gives a low contribution. Therefore the static approach, applied on this kind of building, could provide uncorrected results.
However the modal characteristics of masonry churches significantly influence also the dynamic analysis. The response spectrum analysis, performed taking into account the small contribution of one hundred spanned vibration modes, lead to low seismic forces. The base shears correspond to accelerations much lower than both peak of the recorded pseudo-acceleration and the plateau of the response spectra, provided by the rules. Moreover the distribution of the vibration periods influences the choice of the mode superposition procedure. In particular the SRSS provides results that significantly differ from the CQC procedures,

underestimating the seismic forces. On the other hand, also the CQC procedures gives seismic forces corresponding on average to half of the spectral acceleration of the plateau.

This results, even if they was obtained considering only the linear regime of the material, implies that the high spectral accelerations do not give rise to similar high values of seismic forces, in contrast with what happens on regular buildings. Therefore the seismic forces to be used for verifying these structure can be reduced, and the sample studied suggest that ½ of the maximum spectral acceleration could be applied to the seismic weight of the church.

The fact that the seismic demand on the churches could be reduced is also proved by observing the damage occurred during the earthquakes of the last few decades. These events confirmed the seismic vulnerability of the churches, but at the same time it proved the following: when the construction respects the rules of the art and the restoration works, experienced during the centuries, did not strongly modify the static behavior, the churches supported the high seismic excitation of the earthquake, even if with severe local damage.

Studies done on churches, starting from the observation of damage after the Friuli earthquake in 1976 (Doglioni et al. 1994) and more systematically after the earthquakes in Umbria and the Marches in 1997 (Lagomarsino and Podestà 2004a), Molise in 2002 (Lagomarsino and Podestà 2004b), L'Aquila in 2009 (among the others Lagomarsino 2012) and Emilia Romagna in 2012 (Sorrentino et al.2014) have demonstrated that damage mechanisms in churches have certain recurring characteristics. The collapse usually occurs locally in some parts of churches (façade, nave, triumphal arch, dome, apse, bell tower, etc.). It gave rise to replace the global analysis of the church with the analysis of its constituting parts, the so-called macro-elements. The first suggestion toward this approach is provided by Doglioni et al. (1994) and it was adopted by many researchers: among the others, Siviero et al. 1997, Lagomarsino 1998, Zingone et al., D'Ayala 2000 and more recently Milani 2015, Endo et al.2015, Criber et al. 2015, Giresini 2016).

 In 2006, the macro-element approach was also introduced by the Italian Guidelines for the Cultural Heritage (LL.GG. '06) and at present it is recommended by Italian Guidelines emanated in 2011 (LLl.GG. '11).

The analysis of the modal shapes, provided in section 3.3.2 has further confirmed that these macro-elements are characterized by autonomous structural behavior under seismic loads. Each vibration mode involved

just one among façade, nave walls or bell tower, generally showing considerable out-of-plane deformation.

For the case studies located in L'Aquila: SG, SS, SPC, SMC, a comparison can be carried out between the modal shapes and the damage occurred during the 2009 earthquake. In figure 3.18-3.22 some pictures showing local damage in the church of SG, SPC, SS are reported. It was found consistent with some modal shapes corresponding to a significant value of the modal participating mass ratio.

It can be concluded that invasive restoration works, computed taking into account high seismic forces could be avoided. It could be replaced by interventions calibrated on the analysis of the macro-elements and, in particular the out-of-plane mechanism deduced by the modal shape should be considered.

a)

$M_{pl} = 0\% \; M_{pt} = 3.6\%$
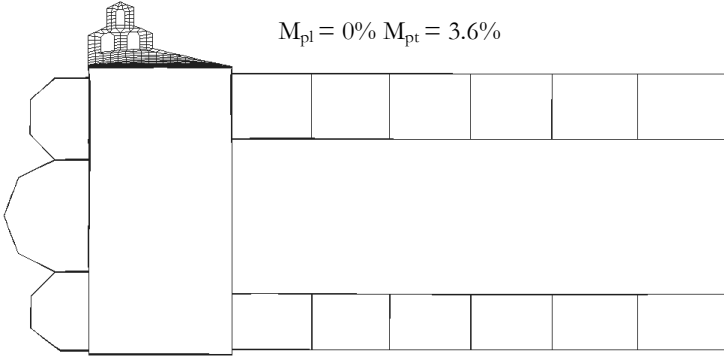
b)

Figure 3.17 S. Giusta church (SG): a) overturning of lateral façade; b) modal shape of 2nd vibration mode

a)

$M_{pl} = 22.7\%$ $M_{pt} = 0\%$
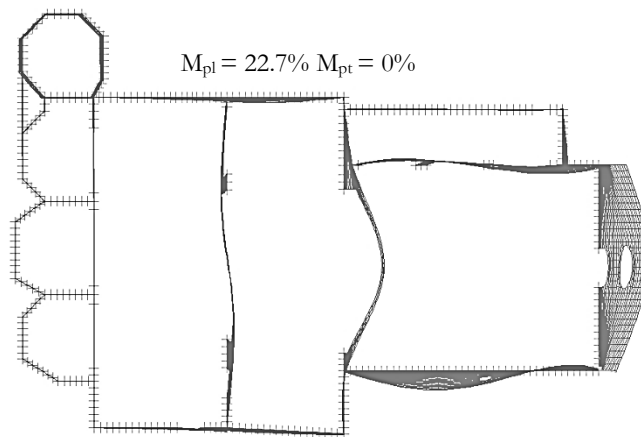
b)

Figure 3.18 S. Pietro di Coppito church (SPC): a) overturning of façade; b) modal shape of 5th vibration mode

a)

$M_{pl} = 0.4\%$ $M_{pt} = 25.5\%$
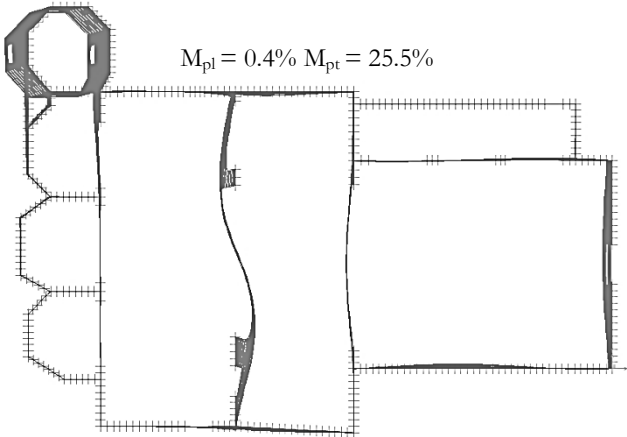
b)

Figure 3.19 S. Pietro di Coppito church (SPC): a) partial collapse of the tower; b) modal shape of 6th vibration mode

a)

$M_{pl} = 14.3\%$ $M_{pt} = 3.7\%$

b)
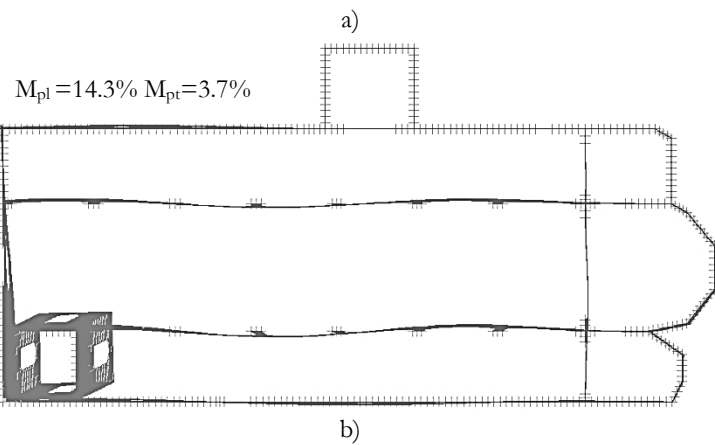
Figure 3.20 S. Silvestro church (SS): a) damage of the tower; b) modal shape of 6th vibration mode

a)

$M_{pl}=0\%$ $M_{pt}=15.3\%$
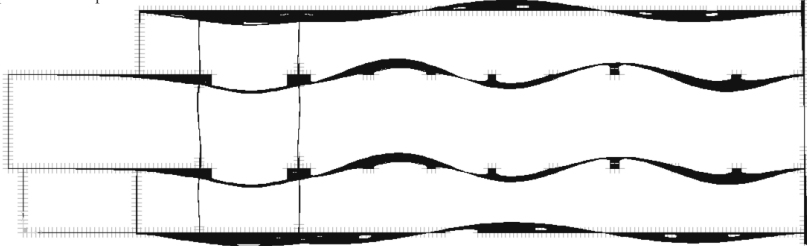
$M_{pl}=0.2\%$ $M_{pt}=8\%$
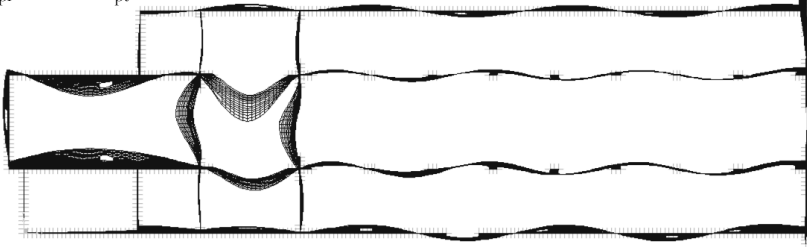
b)

Figure 3.21 S. Maria di Collemaggio church (SMC): a)collapse of the transept; b) modal shape of 15th and 38th vibration modes

4 COMPARISON OF DIFFERENT ANALYSIS METHODS ON A CASE STUDY: SANTA MARIA DEL MAR CHURCH

As discussed in chapter 1, each analysis method is affected by different levels of accuracy and different limitations. Some limitations of the most widely modelling methods, were observed in the seismic analysis of historical masonry building, provided in chapter 2. While, in chapter 3, some questions about the static and the dynamic approach to the seismic analysis of historical masonry churches were pointed out.

Since the lack of only one completely suitable analysis method for the seismic assessment of historical constructions, it should be always evaluated by means of more than one procedures, so that the results would be validated by the comparison and the possible agreement among different approaches.

In this chapter the cathedral of *Santa Maria del Mar* in Barcelona is studied through different analysis methods applied to a FE model of the church. The software DIANA TNO was used to perform the analyses. In detail both linear and non linear static analysis and linear and non linear dynamic analysis were carried out. The results were also compared with the limit analysis performed by other authors in previous study of the cathedral.

4.1 THE CASE STUDY: THE CATHEDRAL OF SANTA MARIA DEL MAR

Based on the informations provided by previous studies (Irizzarry 2004, Roca et al. 2008, Gonzales et al. 2008, Cuzzilla 2009, Roca et al. 2009), a brief description of the church is presented.

4.1.1 History

The *Santa Maria del Mar* church is a gothic cathedral built during the XIV century. Simplicity of form, symmetry and elegance makes it one of the most fascinating example of the Catalan gothic architecture.

The construction started on 25th march 1329, as commemorated by a tablet on the façade that faces the Fossar de les Moreres, and it spanned 54 years. The last stone was collocated in 1383 and the first mass was celebrated on August 1384. The architects in charge were Bernat de Montagut and Ramon Despuig.

The construction process is described in Gonzales et al. 2008, here just some events occurred during the construction are mentioned. In 1379, when the last bay was almost completed, a fire destroyed the scaffoldings and caused some damage to the stone. In 1373, an earthquake in the Pyrenees Region, with an epicentral intensity of VIII-IX (MSK), caused the collapse of the upper body of one of the façade towers.

When the cathedral was already completed, in 1428, a severe earthquake caused the collapse of part of the rose window and, consequently 21 or 22 people died. Later in 1605, another earthquake is said to have damaged the building. The building has also experienced damage during bombardments against the city in1714 (during the Succession War) and the Spanish Civil War (1936-1939), among other episodes. In 1936, another fire caused significant damage to the piers, arches and vault keystones.

In spite of the numerous disaster events occurred, the cathedral of *Santa Maria del Mar* has never suffered very severe damage, resulting in today's uniformity and architectural purity. It proves the good knowledge in the techniques of the construction in rock of the Catalan architects of the XIV century.

4.1.2 Description of the building

Figure 4.1 shows the external and internal views of the *Santa Maria del Mar* church. From outside the church appears as a robust regular building, characterized by two slender octagonal towers at the sides of its principal façade, adorned with a rose window in its central part. From inside, verticality and lightness prevail on the robustness exhibited by the external view. Lateral view, plan and transversal section of the cathedral are provided in fig.4.2.

a)

b)

Figure 4.1 a) external view and b) internal view of *Santa Maria del Mar* cathedral
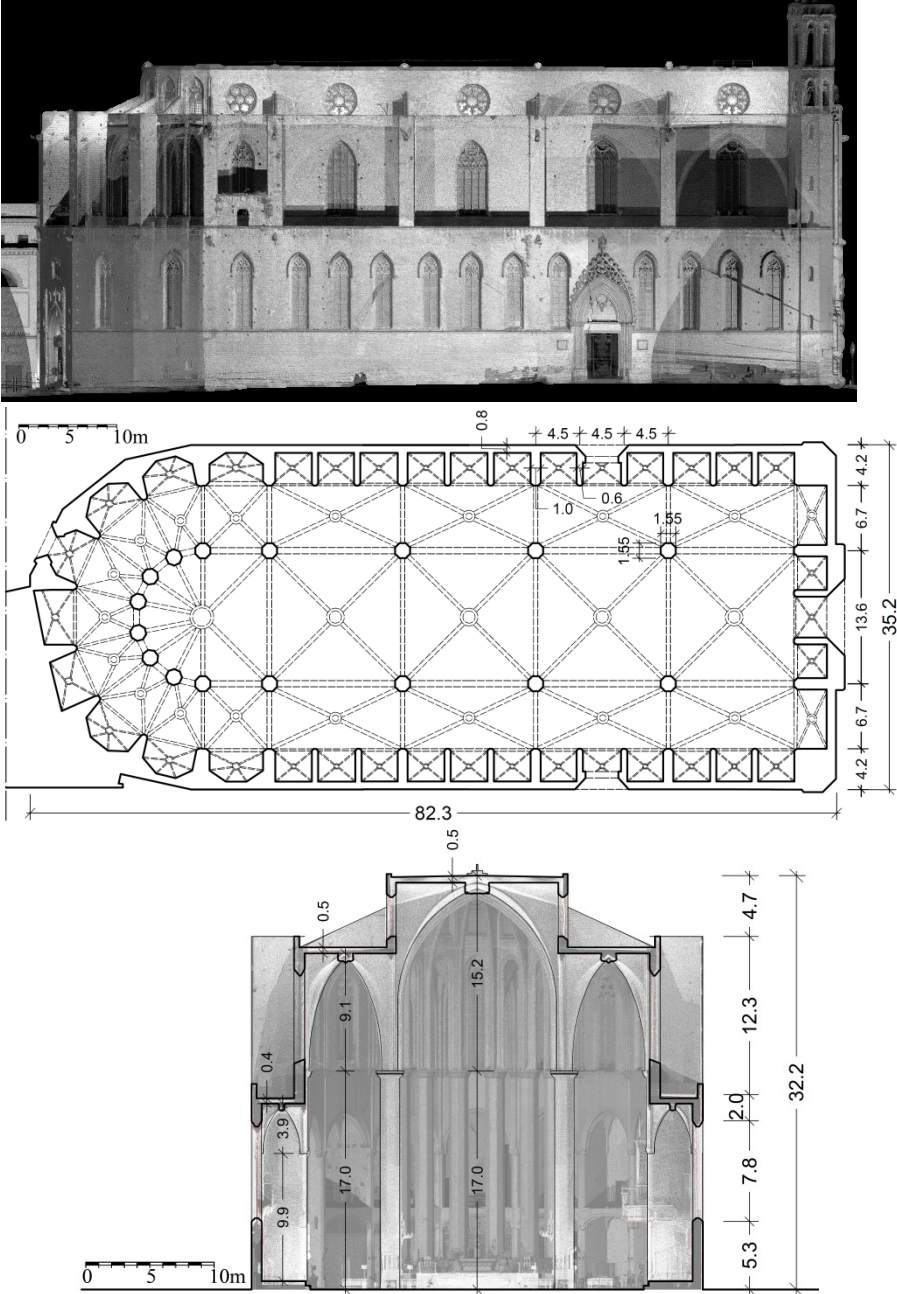
Figure 4.2 Lateral view, plan, transversal section of *Santa Maria del Mar* cathedral

The church has a basilica type plan, 82.3 m long and 35.2 m large, with three naves and lateral chapels. The central nave is divided in four almost square modules (13.5x13.6m), all covered with crossed vaults (fig.4.3a) . The keystones at the apex of the vaults are 32.2 m from the floor. The vaults are supported by octagonal pillars with circumscribed diameter of 1.55 m. The height, of the pillars from the floor to the abutments of the central nave, is equal to 22.6m. Consequently, it can be said that the pillars of *Santa Maria del Mar* church are characterized by an uncommon slenderness.

The lateral nave, divided in four modules as well as the central one, have width approximately equal to half of central nave (6.7m). The four modules are covered by crossed vaults (fig.4.3b) having height equal to 26.6, almost as high as the central ones. The lateral vaults are adequately positioned to receive the lateral thrust of the central vaults and carry it to the buttresses, playing a structural function similar to flying arches, which therefore were not needed (Gonzales et al.2008). The massive buttresses (1m thick) are clearly visible in the lateral view of the church and in the picture of fig.4.1a, where they mark the partition of the naves into four bays.

a)   b)

Figure 4.3 a) Crossed vaults in b) central nave; b) lateral nave

Figure 4.4 Ribbed vault between the apse and the presbytery

The building is completed, at the north side, by the presbytery and the apse divided in seven slices covered by crossed vaults. The apse and the presbytery are connected by a ribbed vault shown in Figure 4.4c. At the south side, there is the façade with the two towers. The façade is built with two large buttresses which are needed to counteract the longitudinal thrust produced by the first square vault.

4.1.3   Previous studies

4.1.3.1   Pioneering studies

Pioneering studies on the Santa Maria del Mar church were carried out by Irizarry (2004). Irizarry evaluated the seismic vulnerability of the principal monuments in the city of Barcelona. A representative monument, the Santa Maria del Mar church, was assessed in detail. One bay (shown in fig. 4.5) was analyzed performing a FE model, consisting of shell elements. Non linear static analysis of the FE model was carried out, giving a maximum value of the load factor equal to 0.14. The results were compared with the limit analysis, which provided a load factor equal to 0.11 (Table 4.1). The capacity curves, obtained by the two analyses, were compared with the seismic demand using the capacity spectrum method. The capacity spectrum method, performed using

mean values for the demand and capacity spectra, showed that a mean damage grade of slight to moderate can be expected for the church.

Finally the expected damage, according to the performed analyses, was compared with the historical seismic damage suffered by the church. The damages was similar to the damage obtained from the analysis.

Figure 4.5 Typical bay studied by Irizarry (Irizarry 2004, fig.9.13, pg. 191)

Table 4.1 Load multipliers obtained by Irizarry (2004)

Element	Analysis	Load Multiplier
Typical bay	FEA (load according to mass)	0.12
	Kinematic limit analysis	0.11

4.1.3.2   Non destructive testing

A multidisciplinary study on morphology, material and structure of Santa Maria del Mar church was carried out by Giraldez et al. in 2007. Non destructive testing (geo-radar, pulse-radar, hole drilling, seismic tomography) were executed in order to prepare and validate more accurate models of the church. The results are also reported in Roca et al. (2008).

The testing provided valuable information on the internal morphology of the structural components (piers, walls, vault fillings). Data about the foundation soil were also given, revealing a poor soil characterized by sandy and clay layers.

The filling of the vaults was investigated through the pulse radar and direct inspection. A superficial previous archaeological pit, during the 80's, had revealed that the upper infill over the vaults of the central nave consisted of empty pottery, fixed with lime mortar (fig. 4.6). The radar

inspection showed that the depth of the pottery infill should be about 1 m in the central nave. The volume between the membrane and this upper pottery layer should be filled with resistant lime concrete, as well as in the lateral vaults.

The compression stresses at the base of the piers was also measured, using the hole-drilling technique, which provided an average value of 3,0 MPa.

Figure 4.6 Pottery filling over the central vaults

4.1.3.3   Seismic assessments: FE and limit analysis

The data obtained by non destructive testing were used to assess, more accurately, the seismic behavior of the church. The multidisciplinary study reported in Giraldez et al. (2007) provided a comparison between non linear static analysis and limit analysis.

The non linear static analysis was carried out on a FE model of one typical bay of the church. Compared with the pioneering Irizarry's study, the updated FE model consisted of solid elements and it took advantage of the improved knowledge of the building. In particular, the model considered the light pottery filling of the central vaults. The results, in terms of load multiplier, are reported in Table 4.2. They are equal to 0.15

and 0.12 respectively for a distribution of horizontal force according to the first mode and to the masses.

Static and kinematic limit analysis were also performed for different macro-elements of the structure: typical bay, façade and towers. The obtained load multipliers are provided in the Table 4.2. The collapse mechanisms evaluated in the limit analysis are plotted in Figure 4.7. Different collapse mechanism were considered for the typical bay, but only the mechanisms providing the lowest load multiplier are reported in the Figure. It was not considered necessary to make a specific study of the apse because it is a structural part particularly rigid, due to the high concentration of buttresses and its favorable radial arrangement. The seismic capacity of the longitudinal section was assumed depending by the capacity of the façade, because it is the weakest element. Consequently the kinematic analysis of the façade was considered sufficient to estimate the capacity of the entire longitudinal section.

The weakest mechanisms corresponded to the overturning of the spandrel over the rose window and the upper gallery of the towers. These are the only parts which experienced severe damage or collapse during the 14th-15th c. earthquakes (see section 4.1.1)

Table 4.2 Load multipliers given in Giraldez et al. 2007

Element	Analysis method	Load Multiplier
Typical bay	FEA (load according to 1st mode)	0.15
	FEA (load according to mass)	0.13
	Static Limit Analysis (load according to 1st mode)	0.12
	Static Limit Analysis (load according to mass)	0.09
	Kinematic Limit Analysis (load according to mass)	0.10
Tower *Global ooverturning*	Kinematic Limit Analysis (load according to mass)	0.14
Tower *Upper body collapse*	Kinematic Limit Analysis (load according to mass)	0.08
Façade *Global overturning*	Kinematic Limit Analysis (load according to mass)	0.11
Façade *Upper body collapse*	Kinematic Limit Analysis (load according to mass)	0.07

$\lambda = 0.097$ $\lambda = 0.098$

$\lambda = 0.142$ $\lambda = 0.08$

$\lambda = 0.105$ $\lambda = 0.07$
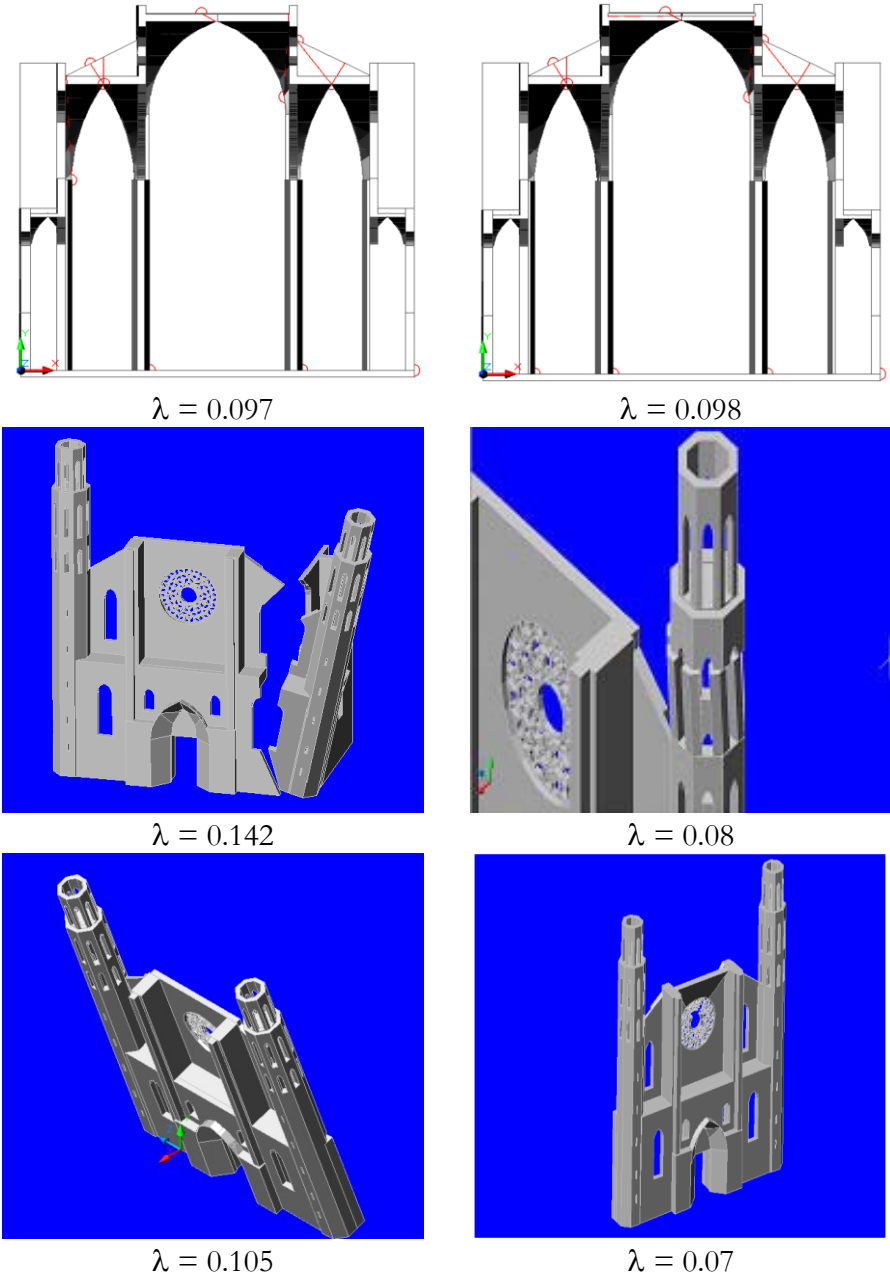
Figure 4.7 Kinematic limit analysis provided in Giraldez et al. 2007

Further FE analyses on a single bay of the cathedral were carried out by Murcia (2008), while further limit analyses were presented by Vacas (2009) and Cuzilla (2009), considering respectively up to 24 and 21 mechanisms. The results, basically in agreement with the previous contributions, are reported in a study by Roca et al. (2009) on the seismic response of gothic churches. Figure 4.8 shows the capacity curves obtained from the most updated FE model of a typical bay of the church. The curves indicate maximum multipliers equal to 0.1 and 0.12, respectively for loads applied according to mass distribution and to the 1st modal shape. These values were slightly lower than the FE results reported in Irizarry and Giraldez et al., but they were more consistent with the limit analysis.
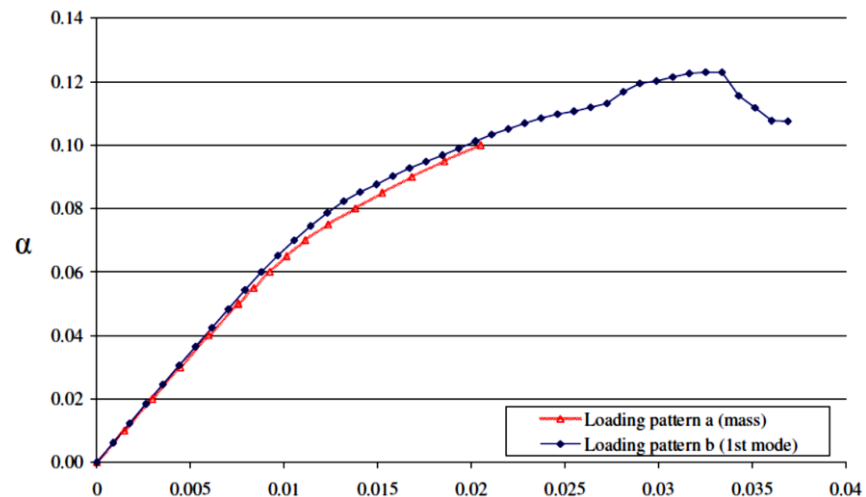
Figure 4.8 Capacity curve of a typical bay, obtained by Roca et al. (2009)

4.1.3.4 More recent studies

All the mentioned studies took into account the behavior of single macro-elements of the church. The global behavior of *Santa Maria del Mar* church was investigated by Chellini et al. (2014). In this study, static, modal and response spectrum analysis were carried out, pointing out possible collapse mechanisms or failure phenomena. In particular the upper part of the facade around the rose window, the facade towers and the transversal nave were the structural parts characterized by higher stress concentrations. Finally, the kinematic analysis permits the

assessment of the safety level for all the identified collapse mechanisms, among which the one involving the upper part of the main facade was characterized by an insufficient safety level for the expected seismic action.

4.2   FE MODEL

The global FE model was prepared on the basis of a terrestrial laser scanner campaign, effected in 2006 by the Virtual City Modelling Lab (LMVC) of the Polytechnic University of Catalonia. Figure 4.9 shows three views of the model: the complete axonometric view, the longitudinal and the transversal sections. It can be noted that all the parts of the cathedral were modelled, except of the vaults in the lateral chapels of the apse.

The model included on the whole 38 068 nodes and 120 404 elements. Among these elements: 73 091 were solid elements and 47 313 were shell elements. The solid elements, four-node three-side isoparametric solid pyramid elements, were used to model the fillings of the vaults and the pillars. The shell elements, including 33 382 three-node and 13 931 four-node elements, were used to model the remaining part of the church.

The size of the mesh was calibrated on a model of a single bay of the cathedral, shown in figure 4.10a. An adequate compromise between accuracy of the results and time spent by the software for the analysis, was searched. Finally a variable size of the mesh was adopted. It is equal to 0.35-0.4m at the connection between each slice of the crossed vaults, and between the vaults and the pillars. It is equal to 0.7-0.8m in the remaining part of the church.
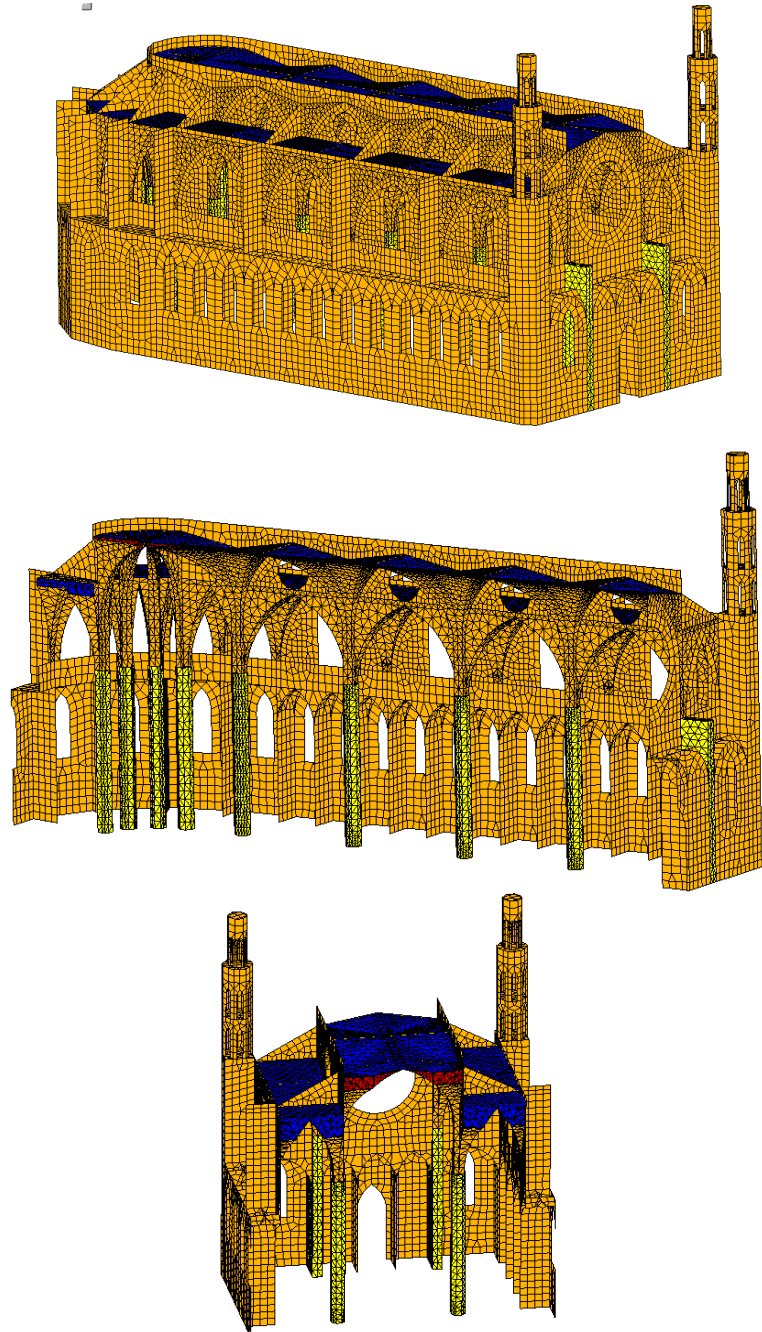
Figure 4.9 Views of the FE model: global view (above), longitudinal section (center), transversal section showing the light filling in the central vaults (below)

A non linear static analysis of the single bay was performed using this mesh size. The capacity curve is plotted in figure 4.10 b . The results were in good agreement with the studies reported in section 4.1.3, therefore the choice about the mesh can be said adequately accurate.
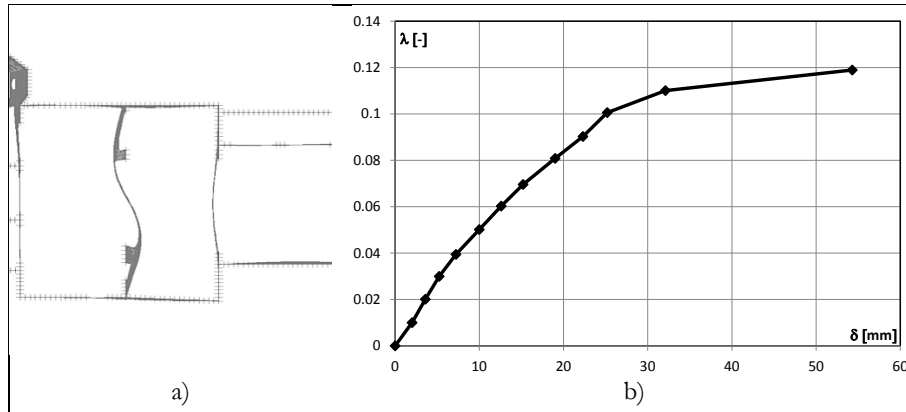
Figure 4.10 a) FE model and b) capacity curve of one bay of the church

The cathedral is almost exclusively made of Montjuïc stone, a siliceous sandstone extracted from the Montjuic mountain. The material properties were assigned according to the previous studies of Giraldez et al. (2007). Four material characteristics were considered and they are indicated with different colors in the views of figure 4.10 and in the table 4.3. The density of the pottery filling, in the central vaults, was considered equal to 1/10 of the other materials. It is noted that the tensile strength was assumed equal to 5% of the compressive strength, according to similar studies on other masonry structures in Barcelona (Elyamani, 2009; Potter, 2011; Saloustros, 2013; Elyamany 2015).

Table 4.3 Material properties

Structural parts	Density [kg/m³]	Poisson's ratio	Young's Module [Mpa]	Compressive Strenght [MPa]	Tensile Strenght [Mpa]
Pillars	2 200	0.3	10 000	12	0.6
Voltes and Walls	2 200	0.3	8 000	8	0.4
Filling of vaults	2 200	0.3	4 000	4	0.2
Pottery filling in central vaults	220	0.3	4 000	4	0.2

4.3 LINEAR ANALYSES

In this section, a preliminary assessment of the structural behavior of *Santa Maria del Mar*, considering only the linear regime, is presented.

4.3.1 Linear static analysis

A linear static analysis for gravity load was carried out to verify the suitability of the FE model. Figure 4.11 shows the contour of the vertical stresses, plotted on the deformed shape obtained from the analysis. The results gave realistic values. The stress state exhibited by the most of the structure is characterized by low compressive stresses. The maximum compressive stress was 3.08 MPa at the base of the, much lower than the compressive strength equal to 12 MPa. This result is in complete agreement with the experimental results discussed in section 4.1.3. Tensile zones were found on the vaults and, partially, on the buttresses. The maximum tensile stress was equal to 0.618 MPa, little higher than the tensile strength of the materials. This will imply little damage in the non linear analysis for dead load. The maximum deflection, almost equal to 8mm at the key of the central vault, was a realistic and acceptable value.
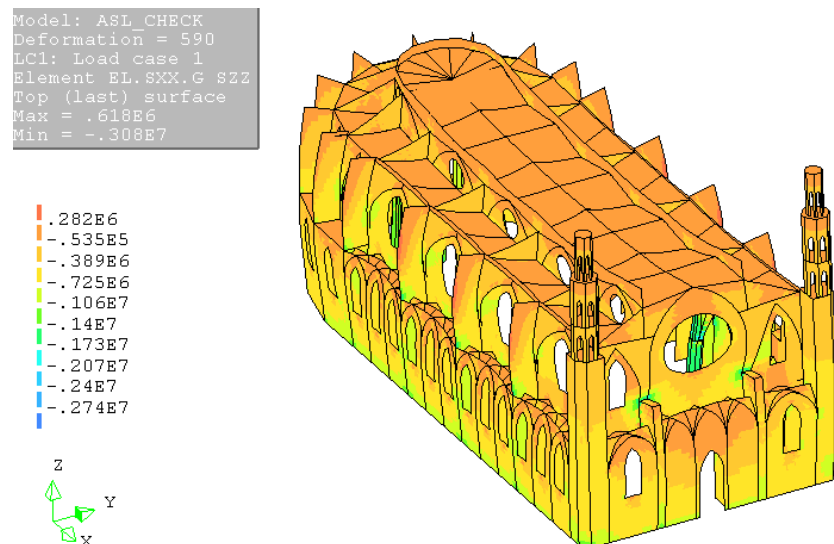
Figure 4.11 Linear static analysis: contour of the vertical stresses on the deformed shape

4.3.2 Modal analysis

The modal analysis was performed in order to find the dynamic properties of the church: frequencies/periods of vibration, modal shapes, participation factors.

The numerical frequencies were compared with the experimental frequencies, provided in 2007 by the *Servicio de Geofísica Aplicada* of the Polytechnic University of Catalonia. The frequencies of the first modes were measured in different points of the church. The values measured in the central bay are considered in the following to compare the results.

The numerical frequencies did not match the experimental data, therefore the stiffness (Young's modulus) of the material was adjusted, in order to obtain a better agreement. The final values assigned to the Young's modulus are reported in Table 4.4.

Table 4.4 Final values of the Young's modulus

	Structural parts	Young's Module [Mpa]
🟨	**Pillars**	6 000
🟧	**Voltes and Walls**	4 800
🟦	**Filling of vaults**	2 400
🟥	**Pottery filling in central vaults**	2 400

Table 4.5 Experimental and numerical frequencies

Experimental frequency	Numerical frequency		Direction
	Initial model	*Final model*	
[Hz]	mode	[Hz]	[Hz]	
1.45	1	1.86	1.46	transversal
2.05	2	2.28	2.12	longitudinal
2.19	3	2.38	2.15	longitudinal
2.4	4	2.61	2.38	longitudinal
2.7	5	2.72	2.42	transversal
2.73	6	3.09	2.45	longitudinal
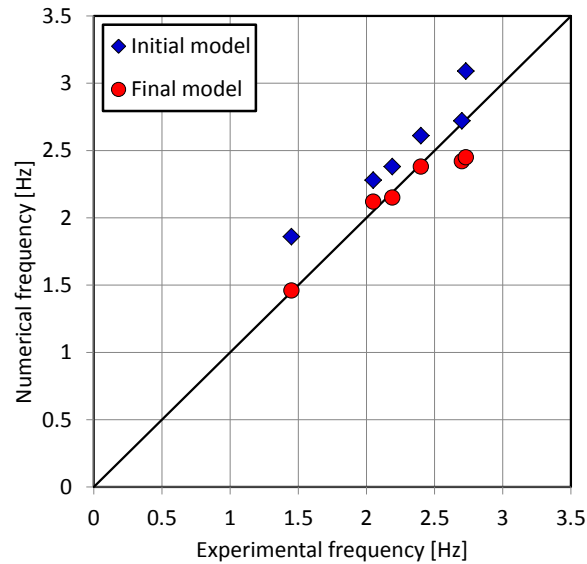
Figure 4.12 Comparison between the experimental frequencies and the numerical frequencies of initial and final models
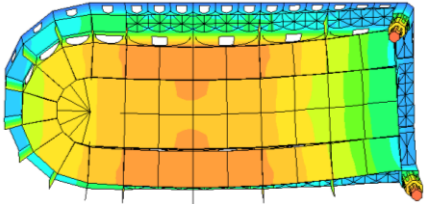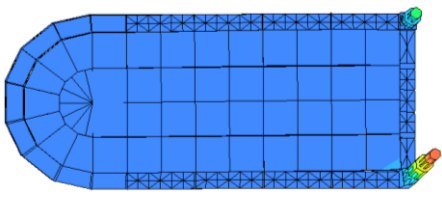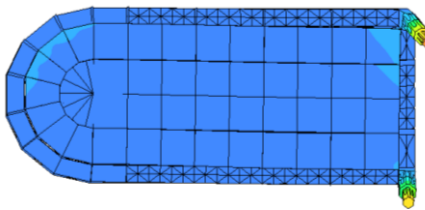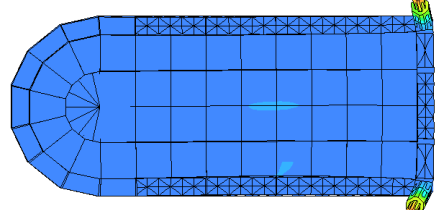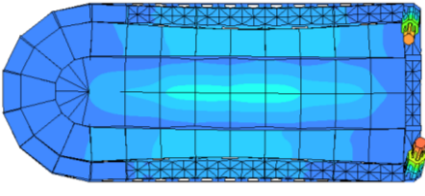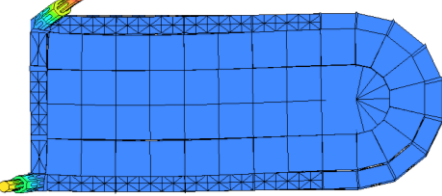
The numerical frequencies, for the first six modes, of initial and final model, are reported with the experimental frequencies in Table 4.5. It can be noted that the first frequency was satisfactorily adjusted, since it corresponded to a transversal mode which involved approximately 70% of the total mass. The other numerical frequencies, even if they were less accurately adjusted, better match the experimental data, as it can be noted from the graph in Figure 4.12.

The graph reports experimental and numerical frequencies respectively on the x and y axes. The numerical frequencies obtained from final and initial model were represented by different indicators. It can be observed that the final model provides better results than the initial one, for all the considered frequencies, except of the fifth.

The modal shape and the corresponding periods and participation factors of the first six vibration modes, are plotted in Figure 4.6. The modes from 2 to 6 are local modes, involving just single macro-elements of the structure (in particular the tower) and they correspond to small values of the participating mass ratio. This result is in agreement with the conclusions of chapter 3, about the dynamic behavior of the masonry churches. However, as mentioned above, the first vibration mode of

Santa Maria del Mar church is a global mode and involves the most of the total mass (66.4%). It can be deduced that the dynamic behavior of this church is quite different, compared with the fourteen case studies, described in chapter 3.

Table 4.6 Modal shapes

Mode 1: T = 0.69s M_{pL}=0% M_{pT}=66.4%	Mode 2: T = 0.47 M_{pL}=32.4% M_{pT}=0.2%

Mode 3: T = 0.47s M_{pL}=23.1% M_{pT}=0.4%	Mode 4: T=0.42s M_{pL}=11.1% M_{pT}=0.0%

Mode 5: T = 0.41s M_{pL}=0.2% M_{pT}=0.0%	Mode 6: T = 0.41s M_{pL}=0.2% M_{pT}=0.0%

The graph type and the dynamic parameters defined in section 3.3.2 are provided also for Santa Maria del Mar church, respectively in Figure 4.13 and in Table 4.7. As it can be observed, except of the sum of the first 100 vibration modes, all the other results are not in line with what has been obtained in chapter 3. Considering the vibration modes corresponding to M_p>5%, approximately 70% of the total mass was reached and, extrapolating ten vibration modes corresponding to the highest values of M_p, 80% was obtained. Moreover, the most of the vibration periods are concentrated at the plateau of the spectrum. It can be explained considering that *Santa Maria del Mar* church has a very

regular, compact structure, as it has been described in section 4.1.2. All the structural parts are well connected each others and, at the north side, the apse with its radial walls forms a considerable rigid elements.
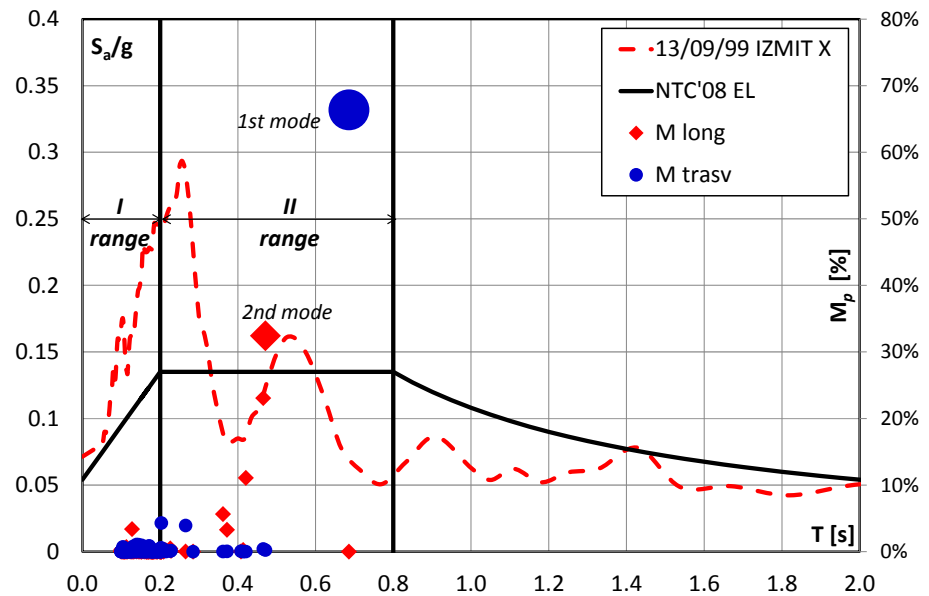
Figure 4.13 Distribution of M_p (modal participating mass ratios) for the first 100 vibration modes and comparison with the response spectra

Table 4.7 Dynamic parameters

	100 v.m.	M_p>5%	10 $M_p$max	I range	II range
ΣM_{plong}	83.9%	72.2%	80.7%	7.3%	76.6%
$\Sigma M_{ptransv}$	84.5%	66.4%	80.5%	7.9%	76.6%

4.4   NON LINEAR STATIC ANALYSIS

A non linear static analysis (NSA) was carried out applying: gravity loads in the first step, increasing horizontal forces, proportional to the masses, in the second step. The analysis was performed in the transversal direction (Y), in the positive (X+) and negative (X-) longitudinal

directions, indicated in Figure 4.14. The capacity curves were obtained considering 8 control points (C.P.) shown in this Figure.
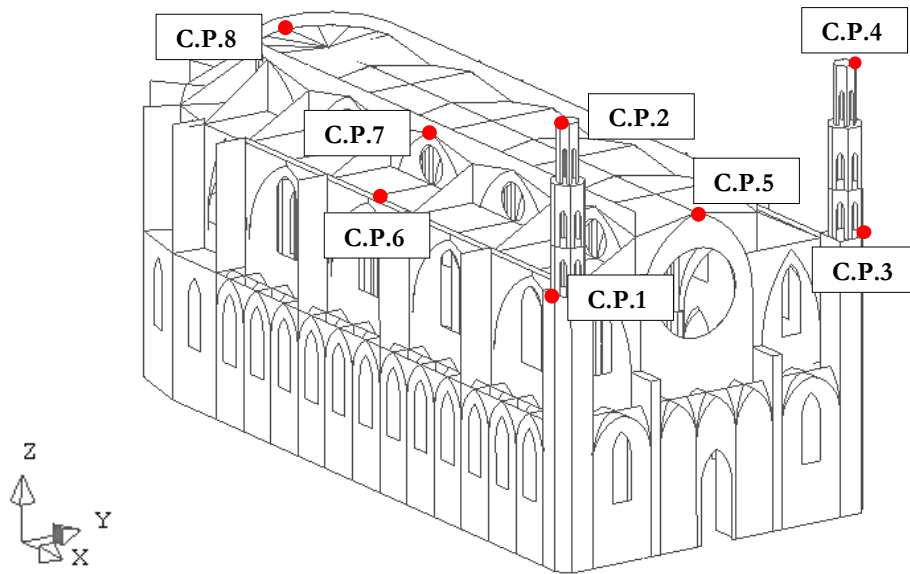
Figure 4.14 Considered control points

To simulate the non linear behavior of the masonry, a fixed smeared cracking model was considered, in detail the multi-directional fixed crack model implemented by DIANA TNO was considered. According to this model, the tensile regime is described as a combination of tension cut-off (fig. 4.15a), tension softening (fig.4.15b) and shear retention (Manie and Kikstra 2014). The tension softening was defined assigning a value of the fracture energy (G_f) equal to 50 N/m². The compressive regime is modeled using the Drucker–Prager failure criterion. This material model was adopted according to similar studies on masonry churches, performed with the same software (among the others Elyamani 2015, Endo 2015a, b). A better modelling of the non linear behavior of the material is provided by a total strain fixed crack model, since it describes the tensile and compressive regime with one stress-strain relationship. However it can be much more costly in terms of time spent to complete the analyses. Therefore, for large scale model, the multi-directional crack model is preferred.
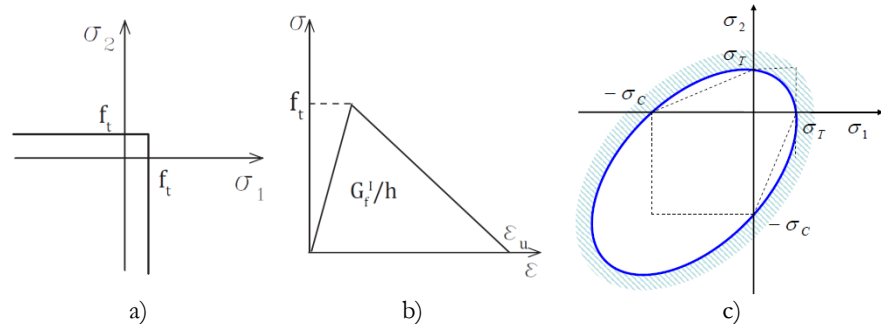
Figure 4.15 Multi-directional fixed crack model: adopted laws for a) tension cut-off ; b) tension softening c) failure criterion for compressive regime

4.4.1   Transversal direction

The NSA in transversal direction was carried out using both the constitutive material models illustrated in the previous section. When the total strain model was used, a bi-linear σ-ε law was adopted. The effect of the geometrical non linearity was also evaluated in this analysis. Figure 4.16 shows the capacity curves (displacements Vs load multiplier) obtained for the transversal direction considering: a) a multi-directional fixed crack model (MDFC); b) a multi-directional fixed crack model and the geometrical non linearity (MDFC+GNL); c) a total strain fixed crack model and the geometrical non linearity (TSFC+GNL). The comparison is presented in the figure considering the displacements of only one control point (C.P. 6). However similar differences were found for the other points. It can be observed that, taking into account the geometrical non linearity, the load multiplier decreases from 0.11 to approximately 0.095. It can be explained considering the considerable slenderness of the pillars (see section 4.1.2) On the other hand, almost identical results, both in terms of displacements and load multiplier, were obtained with the two material model. This comparison confirmed the suitability of the multi-directional fixed crack model, which was used for all the performed analyses, illustrated in the following.

The capacity curves obtained in transversal direction, for each considered control point are presented in figure 4.17.
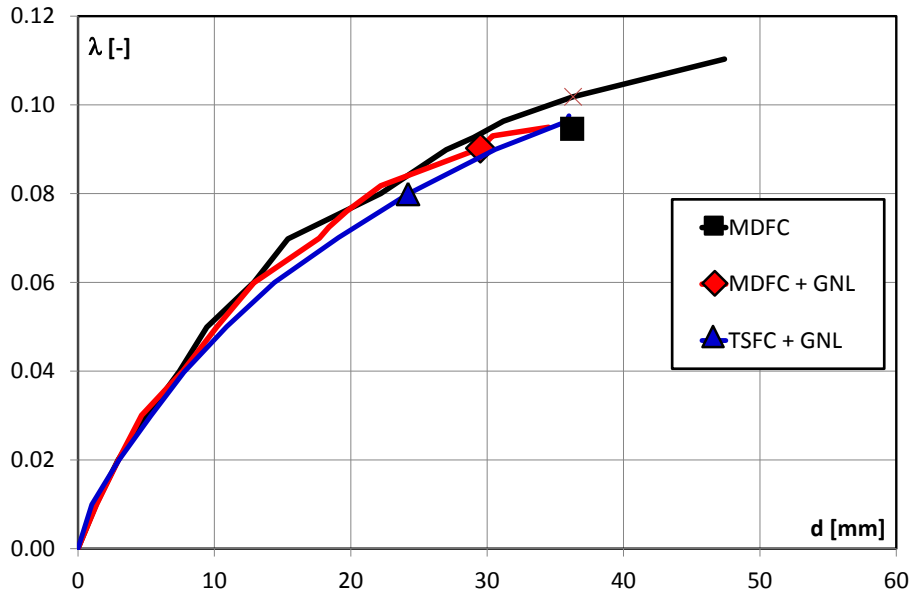
Figure 4.16 Comparison between the capacity curves obtained with different analysis input for the transversal direction of the earthquake (control point 6)
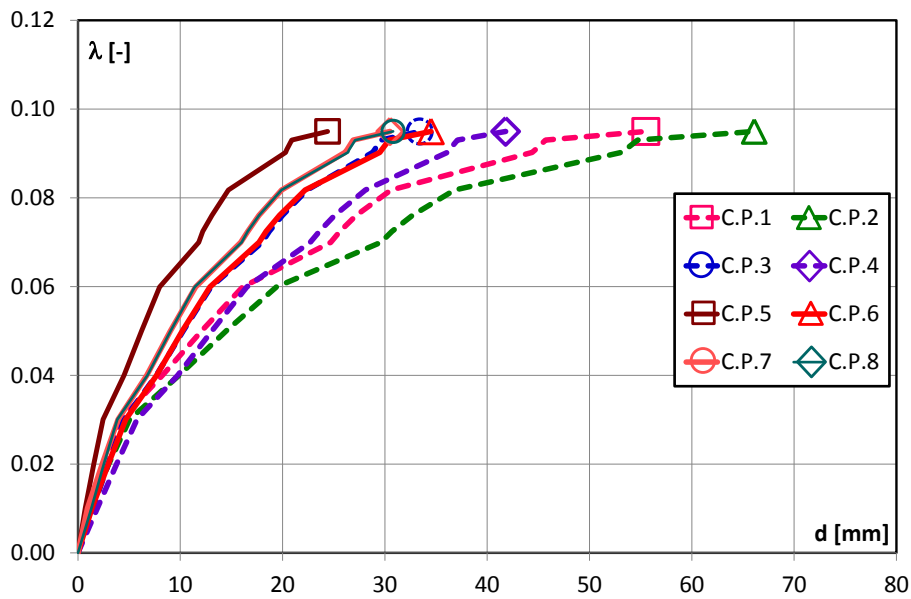
Figure 4.17 Capacity curves at different control points for the transversal direction of the earthquake

The maximum load multiplier is equal to 0.095. The maximum displacements equal to 66mm was found for the C.P.2, which corresponds to the top of the left tower. A similar high value (56mm) was found for C.P.1, which corresponds to an intermediate point of the left tower. The right tower (C.P. 3 and C.P.4) experienced lower displacements. The lowest displacement equal to 24mm was obtained considering the C.P.5, at the top of the façade. The central bay of the cathedral is characterized by intermediate values of the maximum displacement, about equal to 35mm. It is remarkable that these results are in good agreement with the analysis performed on a single bay of the church (see section 4.2, fig. 4.10). The maximum values of the displacement and the load multiplier, on a single bay, were respectively 55mm and 0.12. The higher values of the load multiplier is probably due to the fact that the geometrical non linearity was not taken into account.

To explain how the cathedral failed in this direction, the evolution of the crack pattern has been observed and it is plotted in Figure 4.18 for a bay adjacent to the façade. Moderate damage can be observed on the vaults also for seismic load equal to 0.02–0.04g, as soon as the horizontal loads are applied. It can be explained considering that, in the first step of the analysis, the gravity load was applied and it induced tensile stresses in the vaults, higher than the tensile strength of the material (as it has been found from the linear static analysis in section 4.2.2). With the increase of the lateral loads (0.06-0.08g), a series of disconnections or hinges can be noticed at the abutments and at the keystone of the vaults. Consequently a significant decrease of the stiffness is exhibited by the capacity curves. The collapse occurred when the damage becomes significant also at the base of pillars and of right perimeter walls. Ten hinges, the sufficient number to activate the mechanism, can be found at the ultimate step. The identified failure mechanism is very similar to those provided by the limit analysis, and the load multiplier are almost identical. In detail the mechanism corresponding to $\lambda = 0.097$, (figure 4.7, section 4.1.3.3) is found consistent with the failure mechanism given by the NSA. In fact both of them shows that there are not disconnections at the base of the left walls.

Significant damage can also be observed on the buttresses and, in particular, on the vaults of the small lateral chapel, probably compressed by the much stiffer buttresses. Finally it is remarkable the development of a diagonal crack on the façade of the cathedral, proving its shear damage.

a = 0.020g

a = 0.040g

a = 0.060g

a = 0.080g

a = 0.092g

a = 0.098g
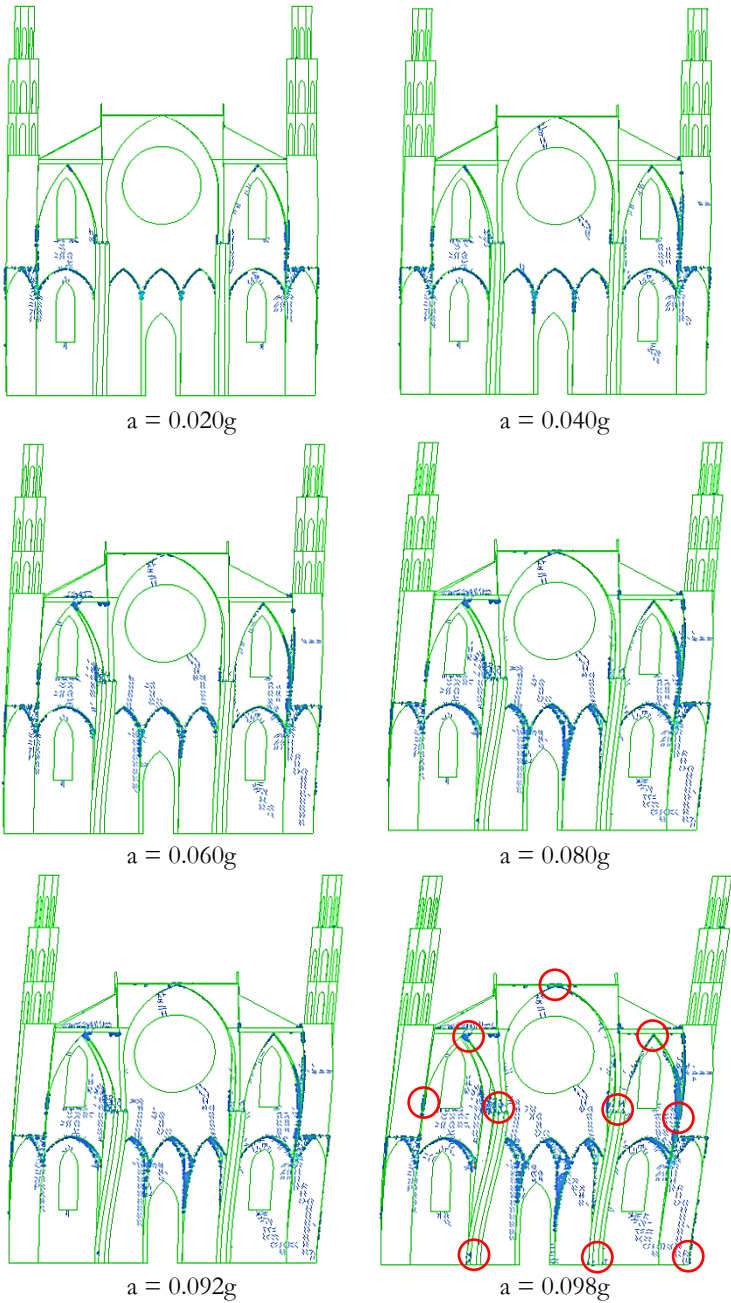
Figure 4.18 Evolution of the crack pattern and the associated seismic load factor, for the transversal direction of the earthquake

4.4.2 Positive longitudinal direction

In view of the results obtained for the transversal direction, the non linear static analyses in longitudinal direction were carried out considering the multi-directional fixed crack model and the geometrical non linearity, assuring a good accuracy of the results.

The capacity curves obtained in positive longitudinal direction, for each considered control point except of C.P.3 and C.P.4, are presented in figure 4.19. The control points 3 and 4 correspond to the right tower which experienced displacements basically identical to the left one.

The maximum load multiplier is equal to 0.097. Due to the greater stiffness of the cathedral in this direction, the obtained displacements are significantly lower in comparison with the transversal ones. As expected, the maximum displacement, equal to 37mm, is given by the C.P.2, namely the highest point of the tower. Similar displacements were found for the C.P.1, namely the intermediate point of the left tower. All the other control points are characterized by similar displacements, quite lower than the tower and at most equal to 15 mm.
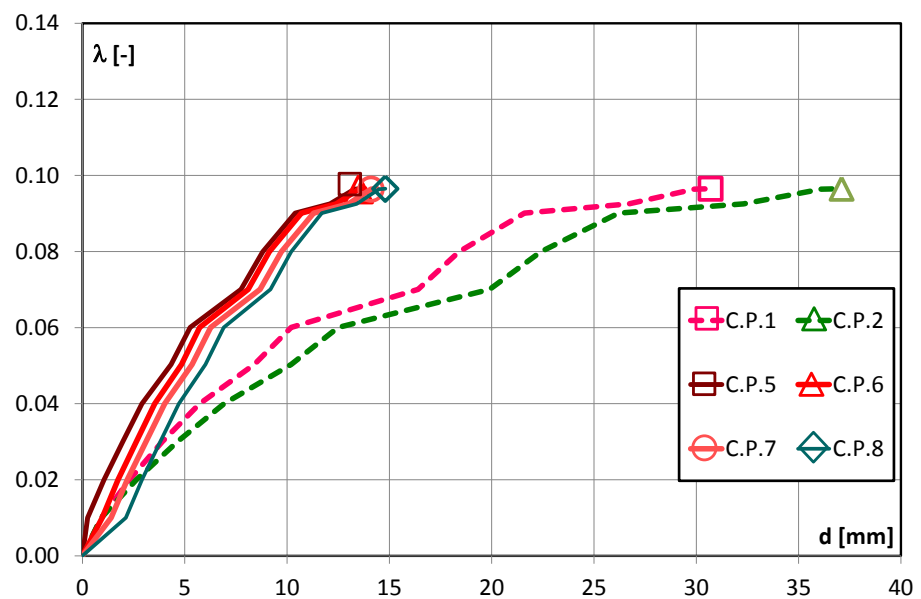
Figure 4.19 Capacity curves (load multiplier Vs displacements) at different control points, for the positive longitudinal direction of the earthquake

It can be deduced that the displacement of the towers during the analysis was independent from the rest of the church and it led to the their overturning. This failure mechanism was confirmed by the crack pattern shown in Figure 4.20. The figure represents the damage at the ultimate state of the analysis. Significant crack can be observed in the vaults of the small lateral chapels, and at the abutments of the lateral vaults, but the most serious damage and deformation was found at the connection between tower and perimeter walls. This result was in agreement with the limit analysis, which gave the overturning of the tower for a load multiplier equal to 0.08, similar to the obtained FE result.

a)

b)
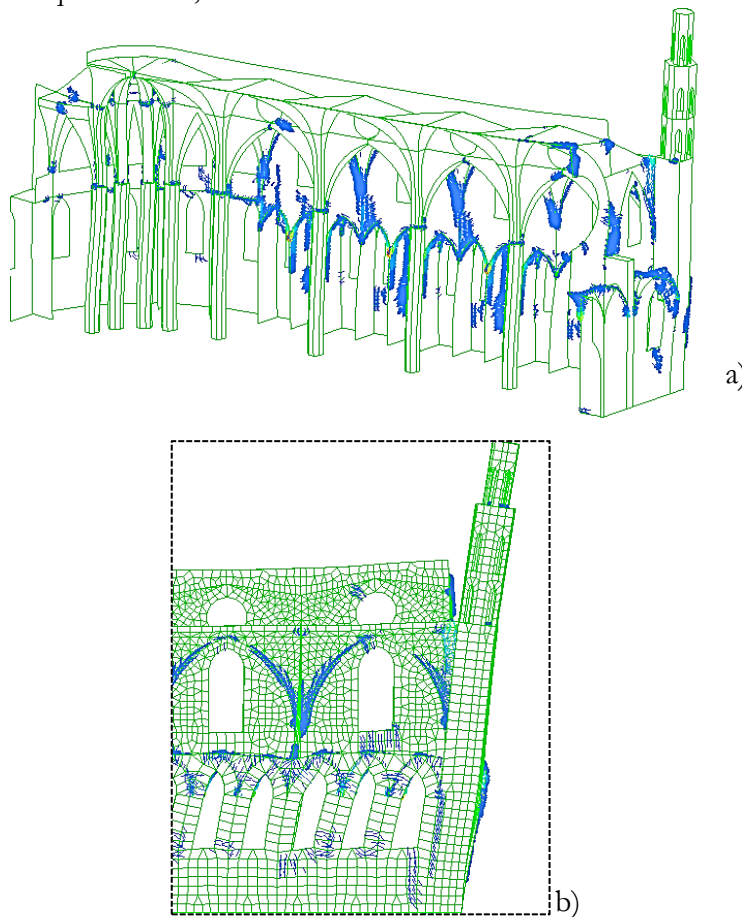
Figure 4.20 Crack pattern at the ultimate state on a) view of the longitudinal section b) zoom of the external lateral view, for the positive longitudinal direction of the earthquake

4.4.3   Negative longitudinal direction

The capacity curves obtained in negative longitudinal direction are presented in figure 4.21. The same control points used for the positive longitudinal direction are considered.

The maximum load multiplier is equal to 0.12, appreciably higher than the result achieved in positive direction. On the other hand, the maximum displacements - providing 34mm and 26mm respectively at the top and at an intermediate point of the tower (C.P.2, C.P.1), and approximately 15mm for the other control points - are very similar compared with the positive direction, As a result, the slope of the capacity curves is greater compared with the curves plotted for both transversal and positive longitudinal direction. It proves the higher rigidity of the church in this direction, due to the presence of the stiff apse at the north side.
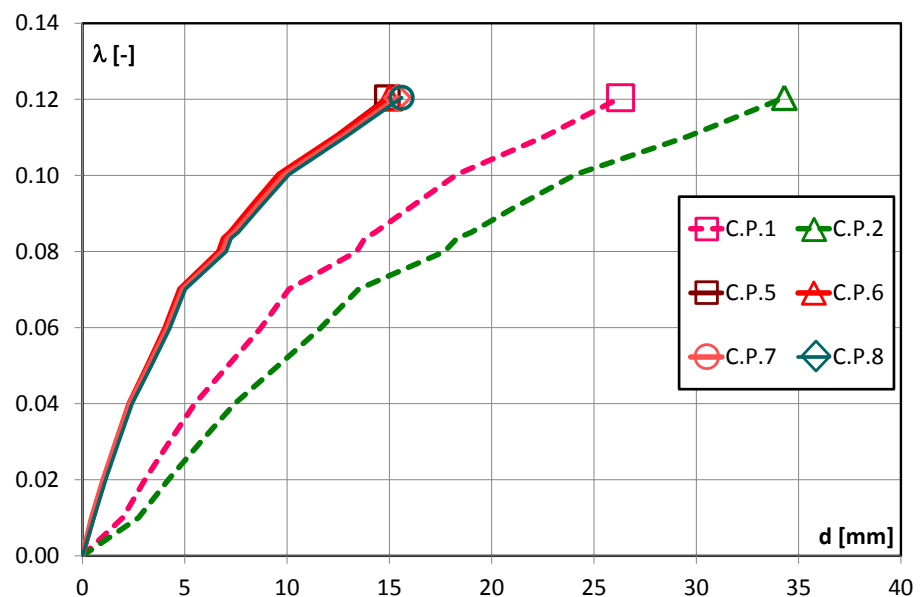
Figure 4.21 Capacity curves (load multiplier Vs displacements) at different control points, for the negative longitudinal direction of the earthquake

The identified failure mechanism for the negative longitudinal direction was attributed to the damage of the pillars. Figure 4.22 shows the crack pattern captured at different states of the analysis.

a=0.07g

a=0.1

a=0.12
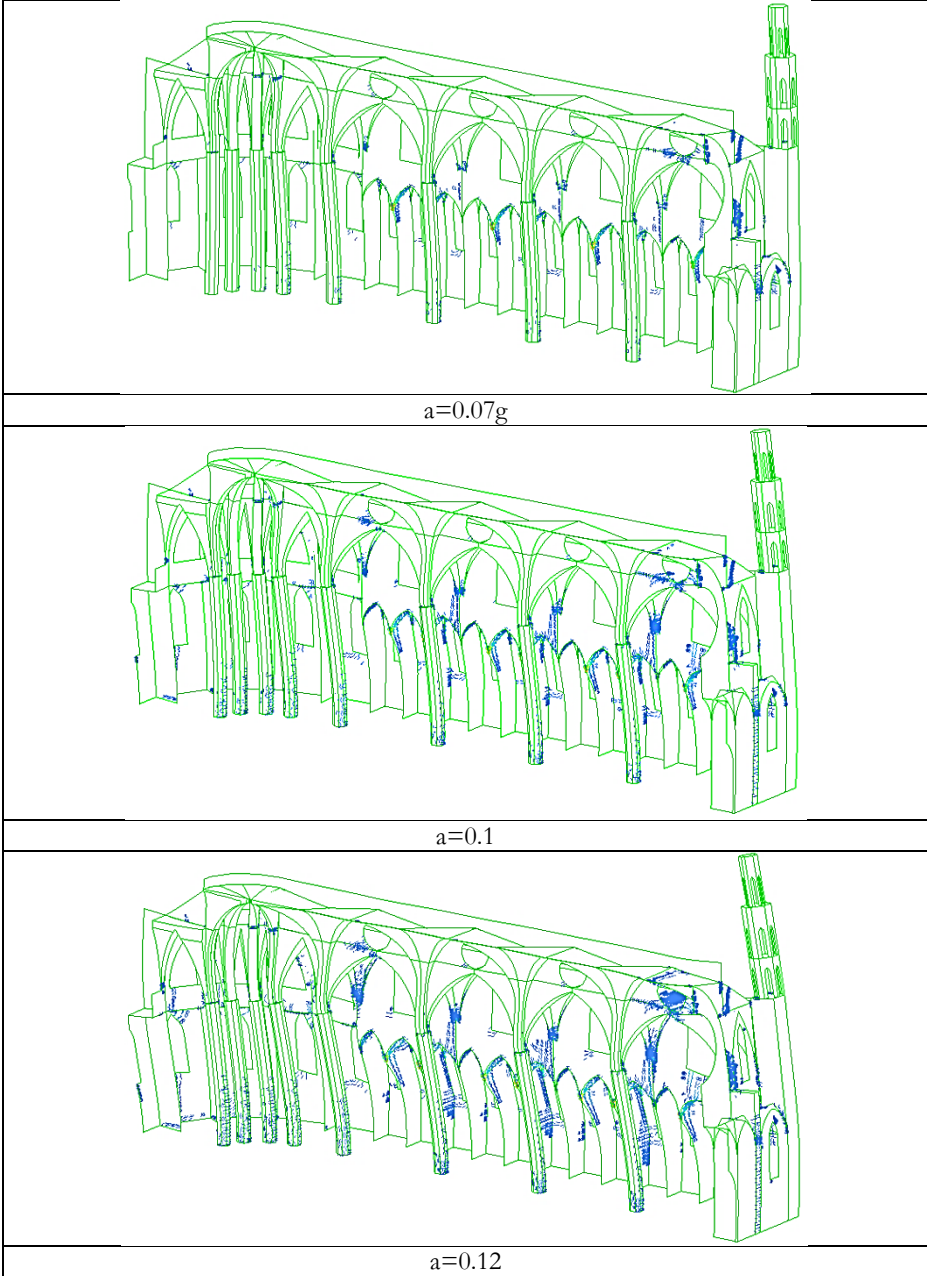
Figure 4.22 Evolution of the crack pattern and the associated seismic load factor, for the negative longitudinal direction of the earthquake

Also for a small value of acceleration of 0.07g, damage was concentrated at the base of the pillars. At this state, a decrease of the slope is observed in the capacity curves. Further decrease is noticed at the acceleration of 0.1g, when the crack pattern clearly shows that the bases of all the pillars was damaged. At the ultimate state the cracks almost reached the half of the pillars in the apse, causing the collapse of the structure.

4.4.4   Comparison with the existent damage

The existent damage of Santa Maria del Mar church is basically due to: fires experienced in 1379 and 1936, which damaged especially the piers; differential settlement, which caused a longitudinal crack developed following the keystones of the lateral vaults (Gonzales et al.2008); earthquakes occurred during XIV, XV and XVII centuries. Since no notable restoration has been undertaken in the past, most of the damage visible today, consisting of distinct cracks in walls and façade, might still be the one caused by the past earthquakes. In this case, the response of the building to earthquakes of such intensity would be still fully readable today in the shape of rather slight or moderate damage (Roca et al.2009). Then the existent damage was compared with the cracks noticed through the NSA. The comparison is given in Figure 4.23 – 4.25. It can be observed that a good agreement was found between the real and the analytical damage.

In detail, the pictures of the façade (fig. 4.23 PF1-PF4) show the same diagonal crack mentioned in section 4.3.1, the only difference being the presence of this crack also in the opposite direction, to form a cross in correspondence of the rose.

On the lateral façade (fig. 4.24, picture PLF1), cracks can be noted at the base of the walls. Other cracks start from the opening of the small chapels and go, slightly inclined, toward the upper part of the wall (fig. 4.24, PLF2-PLF3). The crack inclined towards the tower (PLF3), is probably due to the leaning of the tower during the earthquakes. These cracks were obtained from NSA in positive longitudinal direction.

From inside, some cracks can be observed on the walls of the lateral nave (fig. 4.25 pictures: PI1-PI2) and also on the central vault, where the cracks start at the arches and going up inclined to the circle opening (fig4.25, PI3). Very similar damage was noticed on the longitudinal section of the model, caused by the NSA in positive longitudinal direction.

153

PF-1

PF-2

PF-3

PF-4
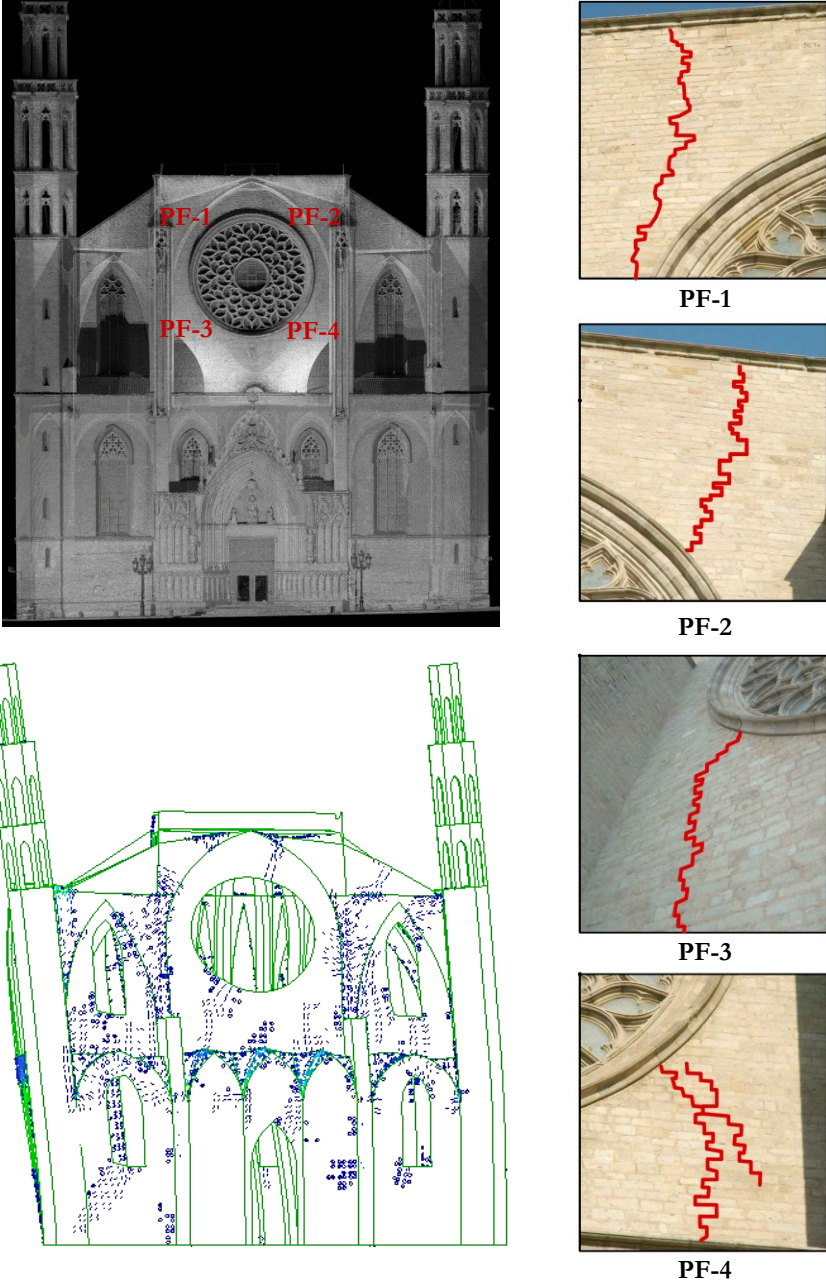
Figure 4.23 Comparison between real damage of the façade and crack pattern provided by the NSA in transversal direction
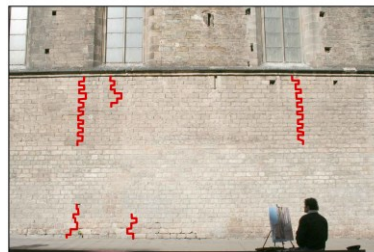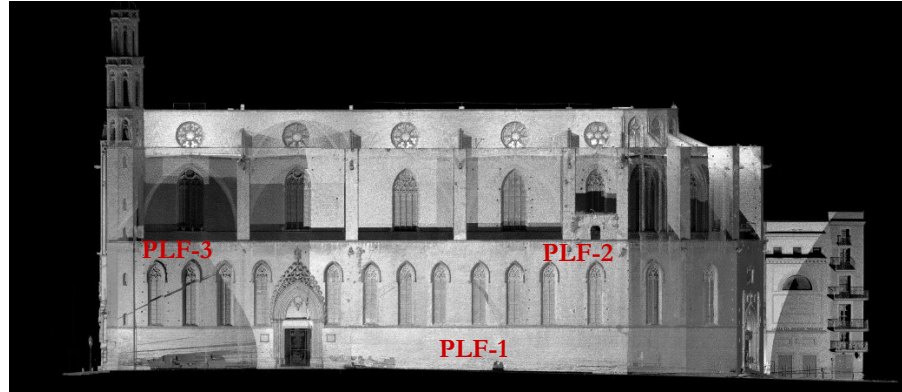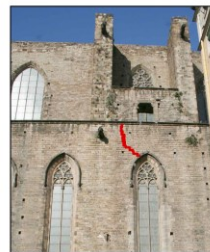
PLF-1 **PLF-2** **PLF-3**
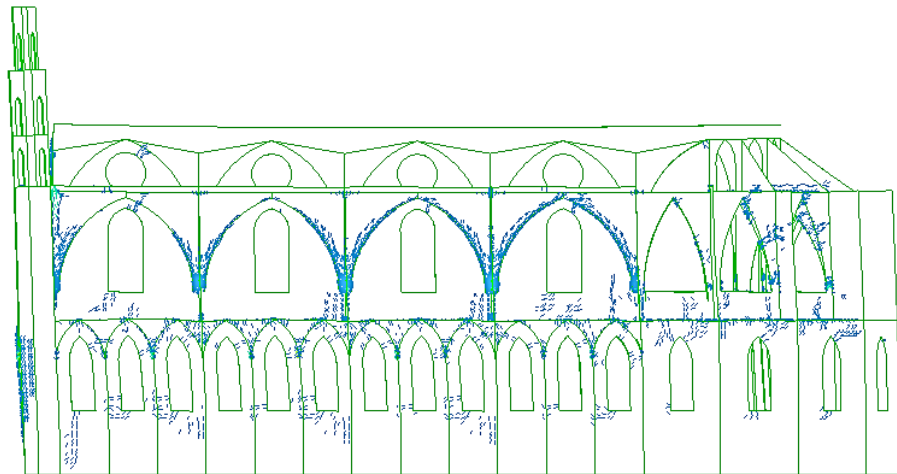
Figure 4.24 Comparison between real damage of the lateral façade and crack pattern provided by the NSA in positive longitudinal direction
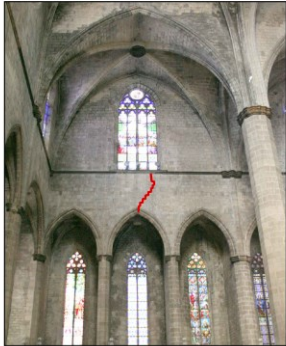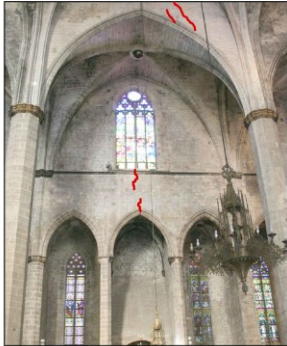
PI-1   PI-2   PI-3
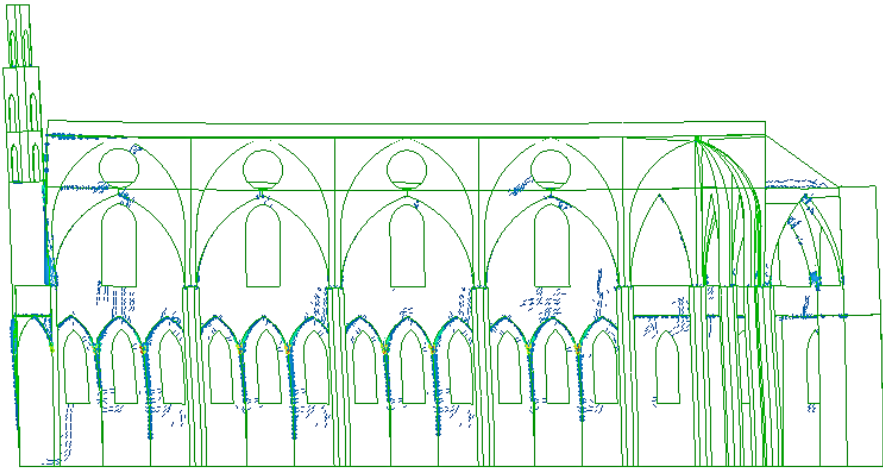
Figure 4.25 Comparison between real damage of internal lateral nave and crack pattern provided by the push-over analysis in positive longitudinal direction

4.4.5 Application of the N2 method

The results obtained from the non linear static analyses were compared with the seismic demand, applying the N2 method. The method has been explained in section 1.2.

The seismic demand was defined by using two codes: 1) the Eurocode 8 (CEN 2004); 2) the Spanish code for seismic design (NCSE-02, 2002). Two return periods, of 475 and 975 years, were considered. A total of four response spectra were used, plotted in Figure 4.26.

The EC-8 spectra were defined considering a basic seismic acceleration equal to 0.04g (corresponding to Barcelona zone). A soil type D was considered due to its poor quality (see section 4.1.3).

The NCSE-02 spectra were determined using the same value of 0.04g for the seismic acceleration and a soil coefficient equal to 1.7, according to the analysis performed in previous study (Giraldez et al. 2007).

Figure 4.7 shows an example of application of the method N2 to evaluate the performance point. The capacity curve obtained in Y direction for the control point CP.6 (central bay) and the Eurocode 8 with a return period of 475 years, are considered in the example. The found displacement corresponding to the performance point was equal to 28mm, lower than the maximum displacement of CP6 in y direction.

Table 4.8 reports the performance displacements obtained for: 3 considered seismic direction, 2 control points, 2 seismic code and 2 return periods. The control points C.P. 2 (top of the tower) and C.P. 6 (central bay) were chosen. By observed the capacity curves plotted in the previous sections, these control points were considered satisfactorily representative of the global capacity of the church. The performance displacements were compared with the maximum displacements reached with the non linear static analysis. The maximum displacements in each direction and for the considered control points are also given in Table 4.8. It can be noted that, in some cases, the maximum displacement is lower than the performance one. The histogram in Figure 4.28 presents the ratio between maximum and performance displacements. The seismic safety, assured when this ratio is higher than 1, was not always verified. It appears that the positive longitudinal direction is the most unsafe, in fact in this case the check is not satisfied neither considering a period of return equal to 475 years. It can be explained considering the greater stiffness of the church in this direction, which limits the displacement capacity.
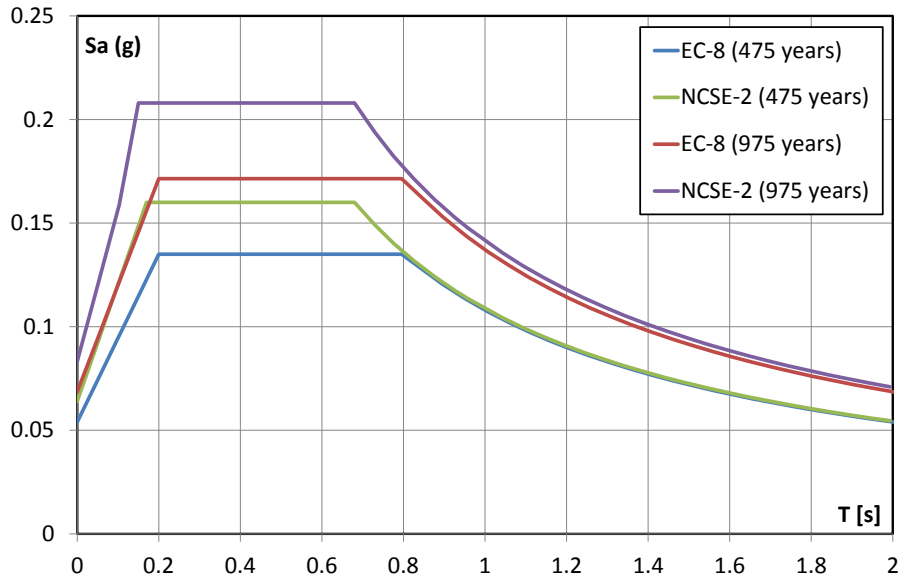
Figure 4.26 Elastic response spectrum provided by Eurocode 8 and Spanish code NCSE-2
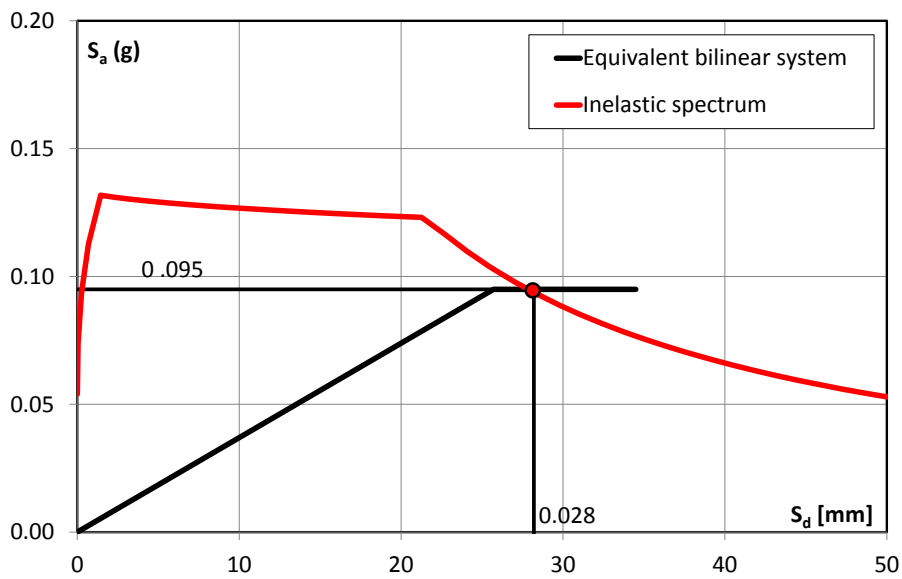
Figure 4.27 Performance point obtained through the N2 method, for control point 6 (central bay), considering the Eurocode 8 with return period of 475 years

Table 4.8 Performance displacements

		C.P. 2	C.P. 6
	d $_{Perf.Point}$ (EC8 475)	44	28
	d $_{Perf.Point}$ (EC8 975)	55	36
Y	d $_{Perf.Point}$ (NCSE-2 475)	44	28
	d $_{Perf.Point}$ (NCSE-2 975)	57	37
	d $_{max}$ (NSA)	**66**	**35**
	d $_{Perf.Point}$ (EC8 475)	26	15
	d $_{Perf.Point}$ (EC8 975)	33	20
X+	d $_{Perf.Point}$ (NCSE-2 475)	26	17
	d $_{Perf.Point}$ (NCSE-2 975)	34	22
	d $_{max}$ (NSA)	**37**	**14**
	d $_{Perf.Point}$ (EC8 475)	20	13
	d $_{Perf.Point}$ (EC8 975)	26	17
X-	d $_{Perf.Point}$ (NCSE-2 475)	21	15
	d $_{Perf.Point}$ (NCSE-2 975)	27	20
	d $_{max}$ (NSA)	**34**	**15**
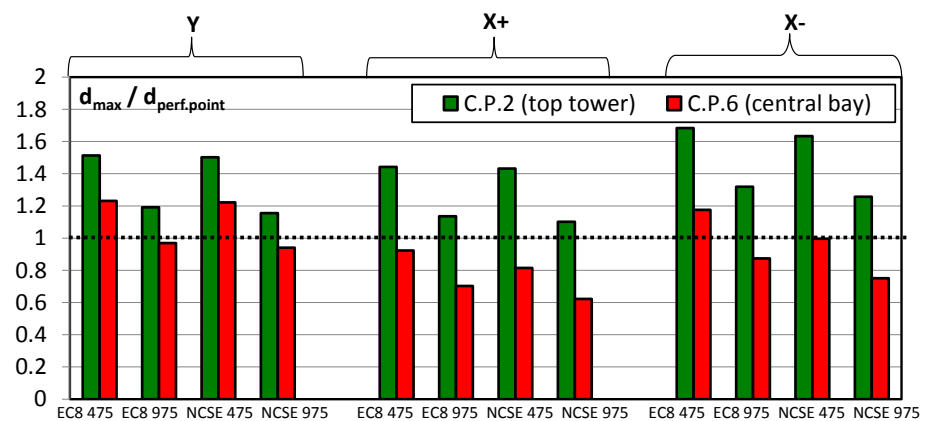
Figure 4.28 Ratio between maximum displacements and performance displacements

4.5 NON LINEAR DYNAMIC ANALYSIS

A non linear dynamic analysis (NDA) was carried both in transversal and in longitudinal direction. As mentioned in section 1.2, the Eurocode 8 (CEN, 2004) permits the use of artificial or real accelerograms to

perform the analysis. A real accelerogram was chosen and it is presented in the following.

4.5.1 Accelerogram

The real accelerogram was obtained by means of the software REXEL v. 3. 5 (Iervolino et al. 2010). The software extracts, from the European Strong-motion Database, a set of real records compatible with a reference spectrum, defined by the user or automatically generated according to Eurocode 8 or Italian seismic code. Tolerance parameters are assigned to define the compatibility between the average spectrum of the set and the reference spectrum.

In this work, the spectrum provided by the Eurocode 8 for a return period of 475 years (see fig. 4.26, section 4.4.5) was considered as reference spectrum. An upper tolerance equal to 20% and a lower tolerance equal to 10% were assumed. A set of seven records was found compatible with the assigned inputs. Figure 4.29 plots the average spectrum compared with the reference one and the upper and lower limits.
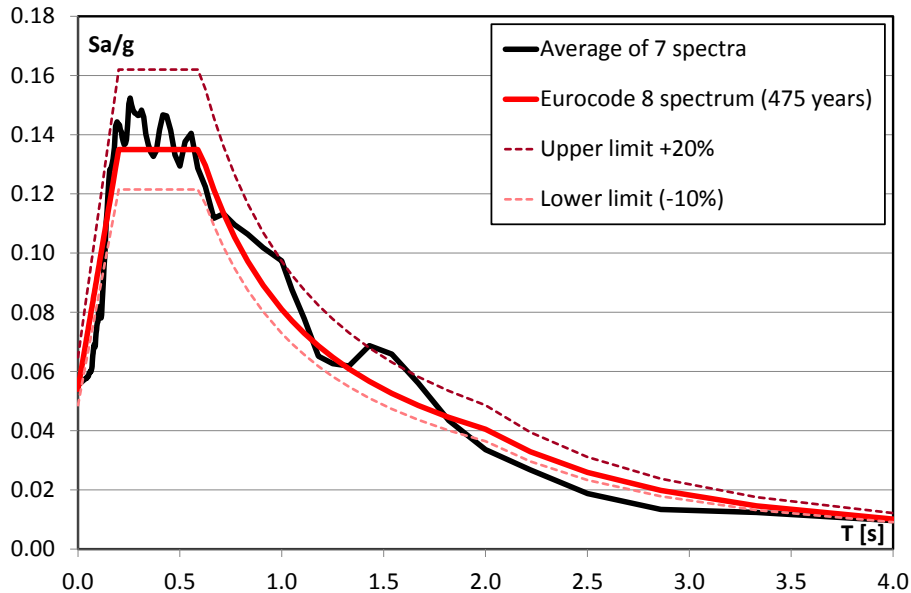
Figure 4.29 Average spectrum corresponding to the records by REXEL and comparison with Eurocode 8 spectrum and the assigned upper and lower limits

The average spectrum is slightly lower than the lower limit for T<0.15 and for T>2s, but these periods are not of interest for *Santa Maria del Mar* church, since the periods of vibration found from the modal analysis (see fig.4.13 section 4.3.2).

The set of seven record is listed in Table 4.9 where the following data are given: earthquake component, station, date of the event, magnitude, peak ground acceleration and, lastly, scale factor. In order to obtain compatible records, matching the Eurocode 8 spectrum, the earthquake signals have to be scaled using the scale factors.

The graphs in Figure 4.30 and 4.31 show the seven accelerograms obtained by scaling the real records provided by the REXEL software.

Table 4.9 Details of the combination of earthquake records provided by REXEL, compatible with the spectrum provided by EC8

Code (return period)	Earthquake name (component direction-station)	Date	M_w	PGA (g)	SF
EC 08 (475)_Soil D	Izmit (y-ST3270)	31/08/1999	5.1	0.358	1.4796
	Izmit (x-ST767)	13/09/1999	5.8	0.3906	1.3562
	Umbria Marche (y-ST229)	26/09/1997	6	0.1846	2.8695
	Izmit (x-ST3267)	31/08/1999	5.1	0.4574	1.1581
	Izmit (x-ST767)	31/08/1999	5.1	0.0354	14.9758
	Izmit (x-ST3270)	13/09/1999	5.8	0.6998	0.75704
	Izmit (y-ST767)	13/09/1999	5.8	0.3258	1.6259

Only the accelerogram indicated as Izmit (x-ST3270) was considered to perform the non linear dynamic analysis. It has duration equal to 79s and maximum acceleration equal to 0.05g.
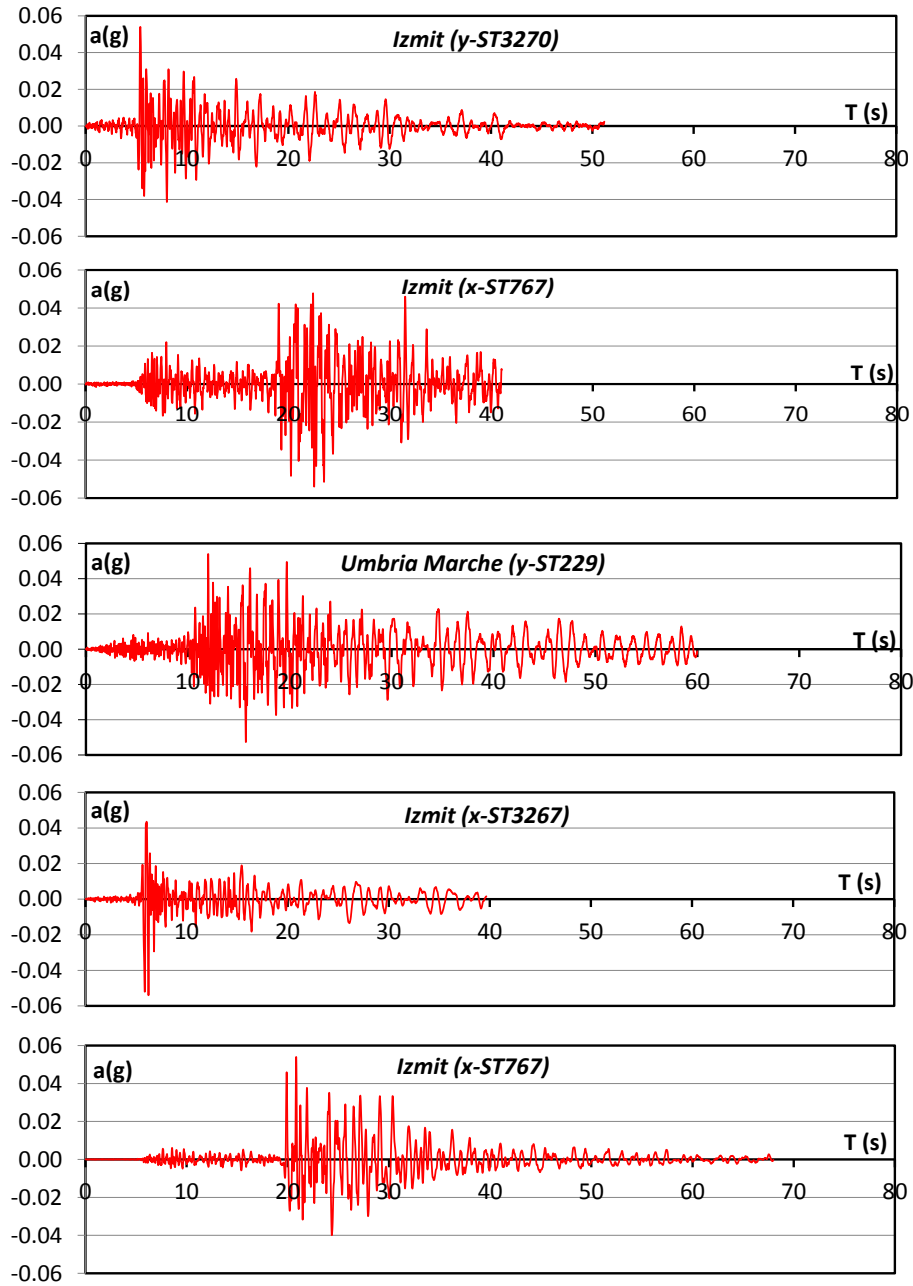
Figure 4.30 Scaled records mentioned in Table 4.9
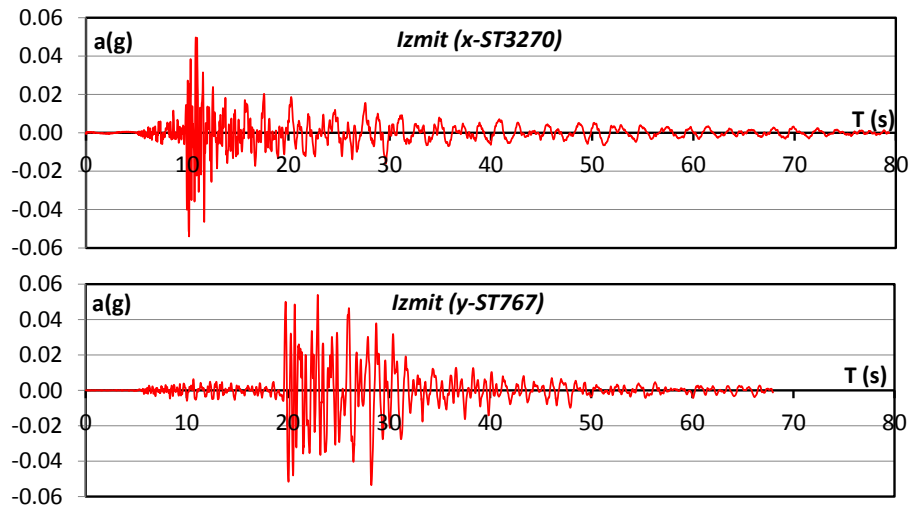
Figure 4.31 Scaled records mentioned in table 4.9 (continuation)

4.5.2 Further analysis inputs

According to similar investigations on masonry buildings (Elyamani 2015, Endo 2015a, b, Pelà 2013), the following analysis inputs were used. The same constitutive material model used for the non linear static analysis was adopted. A Rayleigh damping model is considered, with mass-proportional and stiffness-proportional damping coefficients respectively equal to $a_0=0.5716$ and $a_1=0.0041$. The Newmark-beta method has been used for the integration in the time domain. Constant average acceleration is assumed within each time step, with parameters $\gamma=0.5$ and $\beta=0.25$. Time intervals of 0.02 seconds have been assumed. This value do not respect the recommendation $\Delta t \leq T_h/20$, given in section 1.2, if an highest mode providing a cumulative mass greater than 80% of the total mass was considered. However 0.02s is sufficiently small compared with the accelerogram duration of 79s. Moreover it has been seen (section 4.3.2) that significant values (even if lower than 80%) of participating mass can be obtained also considering only the first vibration modes of the churches.

4.5.3   Transversal direction

The NDA in transversal direction spanned 11 days, 19 hours and 20 min, using a standard pc equipped with an Intel core i5 and 8 GB RAM. The cathedral was able to withstand the complete accelerogram. Figure 4.32 plots three graphs: a) the time history of the absolute displacements for each considered control point, b) the time history of the relative displacements computed with respect to the base displacement, c) the accelerogram compared with the acceleration at the base of the structure. The comparison between graph a) and graph c) shows that, at the beginning, the displacements were in line with the accelerogram, in fact significant increase of the displacements can be observed approximately at 10s, corresponding to the peak of the accelerogram. Between 10 and 30s, the displacements developed further increases, in contrast with the decrease of the acceleration. From 30s even low amplitude oscillations caused a significant increase of non-recoverable deformation in the building, until to obtain a maximum displacement equal to 38mm. This means that even if the building can resist the 80s accelerogram considered, it experienced significant damage and significant plastic deformation.

The graph a) also points out that the different control points gave very similar time history of displacements. Moreover the graph b) shows that the relative displacements assumed very small values, at most equal to 8mm. Figure 4.33 presents a zoom of the graphs a) and b) in the time from 9 to 21s. Small variance between the displacement of towers and rest of the church are readable in the zoom, but it is at most few higher than 5mm. It might be attributed to the observed stiffness and compactness of the church. It seems that the church is so stiff that it hardly undergoes deformation when it experience a low-moderate dynamic excitation.
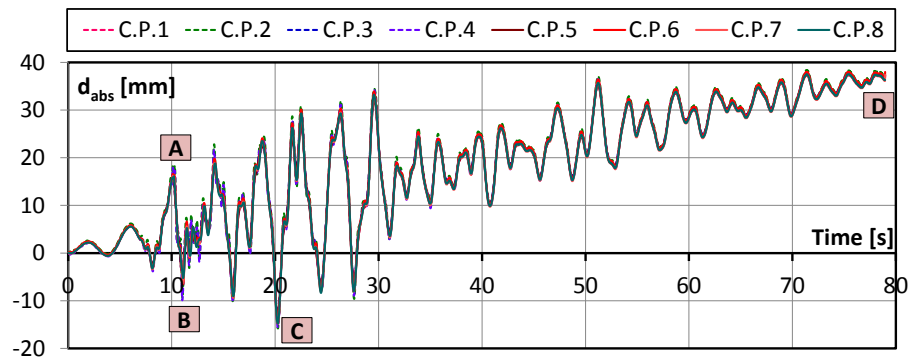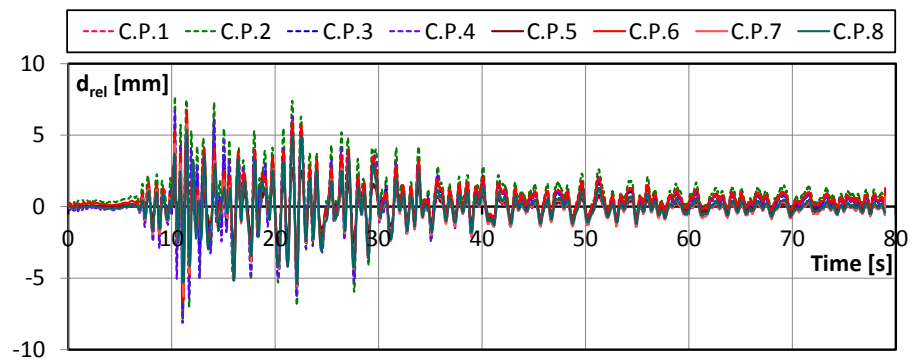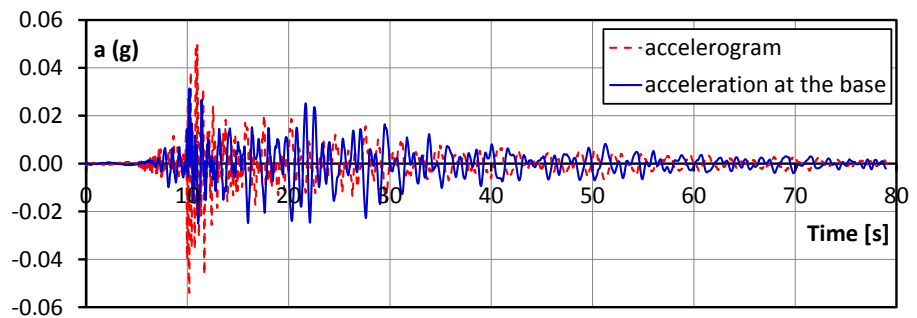
Figure 4.32 NDA in transversal direction: a) time history of the absolute displacements of the considered control points; b) time history of the relative displacements with respect to the base; c) comparison accelerogram vs. acceleration at the base of the structure

a)

b)
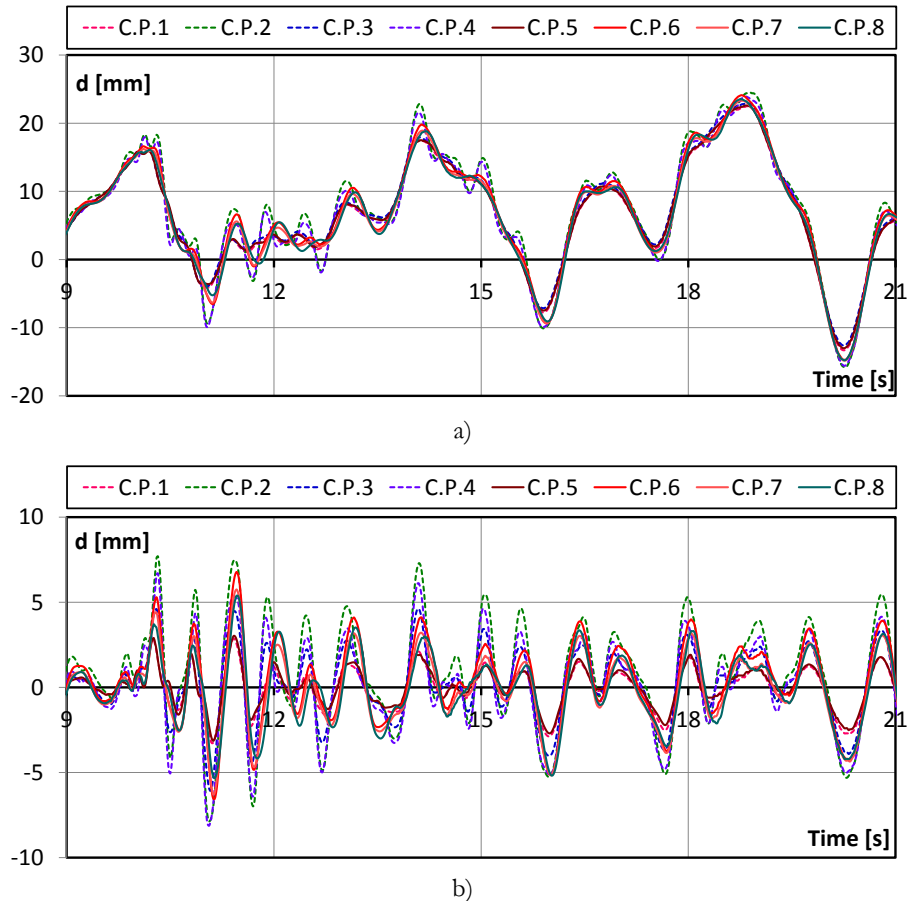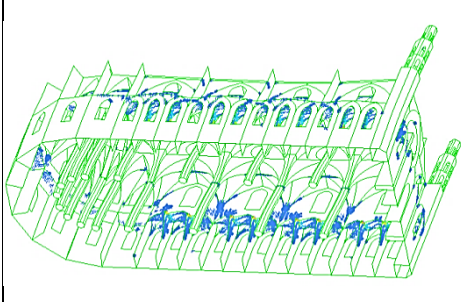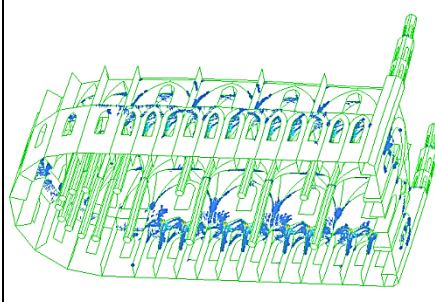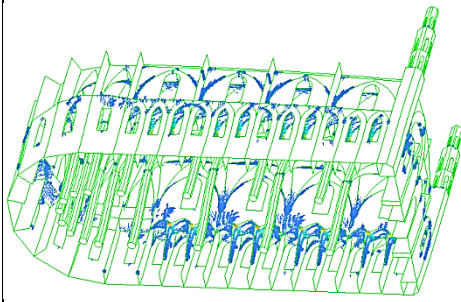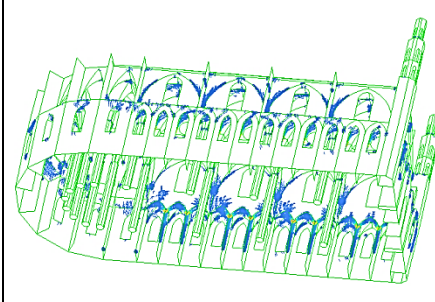
Figure 4.33 Zoom of the time history from 9s to 21s for: a) absolute displacements; b) relative displacements

Four steps are selected on the time history of displacements, and they are indicated as A, B, C, D. The steps A and B correspond to the positive and negative maximum displacement occurred at the peak of the accelerogram (at 10 s); the point C and D correspond to the maximum negative and positive displacement occurred during the entire duration of the accelerogram. Table 4.10 reports for each step: the crack pattern plotted on the deformed shape of the building, the time, the maximum displacement at this step, the corresponding acceleration at the base.

Table 4.10 Crack pattern at different step of the NDA in the transversal direction of the earthquake

A: t = 10.28s d_{max}=18mm a(g)=0.011	**B:** t = 11.04s d_{max}=-9.9mm a(g)=0.023
C: t = 20.28s d_{max}=-15.8mm a(g)=-0.024	**D:** t = 79s d_{max}=36.8mm a(g)=-0.002

Significant damage can be observed at each step especially at the abutments and the keystones of the vaults. The damage of the small later chapels is also considerable, but as it has been seen (see section 4.4.1), it formerly compares for gravity load. However the NDA provoked a damage state less critical than the NSA. The damage observed at the last step of the NSA (Fig. 4.18) exhibited cracks at the base of the pillars and the lateral walls, which were not found in the NDA. A comparison with NSA was carried out also in terms of displacements. Table 4.11 reports for C.P.2 and C.P.6 (top tower and central bay): the maximum displacement obtained with NSA, the performance displacement computed with the Eurocode 8 and return period of 475 years, the maximum displacement obtained from NDA. The analyses provided consistent values for C.P. 6. On the other hand the NDA provided lower displacements for C.P.2. As mentioned above, the greater slenderness of the tower did not give rise of displacements higher than the nave.

Table 4.11 Comparison between NSA and NDA displacements, in Y direction

	d $_{max}$ **(NSA)**	d $_{Perf.Point}$ **(EC8 475)**	d $_{max}$ **(NDA)**
	[mm]	[mm]	[mm]
C.P.2	66	44	36
C.P.6	35	28	38

4.5.1　Longitudinal direction

The NDA in longitudinal direction stopped after 10.2, at the negative peak of the accelerogram. The analysis lasted 1 day, 1 hour and 7 min. with the same pc used for the analysis in transversal direction.

Similarly to NDA in transversal direction, in Figure 4.34 three graphs are provided: a) the time history of the absolute displacements for each considered control point, b) the time history of the relative displacements computed with respect to the base displacement, c) the accelerogram compared with the acceleration at the base of the structure. The maximum displacement achieved at 10.2 s is equal to 18mm at the top of the tower. All the control points provide similar time history of displacements. Small variance at most equal to 5mm can be found between the top of the towers and the rest of the structure The relative displacements are at most equal to 2mm and 5mm respectively on the top of the tower and on the rest of the church. . It confirms what has been said in the previous section about the stiffness exhibited by the cathedral.

Two step are selected on the time history of the displacements and they are indicated as A and B. Table 4.12 shows the crack pattern plotted on the deformed shape of the building, the time, the maximum displacement at this step, the corresponding acceleration at the base. The crack pattern shows considerable damage at the abutments of the vaults. Cracks were also found at the connection between tower and façade, but it did not justify an overturning mechanism. By observing the damage, the problem seems to be connected to the flexibility of the buttresses in the longitudinal direction. In fact the damage is concentrated in these buttresses and their connections to the vaults. On the other hand, in the NDA both the façade and the apse withstand the earthquake. However further investigation should be carried out in order to understand if the cathedral is really not able to withstand the earthquake in longitudinal

direction or a convergence problem avoids the numerical progress of the analysis. However it has to be noted that also the NSA showed a worse seismic performance of the cathedral in longitudinal direction (see section 4.4.5).
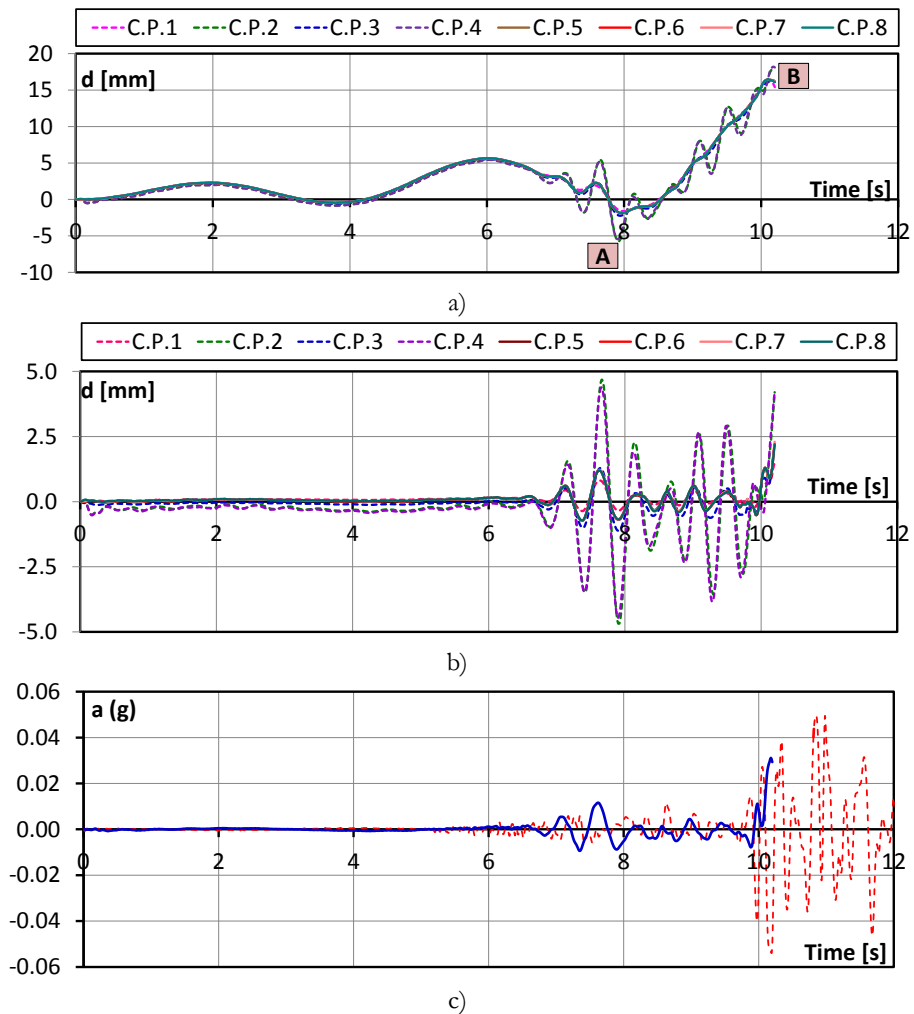
Figure 4.34 NDA in longitudinal direction: a) time history of the absolute displacements of the considered control points; b) time history of the relative displacements with respect to the base; c) comparison accelerogram vs. acceleration at the base of the structure

Table 4.12 Crack pattern at different step of the NDA in the longitudinal direction of the earthquake

A: t = 7.94s d_{max}=5mm a(g)=0.0075

B: t = 10.20s d_{max}=18mm a(g)=-0.03
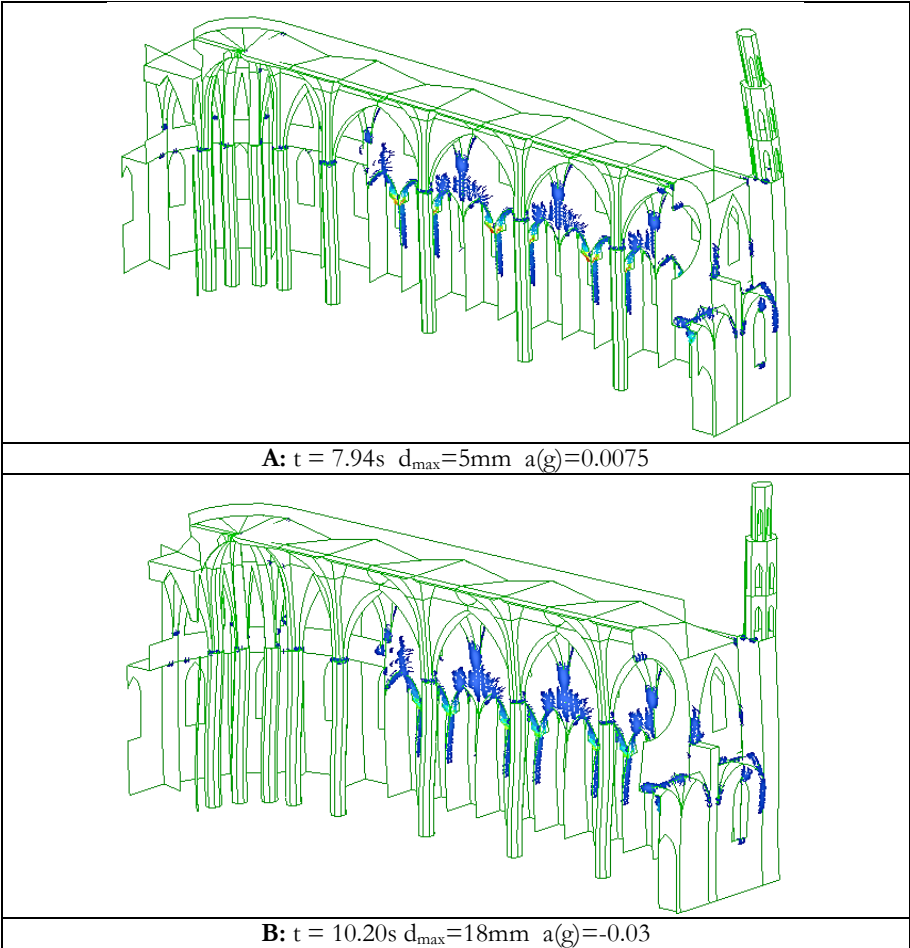
The displacements obtained from NSA and NDA are compared in Table 4.13. It can be noted that consistent displacements were found considering C.P.6, but NDA provided lower displacements of the tower, approximately equal to half of the maximum displacement obtained from NSA.

Table 4.13 Comparison between NSA and NDA displacements, in longitudinal direction

		d $_{max}$ (NSA)	d $_{Perf.Point}$ (EC8 475)	d $_{max}$ (NDA)
		[mm]	[mm]	[mm]
X+	**C.P.2**	37	26	18
	C.P.6	14	15	16
X-	**C.P.2**	34	20	18
	C.P.6	15	13	16

4.6 COMPARISON AND DISCUSSION OF THE RESULTS

The structural analysis of *Santa Maria del Mar* church was carried out using different analysis methods.

The linear static analysis gave realistic values of displacements and stresses, proving the suitability of the model.

However the modal analysis provided numerical frequencies appreciably different from the experimental frequencies. Therefore, the Young's modulus was adjusted in order to obtain a better compatibility especially for the first frequency. The first vibration mode, in fact, involved almost 70% of the participating mass, providing a contribution, significantly prevalent in comparison with the other modes.

Then the non linear static approach was considered suitable to provide a realistic seismic assessment of the church. The non linear static analysis was carried out in transversal, positive and negative longitudinal direction. For the transversal direction a collapse mechanism, caused by the development of ten hinges in the bays, was identified. For the positive and negative longitudinal direction, the overturning of the façade and the significant damage of the pillars in the apse were, respectively, noticed as causes of the collapse.

The results of the NSA were compared with the limit analysis, performed in previous studies of the cathedral. A good agreement was found bot in terms of collapse mechanisms and in terms of maximum load multipliers.

The crack pattern extracted from the NSA was compared with the existent damage of the building, probably caused by the past

Table 4.14 Summary of the results

	Element	Analysis method	λ [-]	d_{max} [mm]	$d_{perf.point}$
Murcia 2008 Roca et al.2009	Typical bay	NSA	0.12	36	23
Giraldez et al.2007 Vacas 2009	Typical bay	Limit Analysis	0.10	-	22
	Tower *Global ooverturning*	Limit Analysis	0.14	-	-
	Upper body collapse		0.08	-	-
	Façade *Global overturning*	Limit Analysis	0.11	-	-
	Upper body collapse		0.07	-	-
Current study	Global model	NSA_ Y	0.09	66 (C.P.2) 35 (C.P.6)	44 (C.P.2) 28 (C.P.6)
		NSA_ X+	0.10	37 (C.P.2) 14 (C.P.6)	26 (C.P.2) 15 (C.P.6)
		NSA_ X-	0.12	34 (C.P.2) 15 (C.P.6)	20 (C.P.2) 13 (C.P.6)
	Global model	NDA_Y	-	36 (C.P.2) 38(C.P.6)	-
		NDA_X	-	18 (C.P.2) 16 (C.P.6)	-

earthquakes. Some of the cracks provided by the analysis were observed on the damage survey of the cathedral.

The seismic performance was assessed by means of the N2 method employed by the Eurocode 8. It pointed out the higher vulnerability of the cathedral in positive longitudinal direction. The great stiffness of the cathedral in this direction gives rise to displacement capacity lower than the seismic demand.

The non linear dynamic analysis confirmed the weakness of the cathedral in longitudinal direction: the church was able to withstand the earthquake in the transversal direction, while in the longitudinal one the analysis stopped in correspondence to the peak of the accelerogram.

However further non linear dynamic analysis should be carried out, first of all, to consider a sufficient number of seismic events and then to verify the result obtained in longitudinal direction. However the NDA

was found to be very time demanding for such a large historical building and it can prevent in-depth analysis.

A summary of the results obtained in terms of load multipliers and displacements is presented in Table 4.14, where the results are compared with previous studies.

5 CONCLUSIONS

This research deals with the structural analysis of historical masonry buildings under seismic loading. The state of the art pointed that the existing modelling strategies and analysis methods are affected by some limitations and different level of accuracy. The thesis is aimed to compare different approaches and to provide simple tools to verify the results of more complex analysis in order to provide a stable assessment of the seismic capacity. Different types of masonry historical buildings were analyzed, including multi-storey buildings (for residence, offices or schools) and churches. Finally an impressive example of gothic cathedral was studied in detail. In the following, the conclusions deduced from the analyses are listed, with reference to each considered typology of historical building.

On the seismic capacity of multi-storey historical buildings

The façade of four multi-storey historical buildings was analyzed by adopting both push-over analysis and the limit analysis approach. In order to perform the push-over analysis, the façades were modelled considering different modelling strategies: simplified modelling, (including equivalent frame and macro-modelling) and finite elements method. A link between the seismic capacity of single wall and complete building was investigated. The main conclusions are:

- The simplified modelling gave capacity curves of the façades appreciably different. They showed a different decreasing of the stiffness of the wall and, moreover, the maximum values of load multipliers and displacement were not always consistent.
- The FE analysis was preliminary calibrated performing a sensitive analysis on a masonry portal frame. I was found that the Fe analysis is significantly sensitive to the tensile strength assigned to the material. Comparing the results obtained with a tensile strength equal to 1% and 10% of the compressive strength, scatters almost equal to 80% were found in terms of load multiplier. This result is alarming due to

the uncertainty, observed also in the literature, about a suitable value has to be assigned to the masonry

- The FE analysis of the façades of the four historical buildings was affected by problems of convergence, which prevents to reach realistic value of the maximum displacement of the wall. However the load multipliers obtained from the FE analysis were comparable with the simplified modelling and variance on average equal to 20% was found.

- The different modelling strategies (simplified and FE) agree on the damage of the facade at the ultimate state. It proved that in the, most of the cases studies, the wall collapsed due to the shear failure of the spandrels. This basically transformed the wall in a sequence of cantilever (namely the piers), which collapsed for the in-plane overturning.

- Since the variability of the results produced by the different modelling, the limit analysis was confirmed to be a fundamental tools to check the analyses. A closed formula, elaborated by the research group of the author, was used to compute the horizontal collapse multiplier. The results were in very good agreement with the maximum load multiplier given by the FE analysis, greater scatters were found from the comparison with the simplified modellings.

- A simplified formula was proposed to evaluate the collapse multiplier of the façades. Since the spandrels have a negligible weight in comparison with the rest of the wall and, moreover, they soon experienced significant damage, the simplified formula is based on a simplified model of the wall consisting of a sequence of cantilever. Then the seismic capacity of the wall can be simply computed through the average ratio between base and height of the cantilevers.

- A very good agreement was found between exact and simplified formula of the limit analysis and also with the results of the push-over analysis. Therefore it can be said that the simplified formula could give a preliminary satisfactory measure of the seismic capacity, being noted only the geometrical characteristics of the wall

- The simplified formula was applied to each wall of the building and an average value of λ was defined. It was compared with the seismic capacity of the whole building, assessed by performing the push-over analysis. Again a good agreement was noticed with the simplified approach. This result should be confirmed performing the analysis on

a larger sample of study. If it was confirmed, it would be remarkable because it gives a good measure of the seismic capacity of an entire building, with a simple ratio between geometrical noted parameters.

On the dynamic behavior of masonry churches

The dynamic behavior of masonry churches was investigated performing modal analysis and dynamic response spectrum analysis on a sample of fourteen masonry churches. The large sample contained churches having different geometry and size, and therefore it provided a certain generality of the results. The main conclusions are:

- The modal analysis of masonry churches produced a great number of vibration modes, all characterized by small participation mass ratios, always lower than 50% of the total mass and generally at most equal to 30-35%. This result implies that the modal analysis of masonry churches does not provide a vibration mode markedly predominant compared with the others, disproving the assumption highlighting the static approaches..

- Since the natural modes are characterized by small participating mass ratio, it was necessary to consider 100 vibration modes in order to obtain a total participating mass almost equal to 80% of the total mass.

- The indications of the Eurocode 8 and the Italian Building Code, which suggest to consider all vibration modes having modal participating mass ratios higher than 5%, is not so significant for masonry churches, because the sum of the vibration modes with $M_p > 5\%$ was found on average equal to 55% of the total mass.

- The obtained modal shapes showed that each vibration modes generally involves one macro-element of the church exhibiting, in the most of the case, out-plane deformation.

- The vibration modes were characterized by a spanned distribution which strongly influenced the results of the response spectrum analysis: the obtained base shears corresponded to accelerations much lower than both peak of the recorded pseudo-acceleration and the plateau of the response spectra, provided by the rules.

- The latter result implies that the high spectral accelerations do not give rise to similar high values of seismic forces, in contrast with what happens for regular buildings. Therefore the seismic forces to be used for verifying the masonry can be reduced, and the sample studied

suggest that ½ of the maximum spectral acceleration could be applied to the seismic weight of the church. In this way invasive intervention of strengthening could result useless and they could be replaced by intervention calibrated on the analysis of the macro-elements and, in particular the out-of-plane mechanism deduced by the modal shape should be considered.

On the Santa Maria del Mar cathedral

The cathedral of *Santa Maria del Mar* was studied by performing on a FE model: linear static analysis, modal analysis, non linear static (push-over) analysis and non linear dynamic analysis.

- The linear static analysis demonstrated the accuracy and reliability of the FE model of the whole cathedral,

- The modal analysis gave a main transversal vibration mode, which involved almost 70% of the church. This result is in contrast with what has been said above on the dynamic behavior of masonry churches. However it could be explained considering the uncommon regularity and compactness of *Santa Maria del Mar:* all the structural parts are well connected each others and, at the north side, the apse with its radial walls forms a considerable rigid elements.

- The push-over analysis in transversal direction revealed a collapse mechanism due to the failure of the typical bay of the cathedral, where ten hinges can be noticed, at the ultimate state of the analysis. In positive longitudinal direction the failure was connected to the overturning of the facade, while in negative longitudinal direction significant damage was concentrated on the pillars, especially in the apse.

- The push-over analysis proved to be reliable because the results were in line with the limit analysis (performed by other authors, in previous studies) and with the real damage of the cathedral, probably due to earthquakes occurred in the past.

- The comparison of the results with the seismic demand was performed by using the N2 method. It pointed out the, in longitudinal direction the capacity of displacement of the cathedral is lower than the spectrum demand. It can be explained considering the great stiffness of the cathedral in this direction, especially due to the structure of the apse. This result implies that, although the cathedral

is in good conservation status, intervention of strengthening should be assessed to improve its seismic performance.

- The non linear dynamic analysis confirmed that the longitudinal direction of the cathedral is the weakest one. The church was able to withstand the earthquake in the transversal direction, while in the longitudinal one the analysis stopped in correspondence to the peak of the accelerogram.

- The non linear dynamic analysis confirmed to be very time-demanding for complex buildings such as gothic cathedral. It was found that the required computational time was in order of ten days, for the analysis in transversal direction. This prevents to carry out the analysis for a sufficient number of accelerograms, but it is noted that the time history analysis is strongly influenced by the considered record.

- The comparison between push-over and non linear dynamic analysis gave consistent results in terms of ultimate displacements at the naves of the church, but significant variance was found for the ultimate displacements of the towers. Moreover the collapse mechanism identified in the longitudinal push over analyses was not in line with failure noticed in the non linear dynamic analysis. The variability of the results, obtained with such complex kind of analysis, confirmed that the simple tool of the limit analysis is needed also for the study of wide size historical constructions.

REFERENCES

[1] Almac U., Schweizerhof K., Blankenhorn G., Duppel C., Wenzel F., *2013 Structural behaviour of Hagia Sophia under dynamic loads.* Vienna Congress on Recent Advances in Earthquake Engineering and Structural Dynamics 2013 (VEESD 2013)C. Adam, R. Heuer, W. Lenhardt & C. Schranz(eds)28-30 August, Vienna, Austria Paper No. 475

[2] Arangio S., Bucchi F., Bontempi F., 2013 *Pushover seismic analysis of masonry buildings with different commercial codes.* In Proceedings of Built Heritage Monitoring Conservation Management, 18-20 November 2013, Milan, Italy.

[3] Araújo A., Lourenço P., Oliveira D., Leite J., 2012. *Seismic Assessment of St James Church by Means of Pushover Analysis – Before and After the New Zealand Earthquake*, The Open Civil Engineering Journal vol.6, (Suppl 1-M5), pp. 160-172

[4] Architecture, Cambridge University Press, ISBN 0521629632.

[5] Baggio C, Trovalusci P. 1998 *Limit analysis for no-tension and frictional three-dimensional discrete systems.* Mech Struct Mach;26(3)pp. 287–304.

[6] Bazzurro P, Luco N. 2003 *Parameterization of non-stationary acceleration time histories.* Report for Pacific Earthquake Engineering Research (PEER). Center Lifelines Program Project 1G00.

[7] Betti M. & Vignoli A., 2008. *Modelling and analysis of a Romanesque church under earthquake loading: Assessment of seismic resistance*, Engineering Structures vol.30, pp. 352-367

[8]   Betti M. & Vignoli A., 2011. *Numerical assessment of the static and seismic behaviour of the basilica of Santa Maria all'Impruneta (Italy)*, Construction and Building Materials vol. 25, 4308–4324

[9]   Boothby T.E., Atamtürktür SH, Erdogmus E, 2006 *Manual for the Assessment of Load-Bearing Unreinforced Masonry Structures*. Louisiana, USA: National Center for Preservation Technology and Training.

[10]   Bracci, J. M., Kunnath, S. K., & Reinhorn, A. M. 1997. *Seismic performance and retrofit evaluation of reinforced concrete structures. Journal of Structural Engineering, 123(1)*, 3-10.

[11]   Brandonisio G, De Luca A, Mele E, Mountuori GM., 2012 *Multi-storey masonry buildings: evaluation of effectiveness of mechanical strengthening*. In: Proc. Of IIX structural analysis of historical constructions (IIX SAHC), 1780–1788, Wroclaw, Poland, 15–17 October.

[12]   Brandonisio G, Mazziotti A, Lucibello G, Mele E, De Luca A., 2014 *Pushover analysis of masonry buildings: comparison of different modelling through four case studies*. In: Proc. of 9th international masonry conference 2014 (9th IMC), Guimarães, Portugal, 7–9 July.

[13]   Brandonisio G., 2007 *Analisi di edifici a pianta basilicale soggetti ad azioni sismiche* Ph.D. Dissertation, Second University of Naples.

[14]   Brandonisio G., De Luca A., Mele E. 2015 *Closed form solution for predicting the horizontal capacity of masonry portal frames through limit analysis and comparison with experimental test results* Engineering Failure Analysis 55, pp. 246-270.

[15]   Brandonisio G., Lucibello G., Mele E. & De Luca A., 2013. *Damage and performance evaluation of masonry churches in the 2009 L'Aquila earthquake*, Engineering Failure Analysis vol.34, pp.693-714.

[16]   Brandonisio G., Mele E., Santaniello R., De Luca A., 2008. *Seismic safety of basilica churches: analysis of ten case studies.* In Proc. of SAHC'08, Bath, England, 2-4 July

[17]   Brenchic A., Lagomarsino S., 1997 *Un modello a macroelementi per l'analisi ciclica di pareti murarie. VIII Congresso ANIDIS, 21-24 September,* Taormina, Italy (in italian).

[18]   Brencich A., Lagomarsino S., 1998 *A macro-elements dynamic model for masonry shear walls.* In Proceedings of the STRUMAS IV—4th Int. Symp. On Computer Methods in Structural Masonry. E&FN Spon: London UK pp. 67–75.

[19]   Breymann GA., 1885 *Trattato generale di costruzioni civili con cenni speciali intorno alle costruzioni grandiose.* Edited by H. Lang e A. Scholtz – italian translation of C. Valentini e Lo Gatto, Antica Casa Editrice dott. Francesco Vallardi – Milano (in Italian).

[20]   Bucchi A., Aprile A., Tralli A., 2009 *Analisi pushover di costruzioni in muratura con codici di calcolo commerciali: problematiche a confronto.* In Proceedings of XIII Conference ANIDIS 2009, 28 June-2 July 2009, Bologna, Italy.

[21]   Caliò I., Marletta M., Pantò B. 2012 *A new discrete element model for the evaluation of the seismic behaviour of unreinforced masonry buildings.* Engineering Structures 40 pp. 327-338.

[22]   Caliò I., Marletta M., Pantò B., 2004 *Un semplice macro elemento per la valutazione della vulnerabilità sismica di edifici in muratura.* In Proceedings of XI National conference *L'ingegneria Sismica in Italia,* 25-29 Jenuary, Genoa, Italy.

[23]   Caliò I., Marletta M., Pantò B., 2005 *A simplified model for the evaluation of the seismic behaviour of masonry buildings.* Proceedings of 10th International Conference on Civil, Structural and Environmental Engineering Computing, August 30 – September 2, Rome, Italy.

[24]   Caliò I., Marletta M., Pantò B., 2008 *A discrete element approach for the evaluation of the seismic response of masonry buildings*. Proceedings of 14th World Conference of Earthquake, October 12 -17 2008, Beijing, China.

[25]   Capecchi D, Vestroni F, Antonacci E, 1990. *Experimental study of dynamic behaviour of an old masonry building. In: Proc 9th Eur conf earth eng, Moscow.*

[26]   Casati, M. J. & Gálvez, J. C. 2009 *The influence of the masonry mechanical properties in the structural behaviour of the Leon's cathedral.* Materiales de Construcción, 59(294), pp. 75-96.

[27]   Castellazzi G., Gentilini C., Nobile L., 2013 *Seismic Vulnerability Assessment of a Historical Church: Limit Analysis and Nonlinear Finite Element Analysis* Advances in Civil Engineering, Article ID 517454, 12 pages http://dx.doi.org/10.1155/2013/517454

[28]   CEN 2004 *Eurocode 8 - Design Provisions for Earthquake Resistance of Structures, Part 1.1: General rules, seismic actions and rules for buildings, European*

[29]   Ceroni F., Pecce M. & Manfredi G. 2009. *Seismic assessment of the bell tower of Santa Maria del Carmine: problems and solutions.* Journal of Earthquake Engineering, Vol. 14, pp. 30-56.

[30]   Chambers J., Kelly T. 2004 *Nonlinear dynamic analysis – the only option for irregular structures* 13th World Conference on Earthquake Engineering Vancouver, B.C., Canada August 1-6, 2004 Paper No. 1389.

[31]   Chellini G., Nardini L., Pucci B., Salvatore W., Tognaccini R., 2014 *Evaluation of seismic vulnerability of Santa Maria del Mar in Barcelona by an integrated approach based on terrestrial laser scanner and finite element modelling.* International Journal of Architectural Heritage, 8 pp. 795–819.

[32] Chopra AK, Goel RK 2002 *A modal pushover analysis procedure for estimating seismic demands for buildings.* Earthquake Engineering & Structural Dynamics, 31(3) pp.561-582

[33] Chopra AK, Goel RK 2004 *A modal pushover analysis procedure to estimate seismic demands for unsymmetric-plan buildings.* Earthquake engineering & structural dynamics, 33(8) pp. 903-927

[34] Chopra, A. K. 2000 *Dynamic of structures* – Theory and Applications to Earthquake Engineering. Prentice Hall.

[35] Choudury T., Milani G., Acito M., Chesi C., Difrancesco C., Carabellese I., Martnes G., De Simone V. , 2014 .*Damage survey and structural assessment of the Rosario Church in Finale Emilia after the May 2012 earthquake in Emilia Romagna, italy.* In Proc. of SAHC'14, Mexico City, Mexico, 14-17 October

[36] Clough R. W., Penzien J., 1975. *Dynamics of structures USA* Mc Graw Hill.

[37] CM'09: *Instruction for the application of the Building Standard for Constructions.* G.U. n. 47 del 26-2-2009. Suppl. Ordinario n.27 – Circolare 2 febbraio 2009, n. 617 (in Italian).

[38] Como M. and Grimaldi A., 1983. *Analisi limite di pareti murarie sotto spinta, Quaderni di Teoria e Tecnica delle Strutture*, Università di Napoli, Istituto di Tecnica delle Costruzioni, Napoli, p.546

[39] Cornell CA. Hazard, 2004 *Ground-motions and Probabilistic assessment for PBSD.* In: Performance based Seismic Design Concepts and Implementation. PEER Report 2004/05. Pacific Earthquake Engineering Research Center: University of California Berkeley.

[40] Coulomb CA., 1773 *Essaisurune application des règles des maximis et minimis à quelques problèmes de statique relatifs à l'architecture.* Paris.

[41] Croci G. 1995 *The Colosseum: safety evaluation and preliminary criteria of intervention.* Structural Analysis of Historical Constructions, Barcelona

[42]   Cundall PA., 1971 *A computer model for simulating progressive large-scale movements in blocky rock systems*. Proc Symp Int Soc Rock Mech; 1 pp.132–50.

[43]   Cundall PA., Strack ODL., 1979 *A discrete numerical model for granular assemblies*. Geotechnique;29 pp.47–65.

[44]   Cuzzilla R., 2009. *Seismic assessment and Retrofit of Historical Masonry Structures*, Ph. D. dissertation. University of Naples Federico II.

[45]   D'Ayala F. 2000 *Establishing correlation between vulnerability and damage survey for churches*. Atti del XII World Conference on Earthquake Engineering (12WCEE). Auckland, New Zealand.

[46]   Dal Cin A., Russo S., 2014. *Influence of the annex on seismic behavior of historic churches*, Engineering Failure Analysis vol. 45, , 300–313

[47]   De La Hire P. 1712 *Sur la construction des voûtesdans les édifices*, Mémoires de l'Académie Royale des Sciences.

[48]   De Luca A., Giordano A., Mele E. 2004, *A simplified procedure for assessing the seismic capacity of masonry arches*. Eng Struct;26 pp. 1915–29.

[49]   Doglioni F, Moretti A, Petrini V., 1994. *Churches and the earthquake*. Ed. LINT, Trieste (in Italian)

[50]   DPCM 9/2/2011. *Linee guida per la valutazione e la riduzione del rischio sismico del patrimonio culturale con riferimento alle Norme tecniche delle costruzioni di cui al decreto del Ministero delle Infrastrutture e dei trasporti del 14 gennaio 2008* [Italian guidelines for the evaluation and the reduction of the seismic risk for the built heritage, with reference to the Italian norm of constructions].

[51]   Elnashai, A. S. 2002 *Do we really need inelastic dynamic analysis?* Journal of Earthquake Engineering, 6(S1), pp. 123-130.

[52]   Elyamani A., 2015 *Integrated monitoring and structural analysis strategies for the study of large historical construction. Application to Mallorca cathedral.* Ph. D. dissertation. Universitat Politècnica de Catalunya, Barcelona.

[53]   Endo Y. 2015a *Modelling and Structural Analysis of historical masonry systems including vaulted structure.* Ph. D. dissertation. Universitat Politècnica de Catalunya, Barcelona.

[54]   Endo Y., Pelà L., Roca P., da Porto F., Modena C., 2015b *Comparison of seismic analysis methods applied to a historical church struck by 2009 L'Aquila earthquake.* Bulletin of Earthquake Engineering 13, Issue 12, pp 3749-3778.

[55]   European Committee of Standardization CEN. 1996. *Design of masonry structures. Part 1-1: General rules for buildings—Reinforced and unreinforced masonry* ENV 1996-1-1, Eurocode 6, Brussels, Belgium.

[56]   Fajfar P., 1999 *Capacity spectrum method based on inelastic demand spectra* Earthquake Engng. Struct. Dyn. Vol. 28, pp. 979 993.

[57]   Fajfar, P. A., 2002 *Structural analysis in earthquake engineering- a breakthrough of simplified nonlinear methods.* In 12th European conference on earthquake engineering, 9-13 September, London, UK.

[58]   Galasco A., Lagomarsino, S. Penna A. & Resemini S. 2004 *Nonlinear seismic analysis of masonry structures.* Proceedings of 13th World Conference on Earthquake Engineering, Vancouver, Canada, August 1-6, Paper N. 843.

[59]   Gambarotta L., Lagomarsino S., 1996, *On dynamic response of masonry panels.* in Gambarotta L. (ed.) Proc. of the National Conference *La meccanica delle murature tra teoria e progetto,* 18-20 September, Messina, Italy (in italian).

[60]   Gattulli V., Antonacci E. & Vestroni F. 2013 .*Field Observations and Failure Analysis of the Basilica S. Maria di Collemaggio after the*

2009 L'Aquila Earthquake, Engineering Failure Analysis vol.34, , pp.715-734

[61]   Gattulli V., Potenza F., Graziosi F., Federici F., Colarieti A., 2015. *Distributed structural monitoring for a smart city in a seismic area*, Key Engineering Materials Vol. 628, pp 123-135

[62]   Gilbert M, Melbourne C., 1994 *Rigid-block analysis of masonry structures.* The Struct Eng;72(21) pp.356–61.

[63]   Gilbert M, Melbourne C., 1995 *Analysis of multi-ring brickwork arch bridges.* In: Melbourne C, editor. Arch Bridges. London: Thomas Telford.

[64]   Giordano A, De Luca A, Mele E, Romano A. 2007 *A simple formula for predicting the horizontal capacity of masonry portal frames.* Eng Struct;29 pp.2109–23.

[65]   Giordano A., 2002 *Sulla capacità sismica delle chiese a pianta basilicale,* Ph.D. Dissertation, University of Naples Federico II

[66]   Giráldez P., Vendrell M., Caballé F., Gonzales R. Roca P. 2007 *La Basílica de Santa Maria del Mar de Barcelona. Estudi històrico-constructiu, materials de construcció i estabilitat estructural,* Report. UB-Patrimoni, Veclus, Universitat Politècnica de Catalunya, Barcelona.

[67]   Giresini L. 2016, *Energy-based method for identifying vulnerable macro-elements in historic masonry churches* Bull Earthquake Eng 14:919–942

[68]   Giresini L., Butenweg C., Andreini M., De Falco A., Sassu M., 2014 *Macro elements identification in historic chapels: the case of st. venerio chapel in Reggiolo.* Emilia Romagna SAHC2014 – 9th International Conference on Structural Analysis of Historical Constructions F. Peña & M. Chávez (eds.) Mexico City, Mexico, 14–17 October

[69]   Giuffrè A.   1990 *Letture sulla meccanica delle murature storiche.* Kappa, Rome

[70]   Giuffrè A., 1993. *Sicurezza e conservazione dei centri storici: Il caso Ortigia*. Editrice Laterza, Bari; [in Italian].

[71]   González R., Caballé F., Domenge J., Vendrell M., Giráldez P., Roca P., González J. L. 2008. *Construction process, damage and structural analysis. Two case studies*. Structural Analysis of Historical Construction V, CRC Press, Taylor & Francis Group, London, pp. 643-650.

[72]   Gruppo Sismica s.r.l., 3D Macro - Manuale Teorico Hart RD, Cundall PA, Lemos JV. 1988 *Formulation of a three-dimensional distinct element model—part II: mechanical calculations*. Int J Rock Mech Mining Sci;25(3) pp.117–25

[73]   Heyman J. 1982 *The masonry arch*. Ellis Horwood Limited, Chichester.

[74]   Heyman J. *The stone skeleton*. Int J Solids Struct 1966;2:249–79.

[75]   Heyman J., 1995. *The Stone Skeleton*. Structural Engineering of masonry

[76]   Huerta S., 2003 *The Mechanics of Catalan Vaults: A Historical Outline*. Essays on the History of Mechanics Berlin, Germany: Birkhauser Verlag pp. 89-134.

[77]   Iervolino I, Maddaloni G, Cosenza E. 2009 *A note on selection of time histories for seismic analysis of bridges* in Eurocode 8. J Earthq Eng;13(8) pp.1125–52.

[78]   Iervolino I., Galasso C., Cosenza E., 2010 *REXEL: computer aided record selection for code-based seismic structural analysis*. B Earthq Eng 8(2) pp. 339–62.

[79]   Irizarry I. P., 2004. *An Advanced Approach to Seismic Risk Assessment. Application to the Cultural Heritage and the Urban System of Barcelona*, Ph. D. dissertation. Universitat Politècnica de Catalunya, Barcelona.

[80]   Ivancic S., Bricena C., Marques R., Aguilar R., Perucchio R., Vargas J. , 2014 . *Seismic assessment of the St Peter Apostle Church of Andahuaylillas in Cusco, Perù*. In Proc. of SAHC'14, Mexico City, Mexico, 14-17 October

[81]   Kappos AJ, Penelis GG, Drakopoulos CG., 2002 *Evaluation of simplified models for lateral load analysis of unreinforced masonry buildings*. J Struct Eng;128(7) pp. 890–7.

[82]   Kaushik Hemant B., Rai Durgesh C., Jain Sudhir K., ASCE M., 2007 *Stress Strain Characteristics of Clay Brick Masonry under Uniaxial Compression* Journal Of Materials In Civil Engineering 19:9 pp. 728-739.

[83]   Koçak A., Köksal T. , 2013 . *An example for determining the cause of damage in historical buildings: Little hagia sophia (Church of St. Sergius and Bacchus) – Istanbul, Turkey*. Engineering Structures vol. 56, pp. 1527–1546

[84]   Krawinkler, H. & Seneviratna, G. D. P. K. 1998 *Pros and cons of a pushover analysis of seismic performance evaluation*. Engineering structures, 20(4), pp. 452- 464.

[85]   Lagomarsino S, Podestà S 2004 a *Seismic vulnerability of ancient churches*. Part 1: damage assessment and emergency planning. Earthq Spectr. 20:377–394, ISSN: 8755-2930

[86]   Lagomarsino S. & Podestà S., 2004. *Damage and vulnerability assessment of churches after the 2002 Molise*, Italy, earthquake, Earthquake Spectra, Vol.20, N.S1, pp.S271-S283

[87]   Lagomarsino S. 1998 *A new methodology for the post-earthquake investigation of ancient churches. XI European Conference on Earthquake Engineering*, Balkema, Rotterdam

[88]   Lagomarsino S. 2009, *Damage assessment of churches after L'Aquila earthquake (2009)* Bull Earthquake Eng (2012) 10 pp.73–92

[89]   Lagomarsino S., Penna, A., Galasco, A., Cattari S., 2013 *TREMURI program: an equivalent frame model for the non linear seismic analysis of masonry buildings.* Engineering Structures 56 pp. 1787-1799.

[90]   Lancioni G., Lenci S., Piattoni Q., Quagliarini E., 2013. *Dynamics and failure mechanisms of ancient masonry churches subjected to seismic actions by using the NSCD method: The case of the medieval church of S. Maria in Portuno.* Engineering Structures vol. 56, pp. 1527–1546

[91]   Lemos JV. 2007 *Discrete element modelling of masonry structures.* Int J Arch Heritage;1:90–213.

[92]   Lemos JV., 1987 *A distinct element model for dynamic analysis of jointed rock with application to dam foundations and fault motion.* Ph.D. Thesis. University of Minnesota.

[93]   Livesley RK., 1978 *Limit analysis of structures formed by rigid blocks.* Int J Numer Meth Eng;12(12) pp. 1853–71.

[94]   Lourenço P., 2002. *Computations on historic masonry structures* Prog. Struct. Engng Mater. Vol. 4, pp. 301–319

[95]   Lourenço P., Roque J.A., 2006. *Simplified indexes for the seismic vulnerability of ancient masonry buildings,* Construction and Building Materials vol.20, pp.200–208

[96]   Lourenço P., Trujillo A., Mendes N., Ramos L., 2012. *Seismic performance of the St. George of the Latins church: Lessons learned from studying masonry ruins* Engineering Structures vol.40, pp. 501–5188.

[97]   Lourenço PB 1996, *Computational strategies for masonry structures.* PhD Thesis. Delft University of Technology, Delft, The Netherlands

[98]   Lourenço PB. 2011 *Types of analysis: linear static, linear dynamic and non linear static.*(<http://www.iaaconservation.org.il/pdf/engineers2011/09_Types% 20of%20analysis.pdf>).

[99]   Lourenço PB., 2002 Computations on historic masonry structures. Progr Struct Eng Mater;4(3) pp. 301–19.

[100] Lucibello G., 2013 *Capacità sismica di edifici monumentali in muratura* Ph.D. Dissertation, University of Naples Federico II

[101] Lucibello G., Brandonisio G., Mele E., De Luca A. 2013 *Seismic damage and performance of Palazzo Centi after L'Aquila earthquake: A paradigmatic case study of effectiveness of mechanical steel ties*. Engineering Failure Analysis, 34 pp. 407–430.

[102] Macchi G, Ruggeri M, Eusebio M, Moncecchi M, 1993 *Structural assessment of the leaning tower of Pisa*. In: Structural preservation of the architectural heritage, IABSE, Zürich, Switzerland, pp 401–408

[103] Magenes G, La Fontana A. 1998 *Simplified nonlinear seismic analysis of masonry buildings*. In: Proceedings of British masonry society, vol. 8 pp. 190–5.

[104] Manie J. and Kikstra W. P. : Diana Finite Element Analysis User's Manual Version 9.5. Deflt: TNO Building and Construction Research, 2014.

[105] Manos G.C., Kotoulas L., Matsou V., Felekidou O., 2013. *Dynamic behaviour of greek post-byzantine churches with foundation deformability and evaluation of their earthquake performance – experimental investigation of stone masonry material properties* In Proc. of COMPDYN, Kos Island, Greece, 12–14 June 2013.

[106] Manos G.C., Soulis V.J., Diagouma A., *Numerical investigation of the behaviour of the church of Agia Triada, Drakotrypa, Greece*, 2008. Advances in Engineering Software vol.39, pp. 284–300

[107] Mazziotti A., Brandonisio G., Lucibello G., Mele E., De Luca A., 2014. *L'analisi e il recupero di edifici monumentali ecclesiastici sotto azioni sismiche: problemi aperti*. In Proc. of Workshop Safe Monuments, Firenze, Italy, 28 March, pp 191-202.

[108]   Mele E., De Luca A., Giordano A., 2003. *Modelling and analysis of a basilica under earthquake loading* Journal of Cultural Heritage vol.4, pp. 355–367

[109]   Milani G, Valente M., 2015 *Comparative pushover and limit analyses on seven masonry churches damaged by the 2012 Emilia-Romagna (Italy) seismic events: possibilities of non-linear finite elements compared with pre-assigned failure mechanisms.* Eng Fail Anal 2015;47 pp.129–61.

[110]   Milani G., Valente M., 2015 . *Comparative pushover and limit analyses on seven masonry churches damaged by the 2012 Emilia Romagna (Italy) seismic events: Possibilities of non-linear finite elements compared with pre-assigned failure mechanisms* Engineering Failure Analysis vol. 47, 129–161

[111]   Milani G., Valente M., 2015 *Failure analysis of seven masonry churches severely damaged during the 2012 Emilia-Romagna (Italy) earthquake: Non-linear dynamic analyses vs conventional static approaches.* Eng Fail Anal;54 pp.13–56.

[112]   Milani G., Venturini G., 2013. *Safety Assessment of Four Masonry Churches by a Plate and Shell FE Nonlinear Approach* J. Perform. Constr. Facil. Vol.27, pp.27-42.

[113]   Mola F, Vitaliani R., 1995 *Analysis, diagnosis and preservation of ancient monuments: the St. Mark's Basilica in Venice.* In: Structural analysis of historical constructions I. CIMNE, Barcelona, Spain, pp. 166–188

[114]   Murcia, J. 2008 *Seismic analysis of Santa Maria del Mar Church in Barcelona.* Master's thesis dissertation, Universitat Politècnica de Catalunya, Barcelona.

[115]   Navier CL., 1833 *Résumé des Leçons donées à L'École des Ponts et Chaussées, sur l'application de la mécanique à l'établissement des constructions et des machines.* Paris.

[116]   NCSE-02 2002 *Norma de construcción sismo resistente – Parte general y edificación.* (In Spanish).

[117] NTC'08. *Italian Building Code for the Constructions* (Norme Tecniche per le Costruzioni). D. M. 14 January 2008 – S.O. n. 30, G. U. n. 29–4; February 2008 [in Italian].

[118] NTC'08: *Italian Building Code for the Constructions (Norme Tecniche per le Costruzioni).* D. M. 14 January 2008 – S.O. n. 30, G. U. n. 29 - 4 February 2008 (in Italian).

[119] O.P.C.M 3431 2005 *Ulteriori modifiche ed integrazioni alla Ordinanza PCM 3274 Primi Elementi in Materia di Criteri Generali per la Classificazione Sismica del Territorio Nazionale e di Normative Tecniche per le Costruzioni in Zona Sismica* (in Italian).

[120] Orduna A, Lourenço PB. 2001 *Limit analysis as a tool for the simplified assessment of ancient masonry structures.* In: Historical constructions, Guimaraes: Universidade do Minho pp. 511–20.

[121] Pagano M., 1968 *Teoria degli edifici, Tomo I: Edifici in muratura*, Liguori Editore, Napoli.

[122] Pegon P, Anthoine A., 1994 *Numerical strategies for solving continuum damage problems involving softening: application to the homogenization of masonry.* In: Topping BHV, Papadrakakis M, editors. Advances in non-linear finite element methods. Edinburgh (UK): Civil-Comp Press; pp. 143–57.

[123] Pelà L., Aprile A., Benedetti, 2013 *Comparison of seismic assessment procedures for masonry arch bridges.* Constr Build Mater 38 pp.381-394

[124] Penna A., Lagomarsino S., Galasco A., 2014 *A nonlinear macro-element model for the seismic analysis of masonry buildings* Earthquake Engng Struct. Dyn.; 43 pp.159–179.

[125] Penna, A. 2002 *A macro-element procedure for the non-linear dynamic analysis of masonry buildings.* Ph.D. Dissertation, Politecnico di Milano

References

[126] Poleni G. 1748 *Memorie istoriche della Gran Cupola del Tempio Vaticano.*

[127] Powell G., 2006 *Nonlinear dynamic analysis capabilities and limitations.* The structural design of tall and special buildings struct. design tall spec. build. 15pp.547–552

[128] *prestandards* ENV 1998, European Committee for Standardization, Brussels.

[129] Ramos L. F. & Lourenço P. B. 2003 *Seismic analysis of the old town buildings in "Baixa Pombalina" - Lisbon, Portugal.* 9th North American masonry conference. June 1-4, Clemson, South Carolina, USA.

[130] Ramos L. F. & Lourenco P. B. 2004 *Modelling and vulnerability of historical city centers in seismic areas: a case study in Lisbon.* Engineering structures, 26(9), pp 1295-1310.

[131] Ramos L. F. & Lourenco P. B. 2005 *Seismic analysis of one heritage compound building of the old Lisbon town.* International conference on 250th anniversary of the 1755 Lisbon earthquake. LNEC, Lisbon, Portugal. pp. 362-368.

[132] Roca P, Cervera M, Gariup G, Pela' L., 2010 *Structural analysis of masonry historical constructions. Classical and advanced approaches.* Arch Comput Meth Eng;17 pp.299–325.

[133] Roca P., Clapés J., Caselles O., Vendrell M., Giráldez P., Sánchez-Beitia, 2008. *Contribution of inspection techniques to assessment of historical structures.* Proceedings of the Interantional RILEM SACoMaTIS 2008 conference, RILEM, Bagnéux, pp. 632-632.

[134] Roca P., Vacas A., Cuzzilla R., Murcia-Delso J., Das A. K., 2009 *Response of Gothic churches in moderate seismic Mediterranean regions.* Assessment and strengthening of historical stone masonry structures subjected to seismic action : proceedings of the ISCARSAH Symposium Mostar-09, 12th July 2009, Mostar, Bosnia and Herzegovina, pp. 53-62.

[135]   Rondelet JB., *Trattato teorico e pratico dell'arte di edificare, Tomo IV-Teoria delle Costruzioni. 1802. Prima edizione napoletana notabilmente migliorata e corretta da Raffaele Pepe.* Napoli 1840 (in Italian).

[136]   Rosenblueth E., 1981. *Design of earthquakes resistant structures* Halsted Press, USA.

[137]   Saloustros S., Pelà L., Roca P., Portal J., 2015. *Numerical analysis of structural damage in the church of the Poblet Monastery* Engineering Failure Analysis vol. 48, pp. 41–61

[138]   Santaniello R., 2010 *Analisi di chiese a pianta basilicale sotto azioni sismiche* Ph.D. Dissertation, University of Naples Federico II

[139]   Silva V. C., Lourenço P.B., Ramos L.F., & Mesquita C.G. 2001 *Accounting for the "block effect" in structural interventions in Lisbon's old "Pombaline" downtown buildings.* In: Lourenço, P.B. and Roca, P. (Eds.) Historical Constructions, University of Minho, Guimarães, pp. 943-952.

[140]   Simulia 2010. ABAQUS *Theory Manual.* USA

[141]   Siviero E., Barbieri A., Foraboschi P. 1997 *Lettura strutturale delle costruzioni.* Città Studi Edizioni, Milano.

[142]   Sorrentino L., Liberatore L., Decanini Luis D. Liberatore D., 2014 *The performance of churches in the 2012 Emilia earthquakes* Bull Earthquake Eng 12 pp. 2299–2331

[143]   Sparacio R., 2009. *Il recupero statico di immobili del centro storico di Napoli*, Ed. Università Suor Orsola Benincasa

[144]   STADATA. *3Muri Program*, Release 5.0.4, 2012 [www.3muri.com].

[145]   Vacas A. 2009 *Seismic analysis of Gothic churches by the capacity spectrum method,* End-of-study dissertation. Universitat Politècnica de Catalunya, Barcelona.

[146]   Zingone G., Cavalieri L., Cucchiara C., Tommaselli A. 1999
          *Valutazione della vulnerabilità globale delle chiese in muratura attraverso
          l'analisi di macroelementi significativi.* Atti del IX Convegno Nazionale
          in L'ingegneria Sismica in Italia, Torino , 20- 23 september .

APPENDIX A

In this Appendix the masonry walls of the historical buildings *Ex prison S. Francesco* and *Palazzo Centi* (described in chapter 2), are shown. For each wall, the capacity curves in terms of: base shear divided by the weight (indicated as λ) and displacements of the control point divided by the total height of the wall (d/H_{tot}), is given. The capacity curves were carried out for a distribution of loads proportional to the first vibration mode and to the masses, both in positive and negative direction. A horizontal line, corresponding to the collapse multiplier computed with the simplified formula (λ_{eq}), is reported on the curves.

EX PRISON S. FRANCESCO: LONGITUDINAL WALLS (X)
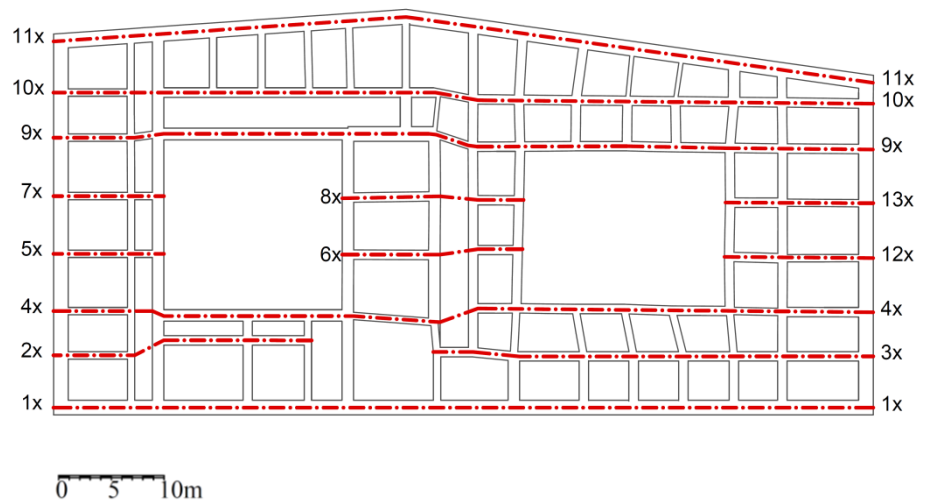
- **WALL 1X**

    H_{tot} = 25.4m

    Weight= 31660KN
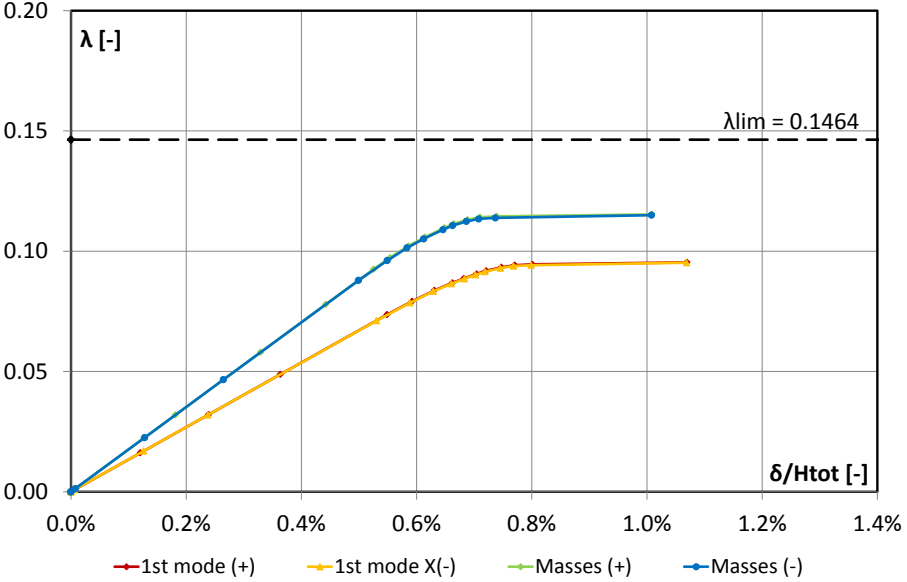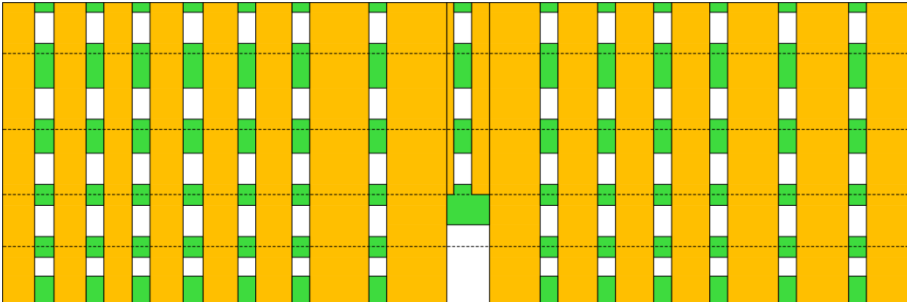
- **WALL 2X**

  H_{tot}= 25.4m

  Weight= 5549kN
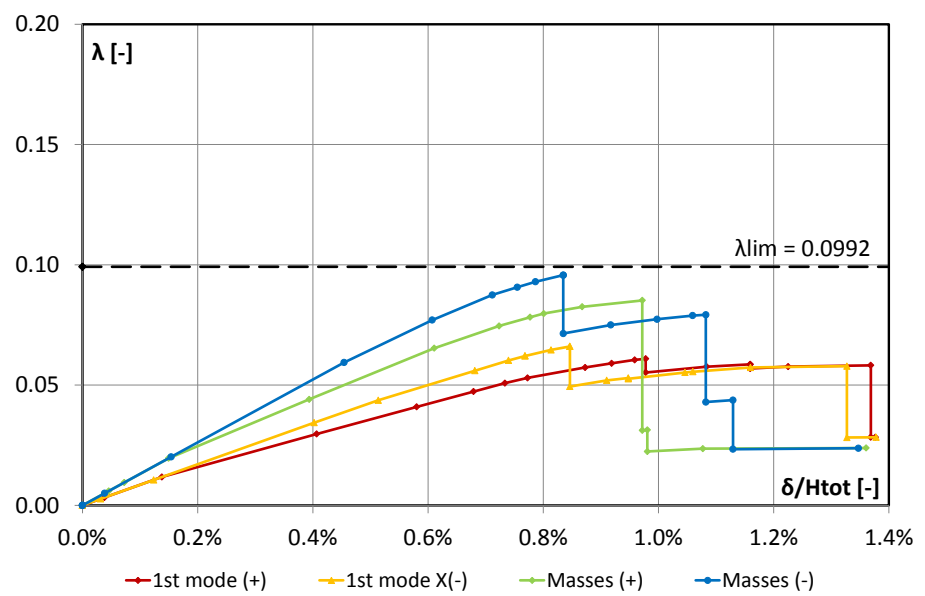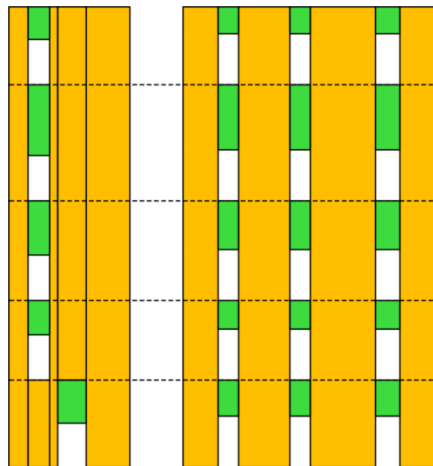
- **WALL 3X**

  H_{tot}= 25.4m

  Weight= 13077kN
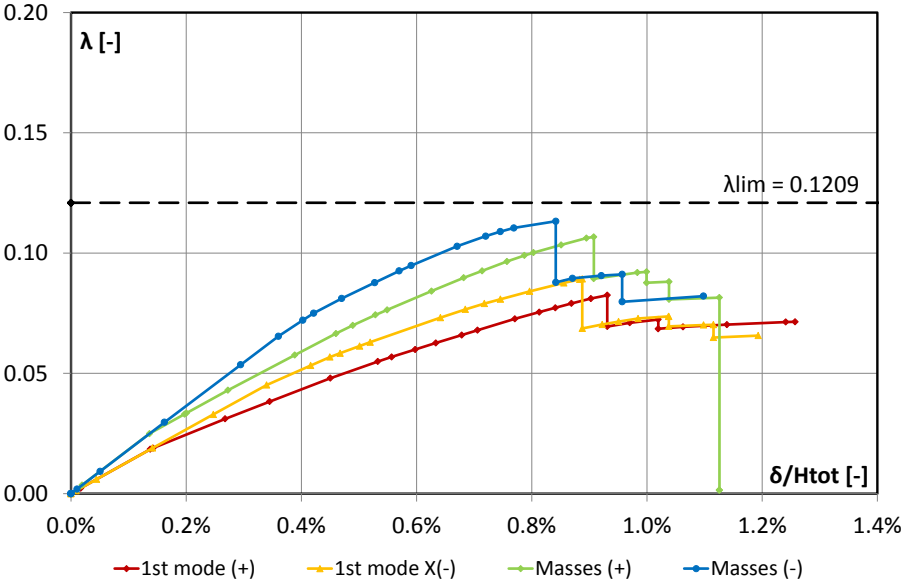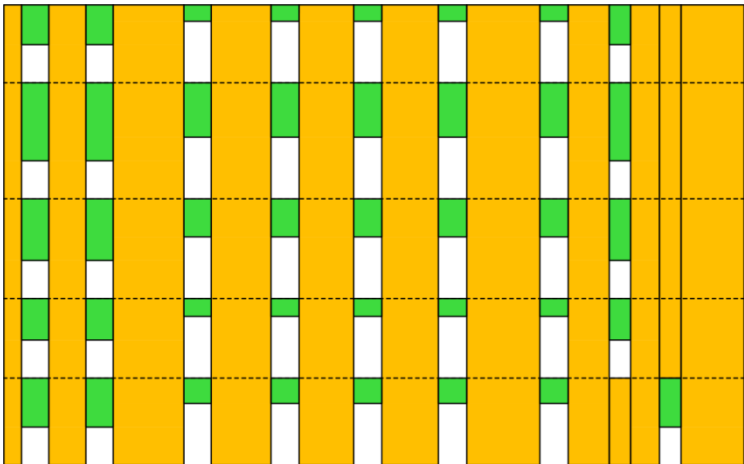
- **WALL 4X**

  H_{tot}= 25.4m

  Weight= 20898kN
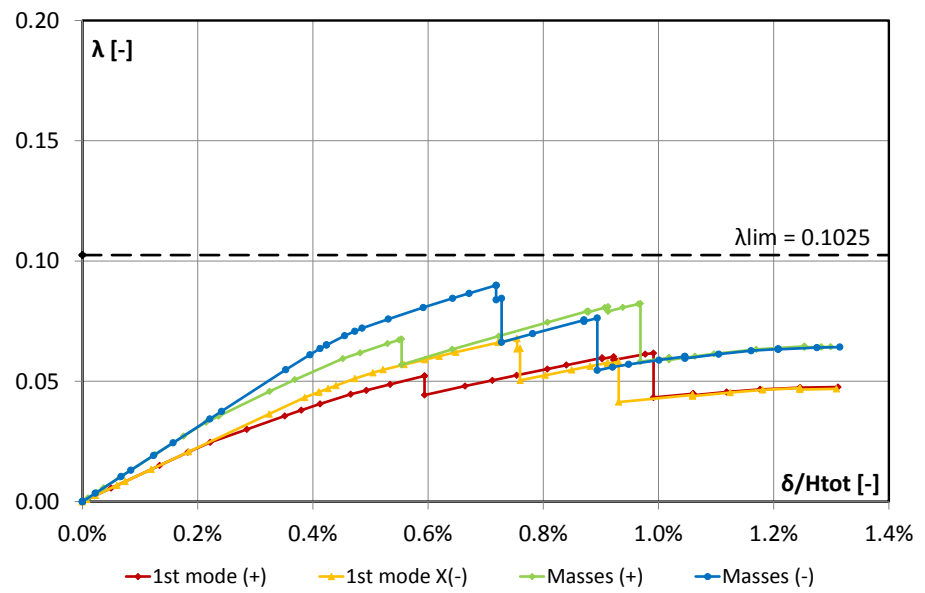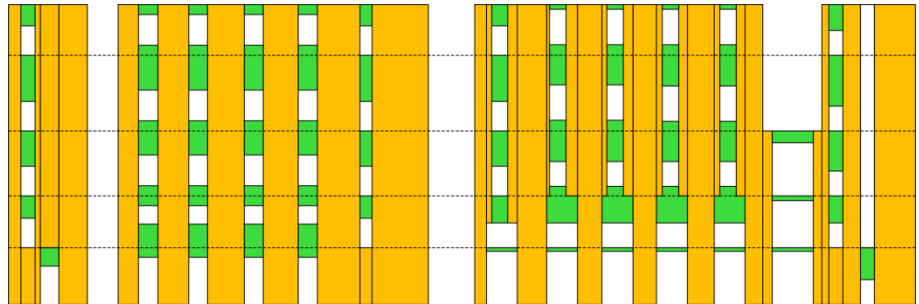
- **WALL 5X**

H_{tot} = 25.4m

Weight= 2850kN
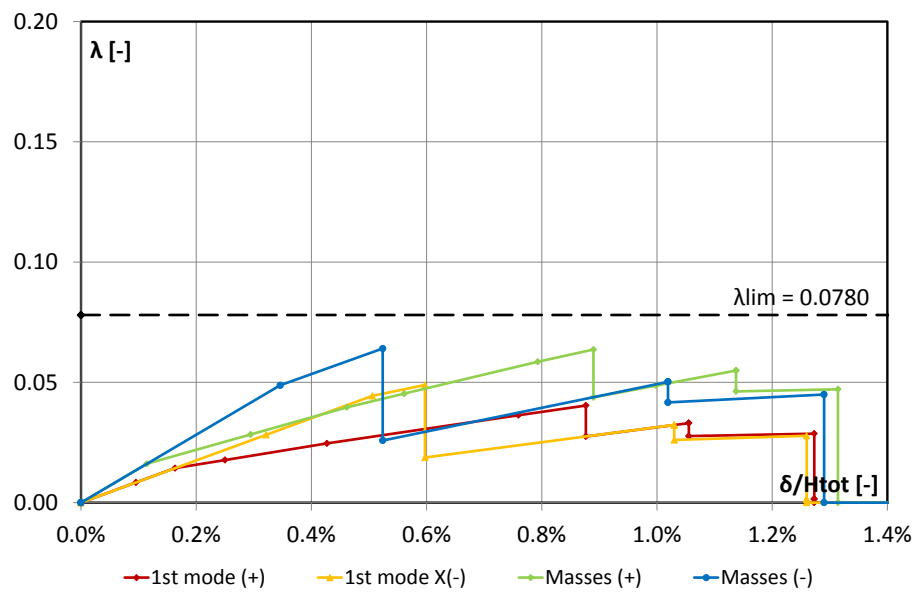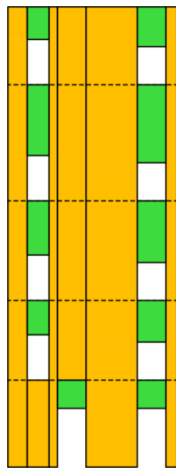
- **WALL 6X**

  H_{tot}= 25.4m

  Weight= 5470kN
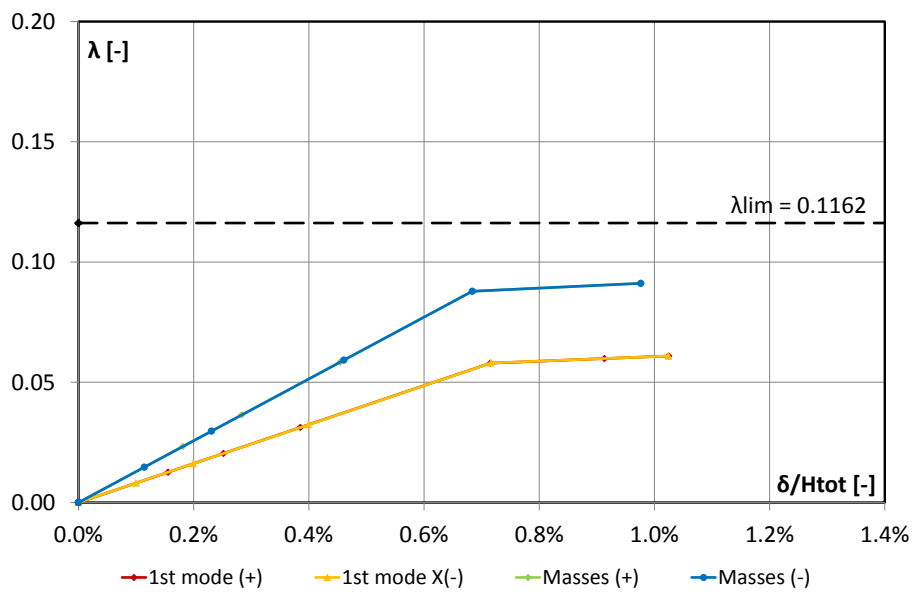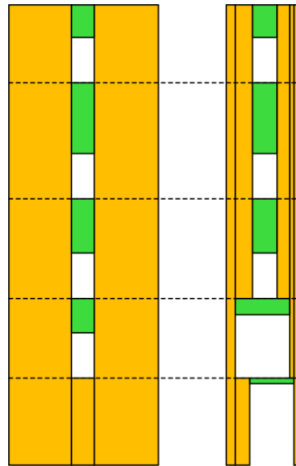
- **WALL 7X**

H_{tot} = 25.4m

Weight= 2860kN
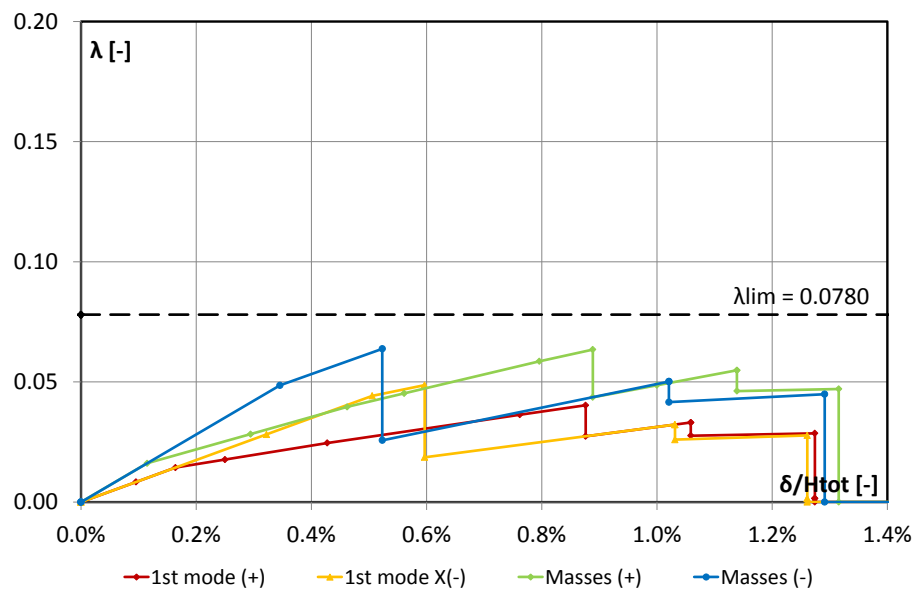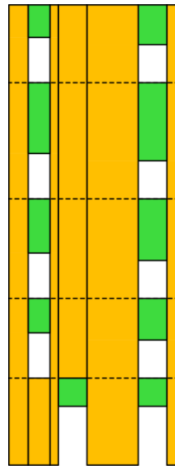
- **WALL 8X**

H_{tot}= 25.4m

Weight= 5492kN
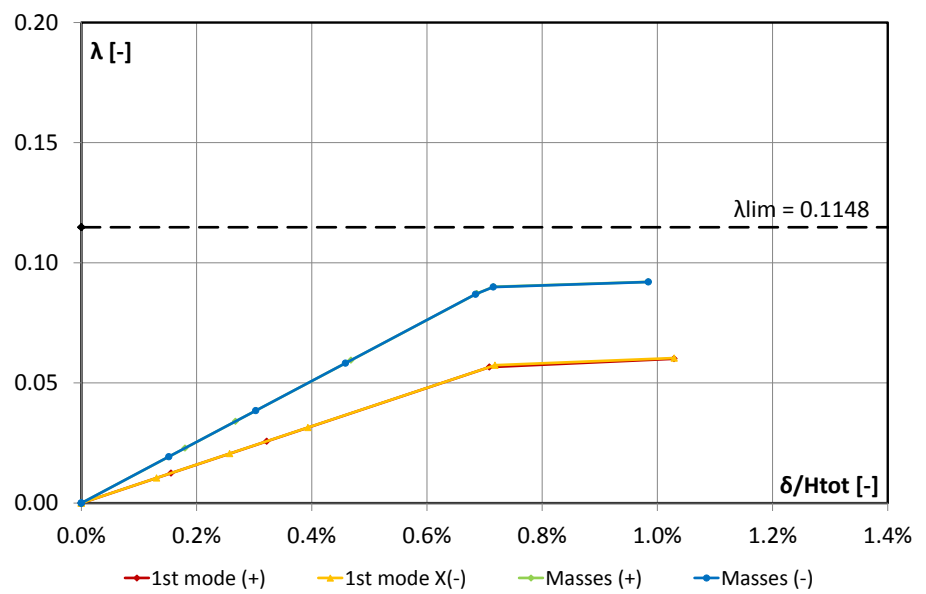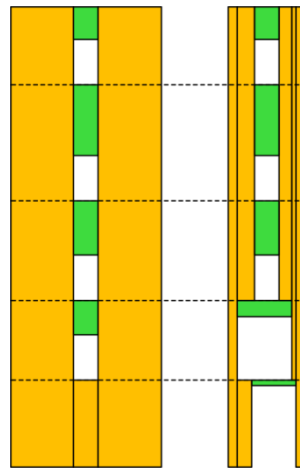
- **WALL 9X**

    H_{tot}= 25.4m

    Weight= 25873kN
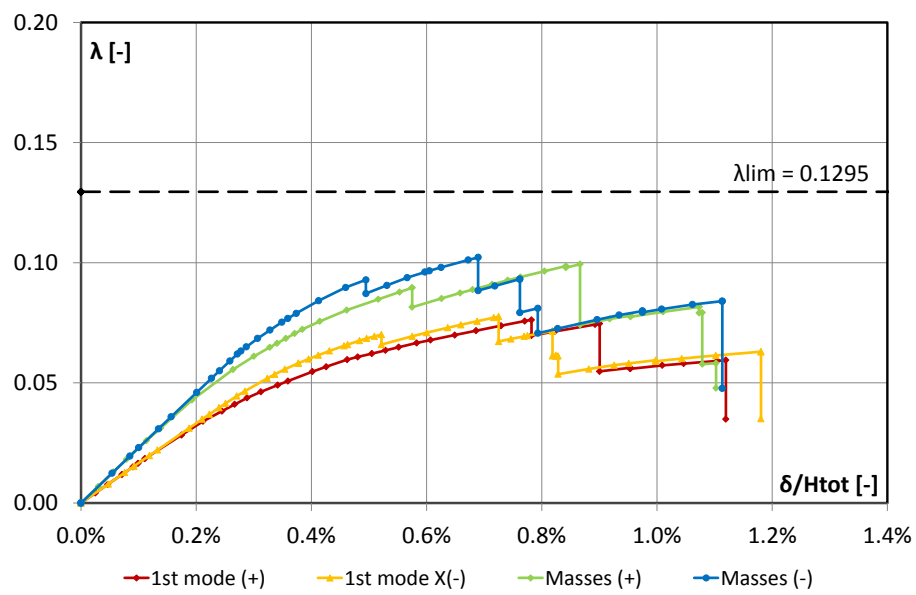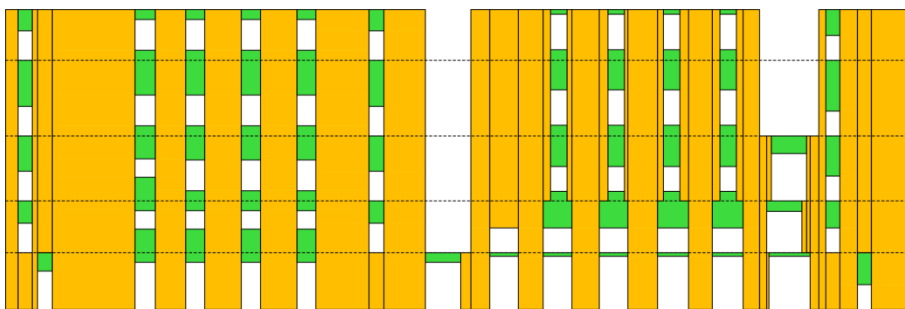
- **WALL 10X**

  H_{tot}= 25.4m

  Weight= 26176kN
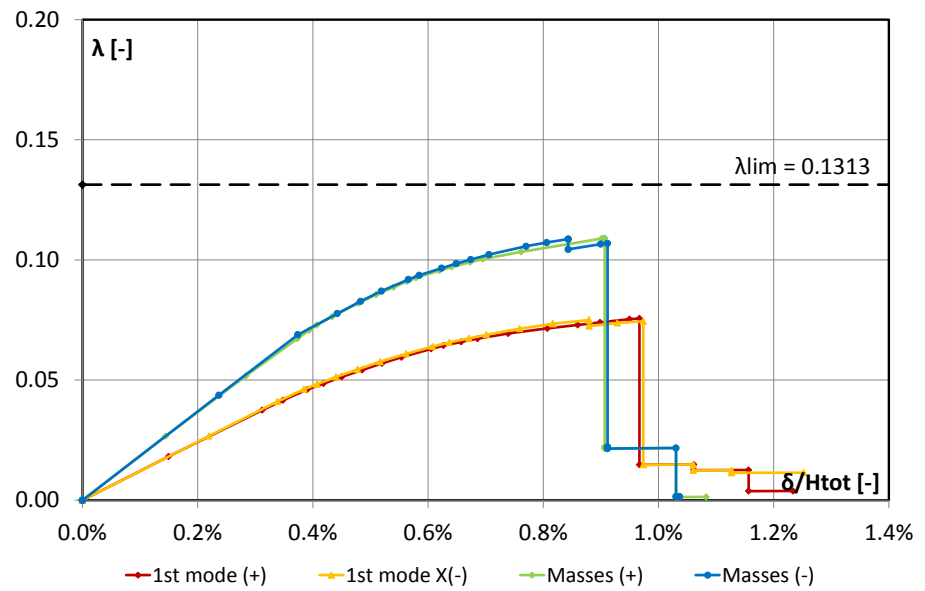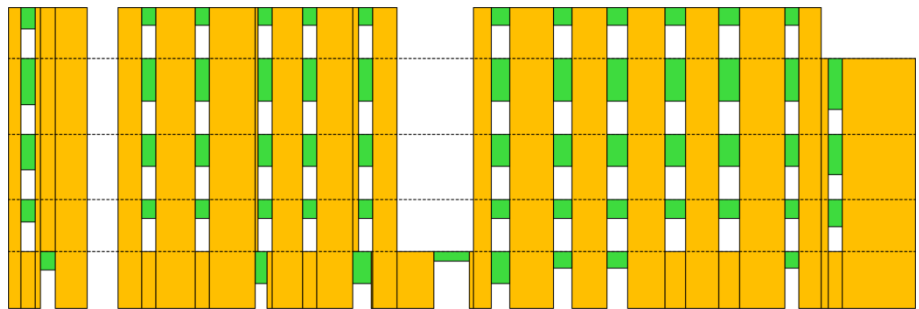
- **WALL 11X**

    H_{tot} = 25.4m

    Weight = 31159kN
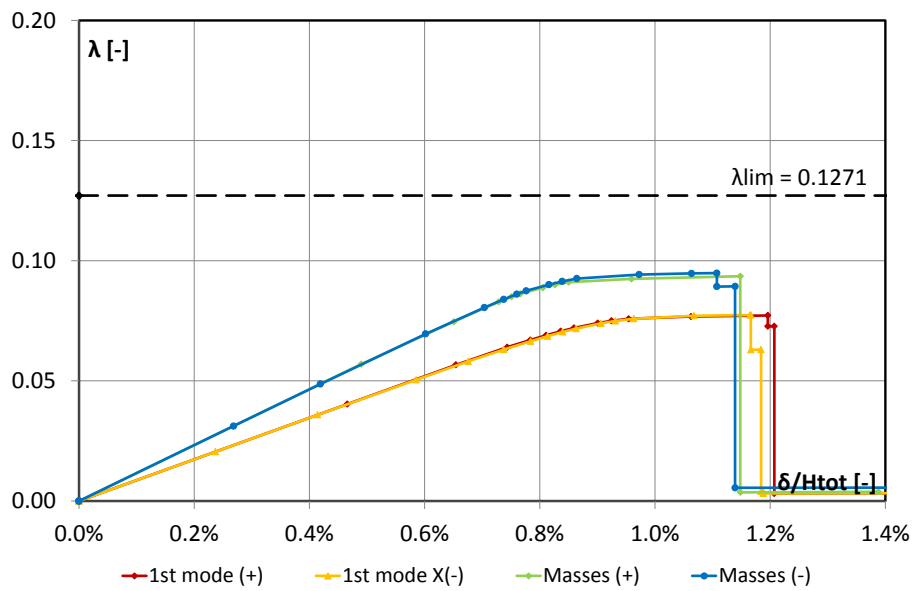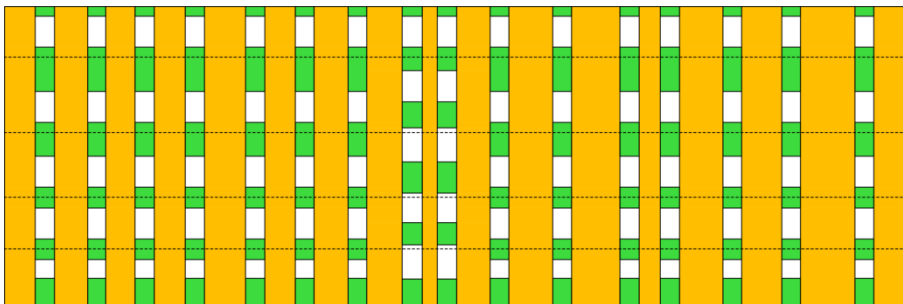
- **WALL 12X**

  H_{tot}= 25.4m

  Weight= 4281kN
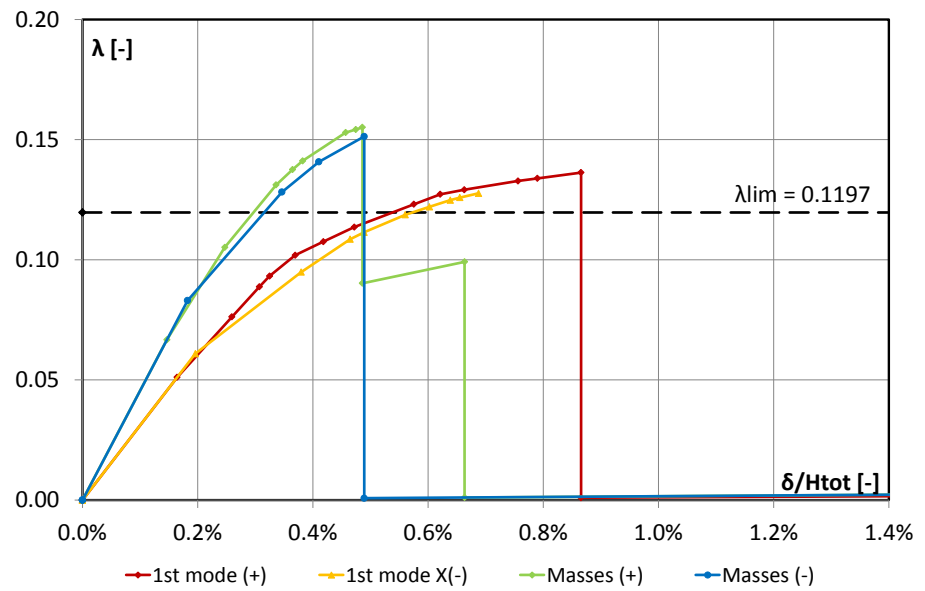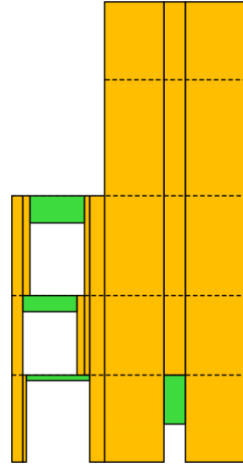
- **WALL 13X**

  H_{tot} = 25.4m

  Weight= 4276kN
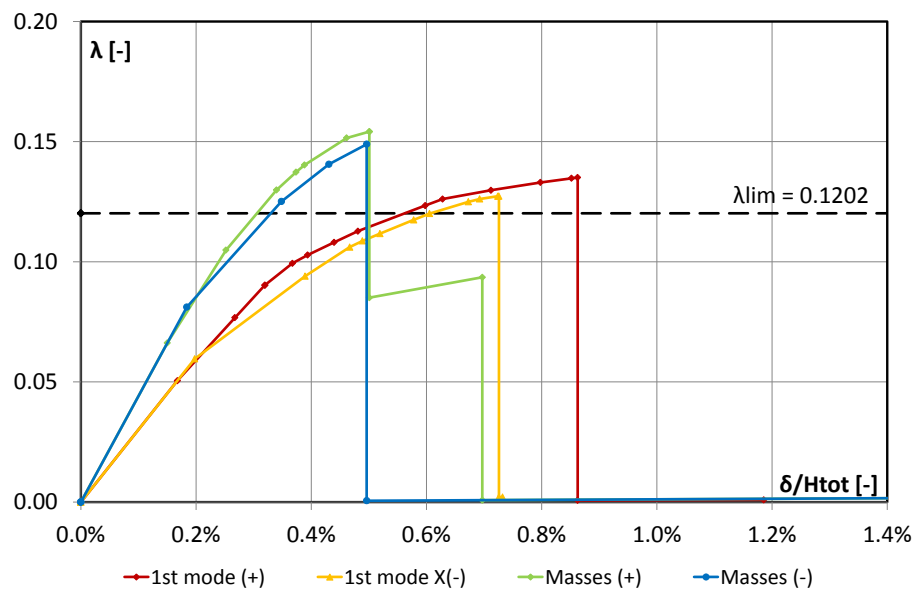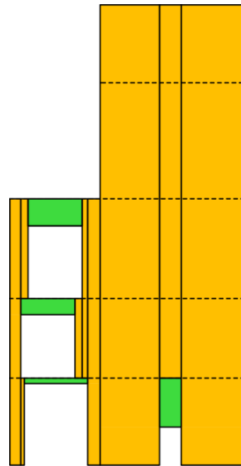
EX PRISON S. FRANCESCO: TRANSVERSAL WALLS (Y)
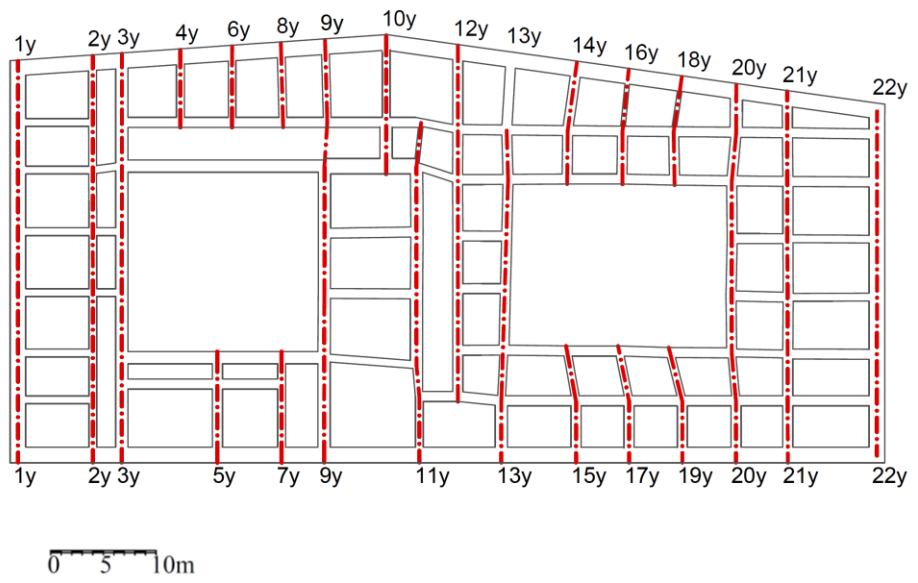
- **WALL 1Y**

H_{tot}= 25.4m

Weight= 14667kN
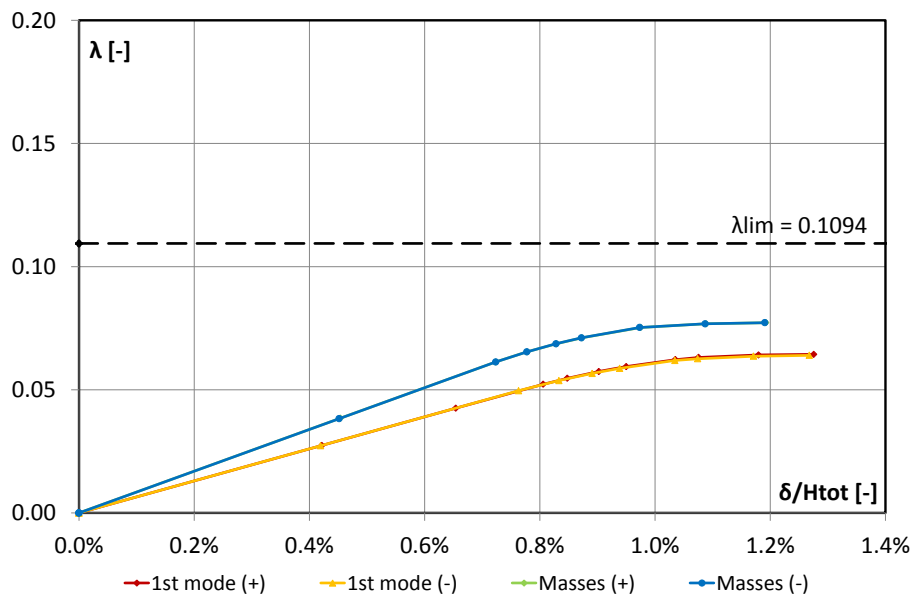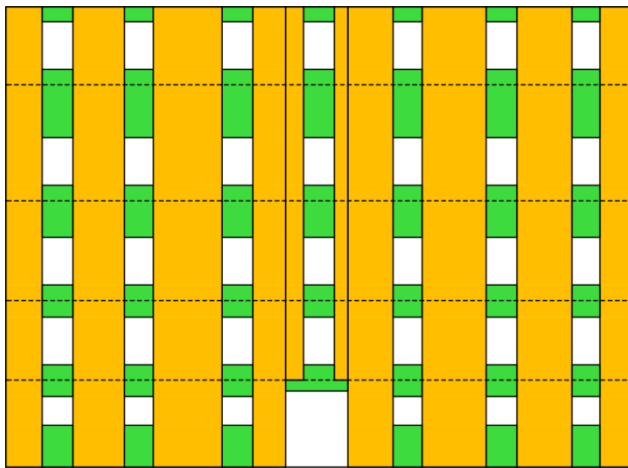
- **WALL 2Y**

    H_{tot}= 25.4m

    Weight= 10661kN
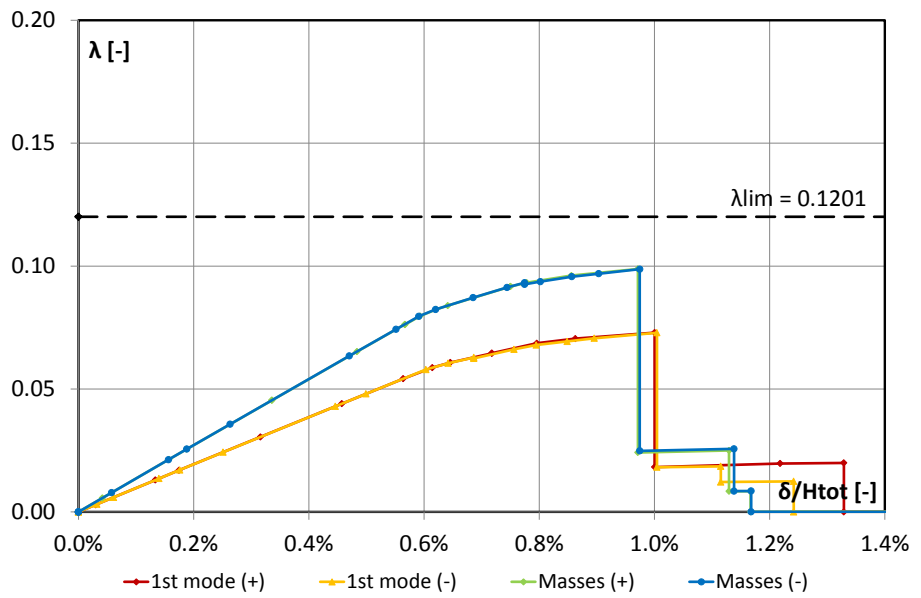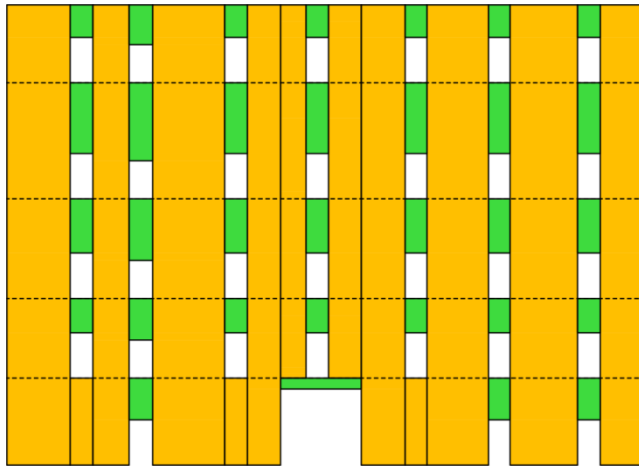
- **WALL 3Y**

H_{tot} = 25.4m

Weight= 14774kN
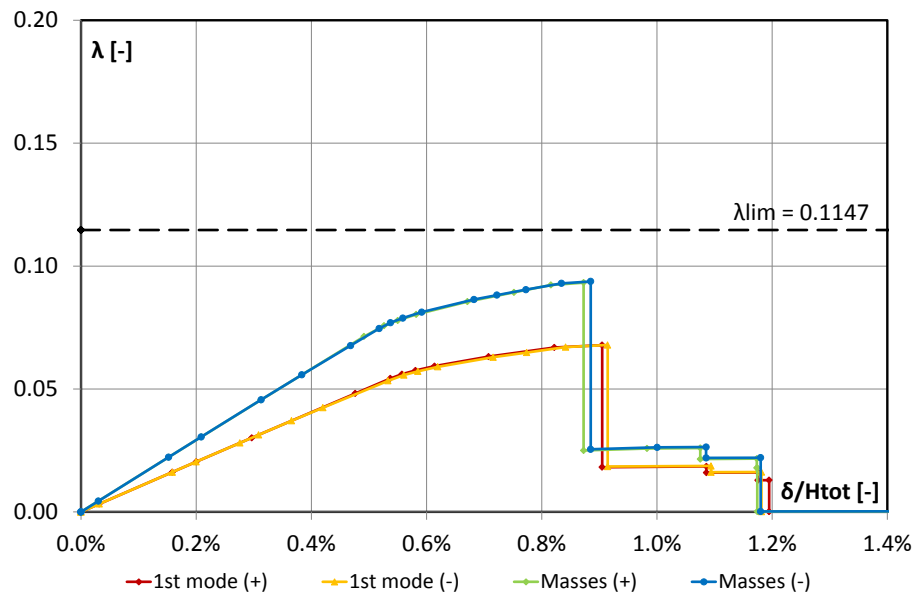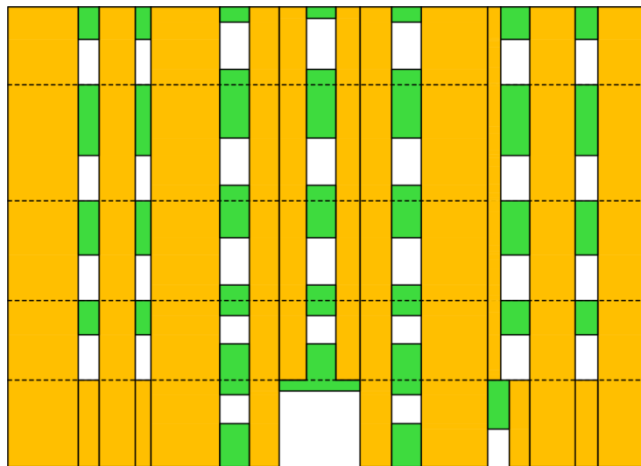
- **WALL 4Y**

  H_{tot}= 25.4m

  Weight= 1811kN
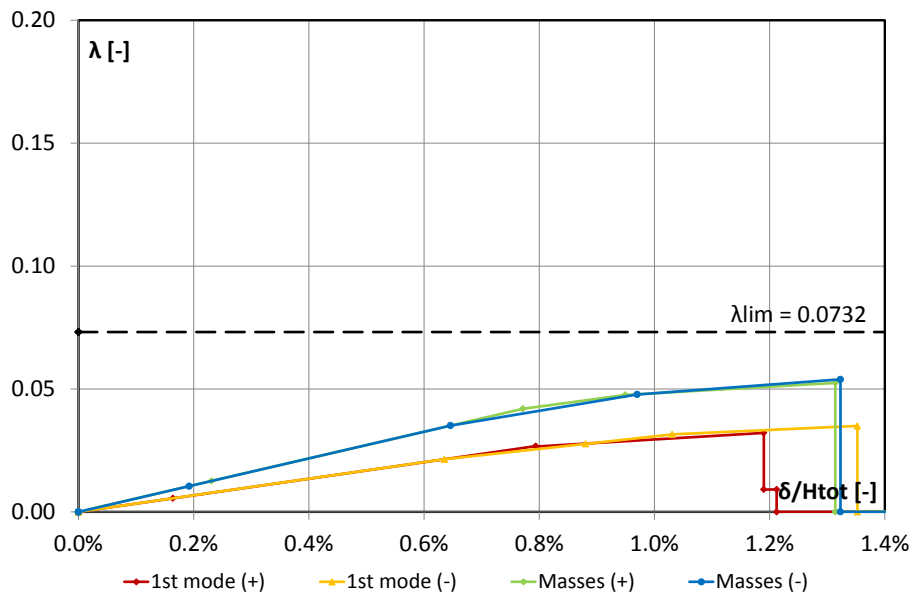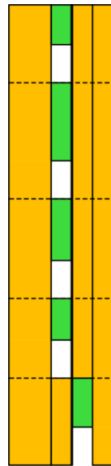
- **WALL 5Y**

H_{tot} = 25.4m

Weight = 4682kN
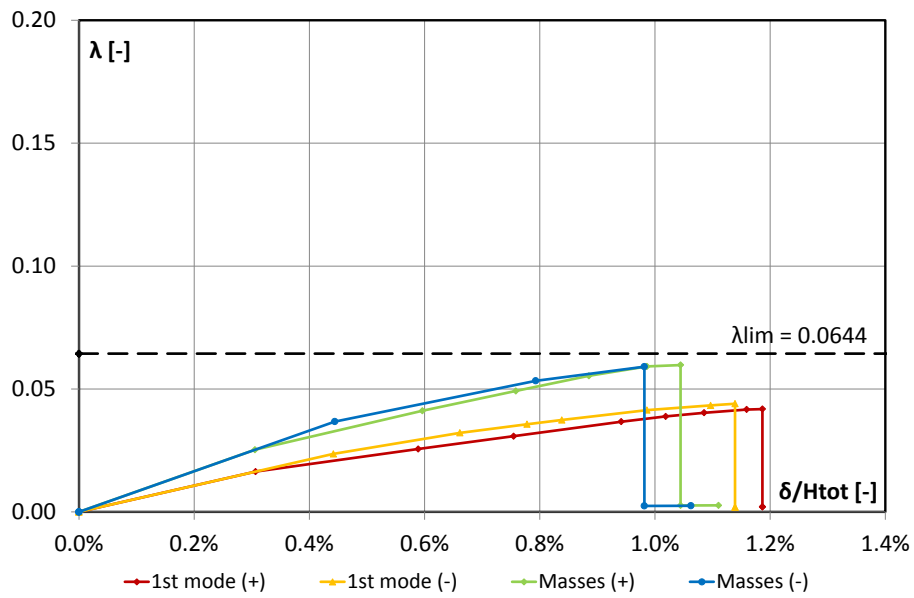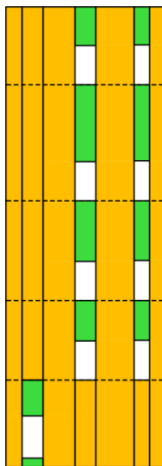
- **WALL 6Y**

H_{tot}= 25.4m

Weight= 1857kN
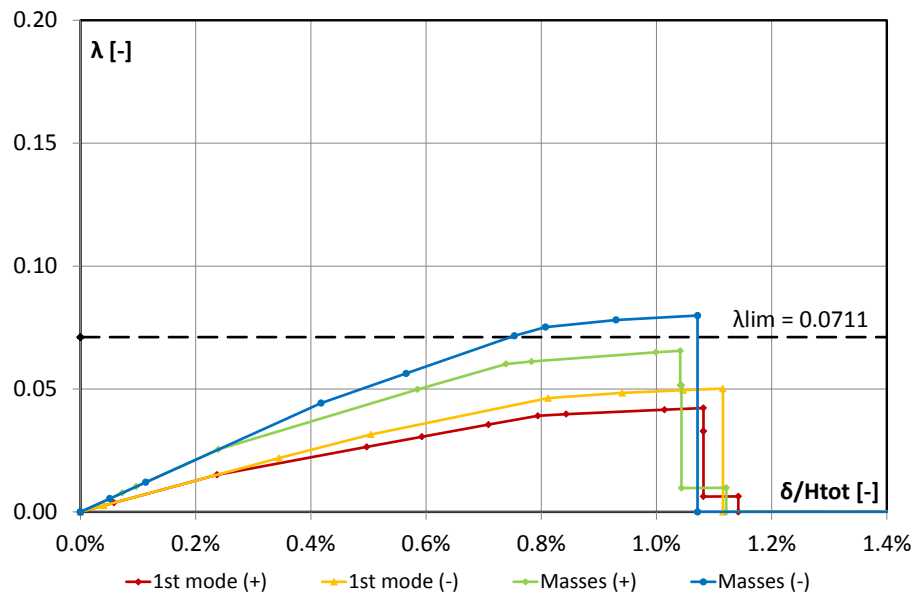
- **WALL 7Y**

  H_{tot} = 25.4m

  Weight= 3369kN
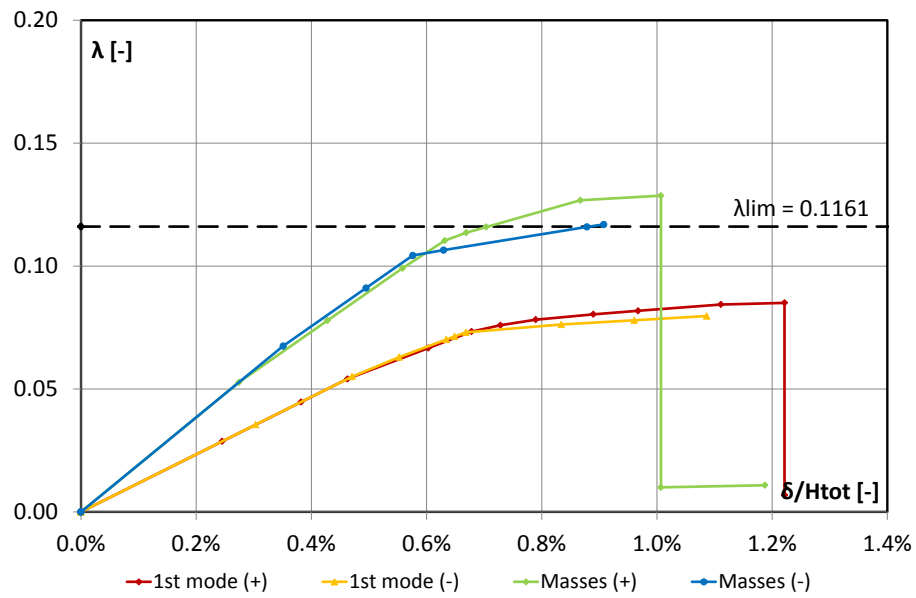
- **WALL 8Y**

    H_{tot}= 25.4m

    Weight= 2326kN
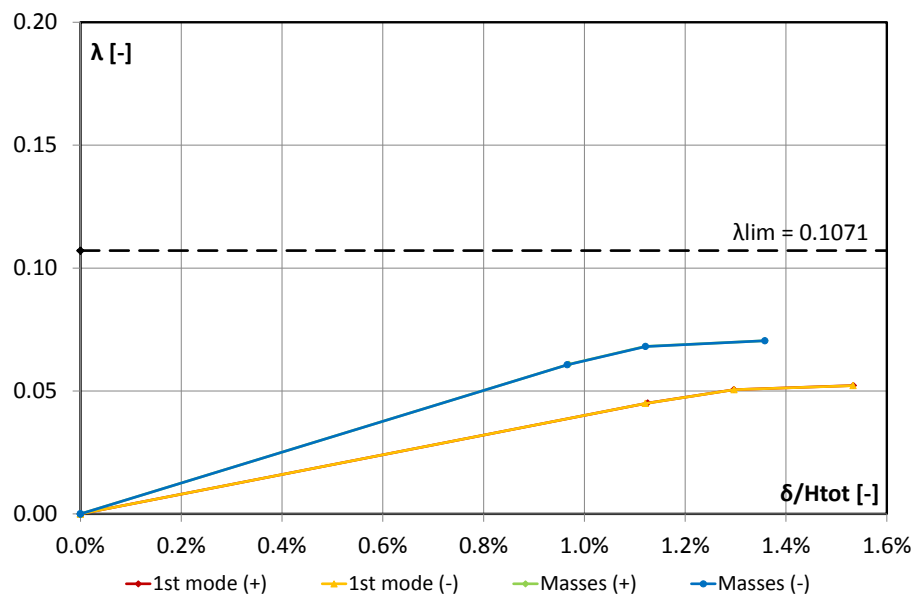
- **WALL 9Y**

  H_{tot} = 25.4m

  Weight= 11362kN
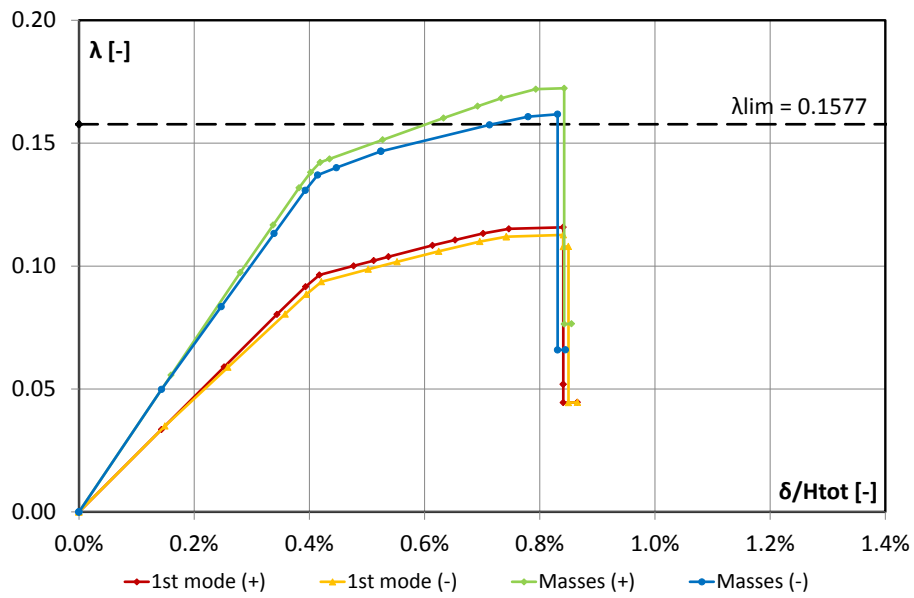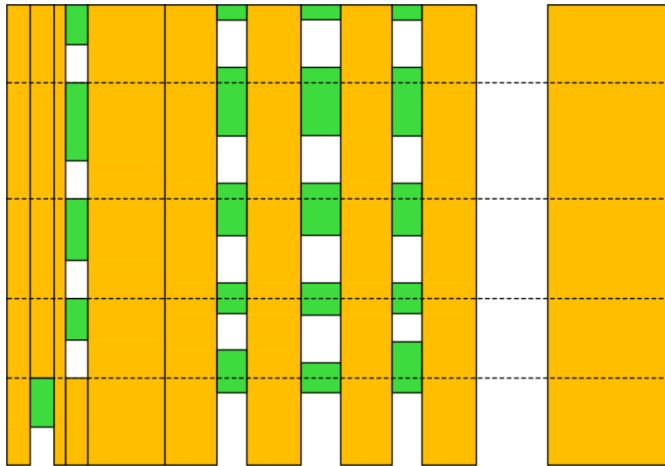
- **WALL 10Y**

    H_{tot}= 25.4m

    Weight= 3490kN
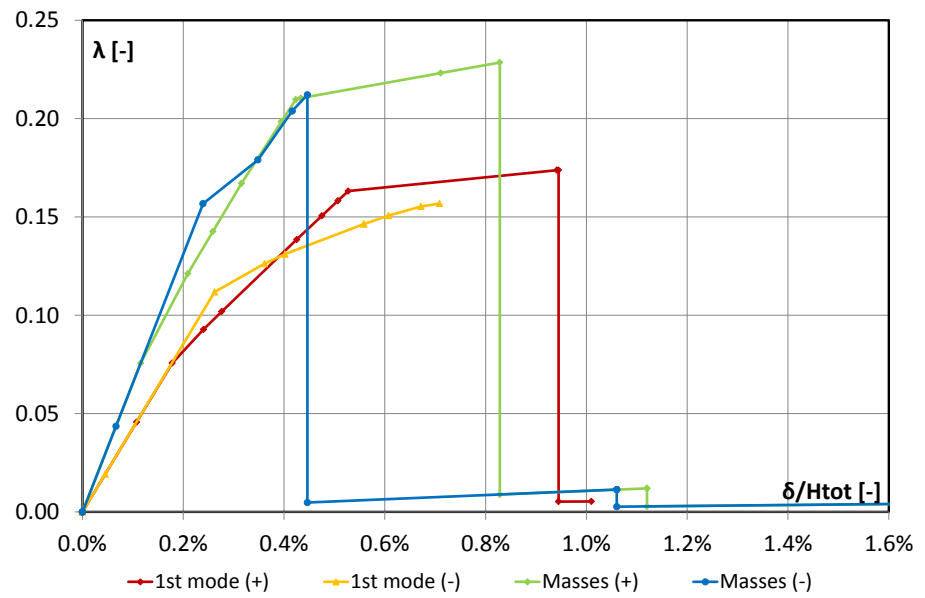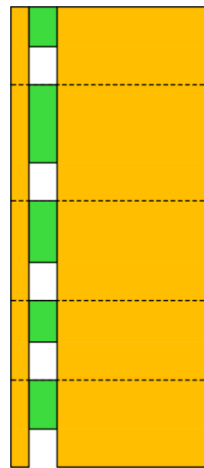
- **WALL 11Y**

H_{tot} = 25.4m

Weight= 9063kN
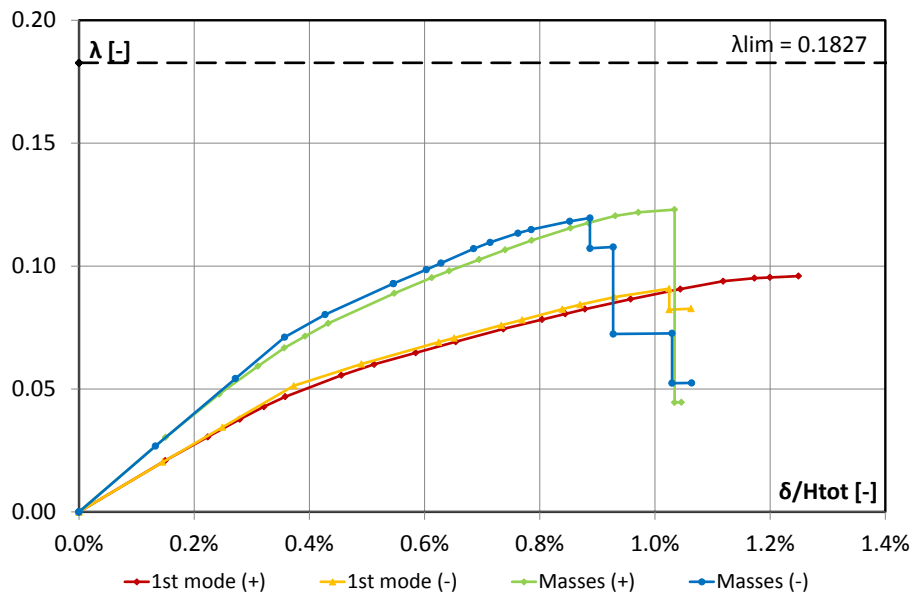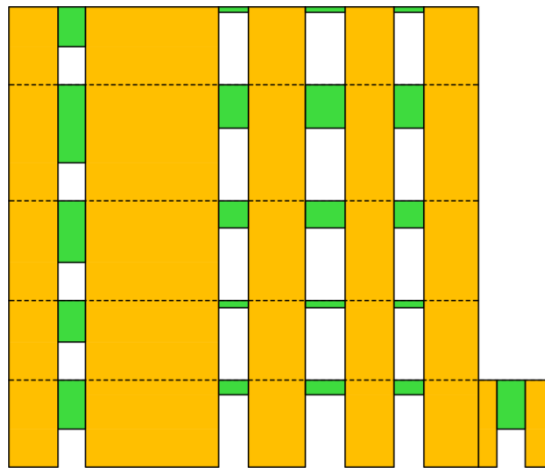
- **WALL 12Y**

  H_{tot} = 25.4m

  Weight= 8858kN
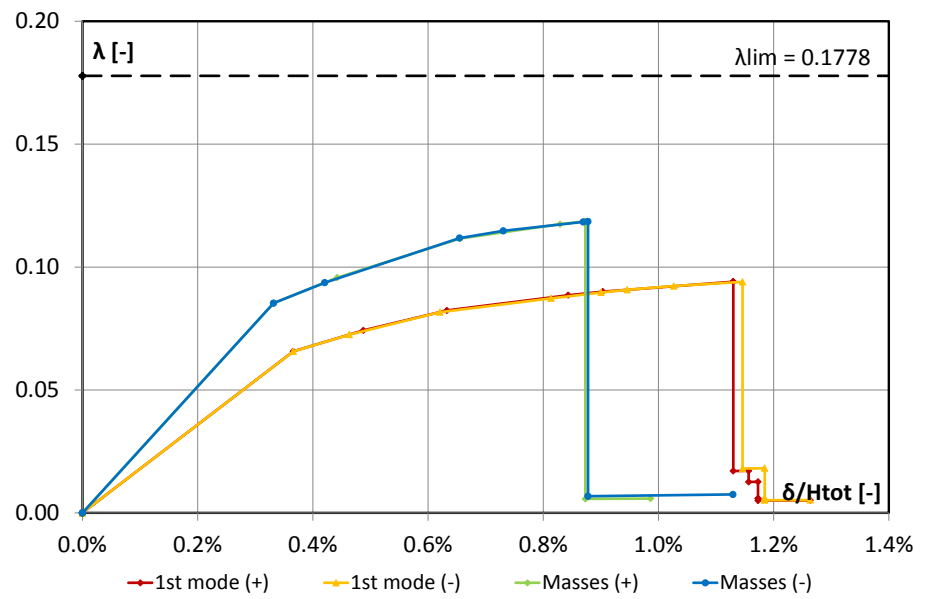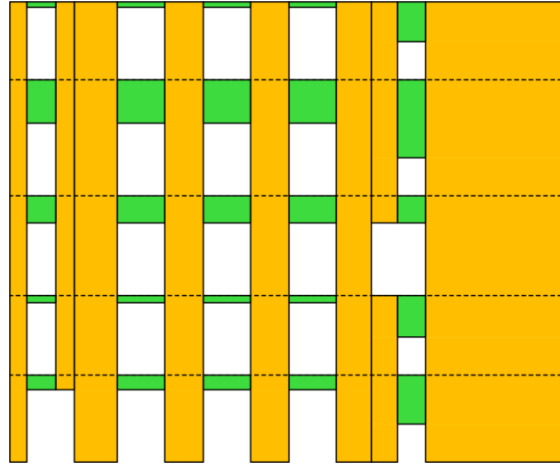
- **WALL 13Y**

H_{tot} = 25.4m

Weight = 9927kN
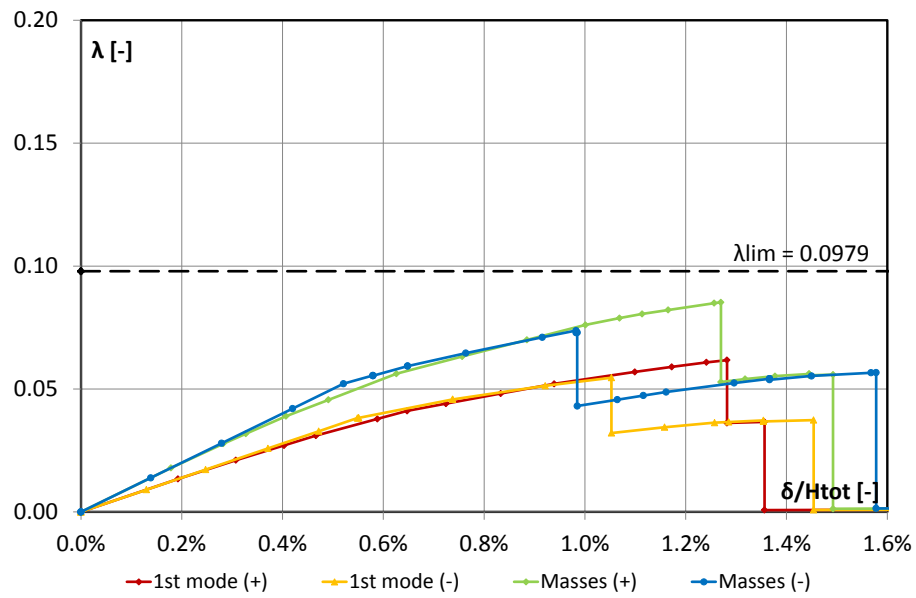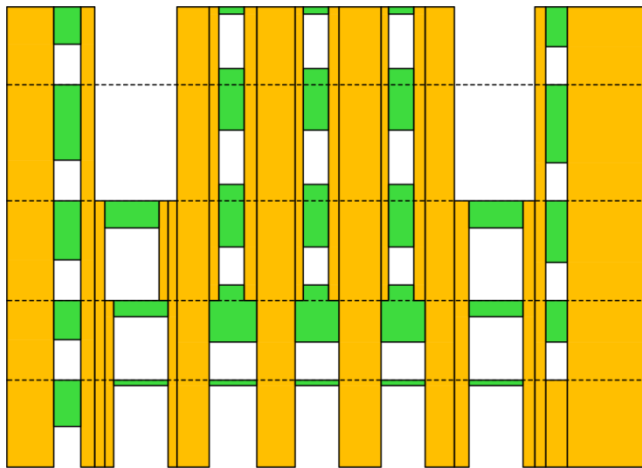
- **WALL 14Y**

    H_{tot}= 25.4m

    Weight= 2429kN
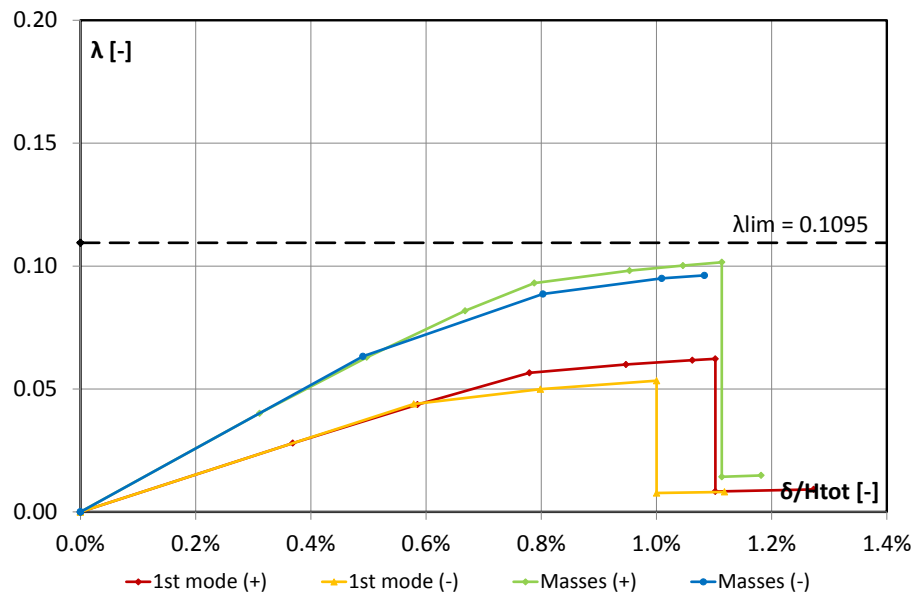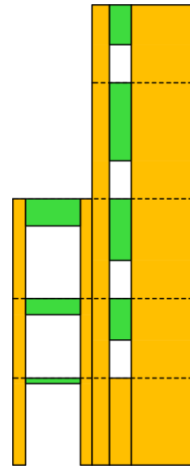
- **WALL 15Y**

  H_{tot} = 25.4m

  Weight= 2519kN
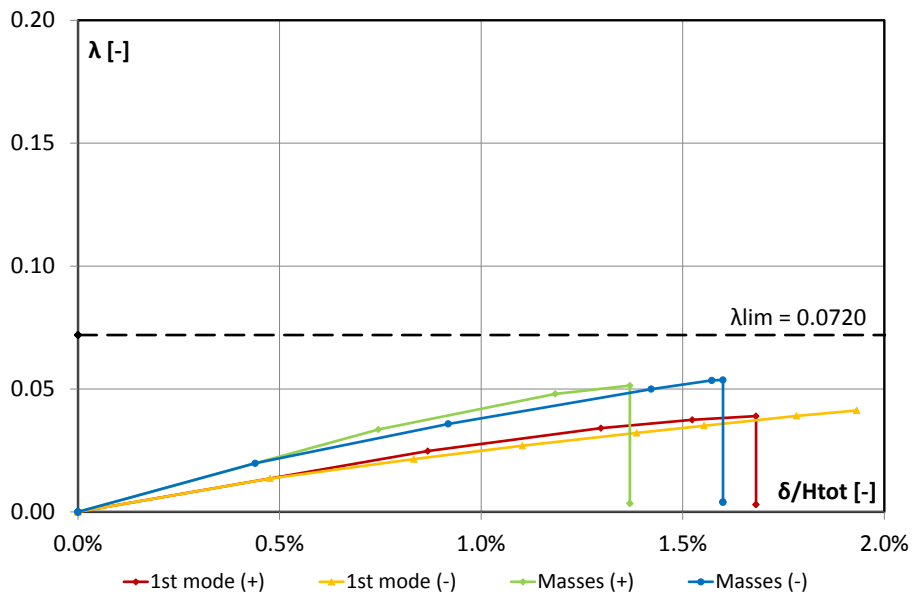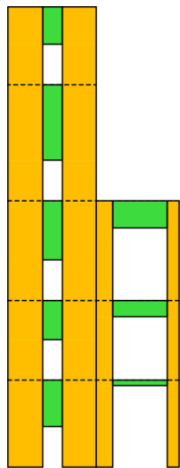
- **WALL 16Y**

  H_{tot}= 25.4m

  Weight= 1403kN
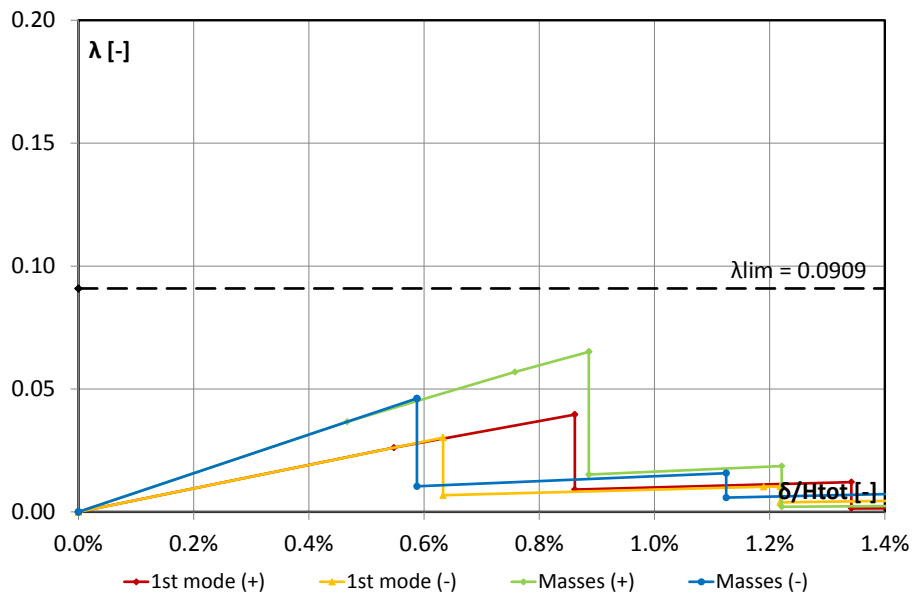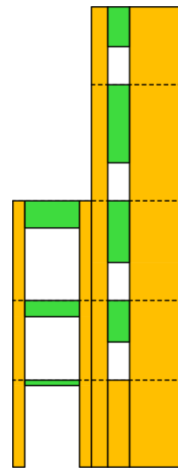
- **WALL 17Y**

  H_{tot} = 25.4m

  Weight = 2315kN
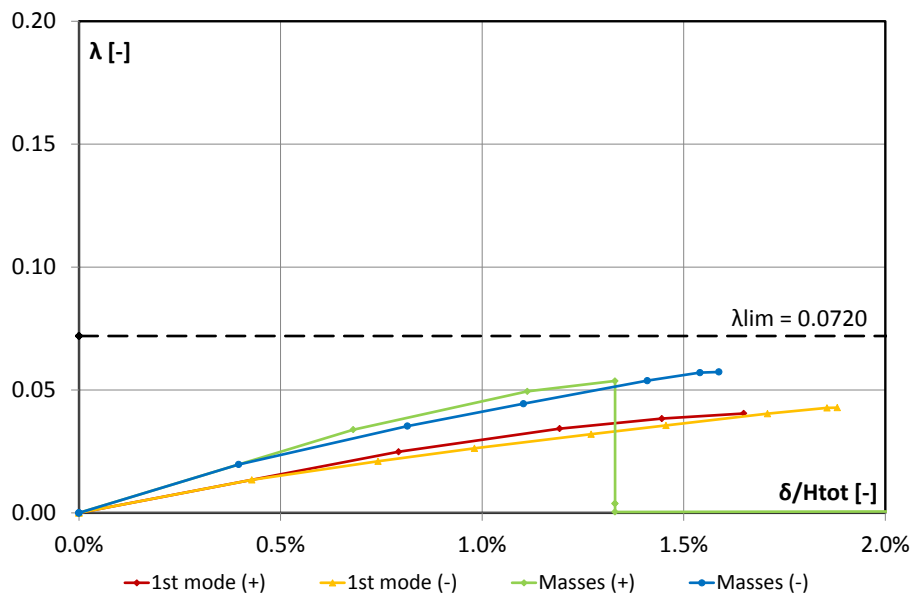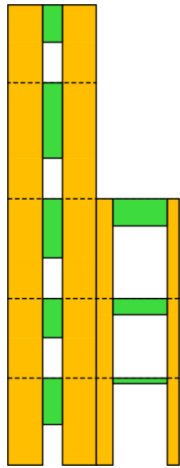
- **WALL 18Y**

  H_{tot}= 25.4m

  Weight= 1312kN
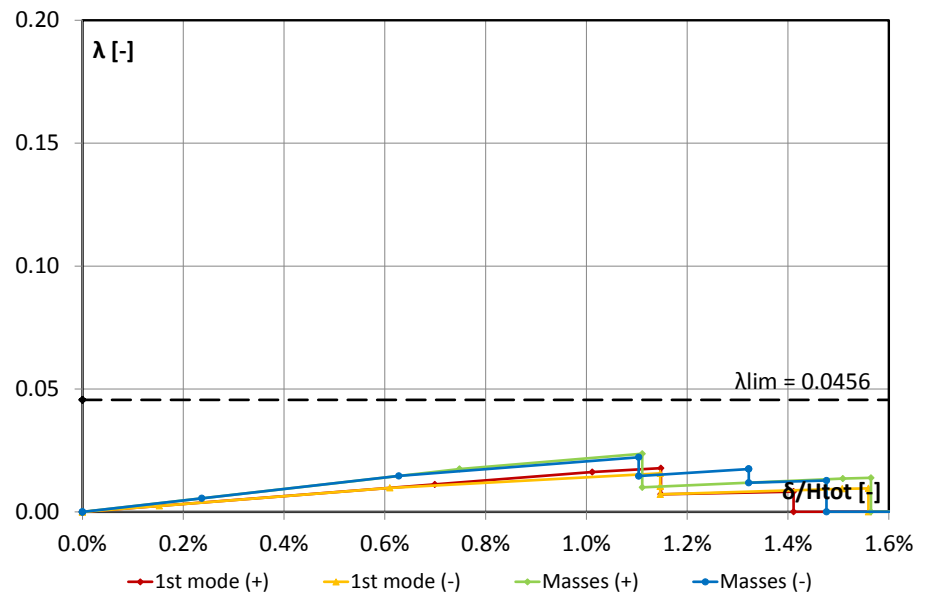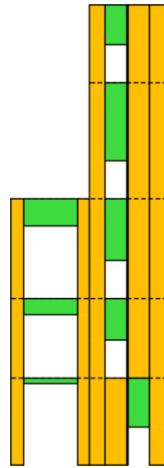
- **WALL 19Y**

  H_{tot} = 25.4m

  Weight= 2330kN
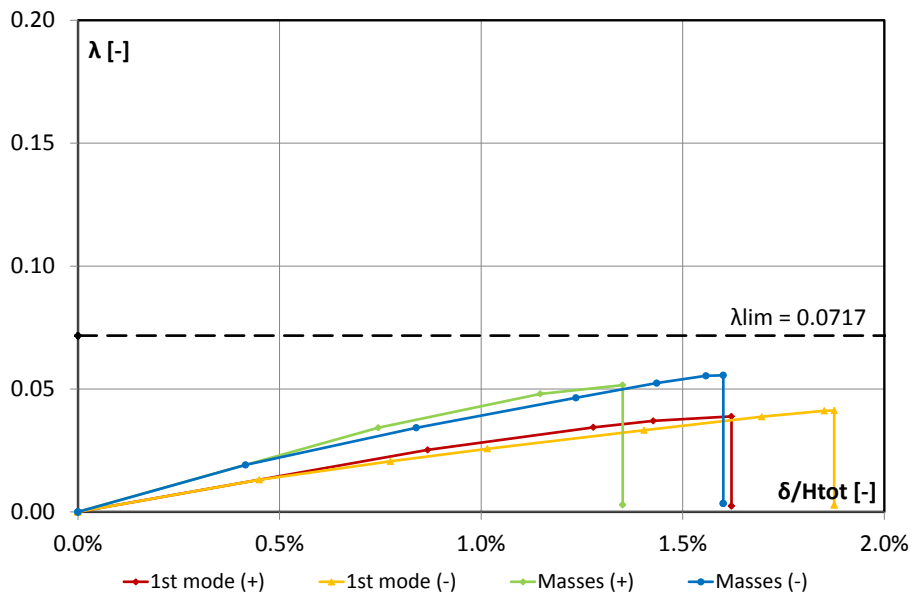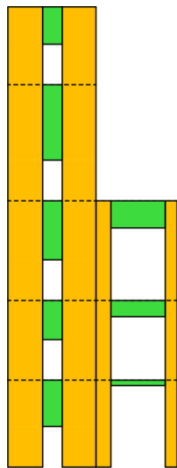
- **WALL 20Y**

  H_{tot}= 25.4m

  Weight= 8331kN
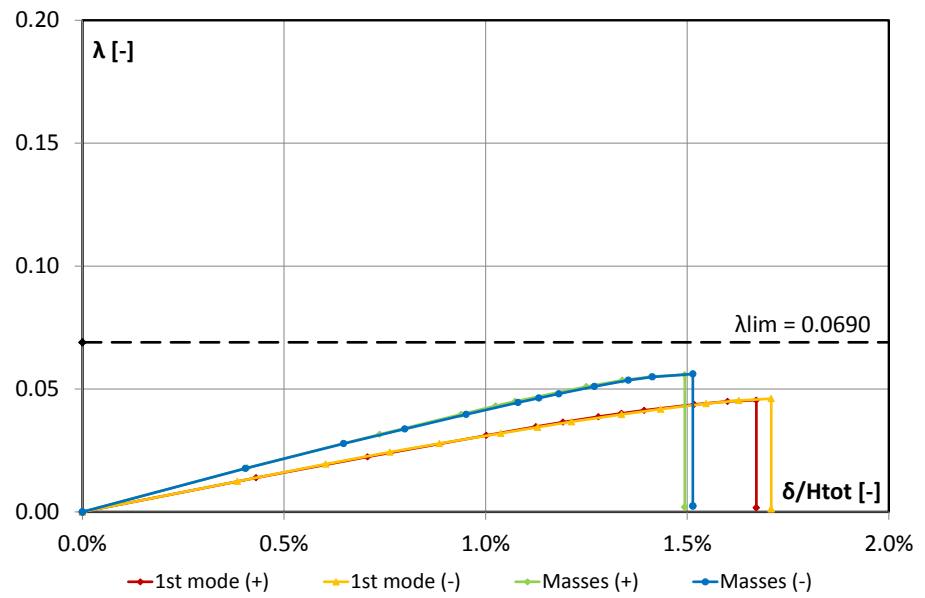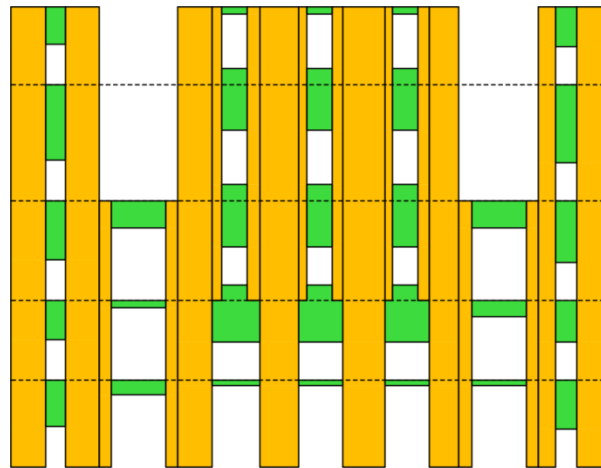
- **WALL 21Y**

H_{tot} = 25.4m

Weight = 9358kN
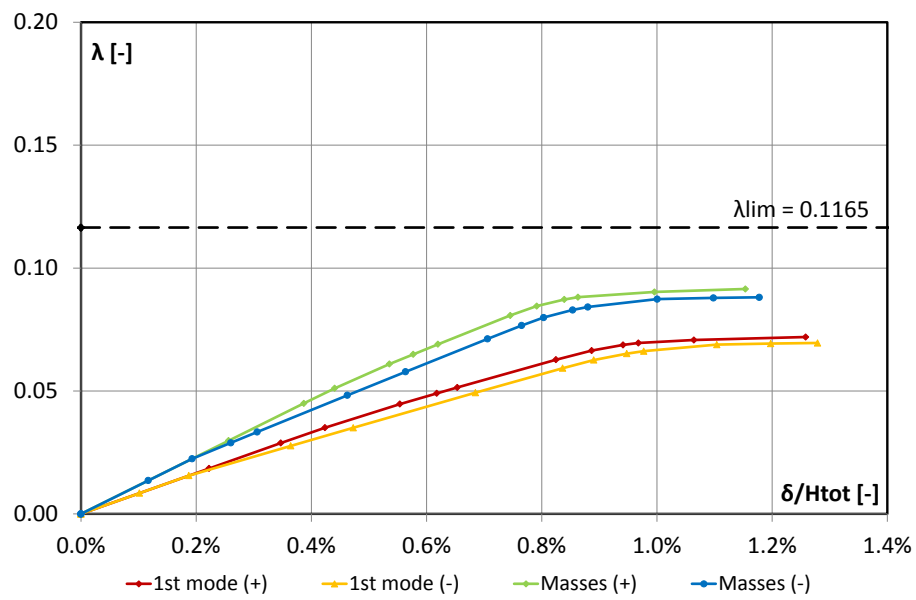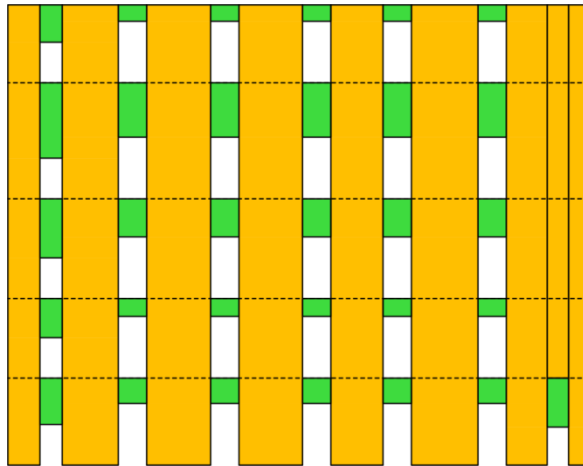
- **WALL 22Y**

H_{tot} = 25.4m

Weight= 11483kN
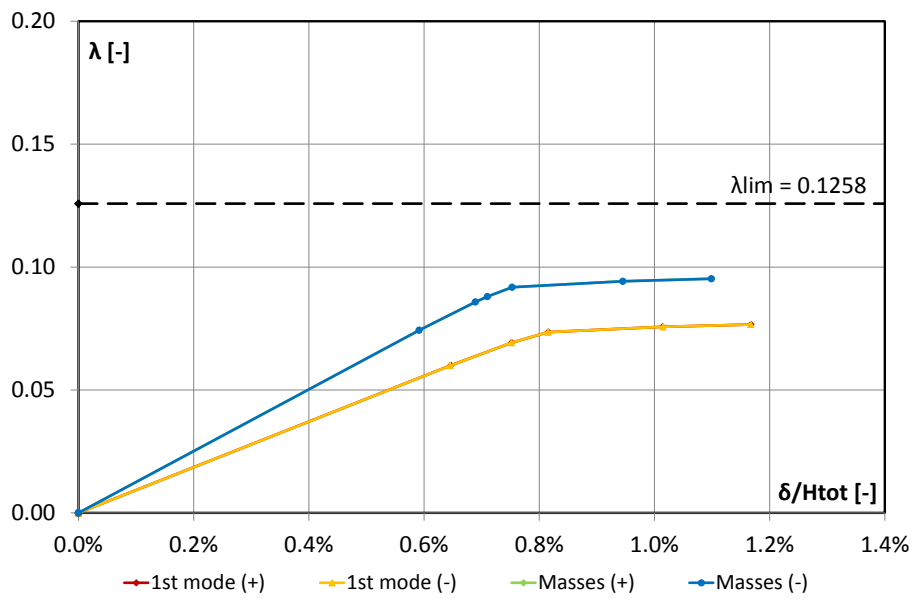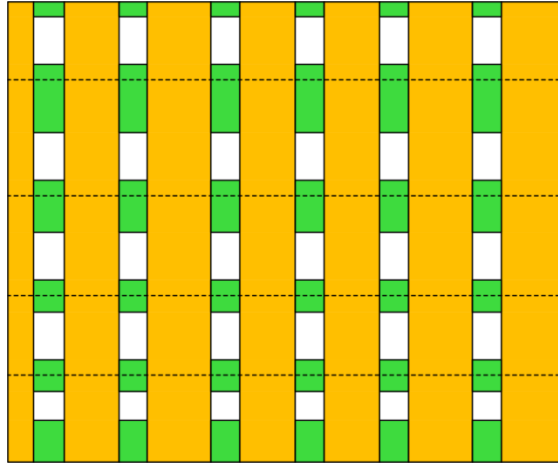
PALAZZO CENTI: LONGITUDINAL WALLS (X)
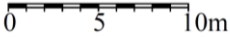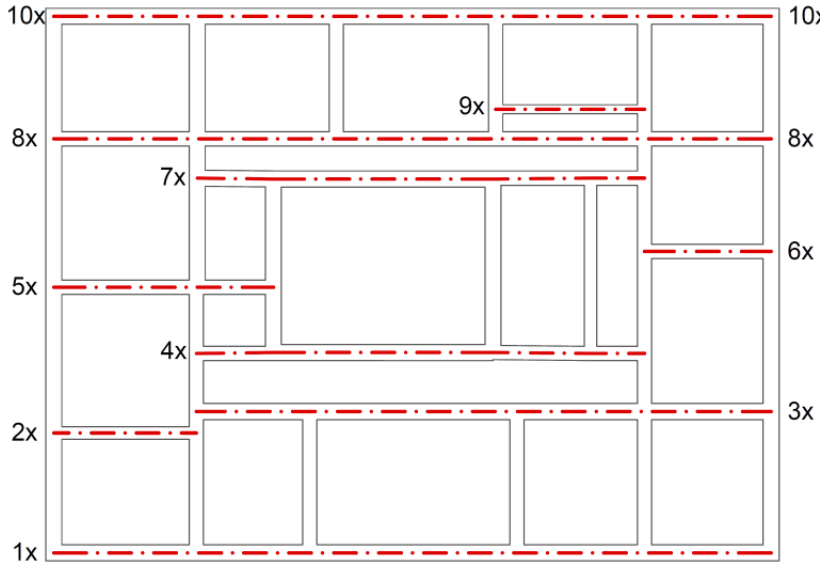
- **WALL 1X**

  $H_{tot} = 16.5$

  Weight = 12209kN
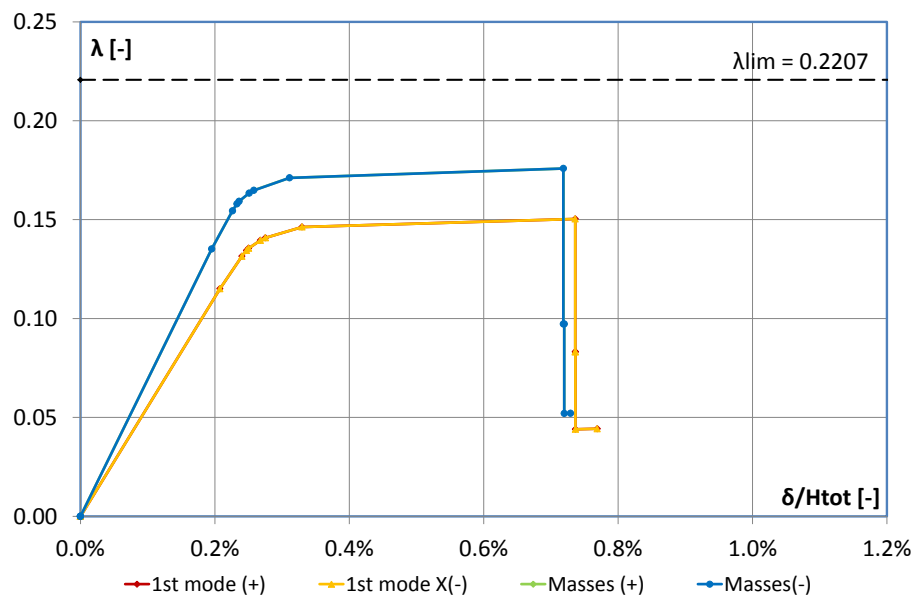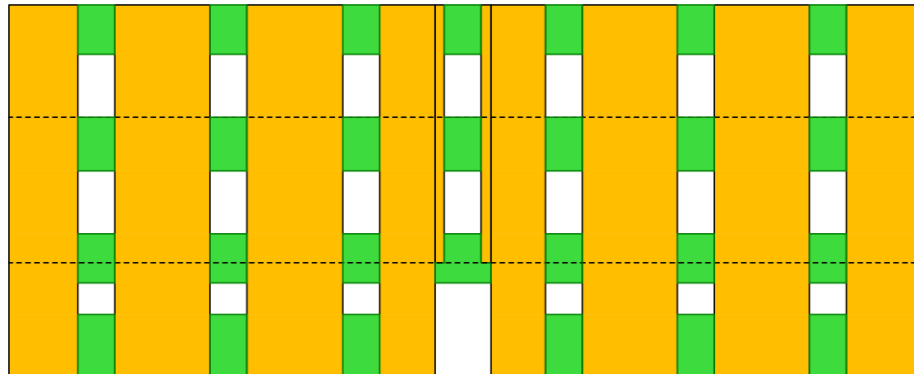
- **WALL 2X**

  H_{tot} = 16.5

  Weight= 2759kN
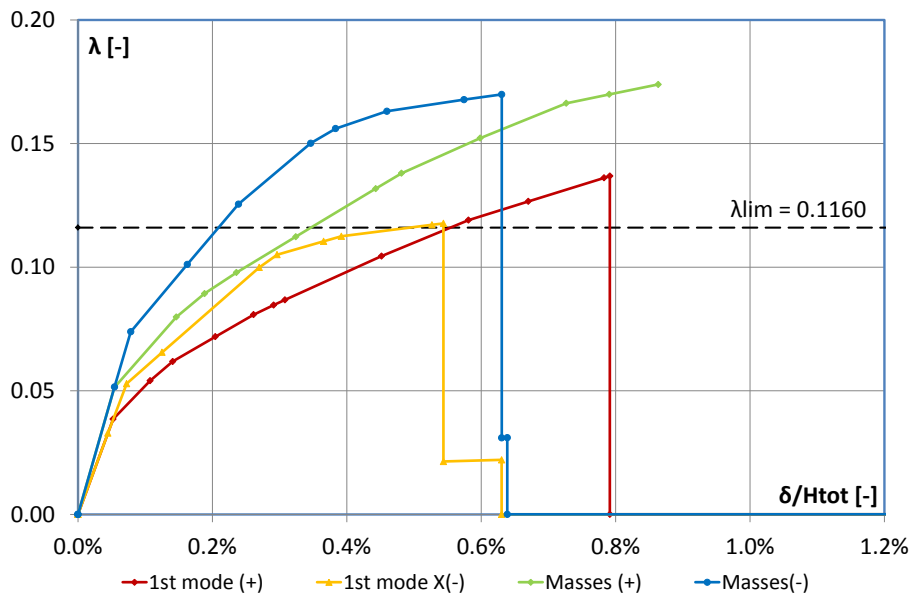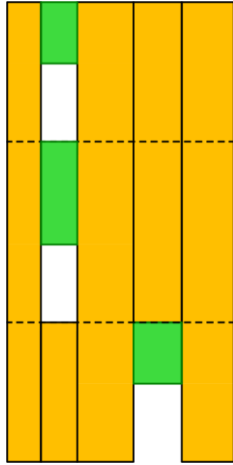
- **WALL 3X**

  H_{tot}= 16.5

  Weight= 12451kN
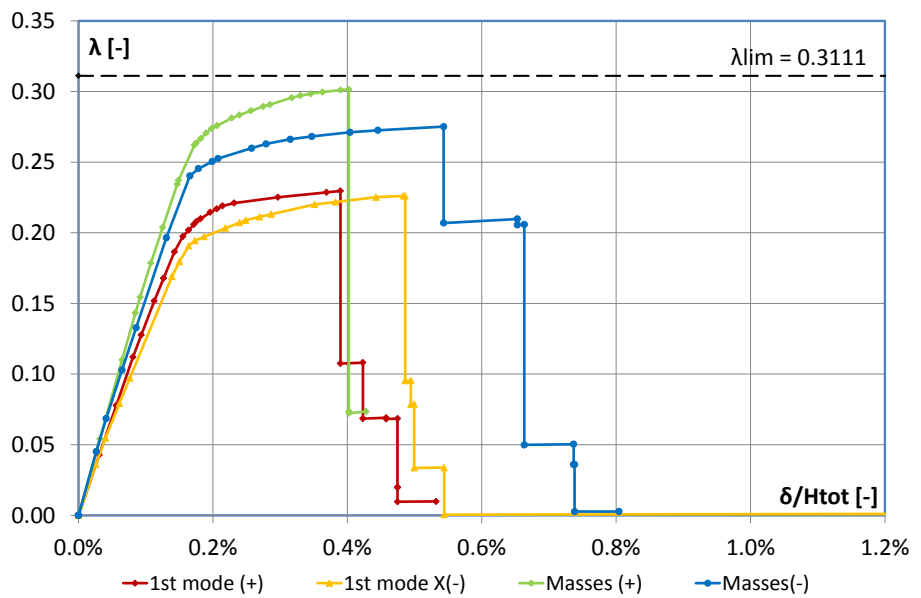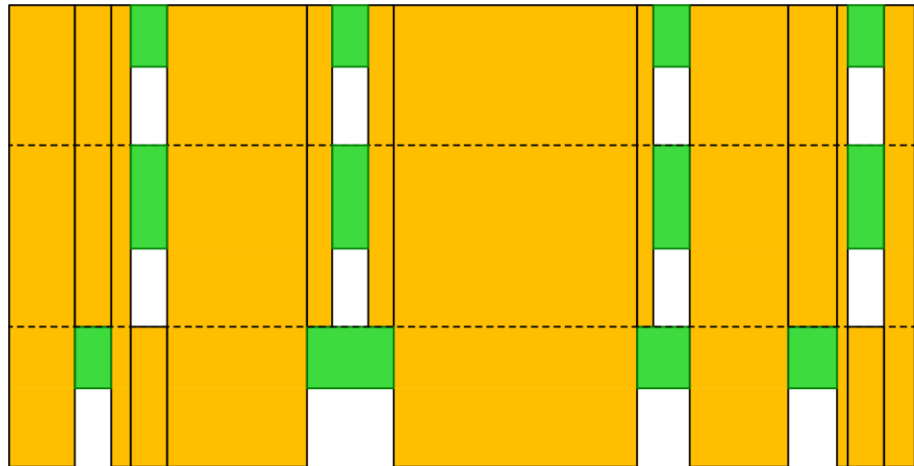
- **WALL 4X**

    H_{tot} = 16.5

    Weight= 5696kN
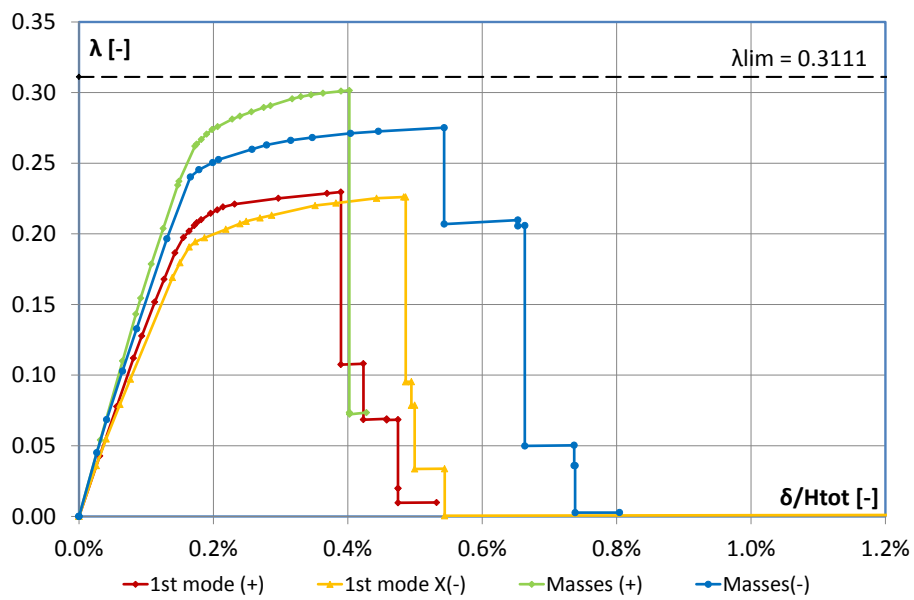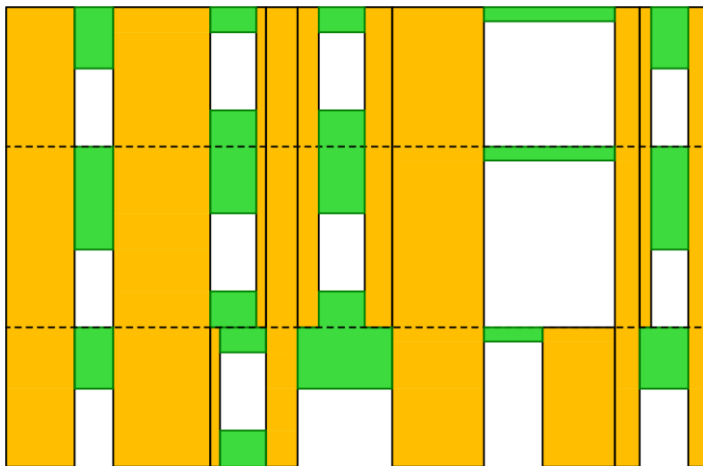
- **WALL 5X**

$H_{tot}= 16.5$

Weight= 3768kN
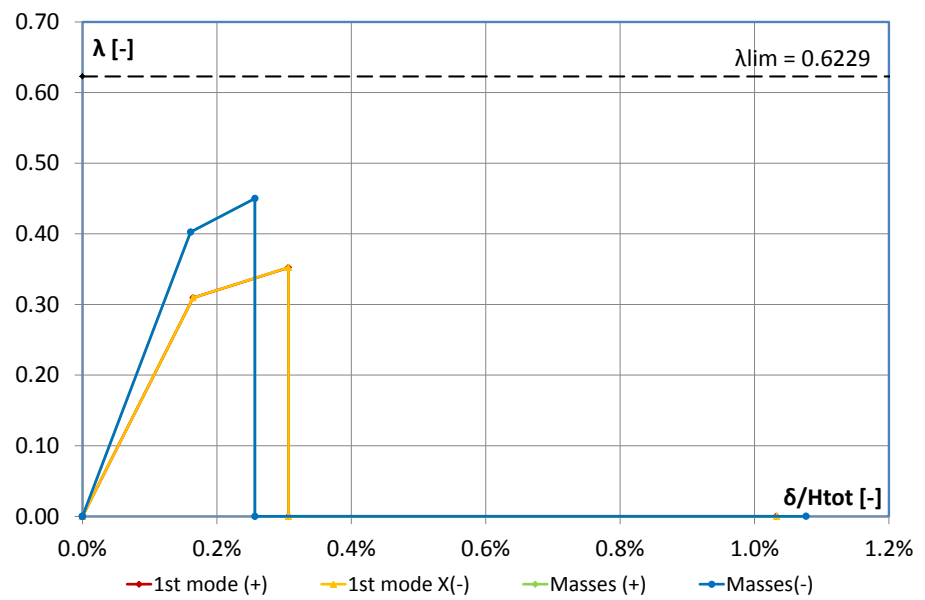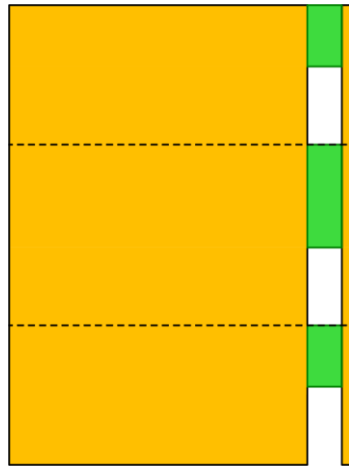
- **WALL 6X**

H_{tot} = 16.5

Weight= 2347kN
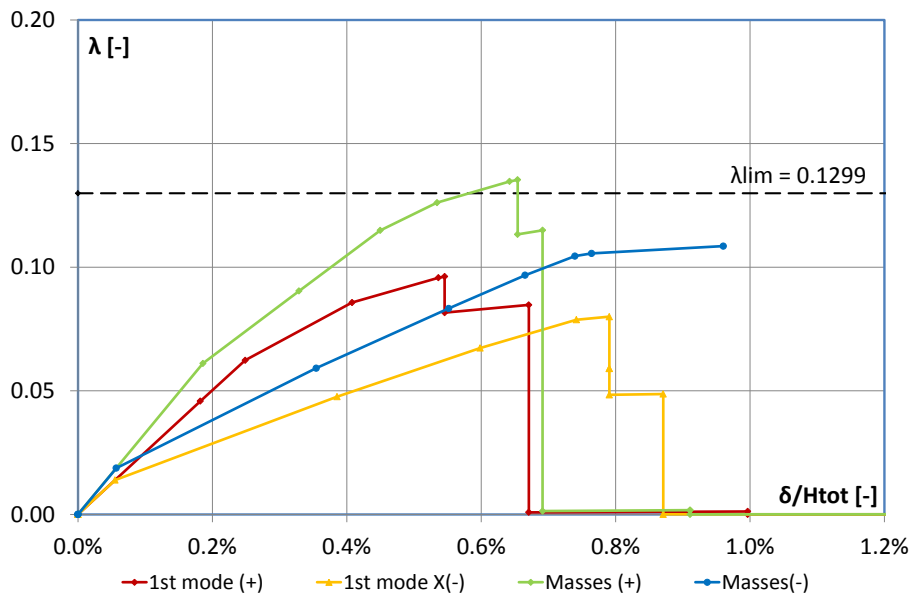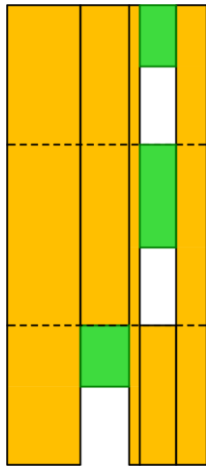
- **WALL 7X**

    H_{tot}= 16.5

    Weight= 5558kN
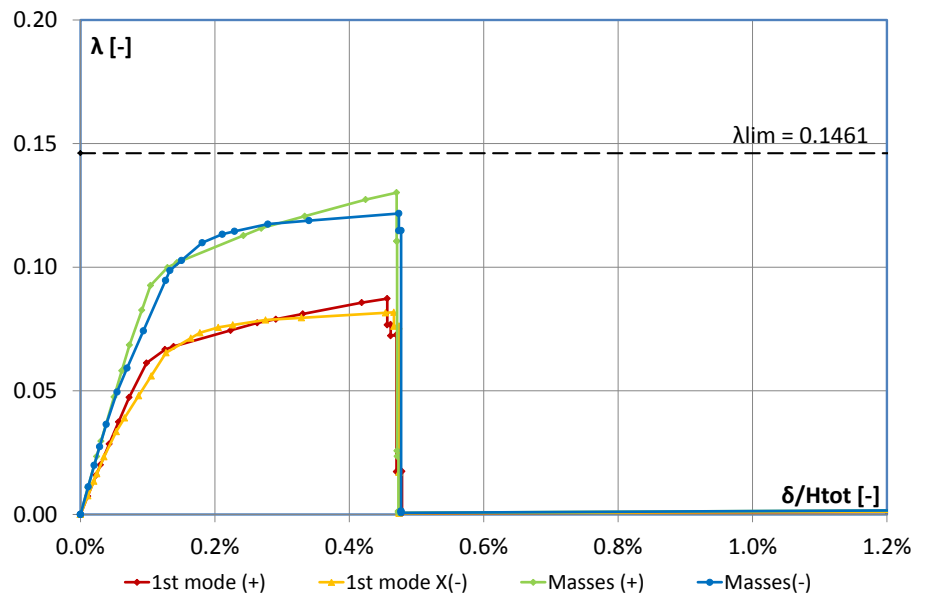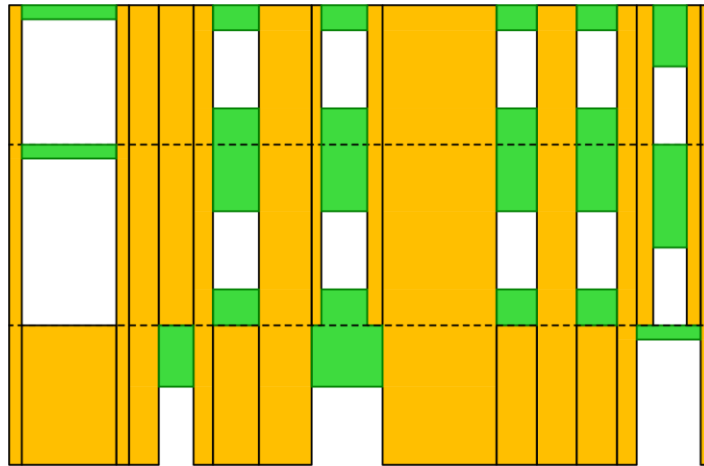
- **WALL 8X**

  $H_{tot} = 16.5$

  Weight = 11686kN
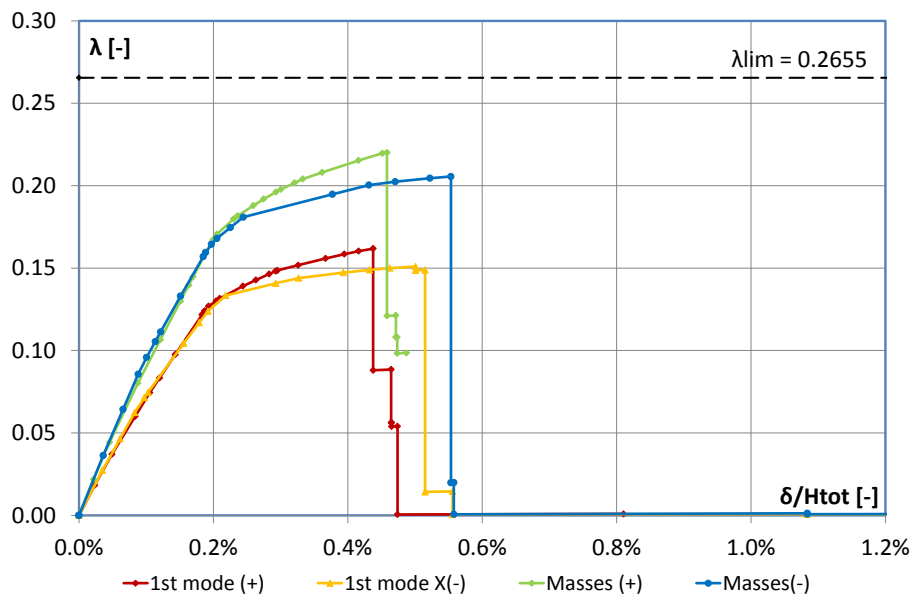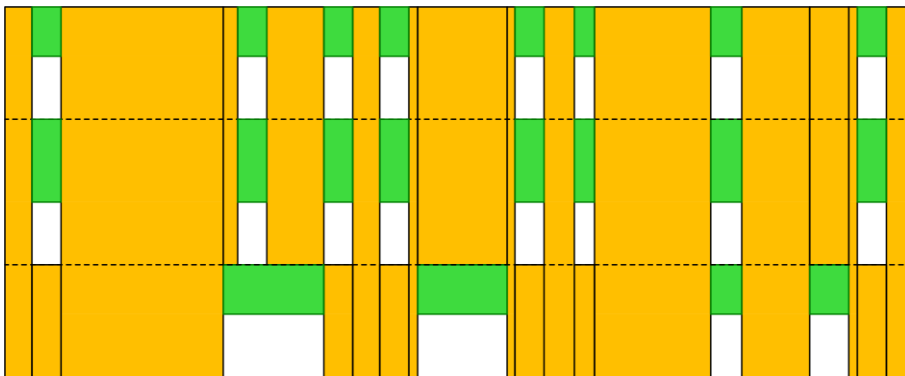
- **WALL 9X**

H_{tot}= 16.5

Weight= 1880kN
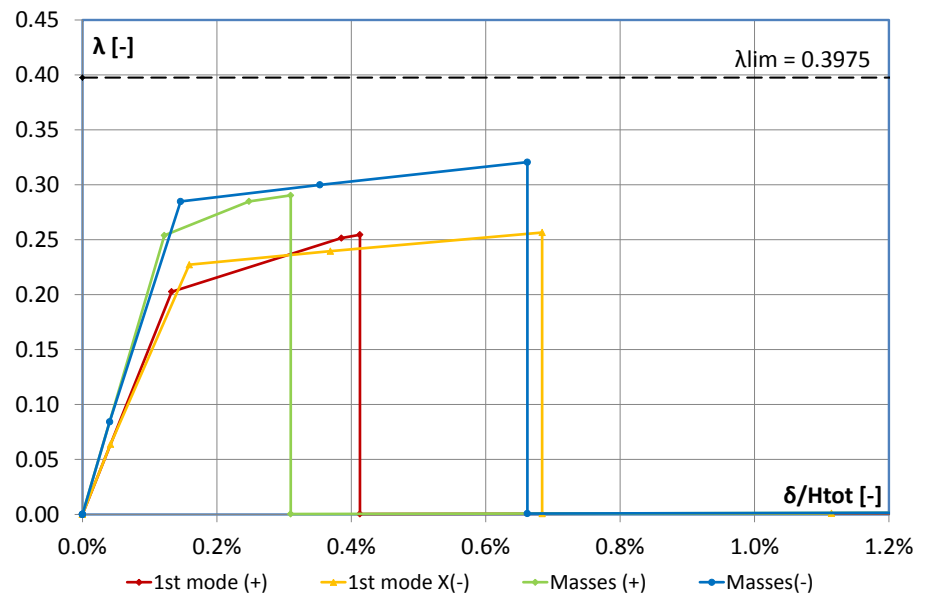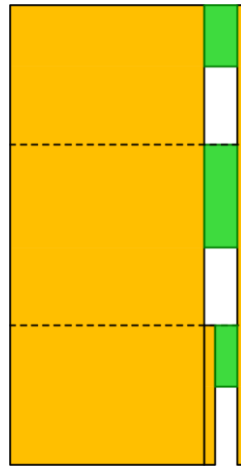
- **WALL 10X**

  H_{tot} = 16.5

  Weight= 11971kN
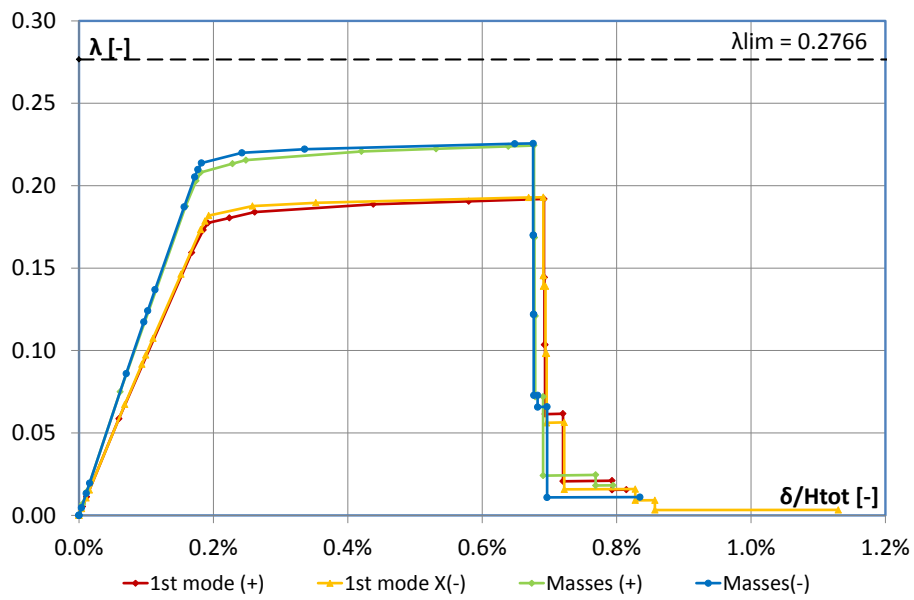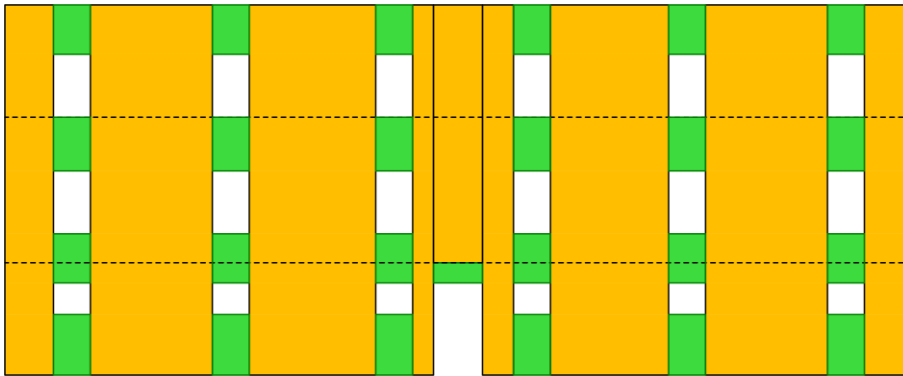
PALAZZO CENTI: TRANSVERSAL WALLS (Y)
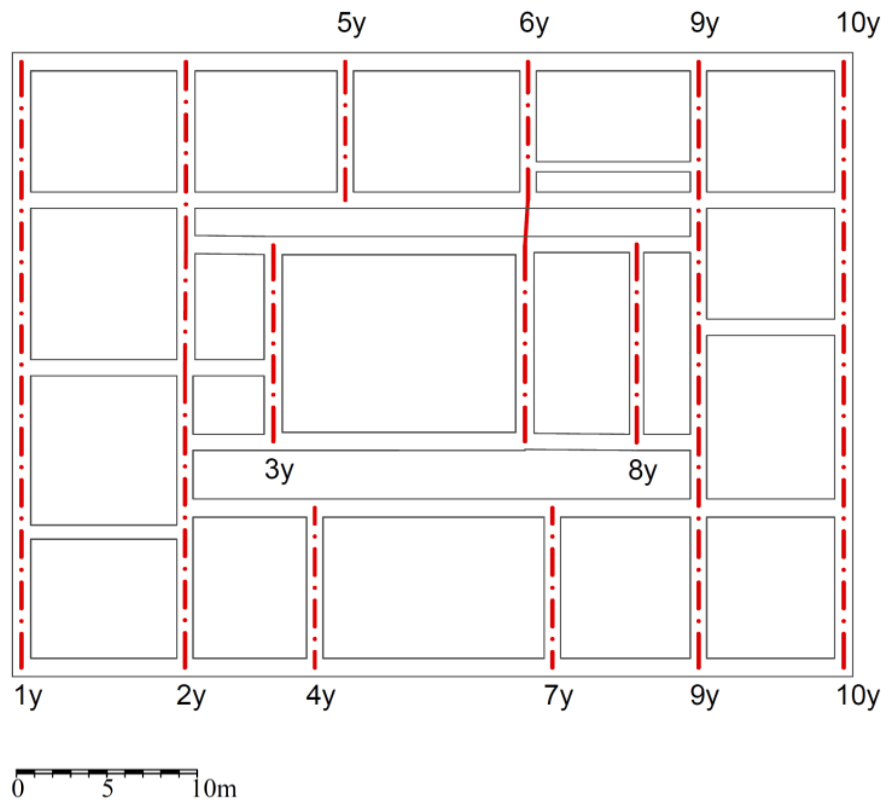
- **WALL 1Y**

  H_{tot} = 16.5

  Weight= 9058kN
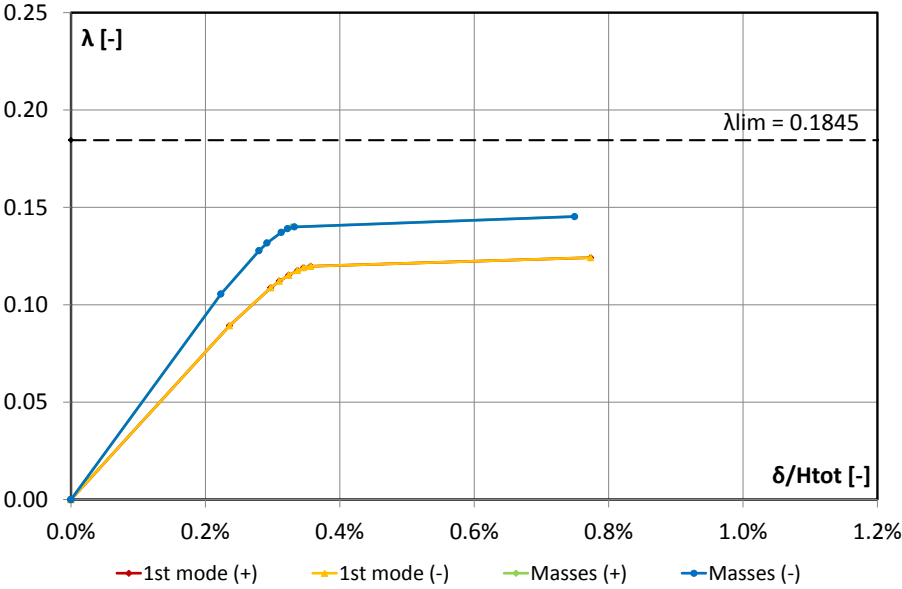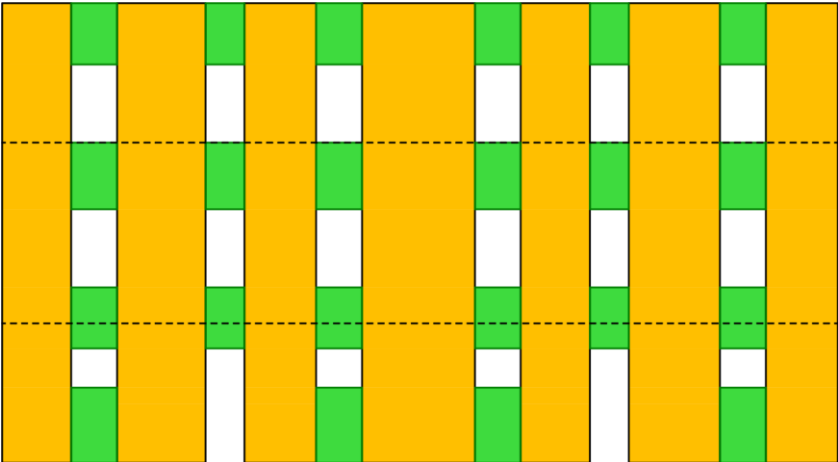
- **WALL 2Y**

  H_{tot} = 16.5

  Weight = 10400kN
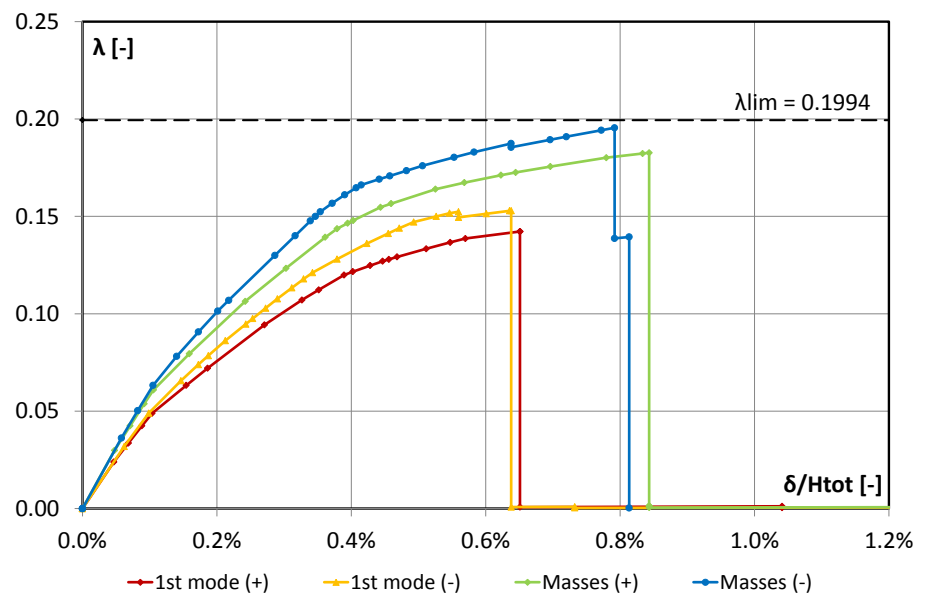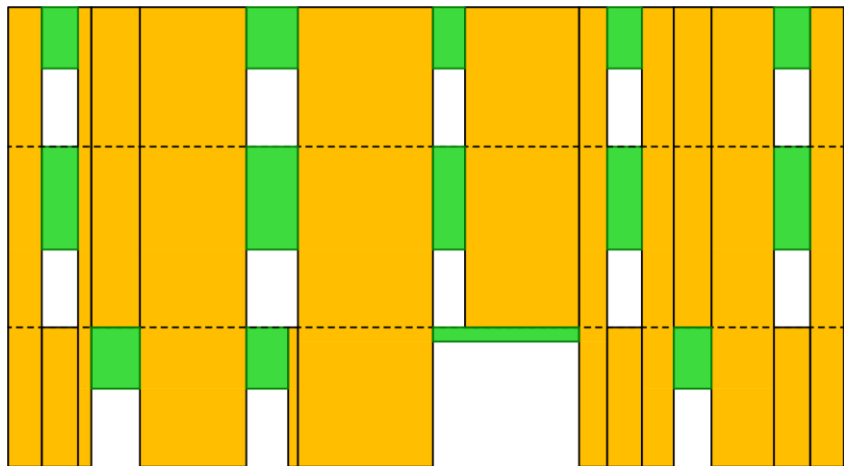
- **WALL 3Y**

  H_{tot} = 16.5

  Weight= 2773kN
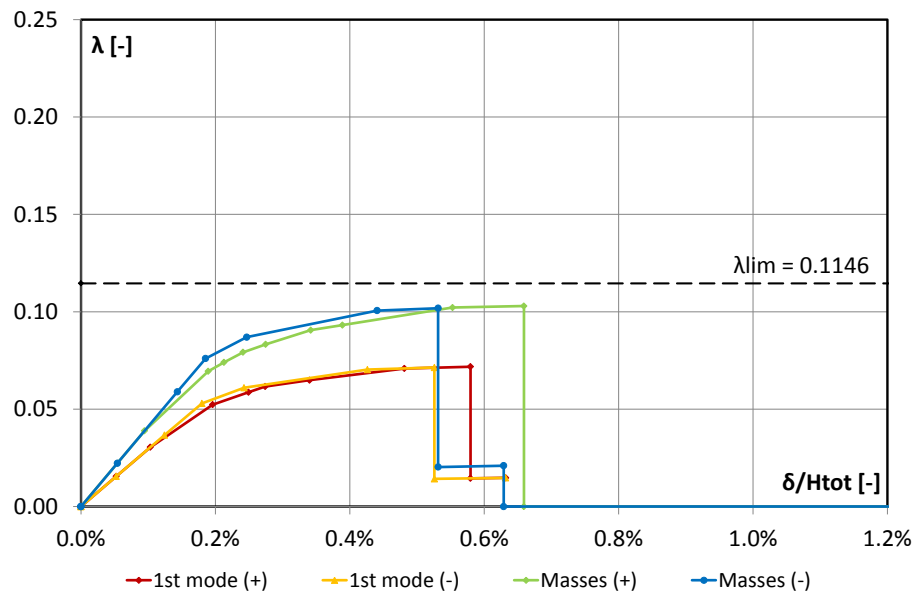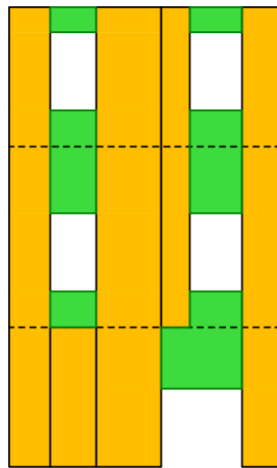
- **WALL 4Y**

    H_{tot}= 16.5

    Weight= 2829kN
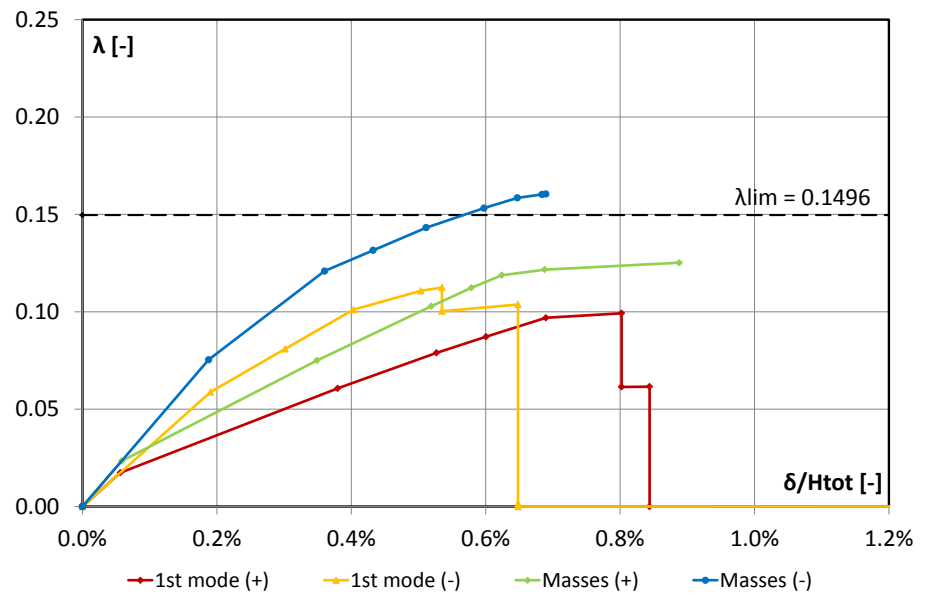
- **WALL 5Y**

  H_{tot} = 16.5

  Weight= 2352KN
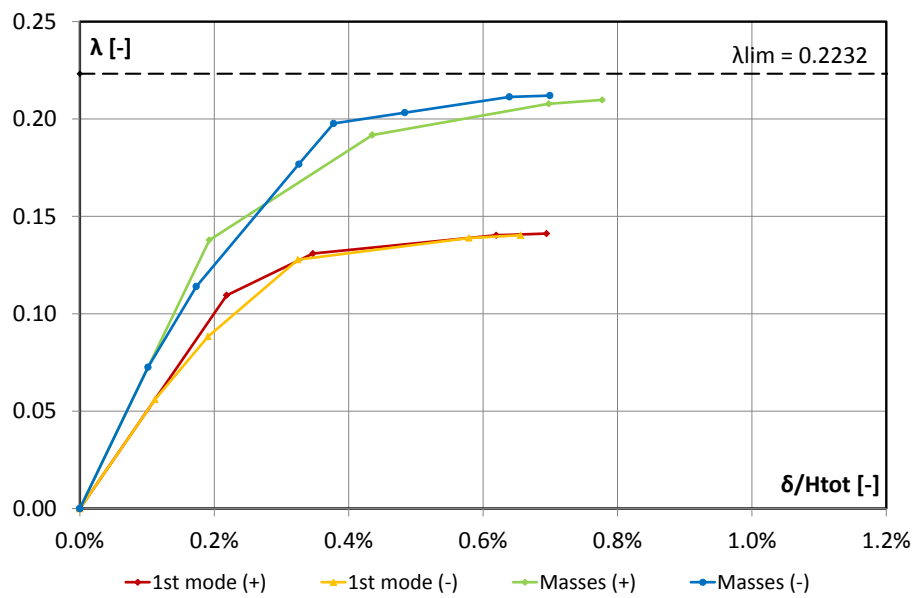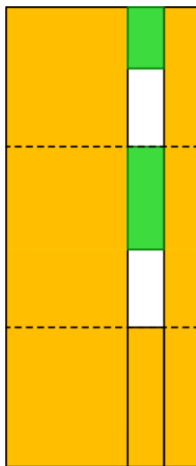
- **WALL 6Y**

  H_{tot}= 16.5

  Weight= 5585kN
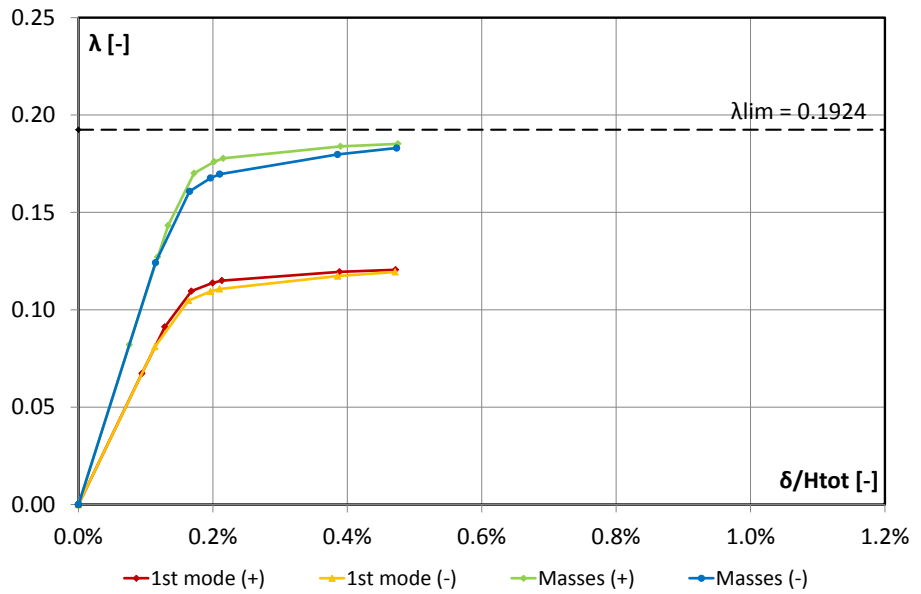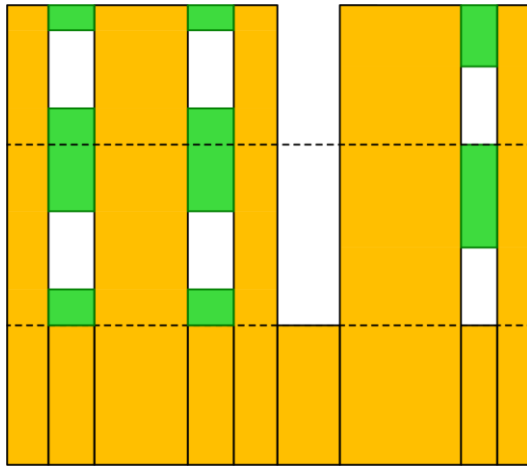
- **WALL 7Y**

  H_{tot}= 16.5

  Weight= 2897kN
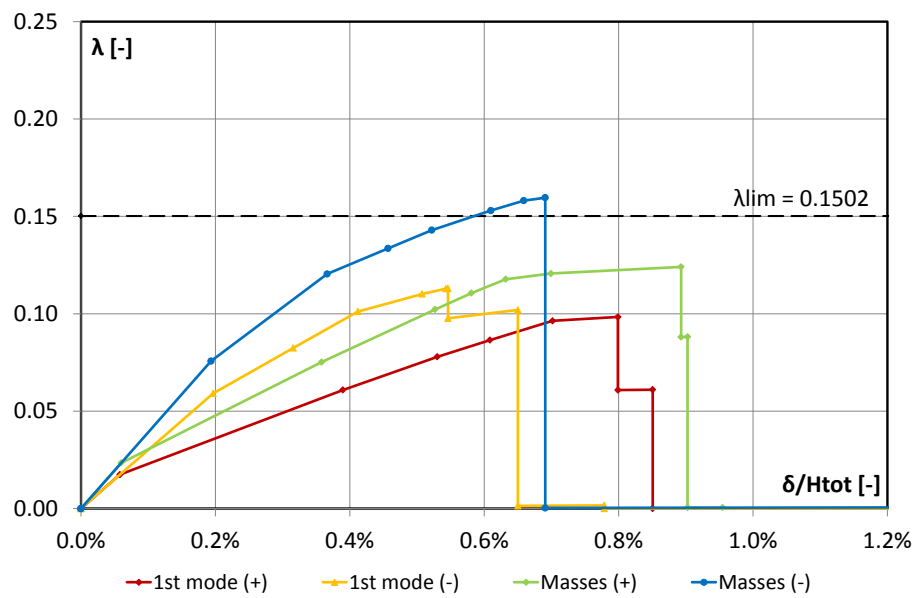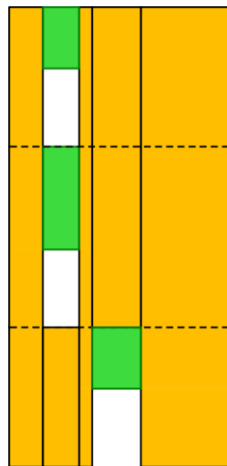
- **WALL 8Y**

  H_{tot}= 16.5

  Weight= 3111kN
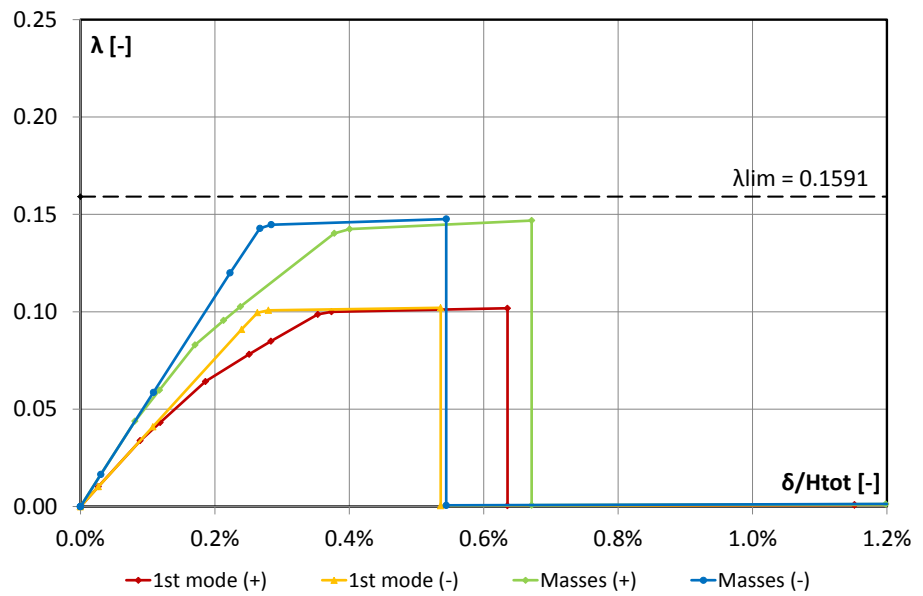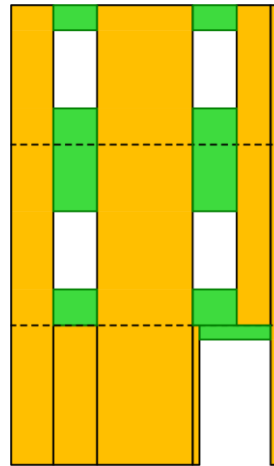
- **WALL 9Y**

  H_{tot} = 16.5

  Weight= 9105kN
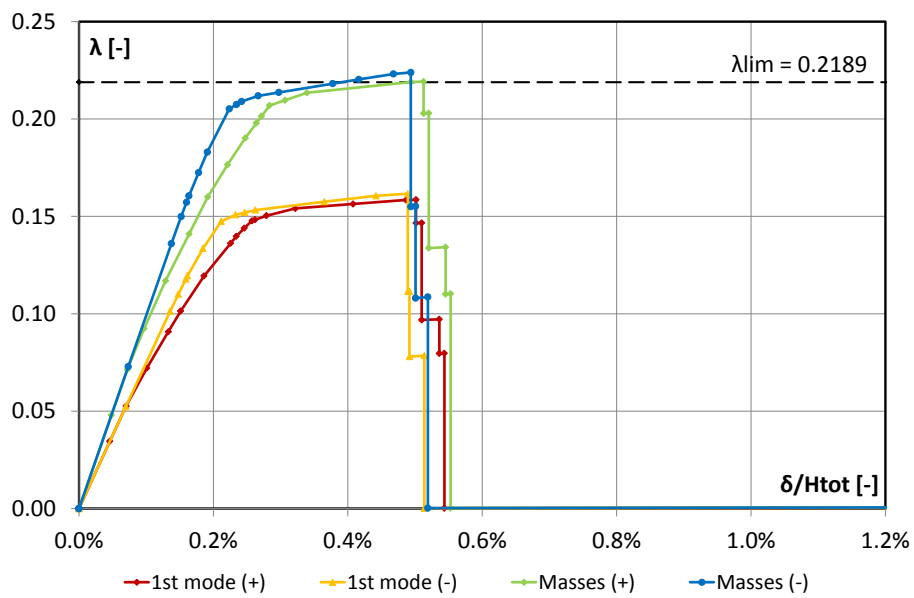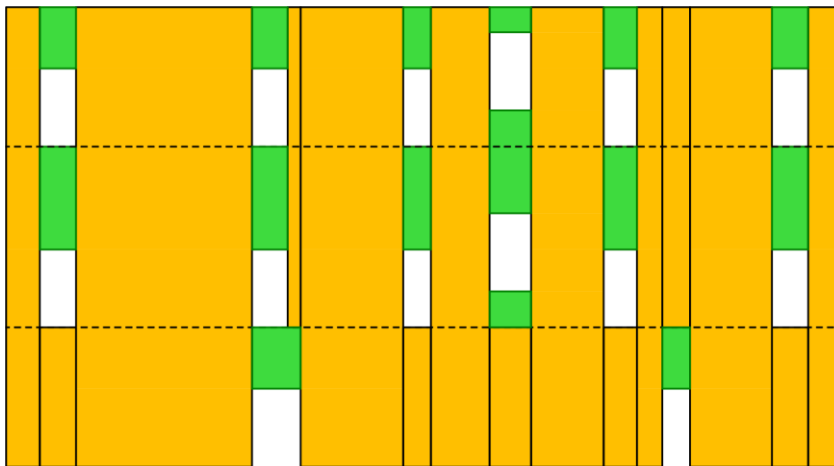
- **WALL 10Y**

  H_{tot}= 16.5

  Weight= 8952kN
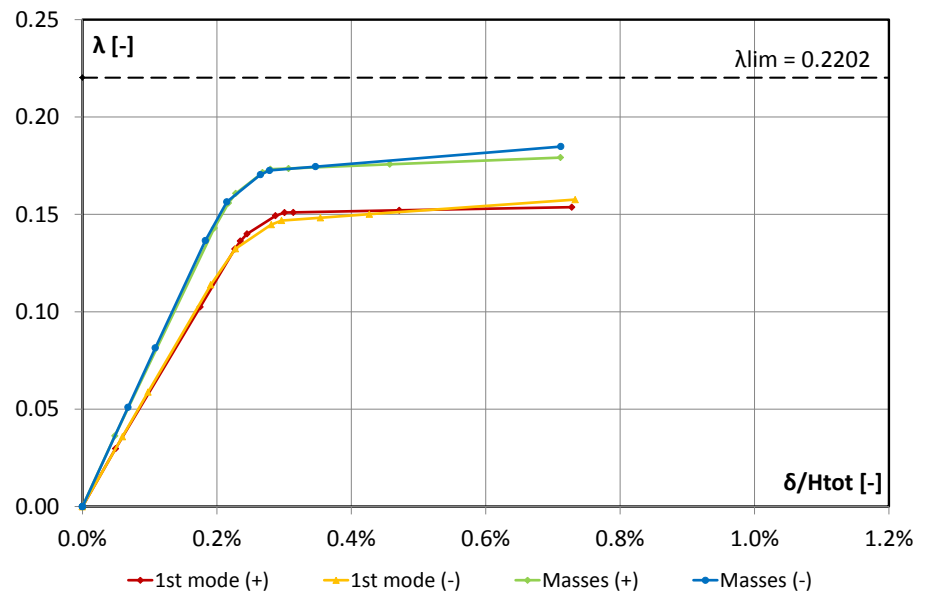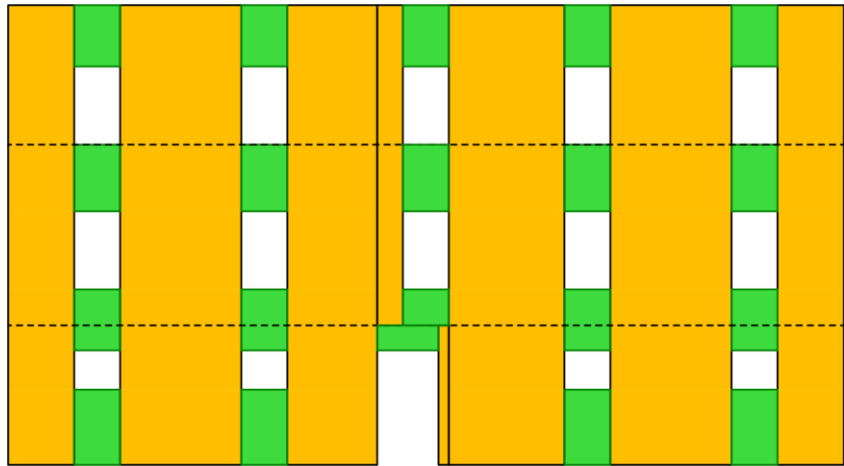
APPENDIX B

In this Appendix, for each masonry churches of chapter 3, the following results are given:

- Table with periods and modal participating mass ratios of the first 100 vibration modes
- Graph showing the distribution of the modal participating mass ratio compared with the response spectrum
- Table of the dynamic parameters used in section 3.3.2
- Modal shape of the main vibration modes

S. GENNARO ALL'OLMO (SGO)

Mode	Period	Longitudinal direction			Transversal direction		
		M_p	ΣM_p	$\Sigma M_p > 5\%$	M_p	ΣM_p	$\Sigma M_p > 5\%$
n°	(s)	(%)	(%)	(%)	(%)	(%)	(%)
1	0.801	1.30%	1.30%	-	2.47%	2.47%	-
2	0.777	0.06%	1.35%	-	35.04%	37.51%	35.04%
3	0.645	0.00%	1.35%	-	1.01%	38.51%	-
4	0.577	0.04%	1.40%	-	0.12%	38.64%	-
5	0.527	0.50%	1.89%	-	0.78%	39.41%	-
6	0.512	0.42%	2.31%	-	0.17%	39.58%	-
7	0.461	0.04%	2.35%	-	0.56%	40.14%	-
8	0.430	0.20%	2.56%	-	0.03%	40.16%	-
9	0.428	0.28%	2.83%	-	0.61%	40.77%	-
10	0.407	0.19%	3.02%	-	0.05%	40.82%	-
11	0.330	0.43%	3.45%	-	4.29%	45.11%	-
12	0.320	4.91%	8.36%	-	1.01%	46.11%	-
13	0.298	28.05%	36.41%	28.05%	0.80%	46.92%	-
14	0.295	9.22%	45.63%	9.22%	2.30%	49.21%	-
15	0.287	2.06%	47.69%	-	0.55%	49.76%	-
16	0.272	0.27%	47.96%	-	0.91%	50.68%	-
17	0.266	0.36%	48.32%	-	0.22%	50.90%	-
18	0.262	0.14%	48.46%	-	15.92%	66.81%	15.92%
19	0.259	0.00%	48.46%	-	0.43%	67.25%	-
20	0.253	0.13%	48.59%	-	0.90%	68.15%	-
21	0.234	0.01%	48.61%	-	1.96%	70.12%	-
22	0.225	0.00%	48.61%	-	0.01%	70.13%	-

| Mode | Period | Longitudinal direction | | | Transversal direction | | |
| | | M_p | ΣM_p | $\Sigma M_p >5\%$ | M_p | ΣM_p | $\Sigma M_p >5\%$ |
n°	(s)	(%)	(%)	(%)	(%)	(%)	(%)
23	0.224	0.00%	48.61%	-	0.89%	71.02%	-
24	0.212	0.03%	48.64%	-	0.50%	71.52%	-
25	0.210	0.15%	48.79%	-	0.38%	71.90%	-
26	0.198	0.04%	48.82%	-	0.00%	71.90%	-
27	0.186	0.06%	48.88%	-	0.15%	72.05%	-
28	0.183	0.05%	48.93%	-	0.00%	72.05%	-
29	0.172	0.36%	49.29%	-	0.51%	72.56%	-
30	0.168	0.29%	49.58%	-	0.07%	72.64%	-
31	0.167	0.51%	50.09%	-	0.09%	72.73%	-
32	0.164	0.29%	50.38%	-	0.54%	73.26%	-
33	0.161	0.01%	50.39%	-	0.17%	73.44%	-
34	0.161	0.09%	50.48%	-	0.04%	73.48%	-
35	0.159	0.02%	50.50%	-	0.56%	74.04%	-
36	0.151	0.02%	50.52%	-	0.04%	74.08%	-
37	0.146	0.20%	50.72%	-	0.00%	74.08%	-
38	0.144	10.68%	61.40%	10.68%	0.40%	74.49%	-
39	0.140	1.91%	63.31%	-	1.76%	76.24%	-
40	0.138	1.17%	64.48%	-	0.11%	76.35%	-
41	0.135	0.00%	64.49%	-	0.02%	76.37%	-
42	0.134	0.01%	64.49%	-	0.76%	77.13%	-
43	0.128	0.01%	64.50%	-	3.31%	80.44%	-
44	0.126	0.03%	64.53%	-	0.00%	80.44%	-
45	0.125	0.87%	65.40%	-	0.15%	80.59%	-
46	0.124	0.17%	65.57%	-	0.22%	80.81%	-
47	0.122	0.26%	65.84%	-	0.00%	80.81%	-
48	0.119	0.91%	66.74%	-	0.00%	80.81%	-
49	0.118	1.21%	67.95%	-	0.07%	80.88%	-
50	0.117	0.30%	68.26%	-	0.19%	81.07%	-
51	0.116	2.17%	70.42%	-	0.51%	81.58%	-
52	0.115	0.49%	70.91%	-	0.01%	81.59%	-
53	0.113	2.40%	73.31%	-	0.07%	81.65%	-
54	0.112	0.18%	73.49%	-	0.00%	81.66%	-
55	0.111	0.21%	73.71%	-	0.01%	81.66%	-
56	0.110	0.11%	73.81%	-	0.00%	81.66%	-
57	0.110	0.63%	74.45%	-	0.07%	81.74%	-
58	0.108	0.56%	75.00%	-	0.12%	81.86%	-
59	0.107	0.59%	75.59%	-	0.19%	82.05%	-
60	0.107	0.11%	75.70%	-	0.14%	82.19%	-
61	0.106	0.09%	75.79%	-	0.39%	82.57%	-
62	0.104	0.31%	76.10%	-	0.09%	82.67%	-

Mode	Period	Longitudinal direction			Transversal direction		
		M_p	ΣM_p	$\Sigma M_p > 5\%$	M_p	ΣM_p	$\Sigma M_p > 5\%$
n°	(s)	(%)	(%)	(%)	(%)	(%)	(%)
63	0.103	0.03%	76.12%	-	0.08%	82.75%	-
64	0.101	0.67%	76.79%	-	0.13%	82.87%	-
65	0.101	0.36%	77.15%	-	0.02%	82.89%	-
66	0.100	0.31%	77.46%	-	0.10%	82.99%	-
67	0.099	0.20%	77.66%	-	0.19%	83.18%	-
68	0.098	0.16%	77.82%	-	0.03%	83.20%	-
69	0.098	0.04%	77.86%	-	0.00%	83.20%	-
70	0.097	0.27%	78.13%	-	0.02%	83.22%	-
71	0.096	0.20%	78.32%	-	0.71%	83.93%	-
72	0.096	0.16%	78.48%	-	0.02%	83.95%	-
73	0.095	1.12%	79.60%	-	0.00%	83.95%	-
74	0.095	0.63%	80.23%	-	0.13%	84.08%	-
75	0.094	0.00%	80.23%	-	0.14%	84.22%	-
76	0.094	0.12%	80.35%	-	0.00%	84.23%	-
77	0.093	0.23%	80.57%	-	0.34%	84.56%	-
78	0.092	0.68%	81.25%	-	0.01%	84.57%	-
79	0.091	1.67%	82.92%	-	0.63%	85.21%	-
80	0.091	0.06%	82.99%	-	0.03%	85.23%	-
81	0.090	0.15%	83.14%	-	0.59%	85.83%	-
82	0.089	0.41%	83.55%	-	0.73%	86.55%	-
83	0.089	0.09%	83.64%	-	0.00%	86.55%	-
84	0.088	0.00%	83.64%	-	0.09%	86.64%	-
85	0.088	0.19%	83.83%	-	0.02%	86.66%	-
86	0.087	0.00%	83.83%	-	0.00%	86.67%	-
87	0.087	0.00%	83.83%	-	0.57%	87.23%	-
88	0.087	0.01%	83.84%	-	0.18%	87.41%	-
89	0.086	0.05%	83.89%	-	0.39%	87.80%	-
90	0.085	0.04%	83.92%	-	0.02%	87.83%	-
91	0.085	0.00%	83.93%	-	0.01%	87.84%	-
92	0.084	0.00%	83.93%	-	0.00%	87.84%	-
93	0.083	1.03%	84.96%	-	0.02%	87.86%	-
94	0.083	0.01%	84.97%	-	0.03%	87.89%	-
95	0.082	0.00%	84.97%	-	0.01%	87.90%	-
96	0.082	0.22%	85.20%	-	0.12%	88.02%	-
97	0.082	0.64%	85.83%	-	0.03%	88.05%	-
98	0.081	0.00%	85.83%	-	0.44%	88.49%	-
99	0.081	0.02%	85.85%	-	0.01%	88.50%	-
100	0.081	0.05%	85.91%	-	0.25%	88.75%	-
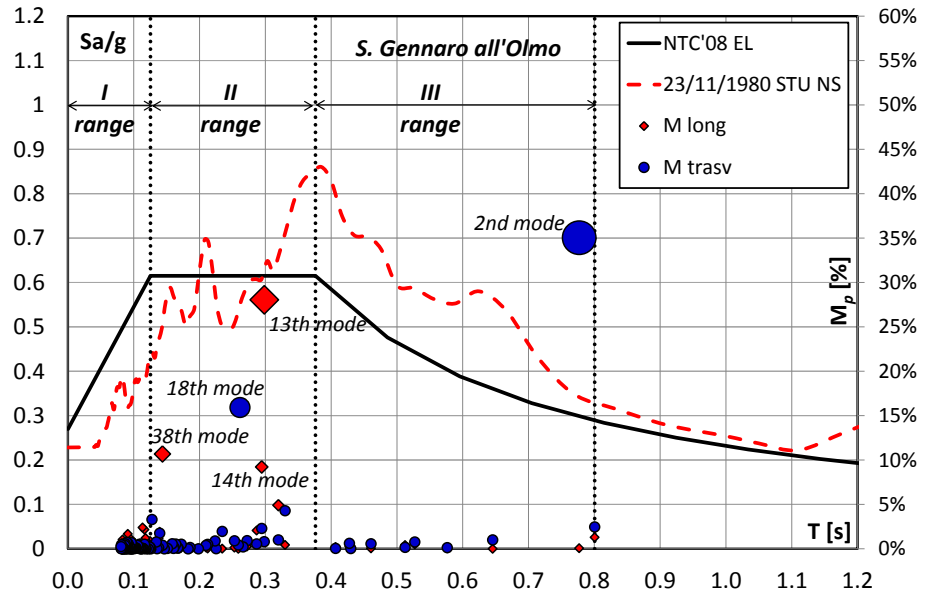
	100 v.m.	M_p>5%	10 $M_p$max	I range	II range	III range
ΣM_{plong}	86%	48%	64%	21%	62%	3%
$\Sigma M_{ptransv}$	89%	51%	69%	8%	40%	41%

2nd mode   13th mode   18 mode
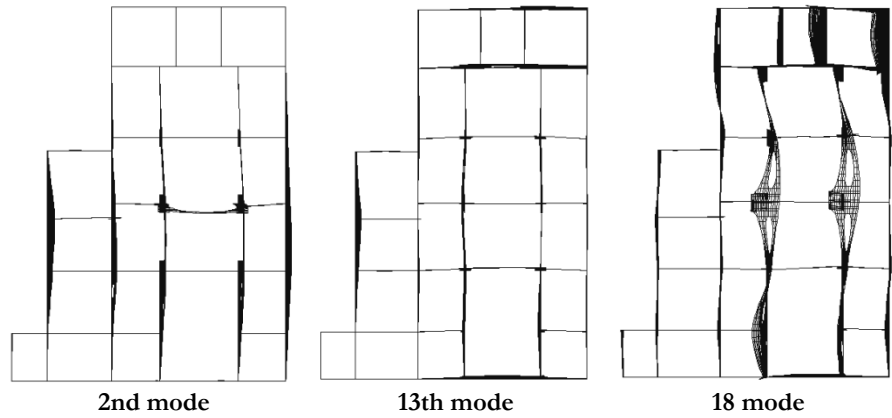
S. GIOVANNI A MARE (SGMR)

Mode	Period	Longitudinal direction			Transversal direction		
		M_p	ΣM_p	$\Sigma M_p > 5\%$	M_p	ΣM_p	$\Sigma M_p > 5\%$
n°	(s)	(%)	(%)	(%)	(%)	(%)	(%)
1	0.519	39.92%	39.92%	39.920%	0.01%	0.01%	-
2	0.506	0.00%	39.92%	-	33.72%	33.72%	33.715%
3	0.424	0.03%	39.95%	-	10.28%	44.00%	10.283%
4	0.407	0.14%	40.09%	-	1.39%	45.39%	-
5	0.381	0.00%	40.09%	-	12.82%	58.21%	12.817%
6	0.335	5.36%	45.45%	5.361%	0.00%	58.21%	-
7	0.290	0.03%	45.48%	-	1.92%	60.12%	-
8	0.282	0.10%	45.58%	-	0.86%	60.98%	-
9	0.277	0.02%	45.61%	-	0.13%	61.11%	-
10	0.270	0.08%	45.68%	-	0.00%	61.11%	-
11	0.250	0.04%	45.72%	-	0.46%	61.57%	-
12	0.241	0.00%	45.72%	-	3.46%	65.03%	-
13	0.235	0.02%	45.75%	-	0.02%	65.05%	-
14	0.231	0.23%	45.97%	-	0.00%	65.06%	-
15	0.223	0.05%	46.02%	-	4.54%	69.59%	-
16	0.221	0.00%	46.02%	-	0.74%	70.33%	-
17	0.212	0.76%	46.78%	-	0.02%	70.35%	-
18	0.210	5.88%	52.66%	5.879%	0.09%	70.43%	-
19	0.208	2.45%	55.11%	-	0.19%	70.62%	-
20	0.202	1.03%	56.13%	-	0.83%	71.45%	-
21	0.192	0.11%	56.25%	-	0.07%	71.52%	-
22	0.187	2.88%	59.13%	-	0.03%	71.55%	-
23	0.186	0.16%	59.28%	-	0.51%	72.06%	-
24	0.180	0.01%	59.30%	-	0.05%	72.11%	-
25	0.179	10.75%	70.04%	10.746%	0.02%	72.13%	-
26	0.171	0.00%	70.04%	-	0.03%	72.16%	-
27	0.166	0.15%	70.19%	-	0.06%	72.22%	-
28	0.165	0.12%	70.31%	-	0.02%	72.24%	-
29	0.162	0.02%	70.33%	-	0.07%	72.32%	-
30	0.160	0.01%	70.34%	-	0.09%	72.41%	-
31	0.159	0.00%	70.34%	-	0.63%	73.03%	-
32	0.155	0.02%	70.36%	-	0.06%	73.09%	-
33	0.149	0.66%	71.02%	-	0.07%	73.16%	-
34	0.145	0.09%	71.11%	-	0.56%	73.71%	-
35	0.145	0.16%	71.27%	-	0.63%	74.34%	-
36	0.143	0.00%	71.27%	-	0.07%	74.41%	-
37	0.141	0.43%	71.71%	-	0.00%	74.41%	-
38	0.137	0.01%	71.72%	-	0.27%	74.67%	-
39	0.135	0.76%	72.48%	-	0.00%	74.68%	-

Mode	Period	Longitudinal direction			Transversal direction		
		M_p	ΣM_p	$\Sigma M_p > 5\%$	M_p	ΣM_p	$\Sigma M_p > 5\%$
n°	(s)	(%)	(%)	(%)	(%)	(%)	(%)
40	0.134	0.08%	72.56%	-	2.17%	76.84%	-
41	0.134	0.01%	72.56%	-	1.95%	78.80%	-
42	0.133	0.00%	72.57%	-	0.03%	78.82%	-
43	0.131	0.02%	72.59%	-	0.01%	78.83%	-
44	0.130	0.01%	72.59%	-	0.15%	78.99%	-
45	0.128	0.01%	72.60%	-	0.00%	78.99%	-
46	0.127	0.08%	72.68%	-	0.02%	79.01%	-
47	0.125	0.38%	73.06%	-	0.01%	79.02%	-
48	0.124	0.00%	73.06%	-	0.23%	79.24%	-
49	0.123	0.27%	73.34%	-	0.04%	79.29%	-
50	0.121	0.01%	73.34%	-	2.68%	81.96%	-
51	0.120	0.00%	73.34%	-	0.00%	81.97%	-
52	0.118	0.00%	73.35%	-	0.00%	81.97%	-
53	0.114	0.00%	73.35%	-	0.09%	82.06%	-
54	0.113	0.14%	73.49%	-	0.00%	82.06%	-
55	0.112	0.03%	73.52%	-	0.02%	82.08%	-
56	0.111	0.25%	73.76%	-	0.02%	82.11%	-
57	0.110	0.00%	73.76%	-	0.06%	82.17%	-
58	0.110	0.02%	73.78%	-	0.03%	82.20%	-
59	0.109	0.01%	73.79%	-	0.00%	82.20%	-
60	0.108	0.39%	74.18%	-	0.00%	82.20%	-
61	0.106	0.14%	74.32%	-	0.03%	82.22%	-
62	0.104	1.08%	75.41%	-	0.00%	82.23%	-
63	0.103	0.08%	75.48%	-	0.00%	82.23%	-
64	0.102	0.19%	75.68%	-	0.04%	82.27%	-
65	0.101	0.06%	75.73%	-	0.02%	82.29%	-
66	0.099	1.00%	76.74%	-	0.08%	82.37%	-
67	0.098	0.08%	76.82%	-	0.23%	82.60%	-
68	0.098	0.12%	76.94%	-	0.05%	82.65%	-
69	0.097	0.04%	76.98%	-	0.19%	82.84%	-
70	0.097	0.01%	76.99%	-	0.03%	82.87%	-
71	0.096	0.03%	77.02%	-	0.08%	82.95%	-
72	0.095	0.42%	77.44%	-	0.00%	82.95%	-
73	0.095	0.18%	77.61%	-	0.10%	83.04%	-
74	0.095	0.14%	77.75%	-	0.51%	83.56%	-
75	0.094	0.76%	78.51%	-	0.10%	83.65%	-
76	0.093	0.11%	78.62%	-	0.31%	83.96%	-
77	0.092	0.10%	78.72%	-	0.13%	84.09%	-
78	0.092	0.00%	78.72%	-	0.13%	84.22%	-
79	0.090	0.61%	79.33%	-	0.05%	84.27%	-

Mode	Period	Longitudinal direction			Transversal direction		
		M_p	ΣM_p	ΣM_p >5%	M_p	ΣM_p	ΣM_p >5%
n°	(s)	(%)	(%)	(%)	(%)	(%)	(%)
80	0.090	0.44%	79.76%	-	0.00%	84.27%	-
81	0.091	0.25%	80.01%	-	0.00%	84.27%	-
82	0.089	0.37%	80.38%	-	0.02%	84.29%	-
83	0.089	0.72%	81.11%	-	0.01%	84.30%	-
84	0.089	0.12%	81.23%	-	0.04%	84.34%	-
85	0.088	0.00%	81.23%	-	0.07%	84.41%	-
86	0.088	0.12%	81.34%	-	0.18%	84.59%	-
87	0.088	0.03%	81.37%	-	0.03%	84.63%	-
88	0.087	0.11%	81.48%	-	0.07%	84.69%	-
89	0.087	0.04%	81.52%	-	0.06%	84.75%	-
90	0.087	0.01%	81.53%	-	0.06%	84.80%	-
91	0.086	0.68%	82.21%	-	0.24%	85.04%	-
92	0.086	0.00%	82.21%	-	0.14%	85.18%	-
93	0.085	0.02%	82.24%	-	0.01%	85.18%	-
94	0.085	0.00%	82.24%	-	0.52%	85.71%	-
95	0.084	0.50%	82.74%	-	0.05%	85.75%	-
96	0.082	0.73%	83.48%	-	0.00%	85.75%	-
97	0.081	0.16%	83.64%	-	0.00%	85.75%	-
98	0.080	0.58%	84.22%	-	0.00%	85.76%	-
99	0.080	0.08%	84.30%	-	0.01%	85.77%	-
100	0.080	0.03%	84.33%	-	0.35%	86.12%	-
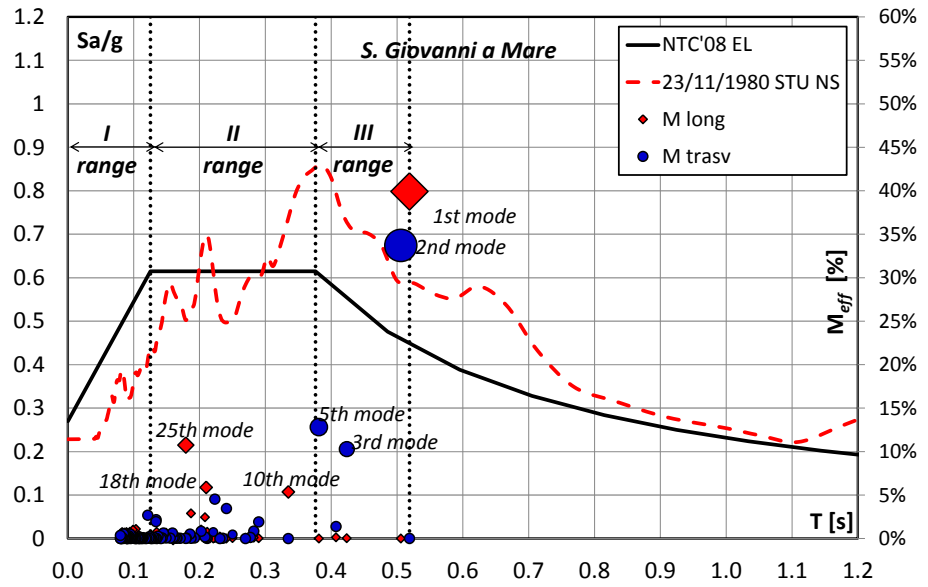
	100 v.m.	M_p>5%	10 $M_p$max	I range	II range	III range
ΣM_{plong}	84%	62%	71%	11%	33%	40%
$\Sigma M_{ptransv}$	86%	57%	75%	7%	21%	58%
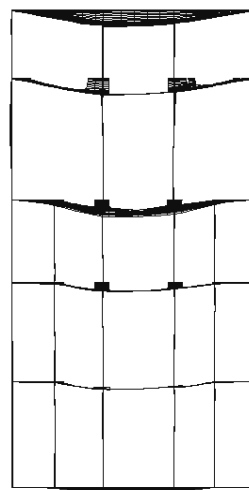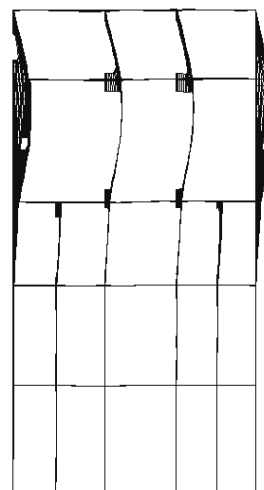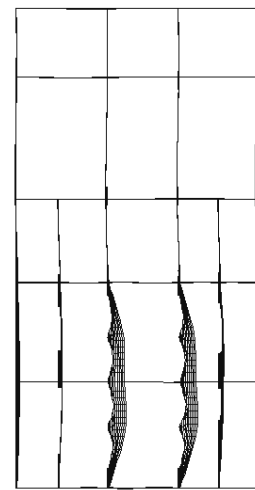
1st mode   2nd mode   5th mode

S. MARIA VERTECOELI (SMV)

Mode	Period	Longitudinal direction			Transversal direction		
		M_p	ΣM_p	$\Sigma M_p > 5\%$	M_p	ΣM_p	$\Sigma M_p > 5\%$
n°	(s)	(%)	(%)	(%)	(%)	(%)	(%)
1	0.811	0.00%	0.00%	-	2.40%	2.40%	-
2	0.675	0.00%	0.00%	-	21.90%	24.30%	21.90%
3	0.568	0.01%	0.01%	-	0.17%	24.47%	-
4	0.406	0.00%	0.01%	-	0.11%	24.58%	-
5	0.377	0.00%	0.01%	-	2.10%	26.68%	-
6	0.363	1.10%	1.11%	-	0.02%	26.69%	-
7	0.340	2.10%	3.21%	-	0.03%	26.72%	-
8	0.313	5.00%	8.21%	-	0.55%	27.27%	-
9	0.312	28.10%	36.31%	28.10%	0.26%	27.53%	-
10	0.290	0.28%	36.59%	-	4.20%	31.73%	-
11	0.288	9.70%	46.29%	9.70%	0.00%	31.74%	-
12	0.286	0.81%	47.10%	-	0.07%	31.80%	-
13	0.281	0.01%	47.11%	-	12.60%	44.40%	12.60%
14	0.269	0.23%	47.34%	-	0.04%	44.45%	-
15	0.268	1.70%	49.04%	-	1.00%	45.45%	-
16	0.262	0.91%	49.94%	-	1.60%	47.05%	-
17	0.260	0.35%	50.30%	-	0.00%	47.05%	-
18	0.253	4.10%	54.40%	-	0.01%	47.06%	-
19	0.248	0.30%	54.70%	-	8.60%	55.66%	8.60%
20	0.242	0.01%	54.71%	-	6.60%	62.26%	6.60%
21	0.232	1.70%	56.41%	-	0.09%	62.35%	-
22	0.230	0.29%	56.70%	-	0.00%	62.35%	-
23	0.221	0.02%	56.72%	-	0.13%	62.48%	-
24	0.200	0.13%	56.84%	-	4.70%	67.18%	-
25	0.197	0.45%	57.30%	-	0.30%	67.48%	-
26	0.191	0.23%	57.52%	-	0.19%	67.68%	-
27	0.188	0.00%	57.53%	-	0.07%	67.75%	-
28	0.184	2.00%	59.53%	-	0.01%	67.75%	-
29	0.183	0.00%	59.53%	-	3.20%	70.95%	-
30	0.178	0.00%	59.53%	-	0.02%	70.97%	-
31	0.174	0.26%	59.79%	-	0.01%	70.98%	-
32	0.171	0.01%	59.80%	-	0.55%	71.52%	-
33	0.167	0.00%	59.80%	-	0.04%	71.56%	-
34	0.165	0.02%	59.82%	-	0.07%	71.63%	-
35	0.165	0.05%	59.87%	-	0.01%	71.63%	-
36	0.163	0.11%	59.98%	-	1.40%	73.03%	-
37	0.160	0.26%	60.24%	-	0.83%	73.86%	-
38	0.159	0.82%	61.06%	-	0.00%	73.86%	-
39	0.156	6.20%	67.26%	6.20%	0.04%	73.90%	-

Mode	Period	Longitudinal direction			Transversal direction		
		M_p	ΣM_p	$\Sigma M_p >5\%$	M_p	ΣM_p	$\Sigma M_p >5\%$
n°	(s)	(%)	(%)	(%)	(%)	(%)	(%)
40	0.145	0.03%	67.28%	-	0.27%	74.17%	-
41	0.145	0.41%	67.70%	-	0.46%	74.63%	-
42	0.142	0.14%	67.84%	-	0.30%	74.93%	-
43	0.141	0.48%	68.32%	-	0.86%	75.79%	-
44	0.139	0.09%	68.41%	-	0.03%	75.83%	-
45	0.135	1.70%	70.11%	-	0.38%	76.21%	-
46	0.133	0.16%	70.27%	-	0.00%	76.21%	-
47	0.131	6.70%	76.97%	6.70%	0.01%	76.22%	-
48	0.129	0.32%	77.30%	-	0.09%	76.31%	-
49	0.128	0.20%	77.50%	-	0.17%	76.48%	-
50	0.126	0.26%	77.76%	-	1.20%	77.68%	-
51	0.126	0.02%	77.78%	-	0.02%	77.70%	-
52	0.124	0.40%	78.18%	-	0.37%	78.07%	-
53	0.120	0.67%	78.85%	-	0.03%	78.10%	-
54	0.118	0.18%	79.03%	-	0.06%	78.16%	-
55	0.117	0.00%	79.03%	-	0.21%	78.37%	-
56	0.116	0.32%	79.35%	-	0.45%	78.82%	-
57	0.115	0.32%	79.68%	-	0.17%	79.00%	-
58	0.113	0.67%	80.35%	-	2.00%	81.00%	-
59	0.112	0.03%	80.38%	-	0.02%	81.02%	-
60	0.111	0.76%	81.14%	-	0.08%	81.10%	-
61	0.110	1.90%	83.04%	-	0.44%	81.54%	-
62	0.109	0.12%	83.16%	-	0.12%	81.66%	-
63	0.109	0.15%	83.31%	-	0.06%	81.72%	-
64	0.108	0.03%	83.34%	-	0.51%	82.23%	-
65	0.106	0.02%	83.36%	-	0.59%	82.82%	-
66	0.103	0.00%	83.36%	-	0.63%	83.45%	-
67	0.103	0.00%	83.36%	-	0.00%	83.46%	-
68	0.101	0.00%	83.36%	-	0.25%	83.70%	-
69	0.101	0.00%	83.36%	-	0.16%	83.86%	-
70	0.100	0.07%	83.43%	-	0.04%	83.91%	-
71	0.099	0.13%	83.57%	-	0.02%	83.93%	-
72	0.098	0.11%	83.67%	-	0.24%	84.17%	-
73	0.097	0.00%	83.67%	-	0.04%	84.21%	-
74	0.097	0.02%	83.70%	-	0.00%	84.21%	-
75	0.096	0.05%	83.75%	-	0.00%	84.21%	-
76	0.096	0.03%	83.78%	-	0.18%	84.40%	-
77	0.095	0.57%	84.35%	-	0.00%	84.40%	-
78	0.094	0.01%	84.36%	-	0.01%	84.40%	-
79	0.094	0.00%	84.36%	-	0.00%	84.40%	-

Mode	Period	Longitudinal direction			Transversal direction		
		M_p	ΣM_p	$\Sigma M_p > 5\%$	M_p	ΣM_p	$\Sigma M_p > 5\%$
n°	(s)	(%)	(%)	(%)	(%)	(%)	(%)
80	0.093	0.02%	84.38%	-	0.02%	84.38%	-
81	0.092	0.00%	84.38%	-	0.00%	84.38%	-
82	0.091	0.01%	84.39%	-	0.01%	84.39%	-
83	0.091	0.00%	84.40%	-	0.00%	84.40%	-
84	0.090	0.04%	84.44%	-	0.04%	84.44%	-
85	0.088	0.06%	84.50%	-	0.06%	84.50%	-
86	0.088	0.03%	84.53%	-	0.03%	84.53%	-
87	0.087	0.05%	84.58%	-	0.05%	84.58%	-
88	0.086	0.06%	84.64%	-	0.06%	84.64%	-
89	0.086	0.00%	84.64%	-	0.00%	84.64%	-
90	0.085	0.00%	84.64%	-	0.00%	84.64%	-
91	0.085	0.60%	85.24%	-	0.60%	85.24%	-
92	0.085	0.05%	85.29%	-	0.05%	85.29%	-
93	0.084	0.00%	85.29%	-	0.00%	85.29%	-
94	0.083	0.00%	85.29%	-	0.00%	85.29%	-
95	0.082	0.05%	85.35%	-	0.05%	85.35%	-
96	0.082	0.02%	85.36%	-	0.02%	85.36%	-
97	0.081	0.01%	85.37%	-	0.01%	85.37%	-
98	0.081	0.00%	85.37%	-	0.00%	85.37%	-
99	0.081	0.12%	85.49%	-	0.12%	85.49%	-
100	0.080	0.00%	85.49%	-	0.00%	85.49%	-
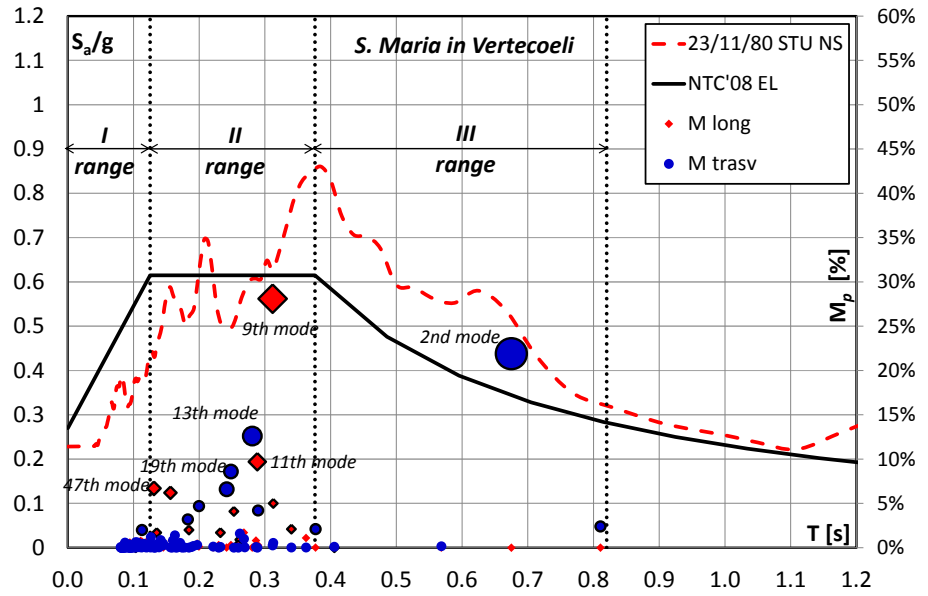
	100 v.m.	M_p>5%	10 $M_p$max	I range	II range	III range
ΣM_{plong}	85%	51%	68%	8%	78%	0%
$\Sigma M_{ptransv}$	86%	50%	68%	9%	51%	27%

2nd mode   9th mode   13th mode

SS. BERNARDO E MARGHERITA A FONSECA (SBM)

Mode	Period	Longitudinal direction			Transversal direction		
		M_p	ΣM_p	$\Sigma M_p > 5\%$	M_p	ΣM_p	$\Sigma M_p > 5\%$
n°	(s)	(%)	(%)	(%)	(%)	(%)	(%)
1	0.386	0.00%	0.00%	-	49.98%	49.98%	49.977%
2	0.310	0.21%	0.21%	-	0.14%	50.11%	-
3	0.273	1.14%	1.35%	-	12.07%	62.18%	12.069%
4	0.238	58.60%	59.95%	58.597%	0.33%	62.52%	-
5	0.235	0.53%	60.48%	-	0.84%	63.36%	-
6	0.221	0.34%	60.81%	-	0.41%	63.77%	-
7	0.217	2.61%	63.42%	-	0.04%	63.80%	-
8	0.212	0.06%	63.49%	-	1.80%	65.60%	-
9	0.205	3.24%	66.73%	-	0.29%	65.89%	-
10	0.198	0.89%	67.62%	-	0.19%	66.08%	-
11	0.191	3.16%	70.78%	-	0.36%	66.44%	-
12	0.182	0.45%	71.23%	-	0.95%	67.39%	-
13	0.180	0.25%	71.47%	-	0.61%	68.00%	-
14	0.172	0.01%	71.48%	-	0.09%	68.09%	-
15	0.169	0.15%	71.64%	-	0.57%	68.66%	-
16	0.167	0.00%	71.64%	-	0.01%	68.67%	-
17	0.165	0.00%	71.65%	-	0.03%	68.70%	-
18	0.163	0.02%	71.66%	-	0.01%	68.71%	-
19	0.155	0.03%	71.69%	-	0.03%	68.73%	-
20	0.152	0.04%	71.73%	-	0.13%	68.86%	-
21	0.152	0.53%	72.26%	-	0.18%	69.04%	-
22	0.151	0.01%	72.26%	-	0.54%	69.57%	-
23	0.147	0.02%	72.28%	-	0.27%	69.84%	-
24	0.146	0.62%	72.90%	-	0.29%	70.13%	-
25	0.143	1.41%	74.31%	-	0.06%	70.18%	-
26	0.141	0.05%	74.36%	-	4.13%	74.31%	-
27	0.139	0.30%	74.66%	-	0.13%	74.44%	-
28	0.136	0.17%	74.83%	-	1.12%	75.56%	-
29	0.135	0.83%	75.65%	-	2.04%	77.60%	-
30	0.133	0.34%	75.99%	-	0.29%	77.89%	-
31	0.131	0.00%	75.99%	-	0.42%	78.31%	-
32	0.129	0.01%	76.00%	-	0.13%	78.44%	-
33	0.127	0.95%	76.95%	-	0.01%	78.45%	-
34	0.126	0.43%	77.38%	-	0.20%	78.65%	-
35	0.123	0.38%	77.76%	-	0.25%	78.90%	-
36	0.120	0.21%	77.96%	-	0.40%	79.30%	-
37	0.118	0.03%	77.99%	-	0.74%	80.04%	-
38	0.113	0.01%	78.01%	-	0.40%	80.44%	-
39	0.112	0.34%	78.35%	-	1.09%	81.54%	-

Mode	Period	Longitudinal direction			Transversal direction		
		M_p	ΣM_p	$\Sigma M_p > 5\%$	M_p	ΣM_p	$\Sigma M_p > 5\%$
n°	(s)	(%)	(%)	(%)	(%)	(%)	(%)
40	0.112	0.22%	78.57%	-	0.00%	81.54%	-
41	0.108	0.00%	78.57%	-	0.34%	81.88%	-
42	0.108	0.01%	78.58%	-	0.23%	82.11%	-
43	0.106	0.02%	78.60%	-	0.50%	82.61%	-
44	0.105	0.03%	78.63%	-	0.35%	82.96%	-
45	0.104	0.00%	78.63%	-	0.00%	82.96%	-
46	0.104	0.14%	78.77%	-	0.03%	82.99%	-
47	0.103	0.41%	79.18%	-	0.08%	83.06%	-
48	0.102	0.15%	79.33%	-	0.01%	83.07%	-
49	0.100	0.49%	79.82%	-	0.05%	83.13%	-
50	0.098	0.37%	80.19%	-	0.10%	83.22%	-
51	0.096	0.33%	80.52%	-	0.01%	83.23%	-
52	0.094	0.11%	80.63%	-	0.00%	83.24%	-
53	0.093	0.06%	80.69%	-	0.14%	83.38%	-
54	0.093	1.07%	81.76%	-	0.31%	83.69%	-
55	0.092	0.18%	81.94%	-	0.03%	83.72%	-
56	0.091	0.00%	81.95%	-	0.35%	84.07%	-
57	0.090	0.02%	81.96%	-	0.32%	84.40%	-
58	0.089	0.00%	81.97%	-	0.15%	84.55%	-
59	0.089	0.12%	82.08%	-	0.02%	84.57%	-
60	0.088	0.18%	82.26%	-	0.09%	84.66%	-
61	0.087	0.11%	82.36%	-	0.03%	84.69%	-
62	0.086	0.22%	82.58%	-	0.04%	84.73%	-
63	0.085	0.00%	82.59%	-	0.32%	85.05%	-
64	0.085	0.01%	82.60%	-	0.03%	85.08%	-
65	0.084	0.07%	82.67%	-	0.09%	85.17%	-
66	0.084	0.00%	82.68%	-	0.00%	85.17%	-
67	0.084	0.07%	82.75%	-	0.05%	85.22%	-
68	0.083	0.47%	83.22%	-	0.00%	85.23%	-
69	0.083	0.39%	83.61%	-	0.00%	85.23%	-
70	0.082	0.07%	83.67%	-	0.00%	85.23%	-
71	0.082	0.01%	83.68%	-	0.23%	85.46%	-
72	0.082	0.01%	83.70%	-	0.04%	85.50%	-
73	0.081	0.01%	83.70%	-	0.07%	85.56%	-
74	0.081	0.01%	83.71%	-	0.08%	85.64%	-
75	0.080	0.04%	83.76%	-	0.01%	85.65%	-
76	0.080	0.00%	83.76%	-	0.03%	85.68%	-
77	0.079	0.65%	84.40%	-	0.03%	85.71%	-
78	0.079	0.00%	84.41%	-	0.08%	85.78%	-
79	0.079	0.15%	84.56%	-	0.00%	85.78%	-

Mode	Period	Longitudinal direction			Transversal direction		
		M_p	ΣM_p	$\Sigma M_p > 5\%$	M_p	ΣM_p	$\Sigma M_p > 5\%$
n°	(s)	(%)	(%)	(%)	(%)	(%)	(%)
80	0.079	0.04%	84.60%	-	0.03%	85.82%	-
81	0.078	0.01%	84.61%	-	0.01%	85.83%	-
82	0.077	0.00%	84.61%	-	0.13%	85.95%	-
83	0.077	0.03%	84.63%	-	0.00%	85.95%	-
84	0.076	0.15%	84.78%	-	0.05%	86.00%	-
85	0.076	0.06%	84.84%	-	0.02%	86.02%	-
86	0.075	0.03%	84.87%	-	0.02%	86.04%	-
87	0.074	0.10%	84.97%	-	0.04%	86.08%	-
88	0.073	0.16%	85.14%	-	0.00%	86.08%	-
89	0.073	0.01%	85.14%	-	0.05%	86.13%	-
90	0.073	0.37%	85.51%	-	0.04%	86.18%	-
91	0.072	0.40%	85.91%	-	0.24%	86.41%	-
92	0.071	0.07%	85.99%	-	0.03%	86.44%	-
93	0.071	0.02%	86.01%	-	0.03%	86.47%	-
94	0.071	0.03%	86.03%	-	0.09%	86.56%	-
95	0.070	0.04%	86.07%	-	0.04%	86.60%	-
96	0.070	0.41%	86.48%	-	0.08%	86.68%	-
97	0.069	0.04%	86.51%	-	0.05%	86.72%	-
98	0.069	0.02%	86.53%	-	0.01%	86.73%	-
99	0.069	0.00%	86.53%	-	0.07%	86.81%	-
100	0.068	0.00%	86.53%	-	0.07%	86.87%	-
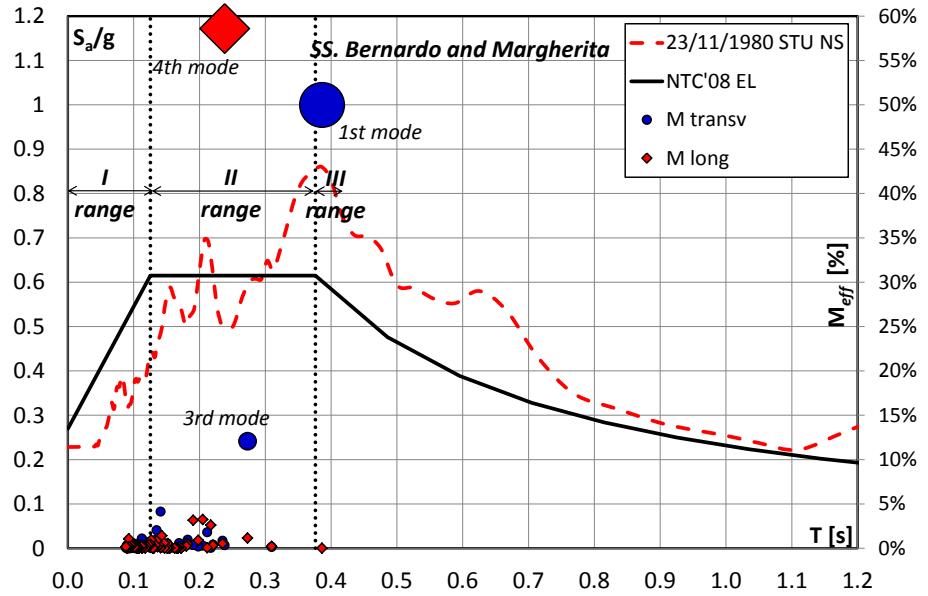
	100 v.m.	M_p>5%	10 $M_p$max	I range	II range	III range
ΣM_{plong}	87%	62%	75%	8%	29%	50%
$\Sigma M_{ptransv}$	87%	59%	74%	9%	77%	0%

1st mode   3rd mode   4th mode
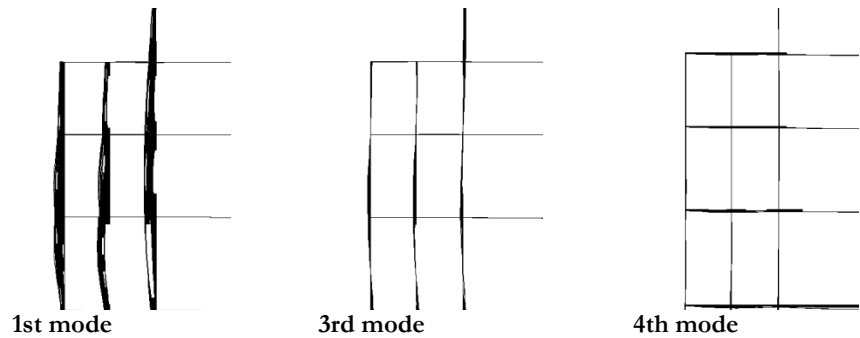
S. MARIA IN DONNAROMITA (SMD)

Mode	Period	Longitudinal direction			Transversal direction		
		M_p	ΣM_p	ΣM_p >5%	M_p	ΣM_p	ΣM_p >5%
n°	(s)	(%)	(%)	(%)	(%)	(%)	(%)
1	0.973	0.00%	0.00%	-	11.33%	11.70%	11.33%
2	0.969	0.01%	0.00%	-	0.40%	12.10%	-

Mode	Period	Longitudinal direction			Transversal direction		
		M_p	ΣM_p	$\Sigma M_p > 5\%$	M_p	ΣM_p	$\Sigma M_p > 5\%$
n°	(s)	(%)	(%)	(%)	(%)	(%)	(%)
3	0.673	3.32%	0.21%	-	0.01%	24.50%	-
4	0.638	0.07%	3.20%	-	12.46%	24.60%	12.46%
5	0.606	0.06%	3.30%	-	0.02%	24.60%	-
6	0.598	0.03%	3.30%	-	12.24%	36.70%	12.24%
7	0.458	1.41%	3.80%	-	0.45%	37.60%	-
8	0.442	49.94%	8.50%	49.94%	0.66%	40.70%	-
9	0.434	3.96%	58.10%	-	2.70%	40.80%	-
10	0.416	0.01%	58.20%	-	0.26%	41.10%	-
11	0.393	0.03%	58.20%	-	0.01%	41.10%	-
12	0.374	0.23%	58.70%	-	0.03%	41.10%	-
13	0.353	1.82%	59.70%	-	0.08%	41.10%	-
14	0.342	0.17%	59.90%	-	0.16%	41.10%	-
15	0.331	0.09%	60.60%	-	0.01%	41.40%	-
16	0.328	0.15%	60.70%	-	0.21%	41.50%	-
17	0.320	1.34%	61.10%	-	1.41%	44.20%	-
18	0.301	2.01%	64.70%	-	1.36%	44.30%	-
19	0.284	1.02%	65.90%	-	4.49%	47.80%	-
20	0.259	0.06%	66.00%	-	2.12%	49.60%	-
21	0.255	0.42%	66.40%	-	0.01%	50.30%	-
22	0.249	0.02%	66.40%	-	10.79%	61.30%	10.79%
23	0.240	0.01%	66.50%	-	0.16%	61.70%	-
24	0.238	0.00%	66.50%	-	7.16%	68.00%	7.16%
25	0.235	0.09%	66.60%	-	0.11%	68.50%	-
26	0.208	0.61%	67.20%	-	0.32%	68.70%	-
27	0.206	0.01%	69.10%	-	0.29%	68.70%	-
28	0.203	0.86%	70.40%	-	0.24%	68.90%	-
29	0.200	2.54%	70.80%	-	0.09%	69.30%	-
30	0.199	0.82%	70.80%	-	0.04%	69.50%	-
31	0.187	0.44%	71.10%	-	0.30%	69.60%	-
32	0.186	0.14%	71.60%	-	0.01%	70.10%	-
33	0.185	0.00%	72.00%	-	1.31%	70.40%	-
34	0.181	0.10%	72.00%	-	0.13%	71.40%	-
35	0.181	0.65%	72.60%	-	0.02%	71.50%	-
36	0.176	0.01%	72.70%	-	0.10%	71.50%	-
37	0.172	0.24%	73.00%	-	0.00%	71.50%	-
38	0.169	0.04%	73.00%	-	0.01%	71.50%	-
39	0.166	0.00%	73.00%	-	1.03%	72.00%	-

Mode	Period	Longitudinal direction			Transversal direction		
		M_p	ΣM_p	$\Sigma M_p > 5\%$	M_p	ΣM_p	$\Sigma M_p > 5\%$
n°	(s)	(%)	(%)	(%)	(%)	(%)	(%)
40	0.163	0.38%	73.00%	-	2.67%	72.00%	-
41	0.160	0.01%	73.30%	-	0.04%	75.50%	-
42	0.152	2.20%	74.30%	-	0.80%	75.80%	-
43	0.150	0.13%	75.00%	-	0.00%	76.00%	-

44	0.147	0.15%	75.00%	-	0.03%	76.30%	-
45	0.145	0.59%	76.00%	-	0.12%	76.40%	-
46	0.144	0.10%	76.00%	-	0.22%	76.50%	-
47	0.142	0.32%	76.40%	-	0.17%	76.50%	-
48	0.141	0.15%	76.80%	-	0.01%	76.80%	-
49	0.139	0.25%	77.00%	-	0.68%	77.40%	-
50	0.137	0.01%	77.00%	-	1.35%	78.50%	-
51	0.136	0.08%	77.00%	-	0.12%	78.50%	-
52	0.134	0.01%	77.00%	-	1.38%	79.70%	-
53	0.134	0.33%	77.30%	-	0.05%	79.80%	-
54	0.127	1.32%	77.30%	-	0.46%	80.50%	-
55	0.126	1.99%	78.80%	-	0.19%	80.60%	-
56	0.126	0.60%	78.90%	-	0.04%	81.00%	-
57	0.125	0.01%	79.70%	-	0.04%	81.10%	-
58	0.124	0.00%	79.70%	-	0.40%	81.20%	-
59	0.123	0.01%	79.70%	-	0.12%	81.20%	-
60	0.122	0.02%	79.70%	-	0.07%	81.20%	-
61	0.121	0.02%	80.70%	-	0.07%	81.20%	-
62	0.121	1.26%	81.50%	-	0.01%	81.60%	-
63	0.120	0.19%	81.80%	-	0.02%	81.60%	-
64	0.119	0.00%	81.90%	-	0.00%	81.60%	-
65	0.118	0.28%	82.00%	-	0.06%	81.60%	-
66	0.117	0.01%	82.30%	-	0.21%	81.60%	-
67	0.116	0.05%	82.40%	-	0.19%	81.80%	-
68	0.115	0.09%	82.80%	-	0.20%	81.80%	-
69	0.114	0.01%	82.80%	-	0.05%	81.90%	-
70	0.114	0.01%	83.00%	-	0.50%	81.90%	-
71	0.113	0.00%	83.30%	-	0.07%	82.00%	-
72	0.113	1.13%	83.30%	-	0.21%	82.00%	-
73	0.113	0.13%	83.50%	-	0.03%	82.40%	-
74	0.112	0.01%	83.50%	-	0.01%	83.10%	-
75	0.111	0.03%	83.60%	-	0.37%	83.30%	-
76	0.111	0.27%	84.20%	-	0.10%	83.30%	-
77	0.110	0.24%	84.20%	-	0.03%	83.50%	-
78	0.108	0.01%	84.70%	-	0.16%	83.50%	-
79	0.108	0.00%	84.70%	-	0.04%	83.70%	-

Mode	Period	Longitudinal direction			Transversal direction		
		M_P	ΣM_P	$\Sigma M_P > 5\%$	M_P	ΣM_P	$\Sigma M_P > 5\%$
n°	(s)	(%)	(%)	(%)	(%)	(%)	(%)
80	0.106	0.02%	84.80%	-	0.05%	83.70%	-
81	0.106	0.32%	85.00%	-	0.03%	83.70%	-
82	0.105	0.20%	85.20%	-	0.00%	83.70%	-
83	0.104	0.00%	85.20%	-	0.00%	83.70%	-

84	0.104	0.00%	85.20%	-	0.01%	83.80%	-
85	0.103	0.03%	85.30%	-	0.04%	83.80%	-
86	0.103	0.01%	85.50%	-	0.16%	83.80%	-
87	0.103	0.00%	85.60%	-	0.12%	83.80%	-
88	0.102	0.06%	85.60%	-	0.02%	83.80%	-
89	0.101	0.00%	85.70%	-	0.00%	84.00%	-
90	0.101	0.00%	85.70%	-	0.00%	84.10%	-
91	0.101	0.00%	85.70%	-	0.01%	84.10%	-
92	0.100	0.04%	85.70%	-	0.03%	84.10%	-
93	0.099	0.00%	85.80%	-	0.00%	84.10%	-
94	0.099	0.06%	85.90%	-	0.12%	84.10%	-
95	0.098	0.36%	86.00%	-	0.08%	84.20%	-
96	0.097	0.01%	86.30%	-	0.05%	84.60%	-
97	0.096	0.58%	86.40%	-	0.11%	84.70%	-
98	0.096	0.00%	86.80%	-	0.00%	84.90%	-
99	0.095	0.03%	86.90%	-	0.89%	85.30%	-
100	0.094	0.00%	87.00%	-	0.00%	85.40%	-
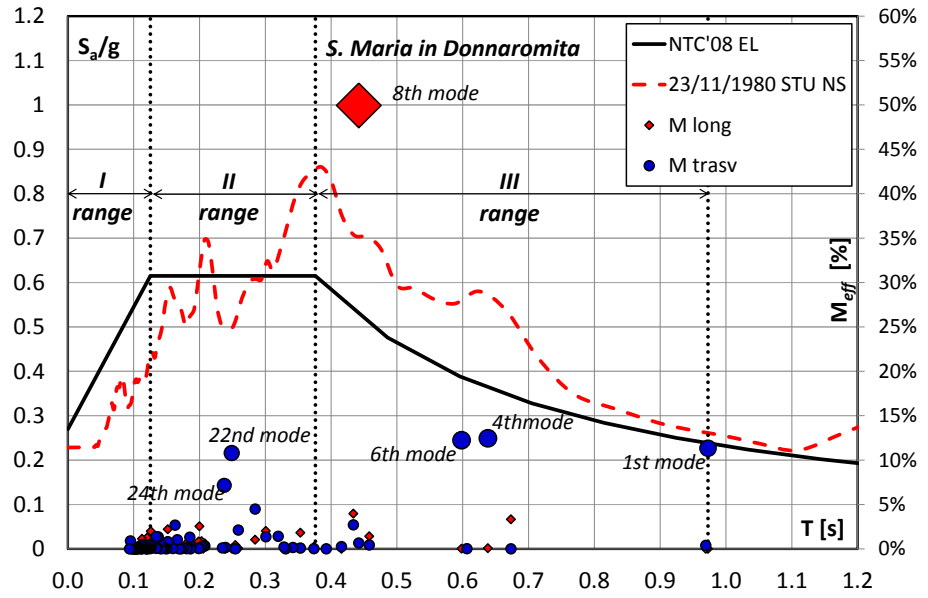
	100 v.m.	$M_p > 5\%$	10 $M_p$max	I range	II range	III range
ΣM_{plong}	87%	50%	71%	0%	24%	63%
$\Sigma M_{ptransv}$	85%	54%	67%	0%	42%	42%

1st mode   **4th mode**   **8th mode**

S. GIUSTA (SG)

Mode	Period	Longitudinal direction			Transversal direction		
		M_p	ΣM_p	$\Sigma M_p > 5\%$	M_p	ΣM_p	$\Sigma M_p > 5\%$
n°	(s)	(%)	(%)	(%)	(%)	(%)	(%)
1	0.610	0.02%	0.02%	-	4.52%	4.52%	-
2	0.539	0.00%	0.02%	-	3.58%	8.10%	-
3	0.430	0.00%	0.02%	-	0.12%	8.21%	-
4	0.398	0.62%	0.64%	-	8.84%	17.06%	8.84%
5	0.362	15.51%	16.16%	15.51%	6.72%	23.78%	6.72%
6	0.359	8.71%	24.86%	8.71%	6.26%	30.03%	6.26%
7	0.344	8.01%	32.88%	8.01%	0.34%	30.37%	-
8	0.328	0.17%	33.04%	-	5.56%	35.93%	5.56%
9	0.311	0.10%	33.14%	-	0.17%	36.10%	-
10	0.291	0.00%	33.14%	-	1.77%	37.87%	-
11	0.287	0.00%	33.14%	-	0.00%	37.87%	-
12	0.265	0.23%	33.37%	-	2.61%	40.48%	-
13	0.255	1.38%	34.75%	-	7.12%	47.61%	7.12%
14	0.247	1.04%	35.79%	-	3.65%	51.26%	-
15	0.238	0.03%	35.82%	-	0.05%	51.31%	-
16	0.215	1.26%	37.07%	-	1.70%	53.00%	-
17	0.208	10.05%	47.12%	10.05%	0.86%	53.86%	-
18	0.203	1.25%	48.37%	-	0.17%	54.03%	-
19	0.194	8.19%	56.56%	8.19%	0.08%	54.11%	-
20	0.192	0.04%	56.61%	-	0.83%	54.95%	-
21	0.187	1.08%	57.68%	-	0.94%	55.89%	-
22	0.186	1.51%	59.19%	-	0.02%	55.91%	-
23	0.181	0.01%	59.20%	-	5.66%	61.57%	5.66%
24	0.180	0.00%	59.20%	-	1.36%	62.93%	-
25	0.176	1.53%	60.73%	-	4.43%	67.35%	-
26	0.173	3.51%	64.24%	-	2.39%	69.75%	-
27	0.167	0.01%	64.25%	-	0.46%	70.21%	-
28	0.161	0.10%	64.35%	-	0.15%	70.36%	-
29	0.158	0.39%	64.74%	-	0.29%	70.65%	-
30	0.156	0.20%	64.94%	-	0.04%	70.69%	-
31	0.151	0.00%	64.94%	-	0.70%	71.39%	-
32	0.149	0.01%	64.95%	-	0.47%	71.86%	-
33	0.144	0.01%	64.96%	-	0.40%	72.26%	-
34	0.141	0.00%	64.96%	-	0.00%	72.26%	-
35	0.139	0.01%	64.97%	-	0.01%	72.27%	-
36	0.135	0.05%	65.03%	-	1.58%	73.85%	-
37	0.135	1.13%	66.15%	-	0.18%	74.02%	-
38	0.134	0.56%	66.72%	-	0.03%	74.06%	-
39	0.129	0.06%	66.77%	-	0.02%	74.08%	-

		Longitudinal direction			Transversal direction		
Mode	Period	M_p	ΣM_p	$\Sigma M_p > 5\%$	M_p	ΣM_p	$\Sigma M_p > 5\%$
n°	(s)	(%)	(%)	(%)	(%)	(%)	(%)
40	0.127	0.34%	67.11%	-	0.02%	74.09%	-
41	0.126	0.00%	67.12%	-	0.46%	74.55%	-
42	0.122	0.08%	67.19%	-	0.08%	74.63%	-
43	0.120	0.00%	67.19%	-	0.01%	74.64%	-
44	0.118	0.06%	67.25%	-	0.01%	74.65%	-
45	0.116	0.32%	67.57%	-	0.13%	74.78%	-
46	0.116	0.12%	67.69%	-	0.00%	74.78%	-
47	0.114	0.01%	67.69%	-	0.00%	74.78%	-
48	0.112	0.39%	68.09%	-	0.06%	74.84%	-
49	0.109	0.03%	68.11%	-	0.70%	75.55%	-
50	0.105	0.13%	68.24%	-	0.07%	75.61%	-
51	0.103	0.15%	68.40%	-	0.24%	75.85%	-
52	0.101	0.99%	69.38%	-	0.05%	75.91%	-
53	0.100	0.01%	69.39%	-	0.01%	75.92%	-
54	0.099	0.40%	69.79%	-	0.41%	76.32%	-
55	0.097	0.61%	70.40%	-	0.35%	76.67%	-
56	0.097	0.01%	70.41%	-	0.32%	77.00%	-
57	0.097	0.01%	70.43%	-	0.57%	77.57%	-
58	0.095	0.77%	71.19%	-	0.17%	77.74%	-
59	0.095	0.71%	71.90%	-	0.04%	77.78%	-
60	0.095	0.29%	72.19%	-	0.44%	78.22%	-
61	0.094	0.14%	72.33%	-	0.37%	78.59%	-
62	0.093	0.00%	72.33%	-	0.20%	78.78%	-
63	0.092	0.08%	72.42%	-	0.22%	79.00%	-
64	0.092	0.22%	72.63%	-	0.10%	79.10%	-
65	0.091	0.21%	72.84%	-	0.14%	79.24%	-
66	0.090	0.02%	72.86%	-	0.01%	79.25%	-
67	0.090	0.04%	72.90%	-	0.01%	79.25%	-
68	0.089	1.34%	74.24%	-	0.41%	79.66%	-
69	0.088	0.00%	74.24%	-	0.01%	79.68%	-
70	0.088	0.01%	74.25%	-	0.04%	79.72%	-
71	0.087	0.03%	74.27%	-	0.07%	79.79%	-
72	0.087	1.10%	75.37%	-	0.37%	80.16%	-
73	0.087	0.34%	75.72%	-	0.23%	80.39%	-
74	0.086	0.48%	76.20%	-	0.03%	80.42%	-
75	0.086	0.16%	76.36%	-	0.14%	80.56%	-
76	0.085	0.04%	76.39%	-	0.37%	80.93%	-
77	0.084	0.08%	76.48%	-	0.13%	81.06%	-
78	0.084	0.28%	76.76%	-	0.00%	81.06%	-
79	0.083	0.03%	76.79%	-	0.47%	81.53%	-

Mode	Period	Longitudinal direction			Transversal direction		
		M_p	ΣM_p	$\Sigma M_p > 5\%$	M_p	ΣM_p	$\Sigma M_p > 5\%$
n°	(s)	(%)	(%)	(%)	(%)	(%)	(%)
80	0.083	0.08%	76.87%	-	0.83%	82.37%	-
81	0.082	0.04%	76.92%	-	0.04%	82.40%	-
82	0.081	0.04%	76.95%	-	0.14%	82.55%	-
83	0.081	0.10%	77.05%	-	0.01%	82.56%	-
84	0.081	0.15%	77.21%	-	0.06%	82.62%	-
85	0.080	0.07%	77.27%	-	0.04%	82.66%	-
86	0.079	0.08%	77.35%	-	0.02%	82.68%	-
87	0.079	1.18%	78.53%	-	0.02%	82.70%	-
88	0.078	0.23%	78.76%	-	0.17%	82.87%	-
89	0.077	0.00%	78.76%	-	0.13%	82.99%	-
90	0.077	0.00%	78.76%	-	0.09%	83.08%	-
91	0.076	0.12%	78.89%	-	0.54%	83.63%	-
92	0.076	0.00%	78.89%	-	0.06%	83.69%	-
93	0.076	0.00%	78.89%	-	0.01%	83.70%	-
94	0.075	0.11%	79.00%	-	0.01%	83.71%	-
95	0.075	0.07%	79.08%	-	0.01%	83.72%	-
96	0.074	0.28%	79.36%	-	0.01%	83.73%	-
97	0.073	0.14%	79.51%	-	0.00%	83.73%	-
98	0.073	0.01%	79.52%	-	0.01%	83.74%	-
99	0.072	0.00%	79.52%	-	0.00%	83.75%	-
100	0.072	0.00%	79.52%	-	0.01%	83.76%	-
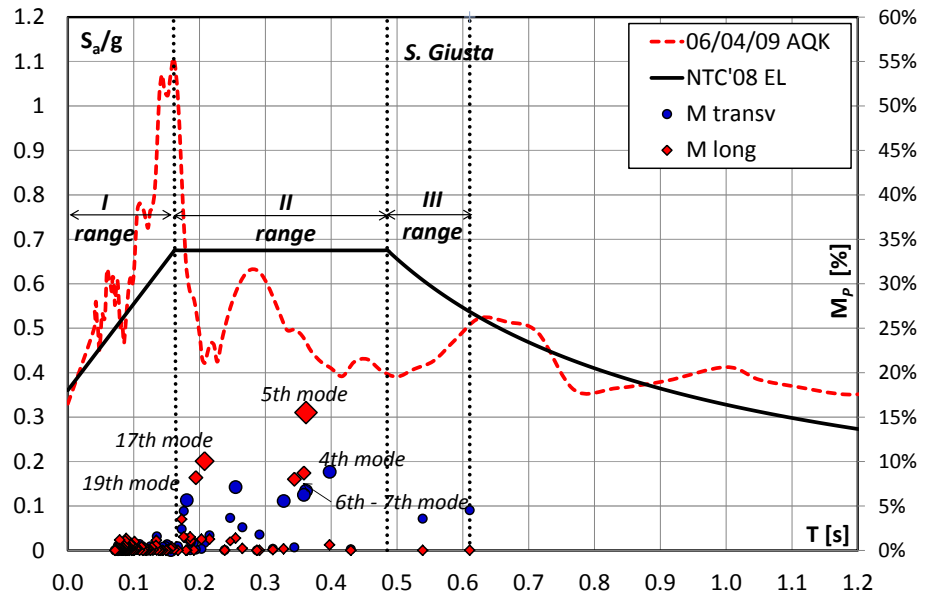
	100 v.m.	$M_p>5\%$	10 $M_p$max	I range	II range	III range
ΣM_{plong}	80%	50%	60%	15%	64%	0%
$\Sigma M_{ptransv}$	84%	40%	56%	13%	62%	8%

4th mode   5th mode   17th mode
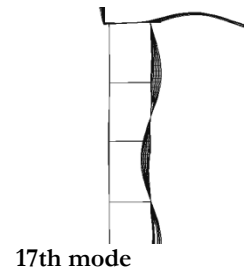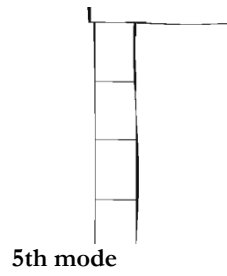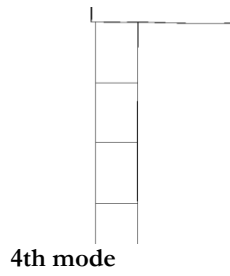
S. IPPOLISTO (SI)

Mode	Period	Longitudinal direction			Transversal direction		
		M_P	ΣM_P	$\Sigma M_P > 5\%$	M_P	ΣM_P	$\Sigma M_P > 5\%$
n°	(s)	(%)	(%)	(%)	(%)	(%)	(%)
1	0.442	0.00%	0.00%	-	46.76%	46.76%	-
2	0.395	13.43%	13.43%	13.43%	5.72%	52.48%	13.43%
3	0.383	40.86%	54.30%	40.86%	1.73%	54.21%	40.86%
4	0.347	0.00%	54.30%	-	7.90%	62.11%	-
5	0.306	0.54%	54.84%	-	3.78%	65.89%	-
6	0.282	6.04%	60.88%	6.04%	0.02%	65.91%	6.04%
7	0.271	0.08%	60.96%	-	0.00%	65.91%	-
8	0.259	0.17%	61.13%	-	0.08%	65.99%	-
9	0.244	0.00%	61.13%	-	0.49%	66.47%	-
10	0.236	0.72%	61.85%	-	0.74%	67.21%	-
11	0.228	0.63%	62.49%	-	0.57%	67.78%	-
12	0.223	0.08%	62.57%	-	0.25%	68.03%	-
13	0.212	0.05%	62.62%	-	0.05%	68.08%	-
14	0.211	0.94%	63.55%	-	0.04%	68.12%	-
15	0.200	0.01%	63.56%	-	2.18%	70.30%	-
16	0.193	0.24%	63.81%	-	2.60%	72.90%	-
17	0.188	0.04%	63.85%	-	0.38%	73.28%	-
18	0.182	1.55%	65.40%	-	0.21%	73.49%	-
19	0.173	3.71%	69.11%	-	0.00%	73.49%	-
20	0.168	0.75%	69.86%	-	1.10%	74.59%	-
21	0.166	0.01%	69.87%	-	0.00%	74.59%	-
22	0.163	0.13%	70.01%	-	0.06%	74.66%	-
23	0.160	0.02%	70.03%	-	1.17%	75.82%	-
24	0.158	0.00%	70.03%	-	0.17%	75.99%	-
25	0.157	0.07%	70.10%	-	1.52%	77.51%	-
26	0.156	0.00%	70.10%	-	0.31%	77.82%	-
27	0.156	0.32%	70.42%	-	2.76%	80.58%	-
28	0.155	0.04%	70.46%	-	0.11%	80.69%	-
29	0.153	0.01%	70.47%	-	0.93%	81.61%	-
30	0.151	0.04%	70.51%	-	0.25%	81.86%	-
31	0.147	0.01%	70.52%	-	0.68%	82.54%	-
32	0.145	0.98%	71.50%	-	0.53%	83.07%	-
33	0.141	1.38%	72.88%	-	0.01%	83.07%	-
34	0.138	1.29%	74.17%	-	0.08%	83.15%	-
35	0.132	0.14%	74.31%	-	0.01%	83.16%	-
36	0.130	0.00%	74.31%	-	0.16%	83.32%	-
37	0.128	0.22%	74.52%	-	0.13%	83.45%	-
38	0.126	1.70%	76.22%	-	0.05%	83.50%	-

Mode	Period	Longitudinal direction			Transversal direction		
		M_P	ΣM_p	ΣM_p >5%	M_P	ΣM_p	ΣM_p >5%
n°	(s)	(%)	(%)	(%)	(%)	(%)	(%)
39	0.124	0.00%	76.22%	-	0.21%	83.71%	-
40	0.122	0.70%	76.92%	-	0.21%	83.92%	-
41	0.121	0.01%	76.93%	-	0.53%	84.45%	-
42	0.119	0.00%	76.93%	-	0.24%	84.70%	-
43	0.114	0.00%	76.94%	-	0.01%	84.70%	-
44	0.114	0.02%	76.96%	-	0.04%	84.74%	-
45	0.113	0.15%	77.10%	-	0.04%	84.78%	-
46	0.111	1.61%	78.71%	-	0.05%	84.83%	-
47	0.110	0.76%	79.47%	-	0.00%	84.83%	-
48	0.108	0.00%	79.47%	-	0.00%	84.83%	-
49	0.107	0.38%	79.85%	-	0.06%	84.89%	-
50	0.104	1.23%	81.08%	-	0.01%	84.90%	-
51	0.102	0.05%	81.13%	-	0.00%	84.90%	-
52	0.100	0.42%	81.55%	-	0.00%	84.90%	-
53	0.099	0.90%	82.44%	-	0.25%	85.15%	-
54	0.098	0.82%	83.27%	-	0.06%	85.22%	-
55	0.098	0.05%	83.32%	-	0.02%	85.24%	-
56	0.096	1.13%	84.45%	-	0.29%	85.52%	-
57	0.095	0.56%	85.01%	-	0.00%	85.52%	-
58	0.094	0.00%	85.01%	-	0.08%	85.61%	-
59	0.093	0.18%	85.19%	-	0.06%	85.67%	-
60	0.093	0.27%	85.45%	-	0.03%	85.69%	-
61	0.092	0.23%	85.68%	-	0.00%	85.69%	-
62	0.092	0.00%	85.68%	-	0.01%	85.71%	-
63	0.091	0.00%	85.68%	-	0.00%	85.71%	-
64	0.090	0.06%	85.75%	-	0.01%	85.72%	-
65	0.089	0.05%	85.80%	-	0.01%	85.73%	-
66	0.089	0.02%	85.81%	-	0.13%	85.86%	-
67	0.088	0.10%	85.91%	-	0.00%	85.86%	-
68	0.088	0.04%	85.95%	-	0.00%	85.86%	-
69	0.087	0.02%	85.97%	-	0.14%	86.00%	-
70	0.086	0.33%	86.30%	-	0.05%	86.05%	-
71	0.085	0.15%	86.44%	-	0.30%	86.36%	-
72	0.084	0.03%	86.47%	-	0.00%	86.36%	-
73	0.084	0.26%	86.74%	-	0.05%	86.40%	-
74	0.082	0.00%	86.74%	-	0.02%	86.42%	-
75	0.081	0.19%	86.93%	-	0.04%	86.46%	-
76	0.081	0.01%	86.94%	-	0.05%	86.51%	-
77	0.080	0.00%	86.95%	-	0.01%	86.53%	-
78	0.080	0.00%	86.95%	-	0.04%	86.56%	-
79	0.079	0.03%	86.97%	-	0.12%	86.68%	-

Mode	Period	Longitudinal direction			Transversal direction		
		M_p	ΣM_p	$\Sigma M_p > 5\%$	M_p	ΣM_p	$\Sigma M_p > 5\%$
n°	(s)	(%)	(%)	(%)	(%)	(%)	(%)
80	0.079	0.03%	87.00%	-	0.04%	86.73%	-
81	0.078	0.00%	87.01%	-	0.46%	87.19%	-
82	0.077	0.00%	87.01%	-	0.13%	87.32%	-
83	0.077	0.00%	87.01%	-	0.17%	87.49%	-
84	0.077	0.03%	87.04%	-	0.08%	87.57%	-
85	0.077	0.01%	87.04%	-	0.02%	87.59%	-
86	0.076	0.03%	87.07%	-	0.36%	87.95%	-
87	0.075	0.00%	87.08%	-	0.03%	87.98%	-
88	0.076	0.00%	87.08%	-	0.01%	87.99%	-
89	0.074	0.00%	87.08%	-	0.03%	88.01%	-
90	0.074	0.01%	87.09%	-	0.05%	88.07%	-
91	0.073	0.06%	87.15%	-	0.02%	88.09%	-
92	0.073	0.46%	87.61%	-	0.11%	88.19%	-
93	0.072	0.05%	87.65%	-	0.41%	88.60%	-
94	0.072	0.18%	87.83%	-	0.00%	88.60%	-
95	0.071	0.07%	87.91%	-	0.37%	88.97%	-
96	0.071	0.12%	88.03%	-	0.00%	88.97%	-
97	0.071	0.05%	88.07%	-	0.00%	88.98%	-
98	0.070	0.09%	88.16%	-	0.02%	88.99%	-
99	0.070	0.07%	88.23%	-	0.02%	89.01%	-
100	0.070	0.01%	88.23%	-	0.03%	89.04%	-
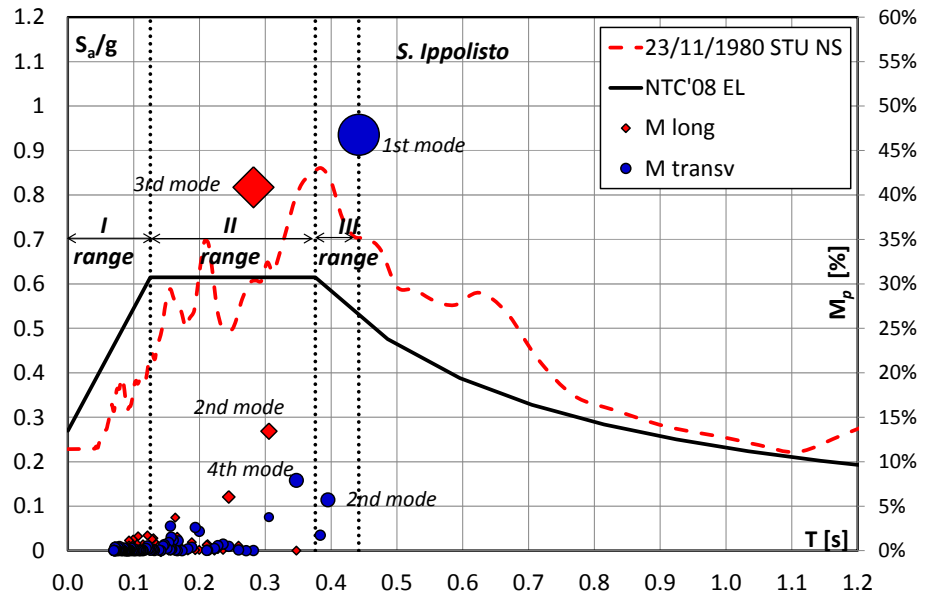
	100 v.m.	$M_p > 5\%$	10 $M_p$max	I range	II range	III range
ΣM_{plong}	88%	60%	68%	12%	22%	54%
$\Sigma M_{ptransv}$	89%	60%	76%	6%	29%	54%
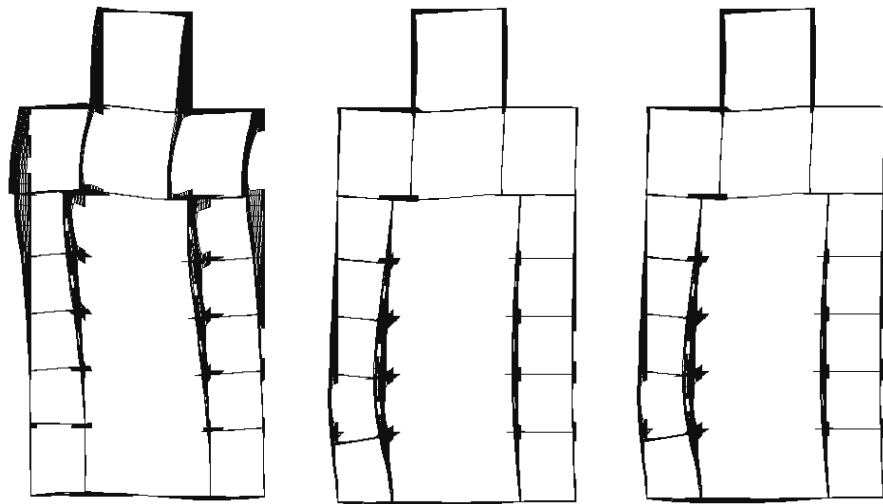
| 1st mode | 2nd mode | 3rd mode |

S. MARIA IN MONTEVERGINELLA (SMM)

Mode	Period	Longitudinal direction			Transversal direction		
		M_p	ΣM_p	ΣM_p >5%	M_p	ΣM_p	ΣM_p >5%
n°	(s)	(%)	(%)	(%)	(%)	(%)	(%)
1	1.120	0.19%	0.19%	-	0.00%	0.00%	-
2	0.759	1.09%	1.28%	-	0.00%	0.00%	-
3	0.664	0.00%	1.28%	-	0.21%	0.21%	-
4	0.566	24.85%	26.13%	-	0.56%	0.77%	-
5	0.544	0.50%	26.62%	7.76%	7.76%	8.53%	7.76%
6	0.501	0.00%	26.62%	13.37%	13.37%	21.89%	13.37%
7	0.467	0.34%	26.96%	15.15%	15.15%	37.04%	15.15%
8	0.463	0.02%	26.98%	-	0.09%	37.13%	-
9	0.455	7.67%	34.65%	-	0.56%	37.68%	-
10	0.446	4.66%	39.31%	-	0.07%	37.75%	-
11	0.441	0.81%	40.13%	10.06%	10.06%	47.81%	10.06%
12	0.431	2.39%	42.51%	-	4.84%	52.65%	-
13	0.403	0.17%	42.69%	-	1.86%	54.51%	-
14	0.397	0.91%	43.60%	-	1.26%	55.77%	-
15	0.393	5.08%	48.68%	-	0.71%	56.48%	-
16	0.380	0.00%	48.68%	-	1.64%	58.12%	-
17	0.372	0.67%	49.35%	-	0.14%	58.26%	-
18	0.352	1.26%	50.62%	-	0.02%	58.27%	-
19	0.350	0.15%	50.77%	-	0.44%	58.71%	-
20	0.344	1.13%	51.90%	-	0.01%	58.72%	-
21	0.339	0.19%	52.09%	-	0.45%	59.16%	-
22	0.326	4.04%	56.12%	-	0.00%	59.17%	-
23	0.307	0.22%	56.35%	-	0.03%	59.19%	-
24	0.300	0.04%	56.39%	6.60%	6.60%	65.80%	6.60%
25	0.279	0.21%	56.59%	-	0.01%	65.80%	-
26	0.271	0.05%	56.65%	-	1.30%	67.10%	-
27	0.269	0.06%	56.70%	-	0.07%	67.17%	-
28	0.267	0.01%	56.71%	-	0.37%	67.54%	-
29	0.263	0.55%	57.26%	-	0.00%	67.54%	-
30	0.258	0.01%	57.27%	-	1.14%	68.68%	-
31	0.243	0.49%	57.76%	-	1.48%	70.15%	-
32	0.231	0.21%	57.97%	-	0.10%	70.25%	-
33	0.229	0.13%	58.09%	-	0.01%	70.26%	-
34	0.226	2.90%	60.99%	-	0.00%	70.26%	-
35	0.221	0.77%	61.75%	-	0.32%	70.58%	-
36	0.220	0.15%	61.90%	-	0.00%	70.58%	-
37	0.218	4.19%	66.09%	-	0.26%	70.84%	-
38	0.218	0.71%	66.80%	-	0.00%	70.84%	-

Mode	Period	Longitudinal direction			Transversal direction		
		M_P	ΣM_p	ΣM_p >5%	M_P	ΣM_p	ΣM_p >5%
n°	(s)	(%)	(%)	(%)	(%)	(%)	(%)
39	0.214	0.14%	66.93%	-	0.18%	71.02%	-
40	0.212	0.46%	67.40%	-	0.25%	71.27%	-
41	0.208	0.73%	68.12%	-	0.01%	71.28%	-
42	0.204	2.09%	70.21%	-	0.27%	71.55%	-
43	0.204	0.14%	70.35%	-	0.02%	71.57%	-
44	0.203	0.92%	71.27%	-	0.00%	71.57%	-
45	0.202	0.03%	71.29%	-	0.04%	71.61%	-
46	0.201	0.24%	71.53%	-	0.01%	71.62%	-
47	0.200	6.16%	77.70%	6.16%	0.09%	71.71%	6.16%
48	0.194	0.08%	77.78%	-	0.03%	71.74%	-
49	0.191	0.03%	77.80%	-	0.01%	71.75%	-
50	0.190	0.14%	77.94%	-	0.71%	72.47%	-
51	0.187	0.00%	77.95%	-	0.18%	72.65%	-
52	0.187	0.01%	77.96%	-	0.09%	72.74%	-
53	0.186	0.00%	77.96%	-	0.32%	73.06%	-
54	0.185	0.01%	77.97%	-	0.41%	73.47%	-
55	0.183	0.02%	77.98%	-	0.03%	73.50%	-
56	0.182	0.03%	78.01%	-	0.00%	73.50%	-
57	0.180	0.00%	78.01%	-	0.04%	73.54%	-
58	0.180	0.00%	78.01%	-	0.18%	73.72%	-
59	0.179	0.00%	78.02%	-	0.00%	73.72%	-
60	0.177	0.01%	78.03%	-	0.02%	73.74%	-
61	0.177	0.03%	78.06%	-	0.09%	73.83%	-
62	0.175	0.08%	78.14%	-	0.07%	73.90%	-
63	0.174	0.26%	78.40%	-	0.55%	74.45%	-
64	0.173	0.20%	78.59%	-	0.51%	74.96%	-
65	0.171	0.00%	78.60%	-	0.16%	75.12%	-
66	0.170	0.01%	78.61%	-	0.08%	75.21%	-
67	0.170	0.02%	78.63%	-	0.30%	75.50%	-
68	0.169	0.03%	78.65%	-	0.02%	75.52%	-
69	0.168	0.14%	78.79%	-	0.00%	75.52%	-
70	0.168	0.01%	78.80%	-	0.22%	75.74%	-
71	0.167	0.03%	78.83%	-	0.01%	75.75%	-
72	0.166	0.00%	78.83%	-	0.04%	75.79%	-
73	0.165	0.02%	78.85%	-	0.01%	75.80%	-
74	0.164	0.01%	78.86%	-	0.00%	75.81%	-
75	0.163	0.01%	78.87%	-	0.43%	76.23%	-
76	0.162	0.06%	78.93%	-	1.23%	77.46%	-
77	0.161	0.16%	79.09%	-	0.00%	77.47%	-
78	0.160	0.14%	79.23%	-	0.06%	77.52%	-
79	0.160	0.05%	79.29%	-	0.10%	77.62%	-

Mode	Period	Longitudinal direction			Transversal direction		
		M_p	ΣM_p	ΣM_p >5%	M_p	ΣM_p	ΣM_p >5%
n°	(s)	(%)	(%)	(%)	(%)	(%)	(%)
80	0.159	0.04%	79.32%	-	0.01%	77.63%	-
81	0.158	0.01%	79.34%	-	0.10%	77.73%	-
82	0.158	0.00%	79.34%	-	0.52%	78.25%	-
83	0.156	0.12%	79.45%	-	0.75%	79.01%	-
84	0.155	0.11%	79.56%	-	0.18%	79.18%	-
85	0.154	0.11%	79.68%	-	0.00%	79.18%	-
86	0.154	0.05%	79.73%	-	0.17%	79.36%	-
87	0.153	0.00%	79.73%	-	0.03%	79.39%	-
88	0.152	0.29%	80.02%	-	0.00%	79.39%	-
89	0.152	0.24%	80.26%	-	0.02%	79.41%	-
90	0.151	0.03%	80.29%	-	0.10%	79.50%	-
91	0.150	0.01%	80.30%	-	0.01%	79.52%	-
92	0.149	0.01%	80.31%	-	0.04%	79.55%	-
93	0.149	0.00%	80.31%	-	0.00%	79.56%	-
94	0.149	0.00%	80.31%	-	0.01%	79.57%	-
95	0.148	0.01%	80.32%	-	0.06%	79.63%	-
96	0.148	0.04%	80.36%	-	0.12%	79.74%	-
97	0.148	0.03%	80.39%	-	0.01%	79.76%	-
98	0.147	0.18%	80.56%	-	0.07%	79.82%	-
99	0.146	0.02%	80.58%	-	0.00%	79.83%	-
100	0.146	0.03%	80.61%	-	0.02%	79.85%	-
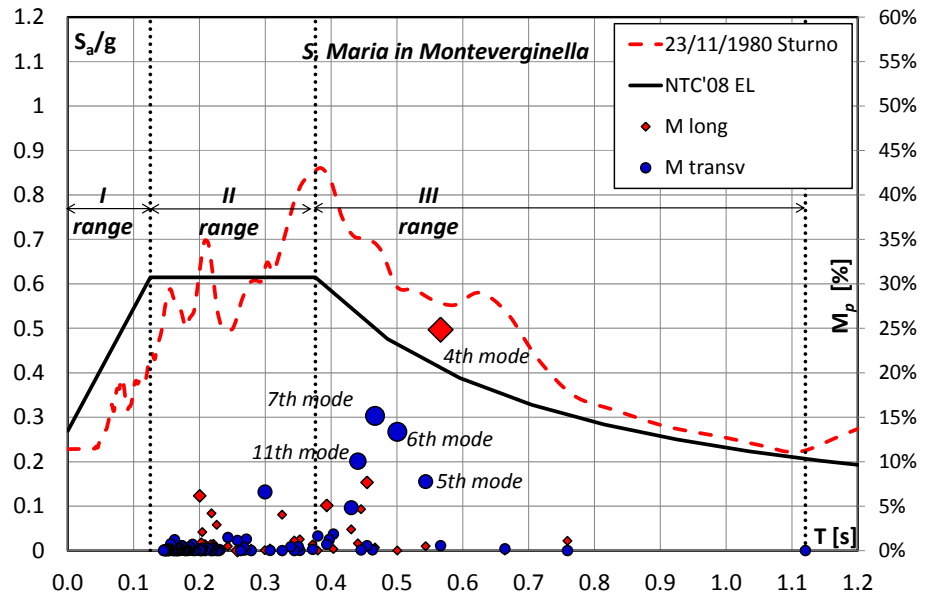
	100 v.m.	M_p>5%	10 $M_p$max	I range	II range	III range
ΣM_{plong}	81%	44%	52%	0%	31%	49%
$\Sigma M_{ptransv}$	80%	53%	64%	0%	22%	58%

4th mode   6th mode   7th mode

S. SILVESTRO (SS)

Mode	Period	Longitudinal direction			Transversal direction		
		M_p	ΣM_p	$\Sigma M_p > 5\%$	M_p	ΣM_p	$\Sigma M_p > 5\%$
n°	(s)	(%)	(%)	(%)	(%)	(%)	(%)
1	2.535	0.00%	0.00%	-	7.66%	7.93%	7.66%
2	2.136	0.00%	0.00%	-	5.65%	13.77%	5.65%
3	1.181	0.02%	0.02%	-	0.01%	13.78%	-
4	0.977	0.00%	0.02%	-	4.08%	17.91%	-
5	0.953	0.04%	0.04%	-	0.47%	18.20%	-
6	0.838	14.29%	14.20%	14.29%	3.71%	22.04%	-
7	0.714	2.17%	14.23%	-	13.34%	25.97%	13.34%
8	0.708	2.93%	19.06%	-	2.31%	38.52%	-
9	0.676	0.03%	19.42%	-	1.35%	38.70%	-
10	0.647	0.00%	19.44%	-	0.08%	38.87%	-
11	0.543	0.01%	19.46%	-	2.06%	40.81%	-
12	0.504	0.03%	19.47%	-	0.84%	41.68%	-
13	0.487	0.67%	19.61%	-	1.05%	42.82%	-
14	0.482	19.13%	39.65%	19.13%	0.15%	43.16%	-
15	0.447	0.71%	40.60%	-	1.73%	44.88%	-
16	0.430	0.03%	40.62%	-	0.08%	44.94%	-
17	0.383	0.14%	40.64%	-	2.83%	45.66%	-
18	0.382	0.00%	40.65%	-	0.19%	48.21%	-
19	0.373	0.12%	40.82%	-	0.01%	48.22%	-
20	0.351	4.46%	40.86%	-	1.56%	48.22%	-
21	0.350	0.35%	45.96%	-	0.55%	50.39%	-
22	0.334	1.58%	47.80%	-	3.03%	53.33%	-
23	0.316	0.49%	48.13%	-	0.09%	53.56%	-
24	0.303	5.74%	48.16%	5.74%	0.61%	53.77%	-
25	0.301	0.68%	54.19%	-	0.21%	54.07%	-
26	0.291	0.64%	54.47%	-	0.66%	54.22%	-
27	0.280	0.27%	54.63%	-	0.72%	54.57%	-
28	0.275	0.12%	54.74%	-	2.27%	56.50%	-
29	0.267	0.99%	55.90%	-	8.74%	60.11%	8.74%
30	0.258	0.00%	56.23%	-	0.25%	66.65%	-
31	0.245	0.00%	56.29%	-	0.45%	67.30%	-
32	0.240	0.01%	56.30%	-	0.26%	67.94%	-
33	0.233	1.00%	56.92%	-	0.55%	69.52%	-
34	0.230	0.02%	57.12%	-	3.76%	72.25%	-
35	0.227	0.00%	57.36%	-	0.35%	72.54%	-
36	0.224	0.16%	57.72%	-	0.13%	72.57%	-
37	0.215	0.97%	59.48%	-	0.05%	72.64%	-
38	0.212	1.14%	60.07%	-	0.14%	72.67%	-
39	0.211	1.34%	60.07%	-	0.57%	72.91%	-

Mode	Period	Longitudinal direction			Transversal direction		
		M_p	ΣM_p	$\Sigma M_p > 5\%$	M_p	ΣM_p	$\Sigma M_p > 5\%$
n°	(s)	(%)	(%)	(%)	(%)	(%)	(%)
40	0.210	0.02%	60.69%	-	0.20%	73.07%	-
41	0.204	0.06%	60.73%	-	0.11%	73.22%	-
42	0.203	0.17%	60.74%	-	0.42%	73.72%	-
43	0.198	0.10%	60.83%	-	0.53%	74.06%	-
44	0.196	0.02%	60.86%	-	0.96%	74.83%	-
45	0.195	0.23%	61.08%	-	0.34%	75.31%	-
46	0.192	0.07%	61.12%	-	0.26%	75.46%	-
47	0.188	0.21%	61.23%	-	0.54%	76.10%	-
48	0.186	0.09%	61.51%	-	0.01%	76.24%	-
49	0.182	0.00%	61.55%	-	0.65%	76.66%	-
50	0.182	0.00%	61.55%	-	0.16%	77.39%	-
51	0.180	0.05%	61.55%	-	1.29%	78.22%	-
52	0.176	0.00%	61.55%	-	0.02%	78.24%	-
53	0.174	0.25%	61.83%	-	0.28%	78.55%	-
54	0.172	0.01%	61.84%	-	0.33%	78.71%	-
55	0.167	0.12%	61.89%	-	0.14%	78.71%	-
56	0.164	0.13%	62.16%	-	0.00%	78.74%	-
57	0.163	0.03%	62.19%	-	0.09%	78.93%	-
58	0.161	0.21%	62.46%	-	0.00%	78.94%	-
59	0.158	0.00%	62.50%	-	0.13%	78.96%	-
60	0.157	0.56%	62.50%	-	0.30%	79.13%	-
61	0.154	0.04%	63.03%	-	0.08%	79.38%	-
62	0.152	0.01%	63.10%	-	0.10%	79.41%	-
63	0.151	0.06%	63.14%	-	0.00%	79.45%	-
64	0.148	0.80%	63.14%	-	0.32%	79.47%	-
65	0.148	0.16%	63.23%	-	0.16%	79.75%	-
66	0.145	0.00%	64.06%	-	0.00%	79.86%	-
67	0.143	0.01%	64.06%	-	0.01%	79.86%	-
68	0.142	0.30%	64.21%	-	0.06%	79.89%	-
69	0.142	0.00%	64.21%	-	0.08%	79.96%	-
70	0.141	0.00%	64.21%	-	0.05%	80.00%	-
71	0.139	0.02%	64.22%	-	0.00%	80.01%	-
72	0.136	0.00%	64.23%	-	0.00%	80.02%	-
73	0.134	0.00%	64.25%	-	0.26%	80.04%	-
74	0.134	0.01%	64.25%	-	0.01%	80.17%	-
75	0.132	0.06%	64.42%	-	0.04%	80.18%	-
76	0.131	0.04%	64.42%	-	1.37%	80.22%	-
77	0.131	0.00%	64.54%	-	0.00%	81.22%	-
78	0.129	0.23%	64.97%	-	0.10%	81.88%	-
79	0.127	2.08%	68.01%	-	0.12%	82.24%	-

Mode	Period	Longitudinal direction			Transversal direction		
		M_p	ΣM_p	$\Sigma M_p > 5\%$	M_p	ΣM_p	$\Sigma M_p > 5\%$
n°	(s)	(%)	(%)	(%)	(%)	(%)	(%)
80	0.125	1.14%	68.05%	-	0.52%	82.52%	-
81	0.124	1.82%	68.14%	-	0.00%	82.66%	-
82	0.123	1.79%	68.75%	-	0.02%	82.66%	-
83	0.121	0.04%	69.19%	-	0.03%	82.67%	-
84	0.121	0.94%	70.05%	-	0.04%	82.69%	-
85	0.119	0.30%	71.65%	-	0.12%	82.73%	-
86	0.118	0.05%	71.68%	-	0.07%	82.88%	-
87	0.117	0.03%	74.58%	-	0.01%	83.31%	-
88	0.115	2.49%	75.28%	-	0.11%	83.37%	-
89	0.114	0.41%	75.59%	-	0.01%	83.41%	-
90	0.114	0.05%	75.90%	-	0.03%	83.42%	-
91	0.113	0.02%	75.98%	-	0.01%	83.62%	-
92	0.113	1.59%	76.08%	-	0.30%	83.62%	-
93	0.112	0.00%	76.08%	-	0.03%	83.65%	-
94	0.112	0.52%	76.24%	-	0.07%	83.65%	-
95	0.111	0.11%	77.34%	-	0.00%	84.12%	-
96	0.110	0.02%	77.48%	-	0.01%	84.14%	-
97	0.110	0.28%	77.48%	-	0.46%	84.18%	-
98	0.109	0.12%	77.77%	-	0.19%	84.20%	-
99	0.107	0.65%	77.86%	-	0.02%	84.23%	-
100	0.106	0.39%	77.90%	-	0.03%	84.24%	-
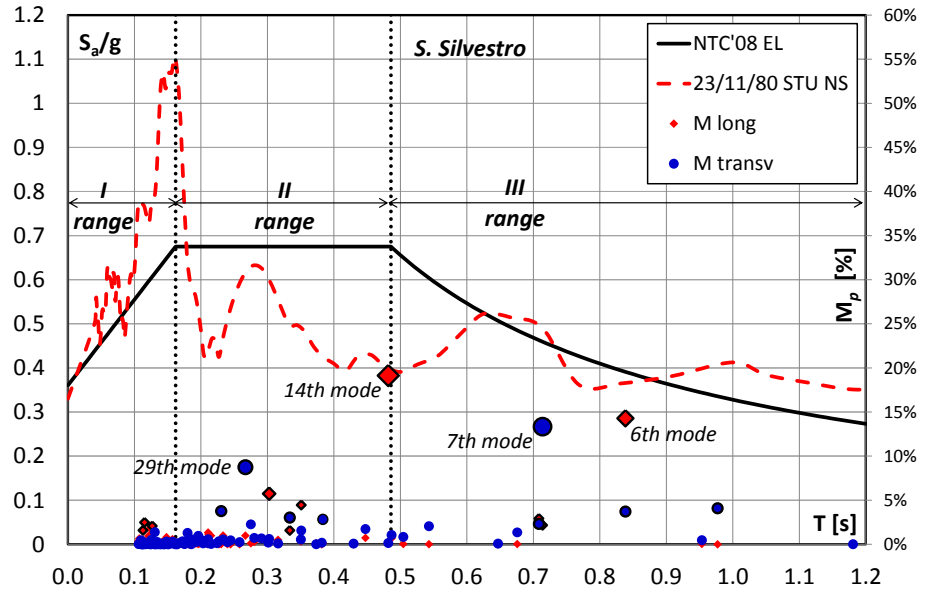
	100 v.m.	M_p>5%	10 $M_p$max	I range	II range	III range
ΣM_{plong}	78%	39%	57%	17%	23%	39%
$\Sigma M_{ptransv}$	84%	35%	55%	5%	36%	43%

6th mode   7th mode   14th mode
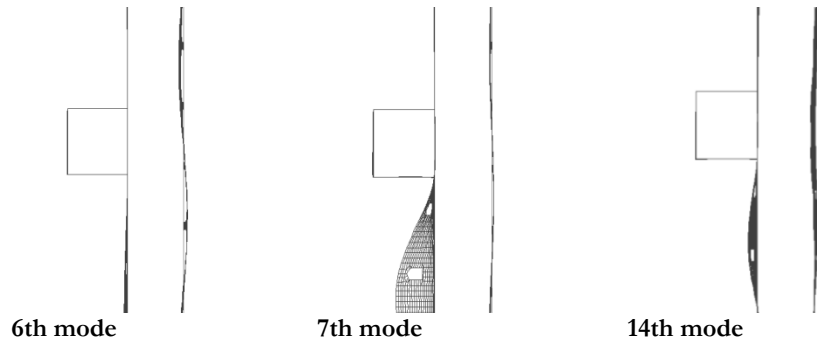
S. PIETRO COPPITO (SPC)

Mode	Period	Longitudinal direction			Transversal direction		
		M_p	ΣM_p	$\Sigma M_p > 5\%$	M_p	ΣM_p	$\Sigma M_p > 5\%$
n°	(s)	(%)	(%)	(%)	(%)	(%)	(%)
1	1.099	2.49%	2.49%	-	0.00%	0.00%	-
2	0.739	0.03%	2.51%	-	1.45%	1.45%	-
3	0.686	0.62%	3.13%	-	5.18%	6.62%	5.18%
4	0.576	5.81%	8.94%	5.81%	1.94%	8.57%	-
5	0.575	22.71%	31.65%	22.71%	0.00%	8.57%	-
6	0.547	0.40%	32.05%	-	25.53%	34.10%	25.53%
7	0.537	0.41%	32.46%	-	6.82%	40.91%	6.82%
8	0.515	0.71%	33.17%	-	0.04%	40.95%	-
9	0.423	0.26%	33.43%	-	0.02%	40.96%	-
10	0.344	0.33%	33.75%	-	0.00%	40.96%	-
11	0.337	1.98%	35.73%	-	0.37%	41.33%	-
12	0.306	0.06%	35.78%	-	0.02%	41.35%	-
13	0.288	0.02%	35.80%	-	0.01%	41.36%	-
14	0.281	1.77%	37.57%	-	0.10%	41.46%	-
15	0.274	0.47%	38.04%	-	0.24%	41.70%	-
16	0.271	5.21%	43.24%	5.21%	0.00%	41.70%	-
17	0.265	5.52%	48.76%	5.52%	1.26%	42.97%	-
18	0.256	0.02%	48.78%	-	0.23%	43.19%	-
19	0.249	0.08%	48.86%	-	2.82%	46.01%	-
20	0.246	0.17%	49.03%	-	0.23%	46.24%	-
21	0.238	1.43%	50.46%	-	4.11%	50.35%	-
22	0.237	0.35%	50.81%	-	3.68%	54.03%	-
23	0.234	0.35%	51.16%	-	5.40%	59.42%	5.40%
24	0.219	0.05%	51.22%	-	0.09%	59.51%	-
25	0.217	0.36%	51.57%	-	0.26%	59.77%	-
26	0.206	0.00%	51.57%	-	0.09%	59.87%	-
27	0.203	0.48%	52.05%	-	0.15%	60.01%	-
28	0.199	1.12%	53.17%	-	0.45%	60.46%	-
29	0.190	2.24%	55.41%	-	0.27%	60.73%	-
30	0.185	7.19%	62.60%	7.19%	1.66%	62.39%	-
31	0.182	1.44%	64.04%	-	0.37%	62.76%	-
32	0.177	0.67%	64.71%	-	0.49%	63.25%	-
33	0.171	0.65%	65.36%	-	0.86%	64.11%	-
34	0.170	2.54%	67.90%	-	8.50%	72.60%	8.50%
35	0.164	0.58%	68.48%	-	0.00%	72.60%	-
36	0.162	0.04%	68.52%	-	0.20%	72.80%	-
37	0.161	0.05%	68.57%	-	0.29%	73.10%	-
38	0.158	0.83%	69.40%	-	0.12%	73.22%	-
39	0.154	0.40%	69.79%	-	0.24%	73.45%	-

Mode	Period	Longitudinal direction			Transversal direction		
		M_p	ΣM_p	$\Sigma M_p > 5\%$	M_p	ΣM_p	$\Sigma M_p > 5\%$
n°	(s)	(%)	(%)	(%)	(%)	(%)	(%)
40	0.149	0.00%	69.80%	-	0.04%	73.50%	-
41	0.149	0.16%	69.95%	-	0.01%	73.50%	-
42	0.146	0.87%	70.83%	-	0.08%	73.58%	-
43	0.142	0.63%	71.46%	-	0.03%	73.61%	-
44	0.141	0.02%	71.48%	-	0.34%	73.95%	-
45	0.139	0.22%	71.69%	-	0.44%	74.38%	-
46	0.137	0.04%	71.73%	-	0.06%	74.44%	-
47	0.135	0.07%	71.80%	-	0.10%	74.54%	-
48	0.135	1.33%	73.13%	-	0.06%	74.60%	-
49	0.135	0.07%	73.20%	-	0.21%	74.80%	-
50	0.129	0.47%	73.67%	-	0.74%	75.54%	-
51	0.125	0.18%	73.85%	-	0.09%	75.63%	-
52	0.121	0.31%	74.15%	-	0.84%	76.47%	-
53	0.119	0.12%	74.27%	-	0.00%	76.47%	-
54	0.119	0.58%	74.86%	-	0.06%	76.53%	-
55	0.118	1.41%	76.27%	-	1.23%	77.76%	-
56	0.116	0.07%	76.33%	-	0.60%	78.37%	-
57	0.116	0.10%	76.44%	-	0.02%	78.39%	-
58	0.115	0.05%	76.48%	-	0.05%	78.44%	-
59	0.112	0.00%	76.48%	-	0.26%	78.69%	-
60	0.111	0.04%	76.52%	-	0.20%	78.89%	-
61	0.110	0.01%	76.53%	-	0.04%	78.93%	-
62	0.110	0.02%	76.55%	-	0.24%	79.17%	-
63	0.108	0.09%	76.64%	-	0.12%	79.29%	-
64	0.108	0.03%	76.67%	-	0.00%	79.29%	-
65	0.106	0.00%	76.67%	-	0.00%	79.30%	-
66	0.105	0.01%	76.68%	-	0.07%	79.37%	-
67	0.104	1.22%	77.90%	-	0.27%	79.63%	-
68	0.102	0.04%	77.94%	-	0.25%	79.89%	-
69	0.101	0.01%	77.94%	-	0.19%	80.07%	-
70	0.100	1.00%	78.95%	-	0.01%	80.09%	-
71	0.099	0.74%	79.69%	-	0.01%	80.10%	-
72	0.097	0.26%	79.95%	-	0.01%	80.11%	-
73	0.095	0.05%	80.00%	-	0.08%	80.19%	-
74	0.095	1.13%	81.13%	-	0.05%	80.24%	-
75	0.094	0.12%	81.24%	-	0.20%	80.44%	-
76	0.094	0.01%	81.25%	-	0.26%	80.70%	-
77	0.093	0.19%	81.44%	-	0.01%	80.71%	-
78	0.092	0.03%	81.46%	-	0.13%	80.84%	-
79	0.091	0.00%	81.47%	-	0.18%	81.02%	-

Mode	Period	Longitudinal direction			Transversal direction		
		M_p	ΣM_p	ΣM_p >5%	M_p	ΣM_p	ΣM_p >5%
n°	(s)	(%)	(%)	(%)	(%)	(%)	(%)
80	0.091	0.09%	81.55%	-	0.12%	81.14%	-
81	0.090	0.00%	81.55%	-	0.00%	81.14%	-
82	0.090	0.08%	81.63%	-	0.06%	81.20%	-
83	0.089	0.00%	81.64%	-	0.00%	81.20%	-
84	0.088	0.64%	82.28%	-	0.19%	81.39%	-
85	0.088	0.01%	82.29%	-	0.60%	82.00%	-
86	0.087	0.01%	82.29%	-	0.23%	82.22%	-
87	0.087	0.03%	82.32%	-	0.00%	82.23%	-
88	0.086	0.01%	82.33%	-	1.02%	83.24%	-
89	0.086	0.25%	82.58%	-	0.14%	83.38%	-
90	0.086	0.05%	82.63%	-	0.36%	83.74%	-
91	0.084	0.12%	82.75%	-	0.83%	84.56%	-
92	0.084	0.00%	82.75%	-	0.06%	84.62%	-
93	0.084	0.10%	82.86%	-	1.28%	85.90%	-
94	0.082	0.00%	82.86%	-	0.01%	85.91%	-
95	0.082	0.06%	82.92%	-	0.22%	86.13%	-
96	0.081	0.02%	82.93%	-	0.00%	86.13%	-
97	0.081	0.00%	82.93%	-	0.13%	86.26%	-
98	0.080	0.06%	83.00%	-	0.01%	86.26%	-
99	0.079	0.04%	83.04%	-	0.02%	86.28%	-
100	0.078	0.00%	83.04%	-	0.00%	86.29%	-
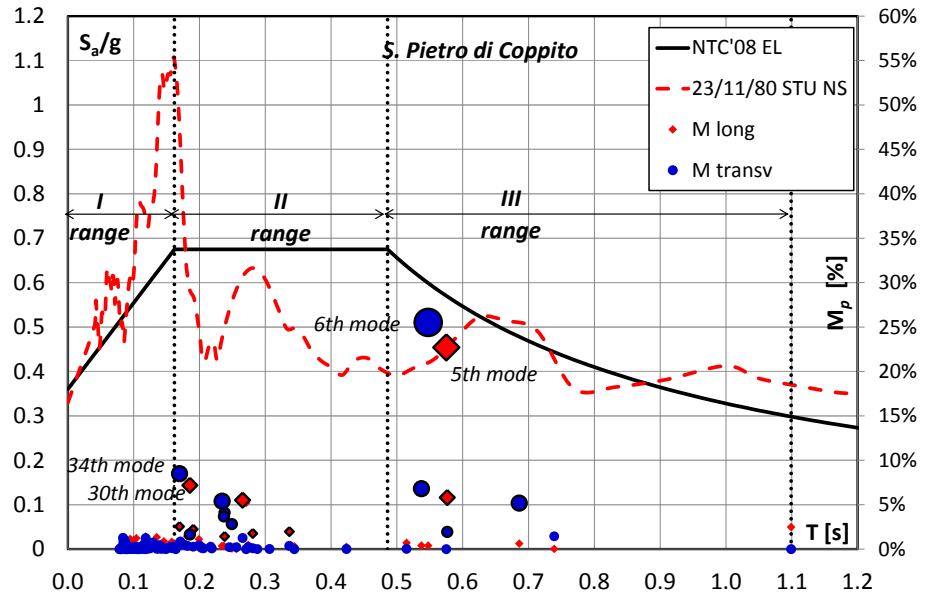
	100 v.m.	M_p>5%	10 $M_p$max	I range	II range	III range
ΣM_{plong}	83%	46%	57%	14%	35%	33%
$\Sigma M_{ptransv}$	86%	51%	66%	13%	32%	41%

| 5th mode | 6th mode | 34th mode |
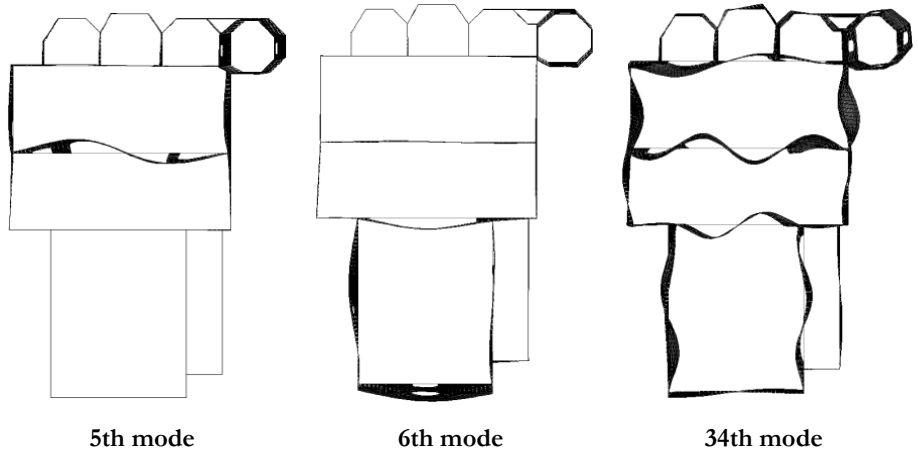
S. GIOVANNI MAGGIORE (SGM)

Mode	Period	Longitudinal direction			Transversal direction		
		M_p	ΣM_p	$\Sigma M_p > 5\%$	M_p	ΣM_p	$\Sigma M_p > 5\%$
n°	(s)	(%)	(%)	(%)	(%)	(%)	(%)
1	0.603	46.19%	46.19%	46.19%	0.00%	0.00%	-
2	0.585	0.00%	46.19%	-	20.30%	20.30%	20.30%
3	0.567	2.56%	48.75%	-	0.00%	20.30%	-
4	0.534	0.03%	48.78%	-	5.40%	25.70%	5.40%
5	0.519	0.02%	48.79%	-	29.45%	55.14%	29.45%
6	0.493	0.01%	48.81%	-	0.23%	55.37%	-
7	0.479	1.50%	50.31%	-	0.00%	55.37%	-
8	0.459	0.00%	50.31%	-	1.80%	57.17%	-
9	0.411	11.46%	61.77%	11.46%	0.01%	57.18%	-
10	0.409	0.66%	62.43%	-	0.30%	57.48%	-
11	0.385	0.34%	62.77%	-	0.00%	57.48%	-
12	0.379	0.00%	62.77%	-	0.18%	57.66%	-
13	0.355	0.02%	62.79%	-	0.00%	57.66%	-
14	0.347	0.01%	62.80%	-	0.13%	57.79%	-
15	0.341	0.22%	63.03%	-	0.02%	57.82%	-
16	0.336	0.08%	63.11%	-	0.00%	57.82%	-
17	0.328	0.62%	63.72%	-	0.46%	58.28%	-
18	0.327	0.79%	64.51%	-	0.17%	58.45%	-
19	0.319	8.54%	73.05%	8.54%	0.02%	58.47%	-
20	0.316	0.00%	73.06%	-	0.00%	58.47%	-
21	0.313	0.00%	73.06%	-	0.03%	58.50%	-
22	0.312	0.03%	73.09%	-	9.71%	68.20%	9.71%
23	0.309	0.00%	73.09%	-	1.30%	69.51%	-
24	0.309	0.00%	73.09%	-	0.26%	69.76%	-
25	0.308	0.00%	73.09%	-	0.00%	69.76%	-
26	0.306	0.00%	73.09%	-	0.00%	69.76%	-
27	0.305	0.67%	73.76%	-	1.54%	71.31%	-
28	0.304	0.00%	73.76%	-	0.00%	71.31%	-
29	0.303	0.00%	73.76%	-	0.00%	71.31%	-
30	0.301	0.01%	73.77%	-	0.00%	71.31%	-
31	0.301	0.00%	73.77%	-	0.00%	71.31%	-
32	0.301	0.02%	73.79%	-	0.05%	71.36%	-
33	0.293	0.23%	74.01%	-	1.35%	72.70%	-
34	0.289	0.00%	74.02%	-	0.05%	72.75%	-
35	0.280	0.59%	74.61%	-	1.13%	73.89%	-
36	0.280	0.07%	74.68%	-	0.08%	73.96%	-
37	0.277	0.01%	74.68%	-	2.34%	76.30%	-
38	0.273	0.00%	74.68%	-	0.00%	76.30%	-
39	0.269	0.69%	75.38%	-	0.31%	76.62%	-

Mode	Period	Longitudinal direction			Transversal direction		
		M_p	ΣM_p	ΣM_p >5%	M_p	ΣM_p	ΣM_p >5%
n°	(s)	(%)	(%)	(%)	(%)	(%)	(%)
40	0.267	0.19%	75.57%	-	0.00%	76.62%	-
41	0.266	0.00%	75.57%	-	0.34%	76.96%	-
42	0.246	0.27%	75.84%	-	0.10%	77.06%	-
43	0.237	0.06%	75.90%	-	0.50%	77.55%	-
44	0.233	0.03%	75.93%	-	0.05%	77.60%	-
45	0.231	0.04%	75.97%	-	1.52%	79.12%	-
46	0.227	0.02%	75.99%	-	0.10%	79.22%	-
47	0.225	0.00%	75.99%	-	0.04%	79.26%	-
48	0.224	0.12%	76.11%	-	0.22%	79.48%	-
49	0.218	0.00%	76.11%	-	0.00%	79.48%	-
50	0.217	0.00%	76.11%	-	0.00%	79.48%	-
51	0.215	0.00%	76.11%	-	0.02%	79.50%	-
52	0.215	0.00%	76.11%	-	0.48%	79.98%	-
53	0.214	0.00%	76.11%	-	0.00%	79.98%	-
54	0.213	0.00%	76.11%	-	0.00%	79.99%	-
55	0.213	0.04%	76.15%	-	0.00%	79.99%	-
56	0.212	0.00%	76.15%	-	0.00%	79.99%	-
57	0.212	0.00%	76.15%	-	0.00%	79.99%	-
58	0.211	0.00%	76.15%	-	0.00%	79.99%	-
59	0.211	0.00%	76.15%	-	0.00%	79.99%	-
60	0.211	0.00%	76.15%	-	0.06%	80.05%	-
61	0.208	0.62%	76.77%	-	0.01%	80.06%	-
62	0.206	0.00%	76.77%	-	0.32%	80.38%	-
63	0.206	0.02%	76.79%	-	0.15%	80.54%	-
64	0.203	0.16%	76.95%	-	0.58%	81.12%	-
65	0.202	0.16%	77.10%	-	1.08%	82.20%	-
66	0.200	0.37%	77.47%	-	0.00%	82.20%	-
67	0.199	0.00%	77.47%	-	0.00%	82.20%	-
68	0.196	0.80%	78.27%	-	0.00%	82.21%	-
69	0.189	0.01%	78.28%	-	0.06%	82.27%	-
70	0.186	0.07%	78.35%	-	0.00%	82.27%	-
71	0.184	0.02%	78.36%	-	0.09%	82.36%	-
72	0.182	0.02%	78.39%	-	0.02%	82.38%	-
73	0.181	0.00%	78.39%	-	0.00%	82.38%	-
74	0.181	0.00%	78.39%	-	0.00%	82.38%	-
75	0.179	0.00%	78.39%	-	0.00%	82.39%	-
76	0.176	0.06%	78.45%	-	0.06%	82.45%	-
77	0.174	0.07%	78.52%	-	0.05%	82.50%	-
78	0.172	0.00%	78.52%	-	0.21%	82.70%	-
79	0.171	0.05%	78.57%	-	0.72%	83.42%	-

Mode	Period	Longitudinal direction			Transversal direction		
		M_P	ΣM_P	$\Sigma M_P > 5\%$	M_P	ΣM_P	$\Sigma M_P > 5\%$
n°	(s)	(%)	(%)	(%)	(%)	(%)	(%)
80	0.169	0.58%	79.14%	-	0.06%	83.48%	-
81	0.167	0.21%	79.35%	-	0.00%	83.48%	-
82	0.166	0.33%	79.68%	-	0.01%	83.50%	-
83	0.165	0.25%	79.93%	-	0.00%	83.50%	-
84	0.162	0.06%	79.99%	-	0.01%	83.51%	-
85	0.162	0.07%	80.07%	-	0.01%	83.52%	-
86	0.161	0.01%	80.07%	-	0.06%	83.57%	-
87	0.159	0.08%	80.15%	-	0.01%	83.58%	-
88	0.158	0.11%	80.26%	-	0.03%	83.61%	-
89	0.156	0.04%	80.30%	-	0.02%	83.63%	-
90	0.154	0.01%	80.31%	-	0.01%	83.64%	-
91	0.151	0.02%	80.33%	-	0.05%	83.69%	-
92	0.150	0.46%	80.79%	-	0.00%	83.69%	-
93	0.149	0.37%	81.16%	-	0.03%	83.73%	-
94	0.148	0.35%	81.51%	-	0.01%	83.73%	-
95	0.147	0.77%	82.28%	-	0.00%	83.73%	-
96	0.144	0.00%	82.28%	-	1.03%	84.76%	-
97	0.144	0.00%	82.28%	-	0.30%	85.06%	-
98	0.143	0.12%	82.40%	-	0.12%	85.18%	-
99	0.143	0.05%	82.45%	-	0.01%	85.19%	-
100	0.141	0.00%	82.45%	-	0.10%	85.29%	-
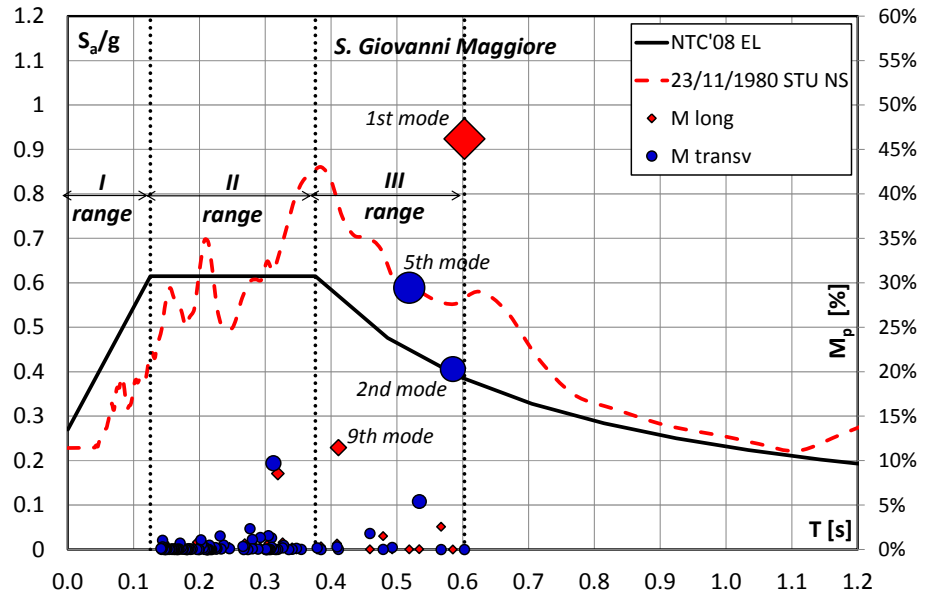
	100 v.m.	M_p>5%	10 $M_p$max	I range	II range	III range
ΣM_{plong}	82%	66%	74%	0%	20%	63%
$\Sigma M_{ptransv}$	85%	65%	76%	0%	28%	58%

1st mode   2nd mode   5th mode

S. MARIA DI COLLEMAGGIO (SMC)

Mode	Period	Longitudinal direction			Transversal direction		
		M_p	ΣM_p	$\Sigma M_p > 5\%$	M_p	ΣM_p	$\Sigma M_p > 5\%$
n°	(s)	(%)	(%)	(%)	(%)	(%)	(%)
1	3.600	0.00%	0.00%	-	0.00%	0.00%	-
2	3.600	0.00%	0.00%	-	11.00%	11.00%	11.00%
3	1.821	0.01%	0.01%	-	0.00%	11.00%	-
4	1.814	0.00%	0.01%	-	0.01%	11.01%	-
5	1.063	0.00%	0.01%	-	4.38%	15.39%	-
6	1.059	0.00%	0.01%	-	0.00%	15.39%	-
7	1.014	0.00%	0.01%	-	4.74%	20.13%	-
8	0.973	0.00%	0.01%	-	4.65%	24.78%	-
9	0.766	0.02%	0.03%	-	0.30%	25.08%	-
10	0.744	0.17%	0.21%	-	0.46%	25.54%	-
11	0.703	0.01%	0.21%	-	2.76%	28.30%	-
12	0.686	1.01%	1.23%	-	0.00%	28.30%	-
13	0.667	0.00%	1.23%	-	1.70%	30.00%	-
14	0.667	0.01%	1.23%	-	0.11%	30.11%	-
15	0.623	0.01%	1.25%	-	15.27%	45.37%	15.27%
16	0.593	31.08%	32.32%	31.08%	0.01%	45.39%	-
17	0.548	0.00%	32.33%	-	0.01%	45.39%	-
18	0.547	0.06%	32.38%	-	0.00%	45.39%	-
19	0.546	0.01%	32.40%	-	0.33%	45.73%	-
20	0.540	0.48%	32.87%	-	0.02%	45.75%	-
21	0.529	0.15%	33.03%	-	0.16%	45.91%	-
22	0.487	0.01%	33.03%	-	0.69%	46.60%	-
23	0.479	0.00%	33.04%	-	0.00%	46.61%	-
24	0.449	0.00%	33.04%	-	2.58%	49.18%	-
25	0.432	0.00%	33.04%	-	0.00%	49.18%	-
26	0.431	0.00%	33.04%	-	0.29%	49.47%	-
27	0.428	0.03%	33.07%	-	0.01%	49.48%	-
28	0.399	0.05%	33.12%	-	0.02%	49.50%	-
29	0.392	0.02%	33.13%	-	1.64%	51.14%	-
30	0.390	0.01%	33.14%	-	2.04%	53.19%	-
31	0.388	0.14%	33.28%	-	2.18%	55.36%	-
32	0.374	0.00%	33.28%	-	1.51%	56.88%	-
33	0.350	0.00%	33.28%	-	2.40%	59.28%	-
34	0.343	0.04%	33.32%	-	0.06%	59.34%	-
35	0.342	0.00%	33.32%	-	0.52%	59.85%	-
36	0.337	0.02%	33.35%	-	0.43%	60.28%	-
37	0.332	1.12%	34.47%	-	0.64%	60.93%	-
38	0.317	0.21%	34.68%	-	8.00%	68.93%	8.00%
39	0.312	0.20%	34.87%	-	0.20%	69.13%	-

Mode	Period	Longitudinal direction			Transversal direction		
		M_p	ΣM_p	$\Sigma M_p > 5\%$	M_p	ΣM_p	$\Sigma M_p > 5\%$
n°	(s)	(%)	(%)	(%)	(%)	(%)	(%)
40	0.303	0.02%	34.89%	-	0.18%	69.31%	-
41	0.301	0.00%	34.89%	-	0.15%	69.46%	-
42	0.290	0.00%	34.89%	-	0.80%	70.26%	-
43	0.284	0.00%	34.90%	-	0.01%	70.27%	-
44	0.278	0.00%	34.90%	-	0.07%	70.34%	-
45	0.276	0.01%	34.90%	-	0.00%	70.34%	-
46	0.270	2.44%	37.34%	-	0.00%	70.34%	-
47	0.259	0.35%	37.69%	-	0.00%	70.34%	-
48	0.255	1.91%	39.60%	-	0.00%	70.34%	-
49	0.252	0.01%	39.62%	-	0.16%	70.50%	-
50	0.242	0.12%	39.73%	-	0.49%	71.00%	-
51	0.235	0.28%	40.01%	-	0.00%	71.00%	-
52	0.229	0.07%	40.08%	-	0.01%	71.01%	-
53	0.229	0.22%	40.30%	-	0.00%	71.01%	-
54	0.228	0.30%	40.60%	-	0.00%	71.01%	-
55	0.227	0.80%	41.39%	-	0.01%	71.02%	-
56	0.219	0.02%	41.41%	-	0.09%	71.11%	-
57	0.212	0.45%	41.86%	-	0.14%	71.25%	-
58	0.212	0.78%	42.64%	-	0.06%	71.31%	-
59	0.209	3.38%	46.02%	-	0.06%	71.37%	-
60	0.206	0.18%	46.20%	-	0.03%	71.40%	-
61	0.204	0.28%	46.48%	-	0.05%	71.45%	-
62	0.201	0.98%	47.46%	-	0.00%	71.45%	-
63	0.198	0.00%	47.46%	-	0.21%	71.65%	-
64	0.198	0.01%	47.47%	-	0.00%	71.66%	-
65	0.198	0.01%	47.47%	-	0.00%	71.66%	-
66	0.196	0.03%	47.51%	-	0.00%	71.66%	-
67	0.194	0.01%	47.52%	-	0.02%	71.68%	-
68	0.194	2.54%	50.06%	-	0.02%	71.71%	-
69	0.191	0.00%	50.06%	-	0.10%	71.81%	-
70	0.189	0.03%	50.09%	-	0.00%	71.81%	-
71	0.189	0.00%	50.09%	-	0.00%	71.81%	-
72	0.186	0.05%	50.14%	-	0.00%	71.82%	-
73	0.184	1.90%	52.04%	-	0.09%	71.90%	-
74	0.182	0.00%	52.04%	-	0.79%	72.69%	-
75	0.180	0.07%	52.11%	-	0.51%	73.19%	-
76	0.178	0.00%	52.11%	-	1.56%	74.75%	-
77	0.178	0.00%	52.12%	-	0.03%	74.78%	-
78	0.177	0.04%	52.16%	-	0.04%	74.81%	-
79	0.177	0.00%	52.17%	-	0.00%	74.82%	-

Mode	Period	Longitudinal direction			Transversal direction		
		M_p	ΣM_p	$\Sigma M_p > 5\%$	M_p	ΣM_p	$\Sigma M_p > 5\%$
n°	(s)	(%)	(%)	(%)	(%)	(%)	(%)
80	0.177	0.00%	52.17%	-	0.07%	74.88%	-
81	0.175	0.00%	52.17%	-	1.58%	76.46%	-
82	0.174	0.25%	52.42%	-	0.38%	76.84%	-
83	0.171	0.05%	52.47%	-	0.21%	77.06%	-
84	0.167	0.01%	52.48%	-	0.12%	77.18%	-
85	0.166	0.28%	52.76%	-	0.00%	77.18%	-
86	0.166	0.06%	52.82%	-	0.02%	77.20%	-
87	0.166	0.13%	52.95%	-	0.12%	77.32%	-
88	0.165	0.01%	52.96%	-	0.00%	77.32%	-
89	0.164	0.03%	52.99%	-	0.00%	77.33%	-
90	0.163	0.01%	53.00%	-	0.00%	77.33%	-
91	0.159	0.00%	53.00%	-	0.03%	77.36%	-
92	0.157	0.73%	53.73%	-	0.30%	77.66%	-
93	0.155	1.09%	54.83%	-	0.01%	77.66%	-
94	0.154	0.28%	55.10%	-	0.02%	77.69%	-
95	0.154	0.87%	55.97%	-	0.04%	77.73%	-
96	0.152	3.50%	59.47%	-	0.00%	77.73%	-
97	0.152	0.08%	59.54%	-	0.00%	77.73%	-
98	0.151	0.09%	59.64%	-	0.28%	78.01%	-
99	0.151	0.09%	59.73%	-	0.00%	78.01%	-
100	0.150	0.17%	59.90%	-	0.10%	78.11%	-
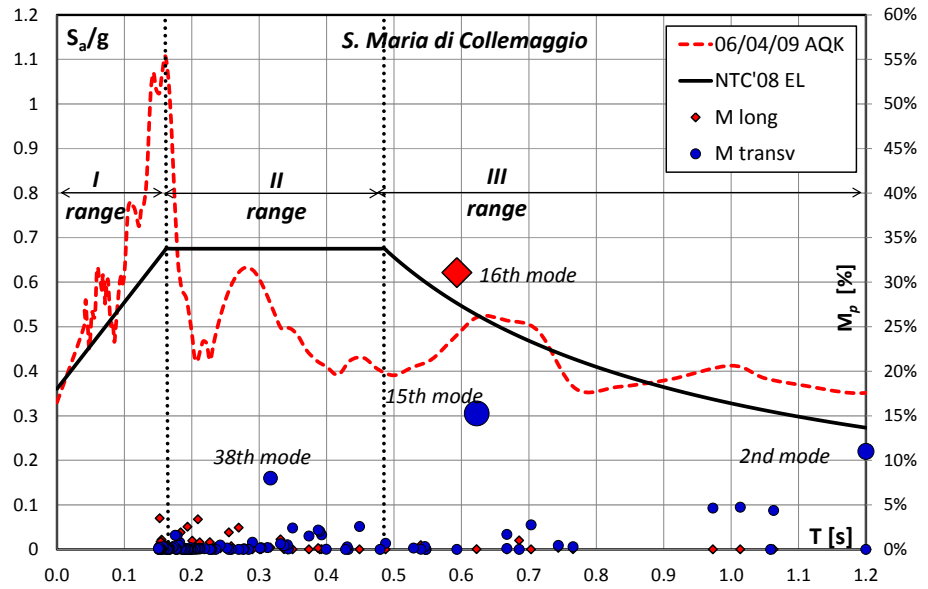
	100 v.m.	M_p>5%	10 $M_p$max	I range	II range	III range
ΣM_{plong}	60%	31%	50%	7%	20%	33%
$\Sigma M_{ptransv}$	78%	34%	58%	1%	31%	47%

1st mode	2nd mode	5th mode

S. AGOSTINO ALLA ZECCA (SAZ)

Mode	Period	Longitudinal direction			Transversal direction		
		M_p	ΣM_p	$\Sigma M_p > 5\%$	M_p	ΣM_p	$\Sigma M_p > 5\%$
n°	(s)	(%)	(%)	(%)	(%)	(%)	(%)
1	0.906	0.00%	0.00%	-	39.66%	39.66%	39.66%
2	0.753	0.84%	0.84%	-	0.81%	40.47%	-
3	0.750	1.12%	1.95%	-	0.78%	41.25%	-
4	0.688	0.07%	2.02%	-	0.00%	41.25%	-
5	0.645	30.28%	32.30%	30.28%	0.00%	41.25%	-
6	0.575	0.01%	32.30%	-	13.55%	54.80%	13.55%
7	0.569	3.77%	36.07%	-	0.01%	54.81%	-
8	0.557	0.01%	36.08%	-	0.00%	54.81%	-
9	0.555	0.03%	36.11%	-	0.00%	54.81%	-
10	0.551	0.03%	36.14%	-	0.10%	54.90%	-
11	0.550	0.01%	36.14%	-	4.24%	59.14%	-
12	0.514	0.04%	36.18%	-	3.43%	62.57%	-
13	0.507	0.63%	36.81%	-	0.03%	62.60%	-
14	0.489	23.66%	60.47%	23.66%	0.00%	62.60%	-
15	0.465	0.03%	60.50%	-	3.56%	66.16%	-
16	0.456	0.68%	61.18%	-	0.00%	66.16%	-
17	0.439	3.99%	65.16%	-	0.00%	66.16%	-
18	0.428	0.00%	65.16%	-	2.48%	68.64%	-
19	0.402	0.01%	65.17%	-	4.76%	73.40%	-
20	0.381	0.04%	65.21%	-	0.01%	73.42%	-
21	0.376	1.51%	66.72%	-	0.05%	73.47%	-
22	0.363	0.00%	66.72%	-	3.50%	76.96%	-
23	0.347	0.20%	66.92%	-	0.19%	77.15%	-
24	0.343	0.03%	66.95%	-	0.86%	78.01%	-
25	0.331	0.77%	67.72%	-	0.09%	78.10%	-
26	0.327	0.19%	67.92%	-	0.72%	78.82%	-
27	0.313	0.12%	68.04%	-	0.17%	78.99%	-
28	0.311	0.02%	68.06%	-	0.01%	79.01%	-
29	0.306	0.58%	68.64%	-	0.01%	79.01%	-
30	0.302	0.00%	68.64%	-	0.07%	79.08%	-
31	0.299	0.71%	69.35%	-	0.00%	79.09%	-
32	0.284	0.04%	69.39%	-	0.49%	79.57%	-
33	0.273	3.63%	73.02%	-	0.04%	79.61%	-
34	0.270	5.52%	78.53%	5.52%	0.00%	79.61%	-
35	0.263	0.08%	78.61%	-	0.07%	79.68%	-
36	0.260	0.11%	78.72%	-	0.01%	79.69%	-
37	0.256	0.35%	79.07%	-	0.07%	79.76%	-
38	0.251	3.39%	82.46%	-	0.02%	79.78%	-
39	0.247	0.01%	82.46%	-	2.78%	82.56%	-

Mode	Period	Longitudinal direction			Transversal direction		
		M_p	ΣM_p	$\Sigma M_p > 5\%$	M_p	ΣM_p	$\Sigma M_p > 5\%$
n°	(s)	(%)	(%)	(%)	(%)	(%)	(%)
40	0.245	0.59%	83.06%	-	0.02%	82.58%	-
41	0.244	0.01%	83.06%	-	0.16%	82.74%	-
42	0.239	0.00%	83.07%	-	0.10%	82.84%	-
43	0.235	0.00%	83.07%	-	0.00%	82.84%	-
44	0.228	0.01%	83.07%	-	1.86%	84.70%	-
45	0.225	0.02%	83.10%	-	0.08%	84.77%	-
46	0.223	0.03%	83.12%	-	0.06%	84.84%	-
47	0.213	0.01%	83.13%	-	0.23%	85.07%	-
48	0.213	0.01%	83.14%	-	0.21%	85.28%	-
49	0.209	0.00%	83.14%	-	0.01%	85.29%	-
50	0.207	0.02%	83.15%	-	0.00%	85.29%	-
51	0.201	0.00%	83.16%	-	0.09%	85.39%	-
52	0.200	0.01%	83.16%	-	0.07%	85.46%	-
53	0.198	0.09%	83.26%	-	0.03%	85.48%	-
54	0.194	0.00%	83.26%	-	0.02%	85.50%	-
55	0.192	0.00%	83.26%	-	0.00%	85.50%	-
56	0.192	0.00%	83.26%	-	0.00%	85.51%	-
57	0.190	0.01%	83.27%	-	0.29%	85.80%	-
58	0.189	0.00%	83.27%	-	0.03%	85.83%	-
59	0.189	0.27%	83.54%	-	0.01%	85.84%	-
60	0.188	0.03%	83.57%	-	0.01%	85.85%	-
61	0.187	0.00%	83.57%	-	0.01%	85.86%	-
62	0.185	0.33%	83.90%	-	0.00%	85.86%	-
63	0.182	0.00%	83.90%	-	0.01%	85.87%	-
64	0.181	0.00%	83.90%	-	0.05%	85.91%	-
65	0.179	0.00%	83.90%	-	0.01%	85.92%	-
66	0.176	0.01%	83.92%	-	0.57%	86.49%	-
67	0.174	0.04%	83.96%	-	0.04%	86.53%	-
68	0.173	0.02%	83.97%	-	0.02%	86.55%	-
69	0.172	0.02%	83.99%	-	0.00%	86.55%	-
70	0.170	0.07%	84.07%	-	0.01%	86.56%	-
71	0.169	0.00%	84.07%	-	0.02%	86.59%	-
72	0.169	0.08%	84.14%	-	0.05%	86.63%	-
73	0.163	0.19%	84.34%	-	0.12%	86.75%	-
74	0.162	0.15%	84.49%	-	0.02%	86.78%	-
75	0.161	0.12%	84.60%	-	0.18%	86.96%	-
76	0.160	0.02%	84.62%	-	0.16%	87.12%	-
77	0.160	0.06%	84.68%	-	0.00%	87.12%	-
78	0.159	0.06%	84.74%	-	0.06%	87.18%	-
79	0.158	0.01%	84.75%	-	0.05%	87.23%	-

Mode	Period	Longitudinal direction			Transversal direction		
		M_p	ΣM_p	$\Sigma M_p > 5\%$	M_p	ΣM_p	$\Sigma M_p > 5\%$
n°	(s)	(%)	(%)	(%)	(%)	(%)	(%)
80	0.157	0.02%	84.77%	-	0.00%	87.23%	-
81	0.156	0.09%	84.86%	-	0.04%	87.27%	-
82	0.155	0.02%	84.88%	-	0.02%	87.29%	-
83	0.154	0.26%	85.14%	-	0.12%	87.40%	-
84	0.154	0.29%	85.43%	-	0.04%	87.45%	-
85	0.153	0.10%	85.53%	-	0.05%	87.50%	-
86	0.152	0.02%	85.55%	-	0.08%	87.58%	-
87	0.152	0.14%	85.69%	-	0.81%	88.39%	-
88	0.151	0.00%	85.69%	-	0.19%	88.57%	-
89	0.150	0.01%	85.71%	-	0.25%	88.83%	-
90	0.149	0.45%	86.16%	-	0.01%	88.84%	-
91	0.148	0.03%	86.19%	-	0.10%	88.94%	-
92	0.147	0.35%	86.54%	-	0.00%	88.94%	-
93	0.147	0.02%	86.56%	-	0.05%	88.99%	-
94	0.146	0.46%	87.02%	-	0.07%	89.06%	-
95	0.146	0.20%	87.22%	-	0.00%	89.06%	-
96	0.145	0.02%	87.24%	-	0.00%	89.06%	-
97	0.143	0.00%	87.24%	-	0.03%	89.10%	-
98	0.142	0.04%	87.29%	-	0.01%	89.11%	-
99	0.141	0.02%	87.31%	-	0.00%	89.11%	-
100	0.140	0.02%	87.33%	-	0.00%	89.11%	-
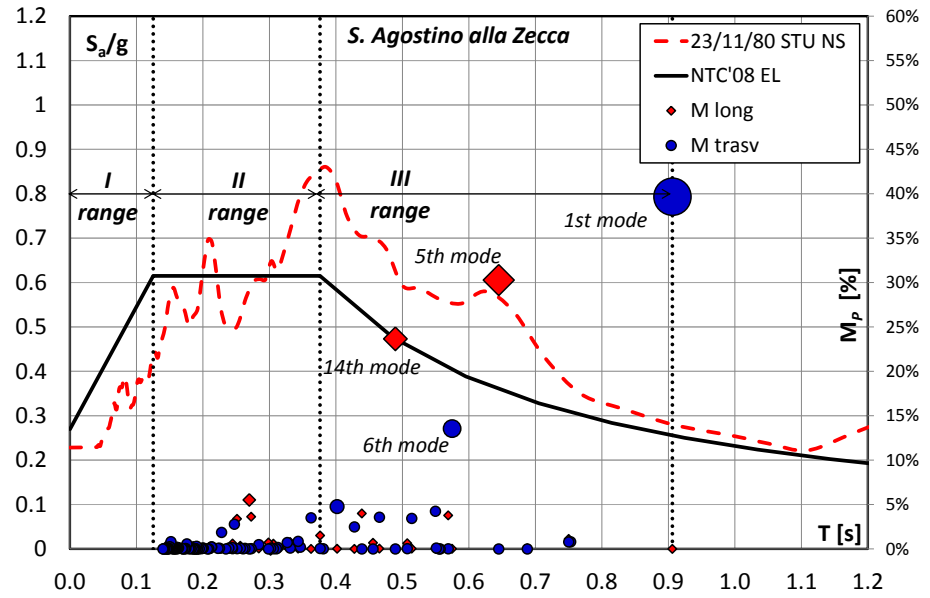
	100 v.m.	$M_p > 5\%$	10 $M_p$max	I range	II range	III range
ΣM_{plong}	87%	59%	78%	0%	21%	67%
$\Sigma M_{ptransv}$	89%	53%	80%	0%	16%	73%

1st mode   5th mode   14th mode
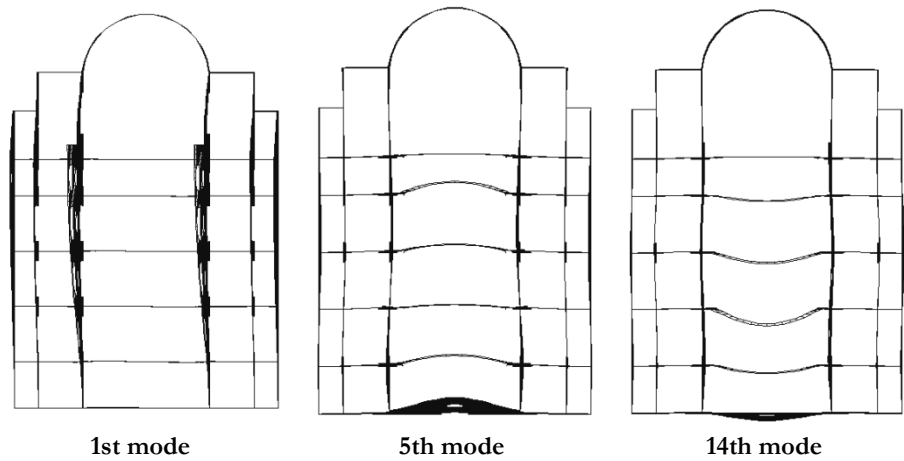
S. PAOLO MAGGIORE (SPM)

Mode	Period	Longitudinal direction			Transversal direction		
		M_p	ΣM_p	$\Sigma M_p > 5\%$	M_p	ΣM_p	$\Sigma M_p > 5\%$
n°	(s)	(%)	(%)	(%)	(%)	(%)	(%)
1	0.820	11.00%	11.00%	11.00%	0.00%	0.00%	-
2	0.771	2.07%	13.07%	-	0.03%	0.03%	-
3	0.765	0.01%	13.08%	-	19.00%	19.03%	19.00%
4	0.637	24.00%	37.08%	24.00%	0.00%	19.03%	-
5	0.586	0.24%	37.32%	-	5.13%	24.16%	5.13%
6	0.580	2.03%	39.34%	-	0.82%	24.98%	-
7	0.569	0.01%	39.36%	-	1.90%	26.88%	-
8	0.516	0.01%	39.37%	-	1.00%	27.87%	-
9	0.505	1.20%	40.56%	-	0.05%	27.92%	-
10	0.459	0.00%	40.57%	-	5.33%	33.26%	5.33%
11	0.430	1.39%	41.95%	-	12.00%	45.26%	12.00%
12	0.424	16.00%	57.95%	16.00%	1.18%	46.44%	-
13	0.413	0.13%	58.08%	-	1.00%	47.43%	-
14	0.395	0.00%	58.08%	-	1.43%	48.86%	-
15	0.381	0.00%	58.08%	-	9.36%	58.22%	9.36%
16	0.376	4.18%	62.26%	-	0.03%	58.26%	-
17	0.356	1.51%	63.77%	-	0.03%	58.28%	-
18	0.349	0.09%	63.86%	-	2.53%	60.81%	-
19	0.324	3.82%	67.68%	-	0.00%	60.81%	-
20	0.317	0.03%	67.70%	-	0.35%	61.16%	-
21	0.308	0.03%	67.73%	-	5.81%	66.97%	5.81%
22	0.305	0.17%	67.90%	-	1.01%	67.99%	-
23	0.297	1.31%	69.21%	-	0.02%	68.01%	-
24	0.289	0.03%	69.24%	-	0.10%	68.10%	-
25	0.283	0.09%	69.33%	-	0.03%	68.13%	-
26	0.281	0.00%	69.33%	-	0.00%	68.13%	-
27	0.274	0.04%	69.37%	-	0.54%	68.67%	-
28	0.267	0.00%	69.38%	-	0.48%	69.15%	-
29	0.265	0.41%	69.79%	-	0.09%	69.24%	-
30	0.262	0.01%	69.80%	-	0.01%	69.25%	-
31	0.261	1.00%	70.80%	-	0.13%	69.38%	-
32	0.256	0.07%	70.87%	-	0.01%	69.39%	-
33	0.253	0.00%	70.87%	-	0.01%	69.40%	-
34	0.252	0.27%	71.15%	-	0.03%	69.43%	-
35	0.248	0.00%	71.15%	-	0.21%	69.64%	-
36	0.245	0.01%	71.16%	-	0.55%	70.20%	-
37	0.244	0.00%	71.17%	-	0.24%	70.43%	-
38	0.242	0.00%	71.17%	-	0.20%	70.63%	-
39	0.238	0.41%	71.58%	-	0.83%	71.46%	-

| Mode | Period | Longitudinal direction | | | Transversal direction | | |
| | | M_p | ΣM_p | $\Sigma M_p > 5\%$ | M_p | ΣM_p | $\Sigma M_p > 5\%$ |
n°	(s)	(%)	(%)	(%)	(%)	(%)	(%)
40	0.236	0.83%	72.41%	0.83%	0.37%	71.83%	-
41	0.232	0.04%	72.45%	0.04%	0.07%	71.90%	-
42	0.226	0.09%	72.54%	0.09%	0.08%	71.98%	-
43	0.225	0.02%	72.56%	0.02%	0.49%	72.47%	-
44	0.225	0.01%	72.57%	0.01%	0.05%	72.52%	-
45	0.219	0.49%	73.07%	0.49%	0.00%	72.52%	-
46	0.219	0.02%	73.09%	0.02%	1.72%	74.24%	-
47	0.217	1.11%	74.20%	1.11%	0.00%	74.24%	-
48	0.211	0.09%	74.29%	0.09%	0.00%	74.24%	-
49	0.210	0.00%	74.29%	0.00%	0.19%	74.43%	-
50	0.205	0.36%	74.65%	0.36%	0.05%	74.48%	-
51	0.204	0.01%	74.66%	0.01%	0.09%	74.57%	-
52	0.203	0.42%	75.08%	0.42%	0.07%	74.64%	-
53	0.202	0.10%	75.18%	0.10%	0.04%	74.67%	-
54	0.197	0.03%	75.21%	0.03%	0.51%	75.18%	-
55	0.195	0.02%	75.23%	0.02%	0.01%	75.19%	-
56	0.192	0.26%	75.49%	0.26%	0.02%	75.21%	-
57	0.190	1.04%	76.53%	1.04%	0.04%	75.25%	-
58	0.189	0.11%	76.64%	0.11%	0.48%	75.73%	-
59	0.188	0.05%	76.69%	0.05%	0.07%	75.79%	-
60	0.185	0.03%	76.71%	0.03%	0.76%	76.55%	-
61	0.184	0.10%	76.82%	0.10%	0.01%	76.56%	-
62	0.183	0.01%	76.83%	0.01%	0.63%	77.19%	-
63	0.181	0.04%	76.87%	0.04%	0.33%	77.52%	-
64	0.178	0.03%	76.90%	0.03%	0.07%	77.59%	-
65	0.176	0.16%	77.06%	0.16%	0.07%	77.66%	-
66	0.175	1.51%	78.57%	1.51%	0.00%	77.66%	-
67	0.175	0.02%	78.59%	0.02%	0.05%	77.72%	-
68	0.174	0.11%	78.69%	0.11%	0.11%	77.82%	-
69	0.173	0.01%	78.70%	0.01%	0.03%	77.85%	-
70	0.173	0.00%	78.71%	0.00%	0.08%	77.93%	-
71	0.172	0.14%	78.84%	0.14%	0.14%	78.07%	-
72	0.170	0.49%	79.34%	0.49%	0.22%	78.30%	-
73	0.170	0.08%	79.42%	0.08%	0.05%	78.35%	-
74	0.168	0.12%	79.54%	0.12%	0.10%	78.45%	-
75	0.167	0.04%	79.57%	0.04%	0.05%	78.49%	-
76	0.166	0.02%	79.59%	0.02%	0.05%	78.55%	-
77	0.163	0.03%	79.62%	0.03%	0.50%	79.04%	-
78	0.161	0.00%	79.62%	0.00%	0.00%	79.04%	-
79	0.159	0.43%	80.05%	0.43%	0.04%	79.09%	-

Mode	Period	Longitudinal direction			Transversal direction		
		M_p	ΣM_p	$\Sigma M_p > 5\%$	M_p	ΣM_p	$\Sigma M_p > 5\%$
n°	(s)	(%)	(%)	(%)	(%)	(%)	(%)
80	0.159	0.05%	80.11%	-	0.20%	79.29%	-
81	0.158	0.70%	80.81%	-	0.06%	79.35%	-
82	0.158	0.38%	81.19%	-	0.01%	79.36%	-
83	0.157	0.02%	81.21%	-	0.50%	79.86%	-
84	0.156	0.07%	81.28%	-	0.04%	79.89%	-
85	0.155	0.00%	81.28%	-	1.55%	81.45%	-
86	0.155	0.21%	81.49%	-	0.00%	81.45%	-
87	0.153	0.00%	81.49%	-	0.14%	81.59%	-
88	0.152	0.00%	81.50%	-	0.12%	81.71%	-
89	0.150	0.28%	81.78%	-	0.01%	81.72%	-
90	0.150	0.02%	81.80%	-	0.03%	81.75%	-
91	0.149	0.00%	81.80%	-	0.06%	81.81%	-
92	0.149	0.00%	81.81%	-	0.00%	81.81%	-
93	0.149	0.00%	81.81%	-	0.04%	81.86%	-
94	0.147	0.01%	81.82%	-	0.31%	82.16%	-
95	0.146	0.00%	81.83%	-	0.06%	82.22%	-
96	0.145	0.30%	82.13%	-	0.10%	82.32%	-
97	0.144	0.11%	82.24%	-	0.04%	82.36%	-
98	0.143	0.09%	82.33%	-	0.16%	82.52%	-
99	0.141	0.02%	82.35%	-	0.01%	82.52%	-
100	0.140	0.04%	82.39%	-	0.00%	82.52%	-
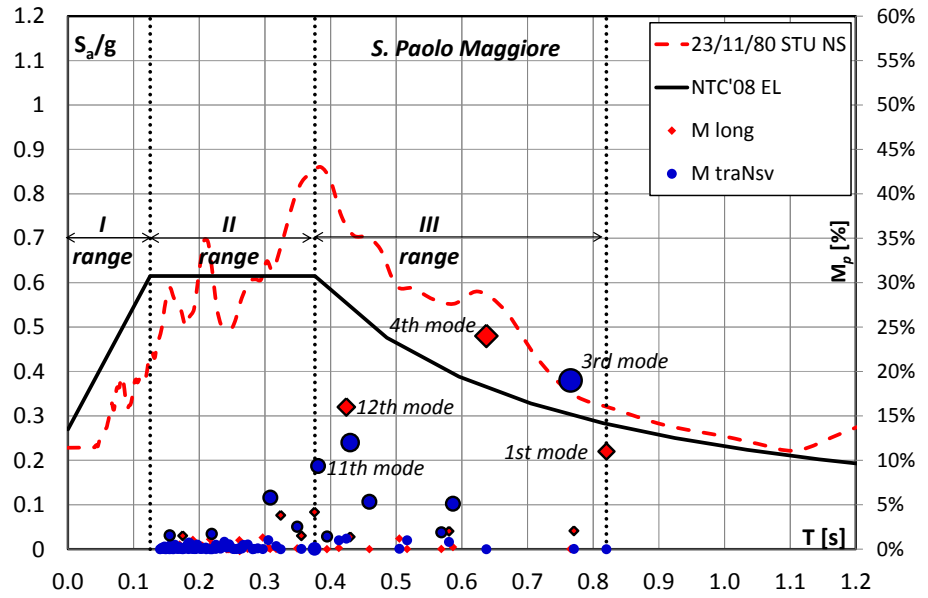
	100 v.m.	M_p>5%	10 M_pmax	I range	II range	III range
ΣM_{plong}	82%	40%	68%	0%	20%	62%
$\Sigma M_{ptransv}$	83%	57%	64%	0%	24%	58%

3rd mode   4th mode   12th mode